

ICMIC 2022 International Conference on Maritime IT Convergence

**"Accelerating Convergence of Maritime,
Terrestrial and Aerial Communications for the 6G Era"**

PROCEEDINGS

Date September 22 (Thur) ~ 23 (Fri), 2022

Venue Sono Calm, Jeju Island, Korea

Organized by



Patrons



General Information

The International Conference on Maritime IT Convergence (ICMIC) will be inaugurated in 2022 with aims to promote convergence activities of maritime and terrestrial communications as well as related wireless communications. Recognizing that maritime communications will usually involve ship-to-ship and ship-to-shore communication, maritime ICT technologies will bring some mature but still evolving terrestrial wired/wireless communication technologies to its own use for future smart maritime communications. More specifically, the conference will focus on addressing challenges of maritime communications with ICT convergence or advanced wireless communications over various industrial sectors, academia and practice engineers. The conference will include keynote speech sessions, invited special sessions and technical paper sessions.

Message from the Chairs

Dear members of The Korean Institute of Communications and Information Sciences (KICS) and participants of the ICMIC 2022.

It is already close to the end of the September 2022. As we slowly move ahead towards the ordinary life, with the long and tiresome COVID-19 pandemic behind, ICMIC 2022 will be held in September, in the Jeju Island. The event will be on/off hybrid since we are not fully freed from COVID-19, but we are happy to be able to provide offline meetings.

This event is undoubtedly the most promising conference in the field of convergence of maritime, terrestrial and aerial communications. The keynote speech by the Prof. Mohamed-Slim Alouini from the KAUST, Makkah Province, Saudi Arabia is prepared along with various oral and poster presentations.

The Sono Calm in Jeju Island seems to be a perfect place for participants to comfortably enjoy offline events and relaxation. It is expected that many professionals in related fields will be able to exchange ideas and collaborate through the event.

Lastly, we would like to thank the organizing committees and staffs for the generous support. We would like to ask many of you to participate online/offline, and wish everyone good health and well-being.

ICMIC chairs

September 2022

Committees

International Advisory Committee

- Woong Seo Kim (KIOST, Korea)
- Yoan Shin (Soongsil University, Korea)
- Zabih Ghassemlooy (Northumbria University, UK)
- Murat Uysal (Ozyegin University, Turkey)
- Dong Jin Kang (Korean Society of Oceanography, Korea)

General Co-Chairs

- Yeon Ho Chung (Pukyong National University, Korea)
- Dong Myung Lee (Tongmyong University, Korea)

Technical Program Committee Co-Chairs

- Seungjae Baek (KIOST, Korea)
- Kyung-Rak Sohn (Korea Maritime and Ocean University, Korea)

Technical Program Committee

- Chanjun Chun (Chosun University, Korea)
- Dong Wook Cho (Chungbuk Provincial University, Korea)
- Hyuntae Cho (Tongmyong University, Korea)
- Inoh Choi (Korea Maritime and Ocean University, Korea)
- Jin Hwan Koh (Gyeongsang National University, Korea)
- Dong Seong Kim (Kumoh National Institute of Technology, Korea)
- Gyung Bae Kim (Seowon University, Korea)
- Sang Ki Jeong (KIOST, Korea)
- Soo Mee Kim (KIOST, Korea)
- Suk Chan Kim (Pusan National University, Korea)
- Sung Hoon Lim (Hallym University, Korea)
- Taewoon Kim (Pusan National University, Korea)
- Wooyeon Choi (Chosun University, Korea)
- Woo Yong Lee (ETRI, Korea)
- Wang Sang Lee (Gyeongsang National University, Korea)
- Yeon Man Jeong (Gangneung-Wonju National University, Korea)
- Yeon S. Chang (KIOST, Korea)
- Yonggang Kim (Kongju National University, Korea)
- Yujae Song (Kumoh National Institute of Technology, Korea)

Finance Chair

- Sang Ki Jeong (KIOST, Korea)

Publicity Chair

- Suk Chan Kim (Pusan National University, Korea)

Registration Chair

- Yonggang Kim (Kongju National University, Korea)

Publication Chair

- Inoh Choi (Korea Maritime and Ocean University, Korea)

Web Chair

- Yujae Song (Kumoh National Institute of Technology, Korea)

Table of Contents

Oral Sessions

Technical Session #1 : Advanced ICT Technologies

Chair : Seungjae Baek (KIOST, Korea)

T1-1) Development of a Deep Learning-Based Condition Diagnosis and Prognosis System for Naval Ship Maintenance.....	1
Dong Seong Kim (Kumoh National Institute of Technology, Korea); Gi Hyeb Kwon (ICT-Convergence Research Center, Korea); Jae-Woo Kim (Kumoh National Institute of Technology, Korea)	
T1-2) Stable Multi Edge Computing System with Blockchain in Industrial Internet of Things.....	3
Yunseong Lee and Sungrae Cho (Chung-Ang University, Korea)	
T1-3) Machine Learning-Based Fault Monitoring on a Digital Twin-Enabled System for Additive Manufacturing	5
Gabriel Avelino R Sampedro (Kumoh National Institute of Technology, Korea & University of the Philippines, Philippines); Made Adi Paramartha Putra, Syifa Maliah Rachmawati, Dong Seong Kim and Jae-Min Lee (Kumoh National Institute of Technology, Korea)	
T1-4) Toward Deeply Understanding Us in Smart Home.....	7
Taesoo Jun (Kumoh National Institute of Technology, Korea)	
T1-5) Performance Evaluation of Metaverse Platform to the Type of Game Server Engine.....	9
Dongeon Yoon, Hyosang Lee, Changseop Lim and Am-Suk Oh (Tongmyong University, Korea)	
T1-6) Lightweight Anomaly Detection Based on Embedded A.I. for Early Failure Detection of Industrial Robots	11
Hyuntae Cho (Tongmyong University, Korea); Wooseok Byun (KAIST)	

Technical Session #2 : Maritime ICT I

Chair : Wooyeol Choi (Chosun University, Korea)

T2-1) Coding Rate Adjustment of Underwater Optical Wireless Communication Based on Deep Reinforcement Learning.....	12
Hui cheol Shin (University of Science and Technology, Korea); Yujae Song (Kumoh National Institute of Technology, Korea); Yongjae Kim (KIOST, Korea)	
T2-2) Anti-Biofouling for Seawater Battery Systems	14
Juhyun Kim (Korea Institute of Ocean Science and Technology, Korea); Seungjae Baek (KIOST, Korea); Sungmin Koo (Korea Institute of Ocean Science and Technology, Korea); Ahyun Park (Marine Equipment Technology Solutions, Korea); Kim Yoonchil (Korea Institute of Ocean Science and Technology, Korea); Saat Mubarrok (Mulawarman University, Indonesia)	
T2-3) Research on the Development of Unmanned Boat Applying Sea-Water Battery for Observation and Detection	16
Juhyun Kim, Hyoun Kang, Jaeho Choi and Sangwoo Kang (Korea Institute of Ocean Science and Technology, Korea); Dayu Wiyati Purnaningtyas (Bandung Institute of Technology, Indonesia)	
T2-4) KIO-Gaon: A Modular Designed Remotely Operated Vehicle for Versatile Operations.....	18
Sungmin Koo and Juhyun Kim (Korea Institute of Ocean Science and Technology, Korea); Yazid Ridla (Oceanovision, Indonesia); Seungjae Baek (KIOST, Korea)	
T2-5) Improved Efficiency of Small Wind Turbine Using Vertical Dual Axis	20
Ah Hyun Park (Marine Equipment Technology Solutions, Korea); Hyoun Kang (Korea Institute of Ocean Science and Technology, Korea); Yong Soo Kang (Dual Wind, Korea); Seungjae Baek (KIOST, Korea); Faizal Ade R. Abdullah (Bandung Institute of Technology, Indonesia)	
T2-6) A Brief Survey of Massive MIMO SWIPT-Enabled IoT Network.....	23
Hyunwoo Jung (University of Maritime ICT, Korea); Yongjae Kim (KIOST, Korea)	

Technical Session #3 : UAV Communications

Chair : Yujae Song (Kumoh National Institute of Technology, Korea)

T3-1) Non-Negative Matrix Factorization Based Optimization Algorithm for Face Age Prediction	24
Man Zhang and Dong Myung Lee (Tongmyong University, Korea)	
T3-2) UAV-Assisted Real-Time Monitoring and Detection of Maritime Infrastructure Defects	25
Min Hyuk Kim and Kwonsoon Yong (Hallym University, Korea); Abdallah A Khereishah (New Jersey Institute of Technology, USA); Sung Hoon Lim and Wonjong Noh (Hallym University, Korea)	

Table of Contents

T3-3) Self-Supervised MIMO System for Autonomous Underwater Navigation Operations.....	27
<i>Simeon Ajakwe (Kumoh National Institute of Technology, Gumi, Korea); Vivian Ukanaka Ihekoronye, Dong Seong Kim and Jae Min Lee (Kumoh National Institute of Technology, Korea)</i>	
T3-4) Aerial Cell Planning Depending on Altitude	30
<i>Yuna Jeong (Chonnam National University, Korea); Jihyung Kim (ETRI, Korea); Intae Hwang (Chonnam National University, Korea); Moonsik Lee (ETRI, Korea)</i>	
T3-5) Maritime UAV Patrol Tasks Based on YOLOv4 Object Detection.....	32
<i>Yi-Yu Chang, John A and Pao-Ann Hsiung (National Chung Cheng University, Taiwan)</i>	
T3-6) DL-Based AUV Position Prediction Using Odometry Data for Internet of Underwater Things	38
<i>Made Adi Paramartha Putra (Kumoh National Institute of Technology, Korea); Nengah Widya Utami and I Gede Juliana Eka Putra (STMIK Primakara, Indonesia); Dong Seong Kim and Jae Min Lee (Kumoh National Institute of Technology, Korea)</i>	

Technical Session #4 : Maritime ICT II

Chair : Yonggang Kim (Kongju National University, Korea)

T4-1) Beam Divergence Angle and Transmission Power Adjustment of Underwater Optical Wireless Communication Based on Reinforcement Learning.....	40
<i>Hui cheol Shin (University of Science and Technology, Korea); Yujae Song (Kumoh National Institute of Technology, Korea); Yongjae Kim (KIOST, Korea)</i>	
T4-2) Single Enhancement Techniques for Underwater Stereo Vision.....	42
<i>Hong-gi Kim (Korea Institute of Ocean Science and Technology, Korea); Jungmin Seo and Soo Mee Kim (KIOST, Korea)</i>	
T4-3) A Brief Survey of Massive MU-MIMO User Scheduling in Various Network.....	44
<i>Hyunwoo Jung and Yongjae Kim (KIOST, Korea)</i>	
T4-4) Development of In-Situ Underwater Gamma-Ray Spectroscopy System	46
<i>Jungmin Seo and Soo Mee Kim (KIOST, Korea)</i>	
T4-5) Analysis of Signal Processing Using Water Surface Elevation Data.....	48
<i>Ukjae Lee (KIOST, Korea); HongYeon Cho (Korea Institute of Ocean Science and Technology, Korea); DongHui Ko (KIOST, Korea); JiYoung Kim (KEPCO Research Institute, Korea); Yunzheng Ge (First Institute of Ocean Energy Research Center, China)</i>	
T4-6) Movable Visualization System for Exterior Monitoring of Outdoor Infrastructures.....	51
<i>Hong Guk Jeong, Jungmin Seo, Jihyeong Lee and Soo Mee Kim (KIOST, Korea)</i>	

Technical Session #5 : Deep Learning Wireless Communications

Chair : Dong Myung Lee (Tongmyong University, Korea)

T5-1) Deep Reinforcement Learning-Based Power Allocation in Multi-Cell Massive MIMO.....	53
<i>Youngwoo Oh and Wooyeon Choi (Chosun University, Korea)</i>	
T5-2) Collaborative Learning for Cyber-Attacks Classification in Maritime Transportation Systems.....	55
<i>Ahmad Zainudin, Jung Hyun Kim, Dong Seong Kim and Jae Min Lee (Kumoh National Institute of Technology, Korea)</i>	
T5-3) FED-MARINE: Federated Learning Framework for DDoS Detection and Mitigation in Maritime-SCADA Network.....	57
<i>Love Allen Ahakonye, Cosmas Ifeanyi Nwakanma, Jae Min Lee and Dong Seong Kim (Kumoh National Institute of Technology, Korea)</i>	
T5-4) Indoor Visible Light LOS Channel Estimation Using Support Vector Regression	60
<i>Yeong Hae Kim, Young Jae Moon, Sudhanshu Arya and Yeonho Chung (Pukyong National University, Korea)</i>	
T5-5) Clustering Algorithm for Cooperative Spectrum Sensing in Cognitive Radio Networks.....	62
<i>Chunghyun Lee (Chun-Ang University, Korea); Junsuk Oh, Taeyun Ha and Donghyun Lee (Chung-Ang University, Korea); Geeranuch Woraphonbenjakul (Chung Ang University, Korea); Sungrae Cho (Chung-Ang University, Korea)</i>	
T5-6) Deep Reinforcement Learning Based Power Allocation Scheme in Uplink NOMA Systems	65
<i>Won Jae Ryu and Dong Seong Kim (Kumoh National Institute of Technology, Korea)</i>	

Table of Contents

Technical Session #6 : Underwater Wireless Communications

Chair : Yeon Ho Chung (Pukyong National University, Korea)

T6-1) A Study on Space Diversity Gain of Reflective LoS Channel in Maritime Long Range Communication	67
Woo Yong Lee and Keunyoung Kim (ETRI, Korea)	
T6-2) Beamforming and Power Optimization Techniques in Cell-Free Networks.....	69
Keunyoung Kim and Woo Yong Lee (ETRI, Korea)	
T6-3) Vessel MMSI Forgery Prevention System.....	70
Sung-Hwa Han and Young-Sik Park (Tongmyong University, Korea)	
T6-4) Density-Based Contention Management for Collision Avoidance in Dense IoT Networks	71
Sejin Choi, Lee Jaewan, Minwoo Kwon and Yonggang Kim (Kongju National University, Korea)	
T6-5) Transmission Loss Analysis of SATCOM Radomes with Wide Incident Angle	73
Taehyeon Kim and Wang-Sang Lee (Gyeongsang National University, Korea)	
T6-6) Channel Estimation for RIS Aided Multi-User SISO System Using Super-Resolution.....	75
Jeongbin Seo (Pusan National University, Korea); Donghwan Kim and Suk Chan Kim (Pusan National University, Korea)	

Poster Session

Poster Session

P-1) Voice Spoofing Countermeasure Using Residual Convolutional Neural Networks and Self-Attention	76
Changhwan Go, Wooyeon Choi and Chanjun Chun (Chosun University, Korea)	
P-2) A Study on the Control of Small Unmanned Surface Vehicles Using Disturbance Learning.....	78
Sang Ki Jeong, Jihyeong Lee and Haeyoung Park (KIOST, Korea); Wen-Hsiang Hsieh (National Formosa University, Taiwan); Dae Hyeong Ji (KIOST, Korea)	
P-3) A Study on the Swarm Control Algorithm of Unmanned Surface Vehicles.....	81
Jihyeong Lee, Sang Ki Jeong and Haeyoung Park (Korea Institute of Ocean Science and Technology, Korea)	
P-4) Fingerprint-Aided Coordinated mmWave Beam Selection for mmWave UAV Communications	83
Yuna Sim, Seungseok Sin, Yuna Jeong and Jihun Cho (Chonnam National University, Korea); Sangmi Moon (Korea Nazarene University, Korea); Intae Hwang (Chonnam National University, Korea)	
P-5) Experiments of Long-Range Underwater Communication in the East Sea	85
Donghyeon Kim, Jeongha An, Jeasoo Kim and Kiman Kim (Korea Maritime and Ocean University, Korea); In-soo Kim (Agency of Defense Development, Korea)	
P-6) Utility-Centric Partial Offloading in Parked Vehicle-Assisted Multi-Access Edge Computing.....	87
Xuan-Qui Pham and Dong Seong Kim (Kumoh National Institute of Technology, Korea)	
P-7) Prospect and Industry Issues of Metaverse and Digital Twin Adoption in Nigerian Maritime.....	89
Cosmas Ifeanyi Nwakanma and Judith Nkechinyere Njoku (Kumoh National Institute of Technology, Korea); Cajethan Onyekachi Okafor (Federal University of Technology Owerri, Nigeria); Dong Seong Kim (Kumoh National Institute of Technology, Korea)	
P-8) A Study of Open-Source Netwrok Simulator	93
Jae Woo Kim, Gi Hyeb Kwon and Dong Seong Kim (Kumoh National Institute of Technology, Korea)	
P-9) Primary User Emulation Attack Detection	95
Vladimir V. Shakhov (University of Ulsan, Korea)	
P-10) A Study on the Problems and Solutions in the NFT Ecosystem	96
Yongbin Choi and Am-Suk Oh (Tongmyong University, Korea)	

Oral Sessions

Development of a deep learning-based condition diagnosis and prognosis system for naval ship maintenance

Ki-Hyeob Kwon

ICT Convergence Research Center
Kumoh national institute of Technology
Gumi, Republic of Korea
navkwon@kumoh.ac.kr

Jae Woo Kim

ICT Convergence Research Center
Kumoh national institute of Technology
Gumi, Republic of Korea
jaewookim@kumoh.ac.kr

Dong-Seong Kim

Dept. of IT Convergence Engineering
Kumoh national institute of Technology
Gumi, Republic of Korea
dskim@kumoh.ac.kr

Abstract—This paper proposes a condition diagnosis based system for efficient maintenance of naval warship combat and propulsion systems using deep learning. In addition, a state based prognosis mechanism is integrated into the system to enhance the maintenance process using convolution neural network (CNN) algorithms. Finally, a test-bed experiment is conducted to verify the proposed maintenance systems.

Index Terms—Condition-Based Maintenance, Deep Learning, Naval Ship Maintenance

I. INTRODUCTION

Smart technology is gradually being applied to improve the management and improvement of ship combat and propulsion systems [1]. Condition-based maintenance of the ship combat/propulsion system analyzes the specified data through the sensor attached to a specific part of the equipment to diagnose the current status, and predict failures through the analysis of data trends to prevent failures technology [2].. In the existing plan-based maintenance, maintenance is performed based on the usage time of parts recommended by the equipment manufacturer, but unnecessary costs may occur because the condition of the equipment is not considered, and there may be insufficient preparation for sudden failure. In other words, condition-based maintenance is a method to reduce costs and prepare for failures because maintenance is carried out by tracking the state of equipment or parts and predicting failure situations. For condition-based maintenance, accurate condition diagnosis and prediction are important factors. However, in the case of the Navy's condition-based maintenance (using the ICAS condition diagnosis program), the following problems may occur.

- Format for displaying simple statistical data.
- Lack of analysis system for predictive management of soundness.
- Lack of diagnostic and prediction functions using real-time data.
- Difficult to modify and add functions for user convenience.

This paper proposes a state diagnosis technique using deep learning to supplement the existing state diagnosis technology.

In order to replace ICAS, which is in charge of real-time status diagnosis and trend analysis of propulsion and combat system rotational equipment in naval ships, we propose a deep learning technology-based status diagnosis and predictive model design. To this end, the deep learning-based state diagnosis technology development process was defined and the technology of each process was described. Figure 1 shows the proposed deep learning-based state diagnosis and prediction system model.

II. MAIN SUBJECT AND CONCLUSION

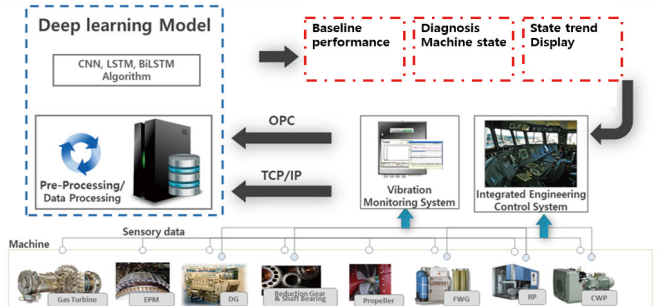


Fig. 1. Proposed ship condition diagnosis and predication system model

In this paper, as shown in Figure 1, a state-based maintenance technology system for efficient maintenance of naval ships based on deep learning is proposed. The proposed state-based maintenance system uses an adaptive preprocessing process and CNN-based deep learning model to predict the abnormal state of parts of the ship combat and propulsion system. Finally, an actual test bed was designed to verify the proposed state diagnosis and prediction system. The proposed condition diagnosis system can further increase the prediction accuracy compared to the statistics-based condition diagnosis, and can contribute to the localization of the condition diagnosis system used in the existing navy. As a future study, we plan to implement conceptual design and evaluate the performance of the proposed system using real data.

ACKNOWLEDGMENT

This research was supported by the MSIT(Ministry of Science and ICT), Korea, under the Grand Information Technology Research Center support program (IITP-2022-2020-0-01612) supervised by the IITP(Institute for Information communications Technology Planning Evaluation). This research was supported by Basic Science Research Program through the National Research Foundation of Korea(NRF) funded by the Ministry of Education(2022R1I1A1A01071058).

REFERENCES

- [1] Kim, Seung-Han, Da-Hye Kim, and Dong-Seong Kim. "Design of Smart Platform-based Event-Log Analysis and Parameter-modifying Software for Naval Combat Systems." IEIE Transactions on Smart Processing Computing 7.5 (2018): 385-391.
- [2] Pack, In-Tack, Seung-Hwan Kim, and Dong-Seong Kim. "Design and Performance Evaluation of a Marine Engine Fault Detection System Using a Proximity Sensor for a Marine Engine." Journal of Institute of Control, Robotics and Systems 22.8 (2016): 619-626.

Stable Multi Edge Computing System with Blockchain in Industrial Internet of Things

Yunseong Lee

*School of Computer Science and Engineering
Chung-Ang University
Seoul, Republic of Korea
yslee@uclab.re.kr*

Sungrae Cho

*School of Computer Science and Engineering
Chung-Ang University
Seoul, Republic of Korea
srcho@cau.ac.kr*

Abstract—In edge computing systems in industrial Internet of Things (IIoT) environment, accommodating significant data generated by IIoT devices is a primary concern. This paper proposes a stable multi edge computing system for IIoT with blockchain network.

Index Terms—Edge Computing, Blockchain, IIoT, Hyperledger Fabric

I. INTRODUCTION

Blockchain provides support for various application services such as secure data management, smart grid, and payment in vehicle networks [1], [2]. Blockchain allows secure transactions with companies that may want to utilize data generated by various Industrial Internet of Things (IIoT) devices. For such companies, transactions are stored in the distributed ledger of the blockchain network. Since several critical messages are exchanged over connected links between EGs and ES in an edge computing based IIoT system. Therefore, it is important to secure critical IIoT data from malicious clients that enter the IIoT network. Blockchain offers an authentication mechanism to verify the identity of IIoT clients and isolate legitimate clients from malicious clients. However, blockchain platform faces problems of complexity of installation and operation when applied to massive IIoT devices in industrial environments. In addition, a large amount of real-time sensory data and control traffic generated by the IIoT devices in a blockchain network increases network load significantly. In particular, since the Hyperledger Fabric platform adopts a centralized approach for transaction processing, it is challenging to achieve high throughput performance and low latency in a blockchain based IIoT network [3]. To resolve this problem, we consider a novel blockchain framework that achieves efficient transaction processing as shown in Fig. 1. In this paper, we propose a three-layered architecture of the IIoT blockchain networks. To distribute the IIoT blockchain network traffic, the IIoT blockchain network is divided into three-layers: namely, 1) *IIoT layer*, 2) *edge computing layer*, and 3) *Internet cloud*. The IIoT layer comprises of IIoT clients that generate network transactions based on real-time IIoT data, and the edge computing layer consists of endorsers and committers that perform IIoT data distribution and transactions management. While the ordering system generates and propagates

II. SYSTEM MODEL

The Hyperledger Fabric has a different system structure than the existing blockchain platforms such as Bitcoin and Ethereum [4], [5]. Unlike the conventional blockchain platforms, that consist of only normal and minor nodes, blockchain nodes in the Hyperledger Fabric comprise of clients, endorsers, committer, and orderer. In an IIoT environment, a client can be an IIoT device or customer who uses an authenticated smart device. For example, a client can be a buyer who may want to utilize IIoT data for big data analysis, or it can be an IIoT device that wants to automatically store data in an edge server. The service providers can choose the most suitable edge server for the supportive services among blockchain platforms. The users who want IIoT data need to subscribe to the blockchain network membership in advance. When the user's authentication process is completed, the information of data, such as the name and type is sent to the blockchain network comprising of edge servers. The hash value of the data is compared with the hash value in the distributed ledger, and the data transmission is requested from the edge server that stores the data by executing smart contract. Before the data created by the IIoT device is stored in the edge server, the hash value of the data and the location of the edge server to be stored are recorded in the distributed ledger.

There are two types of peer nodes that conduct different roles in a Hyperledger Fabric network. The endorser node is responsible for executing the chaincode owned for a client's transaction according to endorsement policy. The chaincode is a specific program to execute the client's transaction and it runs in the Docker container. The endorser, even though, executes a transaction, it does not register directly to own the distributed ledger rather it sends the execution results to the client. In an IIoT system, endorsers can be devices operated by an administrator or it can be the IIoT devices based on specific configuration. On the other hand, the committer peer node does not conduct the endorsement function, but performs transaction validation and manages the distributed ledger.

III. BLOCKCHAIN AND IIOT BASED EDGE COMPUTING FRAMEWORK

Private blockchain-based edge computing systems aim to manage distributed data generated by IIoT devices in a se-

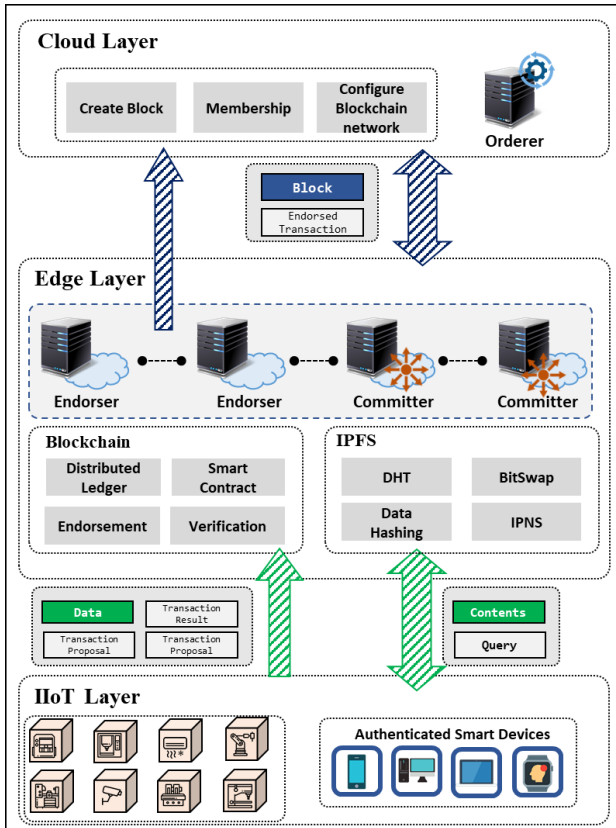


Fig. 1. System architecture

cured way. Although edge computing system offers several advantages over traditional cloud systems, challenges in terms of limited capacity and access to distributed data efficiently need to be resolved yet. In this section, we present our proposed Integration of blockchain and edge computing for IIoT, latency reduction scheme, and IPFS system for accessing the IIoT data. Although some of the existing studies have proposed the combination of blockchain and edge computing into one system [6], they are not suitable for use with private blockchain-based IIoT networks. The nodes in the Hyperledger fabric, which play different roles, generate different kinds of packets, and cause traffic overhead in IIoT network. For example, due to the transaction proposal messages generated by many clients, the delay for other messages transmitted to the orderer, which does not need to receive transaction proposals, increase. In another case, the clients do not need to receive propagated block messages because they do not store ledgers, but in a typical block-chain network, the propagated block message can affect client data transmission. Therefore, it is important to design a network infrastructure that is operationally suitable with Hyperledger Fabric by considering the flow of various packets transmission in the network for efficient transaction processing.

In this paper, we propose a new architecture to manage the IIoT system efficiently and reliably with Hyperledger Fabric platform. The IIoT system with Hyperledger Fabric

is classified into the following three layers: (1) IIoT layer, (2) edge layer, and (3) cloud layer. The IIoT layer consists of blockchain enabled IIoT devices, committers that own a distributed ledger and verify the block, and clients that require application services. The IIoT device or client that generates the transaction proposal transmits the transaction proposal to the peer endorser located at the edge layer or, it can transfer the transaction proposal directly to the cloud layer which manages multi edge layers when the adjacent edge layer is congested.

In addition, since the committer performs relatively simple tasks such as transaction validation and managing ledger of newly created blocks, the low-end performance devices i.e., switches and routers can assume the role of committers in the IIoT blockchain network. The edge layer consists of endorsers and committers, and is physically adjacent to the IIoT devices. Thus, the transaction proposals generated in the IIoT layer are processed in the edge layer by reducing the network load of the cloud layer where orderer exists, and guarantees the transactions to be delivered in the IIoT layer efficiently. In addition, most of the blocks generated by the orderer located in the cloud layer are handled by the edge layer, thus minimizing the number of blocks propagated to the IIoT layer. Therefore, the endorsers located in the edge layer require high-end performance devices and are configured with general server settings to perform complex tasks such as validation, chaincode execution for transactions and managing the distributed ledgers.

IV. CONCLUSION

In this paper, we design a novel architecture to manage the IIoT system efficiently and reliably with Hyperledger Fabric. The proposed system guarantees less traffic overhead than the conventional scheme for IIoT applications.

ACKNOWLEDGMENT

This research was supported by the MSIT(Ministry of Science and ICT), Korea, under the ITRC(Information Technology Research Center) support program(IITP-2022-RS-2022-00156353) supervised by the IITP(Institute for Information & Communications Technology Planning & Evaluation)

REFERENCES

- [1] H. Yao, *et al.*, “Resource Trading in Blockchain-Based Industrial Internet of Things,” *IEEE Trans. Industrial Informatics*, vol. 15, no. 6, Jun. 2019, pp. 3602-3609.
- [2] A. Dorri, *et al.*, “SPB: A Secure Private Blockchain-Based Solution for Distributed Energy Trading,” *IEEE Commun. Mag.*, vol. 57, no. 7, Jul. 2019, pp. 120-126.
- [3] C. Cachin, “Architecture of the Hyperledger Blockchain Fabric,” in *Workshop on Distributed Cryptocurrencies and Consensus Ledgers*, 2016.
- [4] P. Thakkar, S. Nathan, and B. Viswanathan, “Performance Benchmarking and Optimizing Hyperledger Fabric Blockchain Platform,” *IEEE MASCOTS*, 2018
- [5] H. Sukhwani, *et al.*, “Performance Modeling of Hyperledger Fabric (Permissioned Blockchain Network),” *2018 IEEE 17th International Symposium on Network Computing and Applications (NCA)*, 2018, pp. 1-8.
- [6] H. Liu, Y. Zhang, and T. Yang, “Blockchain-Enabled Security in Electric Vehicles Cloud and Edge Computing,” *IEEE Network*, vol. 32, no. 3, May/Jun. 2018, pp. 78-83.

Machine Learning-Based Fault Monitoring on a Digital Twin-Enabled System for Additive Manufacturing

Gabriel Avelino Sampedro*, Made Adi Paramartha Putra†, Syifa Maliah Rachmawati, Dong-Seong Kim, Jae-Min Lee

Department of IT Convergence Engineering, Kumoh National Institute of Technology, Gumi, South Korea

†Informatic Engineering, STMIK Primakara, Denpasar, Indonesia

*Faculty of Information and Communication Studies, University of the Philippines—Open University, Los Baños, Philippines

*Research and Development Center, Philippine Coding Camp, Manila, Philippines

Email: {garsampedro, mdparamartha95, syifamr, dskim, ljmpaul}@kumoh.ac.kr

Abstract—In maritime engineering, the emergence of additive manufacturing technology is starting to change how maintenance and repair work is done. Additive manufacturing is currently being used for fast production to develop tangible representations of objects modeled using computer-aided design (CAD) software. Despite its functionality, using additive manufacturing technology can be tricky, as the process is still subject to unavoidable errors. Errors caused by unfavorable operational conditions can cause a development job to be delayed, thus wasting time and resources. To help optimize environmental and operational conditions, fault monitoring using a digital twin is being developed. The digital twin will replicate the different qualities of its physical counterpart in the digital world. In this research, machine learning algorithms such as multilayer perceptron, long short-term memory, and convolutional neural networks will be explored to predict how the digital twin will behave in various conditions. Overall, LSTM has proven to be the most accurate of the three, and its values do not stray far from its regression line.

Index Terms—additive manufacturing, digital twin, long short-term memory (LSTM), machine learning.

I. INTRODUCTION

Additive manufacturing is an emerging technology that uses basic materials such as plastic, metal, or glass to create actual products layer-by-layer [1], [2]. In the maritime industry, additive manufacturing has been used to develop maritime parts and has been widely adopted. Shipping companies are shifting from ordering parts to developing their parts themselves using 3D printers [3]. The technology has been proven to be more time-efficient and cost-effective. Early adopters of 3D printing technology include major European industry players.

Despite the efficiency of additive manufacturing in the maritime industry, the additive manufacturing process is far from perfect and 3D printers often run into errors. The 3D printing process takes much time and can run from a few hours to even days. Furthermore, 3D printers are often unable to detect errors and the printing process keeps going even if errors occur. Continuous printing may lead to printer damage and output waste. While errors are unavoidable, they can still

be caught early, and the cost of errors can be mitigated [4]. Performing experiments on actual 3D printers may prove both costly and time-consuming. Limited studies have been found to improve the simulation process through a virtual version of the 3D printer. The need to develop a digital twin-enabled monitoring device is established.

To address the growing issue in monitoring 3D printers, a digital-twin enabled system is developed to further understand the behaviour of a 3D printer without having to test on an actual printer. In addition, the system applies machine learning-based algorithms such as long short-term memory and convolutional neural networks to understand what the measurements obtained from the 3D printer's different parts say about the operational condition of the printer.

II. METHODOLOGY

This research focuses on developing a machine learning model to be used on a digital twin for diagnosing the operational conditions of a 3D printer and predicting its future behaviour. The difficulty of a manual process has been identified in various disciplines, specifically engineering. Currently, several proposed solutions explore the application of machine learning algorithms for fault detection using sensor-based and image-based monitoring. Despite the various solutions presented, none use digital twin technology, which is essential in enabling a smart industrial system [5].

Fig. 1 shows the system architecture of the fault monitoring system developed for this research. The research aims to obtain input from the different sensors of a 3D printer to predict future behaviour and to develop a more accurate digital twin of a 3D printer. Within the system, two major processes occur - training and prediction. The significant processes are modeled after three machine learning algorithms - multilayer perceptron, long short-term memory, and convolutional neural networks - long short-term memory. All three machine learning models are tested and compared in terms of performance.

In the training phase of the system, a dataset of historical sensor data is used within the machine learning model. The

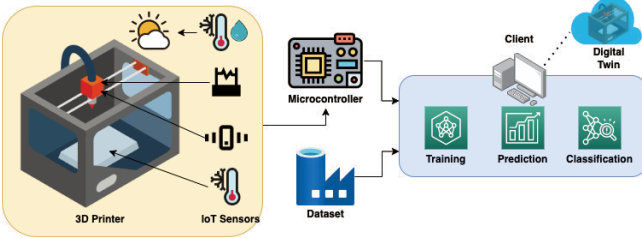


Fig. 1. The conceptual framework of the proposed system shows how machine learning is used to both diagnose and predict future behaviour of a 3D printer.

dataset includes sensor values from the temperature of a 3D printer extruder over 36 hours. The system then extracts features from the collected data and look for specific patterns which can help predict the behaviour of a printer. In addition to the training phase, the prediction of the operational condition of the 3D printer extruder is made using three machine learning-based algorithms.

III. PERFORMANCE EVALUATION

In evaluating the different machine learning models, the different machine learning models are compared with the actual results from actual 3D printing. The results from the test determines which machine learning model is ideal for developing a 3D printer digital twin. The three models are evaluated after a series of preprocessing methods, including removing outliers within the results to optimize the outcome. From there, performance metrics such as the root-mean-square error (RMSE), mean absolute error (MAE), symmetric mean absolute percent error (SMAPE), the coefficient of determination (CD), and the computational time (CT) are evaluated.

After running the models over a period of 100 epochs, fig. 2 illustrates how each model performed. In terms of accuracy, the application of LSTM performed the best with an RMSE of 0.3243, MAE of 0.1514, and a SMAPE of 0.0938. Given that the following error rates are lower than that of MLP and CNN-LSTM, the use of LSTM predicts values that are close to how the printer behaves in the future. As for the coefficient of determination, LSTM also performs better with a higher value than all other models. The high coefficient demonstrates how the values indicate a better fit for the model. The predicted values do not stray from the regression model, and consistency is seen in the results. Despite the better performance of LSTM, a trade-off of the system would be in terms of CT. The use of LSTM is slower than MLP and CNN-LSTM, with a computational time of 1.5109. The slow computational time of LSTM may be attributed to the complexity of the model and its sequential computation.

IV. CONCLUSION

Developing a digital twin-enabled system for testing a 3D printer would mean recreating the system to behave similarly to its physical counterpart. Applying a machine learning-based model for predicting future behaviour is essential for creating an effective digital twin. Based on the various tests conducted

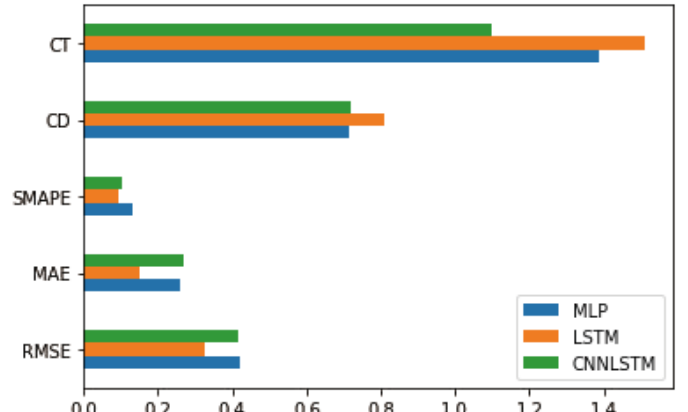


Fig. 2. The performance evaluation of the three different machine learning models are compared in terms of error and processing time.

in evaluating performance, the application of LSTM was observed to be the best fit for the development of the system. LSTM has proven to be more accurate, and its values do not stray far from its regression line. Despite its performance, the trade-off to accuracy would be its computational time.

The next phase of this research would be to try to improve the LSTM model to reduce the computational time while minimizing the accuracy reduction. Furthermore, applying the model to other parts of the 3D printer would help improve the development of the digital twin-enabled system.

ACKNOWLEDGMENT

This work was supported by Priority Research Centers Program through the National Research Foundation of Korea (NRF) funded by the Ministry of Education, Science and Technology (MEST) (2018R1A6A1A03024003). It is also supported by the Ministry of Science and Information and Communication Technology (MSIT), Korea, under the Grand Information Technology Research Center support program(IITP-2022-2020-0-01612) supervised by the Institute for Information & communications Technology Planning & Evaluation (IITP), Korea.

REFERENCES

- [1] G. A. Sampedro, M. A. Paramartha Putra, D.-S. Kim, and J.-M. Lee, “3d printer state prediction: A deep learning model approach,” in *2021 1st International Conference in Information and Computing Research (iCORE)*, 2021, pp. 135–138. [Online]. Available: <https://ieeexplore.ieee.org/document/9681405>
- [2] G. A. R. Sampedro, D. J. S. Agron, G. C. Amaizu, D.-S. Kim, and J.-M. Lee, “Design of an in-process quality monitoring strategy for fdm-type 3d printer using deep learning,” *Applied Sciences*, vol. 12, no. 17, 2022. [Online]. Available: <https://www.mdpi.com/2076-3417/12/17/8753>
- [3] E. Kostidi and N. Nikitakos, “Exploring the potential of 3d printing of the spare parts supply chain in the maritime industry,” in *Safety of Sea Transportation*. CRC Press, 2017, pp. 171–178.
- [4] M. A. P. Putra, D.-S. Kim, and J.-M. Lee, “Adaptive lrfu replacement policy for named data network in industrial iot,” *ICT Express*, vol. 8, no. 2, pp. 258–263, 2022.
- [5] M. P. Ciano, R. Pozzi, T. Rossi, and F. Strozzi, “Digital twin-enabled smart industrial systems: a bibliometric review,” *International journal of computer integrated manufacturing*, vol. 34, no. 7-8, pp. 690–708, 2021.

Toward deeply understanding us in smart home

Taesoo Jun

Department of Computer Software Engineering, Kumoh National Institute of Technology, Korea
taesoo.jun@kumoh.ac.kr

Abstract—This work proposes a home edge system to help understand family members therein. By keeping the user data within the home, recent privacy concerns can be mitigated. System requirements are firstly presented, and software components are followed. The work discusses design points for an edge device at home, leading to remaining works to complete.

I. INTRODUCTION

The recent advance in IT and manufacturing brings cutting-edge technologies into smart devices. While some traditional appliances (e.g., smart fridge) and gadgets (e.g., smart door lock) are upgraded with smart capabilities, new device groups (e.g., smart home hub) are introduced to consumers. We easily buy smart products from a market and use them in our daily lives. As people install large smart consumer devices at home and carry small handheld devices, their residence is equipped with multiple smart devices, being ready to be a smart home.

A typical scenario for a smart home is a home automation [1]; it turns on the lights and plays favorite music when a family member enters the kitchen in the morning. Although such scenarios are popular, more attractive use cases can be imagined. Let's imagine a 30' woman who lives alone in the smart home, and she likes to be neat and clean. Once her patterns are predicted, relevant smart services can be prepared; for example, her smart robot cleaner suggests a cleaning schedule during her working hours, and a smart washing machine proactively tells her the time to buy a detergent.

To support such a smart scenario, residents in the smart home need to be profiled. Understanding family members in the home inevitably requires data about them which is helpful to identify their patterns and inclination. While data could be taken via their direct input, it seems to be annoying to them and fails to succeed to gather. One feasible way to find user's taste is to leave the user's life pattern in logs, collect, and analyze them, resulting in discovering user preferences.

Basically, the user's life log is sensitive and needs to be handled carefully under the user's permission. Some countries impose an obligation to restrict to use of individual's data by law; for example, European countries require companies to obey GDPR (General Data Protection Regulation). Most of the platform players (e.g., Google, Amazon) store user data in their cloud and utilize it for their purposes. In addition, we often listen to news about user information hacking in such companies since they are the main target by hackers. While platform companies keep privacy regulations and maintain the security system, sinking user data in the remote server is supposed to make a potential concern to the data owner [2].

This work describes an edge data platform for home data that infers the family's lifestyle. Firstly, functional requirements are listed, and the corresponding software modules are presented. Then, the design points of the edge platform are discussed and the paper concludes this work with future work.

II. HOME EDGE DATA PLATFORM

This section describes the home edge data platform which gathers home data and discover the insight about the family.

A. Home Edge System Overview

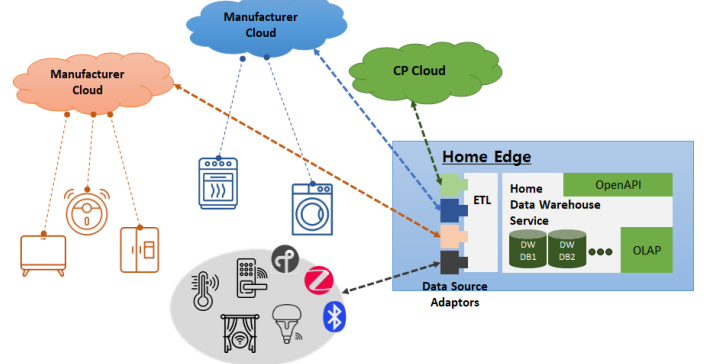


Fig. 1. Home Edge System for Data Platform

Although home data sources are versatile, this work focuses on data from smart devices or gadgets at home. Recent smart devices are on-boarded to specific clouds that the manufacturers guide. On the other hand, some devices are connected to a nearby control hub, using local network protocols such as Zigbee. Fig. 1 shows smart devices at home where smart devices from two vendors are connected to their clouds and smart gadgets that are locally connected to a home edge device. In addition, the home edge data platform is fed from CP (Content Provider) clouds such as weather contents.

In the first step, requirements are considered for the home edge data platform and software components to implement the requirements are depicted.

Major Requirements

- **R1:** Support various data sources: data model, protocol
- **R2:** Store various user data
- **R3:** Maintain data enough to analyze user preference
- **R4:** Report analysis result
- **R5:** Fit for a home edge device with limited resource: computing, storage

To fulfill the above requirements, the home data platform is to be light-weighted. By the way, we have several data platforms for *Big Data* domain, where the platform is designed to handle a huge amount of data. As the data platform in this work manipulates available home data, existing big data platform solutions seem to be good references.

Major Software Components

- **S1:** Data Source Adaptor
- **S2:** ETL (Extract, Transform, Load)
- **S3:** Home Data Warehouse Service: OpenAPI, OLAP (On-Line Analytical Processing), DW DB

The home edge data platform in the work consists of *data source adaptors*, *ETL*, and a *home data warehouse service* which supports OLAP, storage management, and OpenAPI to serve analysis results. The data source adaptors which feed data to the platform are grouped into three: adaptors for vendor clouds, local devices, and external CPs. When owners take a smart device out of the box, they make on-boarding of the device to a cloud by an initial setup guide. Furthermore, it is not allowed to modify device software at will. However, some device vendors serve RESTful OpenAPIs for their smart device [3]. Some vendors don't provide OpenAPI by their policy, but their smart home service works with major platform companies such as Google, which provides OpenAPI for the smart devices instead [4]. A data source adaptor for local devices is to retrieve the device information via local network protocols directly or via hub devices. Lastly, data adaptors toward CP supply information via OpenAPI in CP clouds.

In data engineering, ETL is broadly accepted as a process to put data together from multiple sources. Traditional ETL focuses on adaptation to various bulk data sources whereas ETL in the work considers the operational environment, which requires light-weighted processing. Home Data Warehouse Service provides analysis results of collected home data after it is fed from ETL process. The service implements OLAP engine to handle multiple queries about family characteristics, a storage manager to maintain the limited storage resource in home edge devices, and an API layer to serve analysis reports.

B. Design Considerations

A home edge device where the edge data platform operates might be not as powerful as an edge in MEC (Mobile Edge Computing). With relatively moderate specifications in a home edge device, the following points are considered.

Flexible Architecture: We buy smart home devices from various vendors and connect them via different protocols. Among those devices, internet-capable devices are on-boarding to the corresponding cloud for smart services. Because of multiple manufacturers, home edge devices are to connect to multiple clouds. Due to a recent trend to open IoT platforms, a home edge device can access the device clouds with authorized user accounts. Also, we have locally connected devices that create a network among inter-operable devices. In addition, the home edge acquires useful data from external CP clouds; for example, a home edge device can find temperature within the home from a smart device as well as out of the

home from CP cloud. To leverage various data sources for a home edge, extensible architecture is preferred. In this study, we design data source adaptors that correspond to data sources.

Data Storage: With the total number of IoT messages and connected devices, we can calculate the daily generated device message count on average. The parameters can be collected from a separated L3 router where all smart devices are connected. From a quick case study, smart appliances generated about 360KB per day and smart display devices created about 30KB in case of 3 hours of daily watching [5]. To estimate required data storage, the smart home is supposed to have 8 smart appliances, 2 smart TV, and 10 small things. As for the amount of data from small things, each device is supposed to send 1KB data every hour to the home edge. From the smart home setting, we can get daily data size for the home edge device as 3.2 MB¹. Based on the daily data, the required data storage is calculated².

Security: The home edge approach is motivated by privacy concerns in which personal data is stored in the cloud. To alleviate such concerns, personal data stays within the home. In addition, the home edge device should be able to defend against various internet attacks with a help of security tools such as software firewall, secure connection, and so on.

Operation Policy: As most of the people in the world reside in four seasons climate zone, their life pattern repeats annually. Thus, the home edge device keeps home data for a year; the edge device requires about 1068.5MB. The data should be written in a rolling manner, keeping it for one year.

III. CONCLUSION AND FUTURE WORK

In this work, a home edge design was proposed to enhance family lifestyle understanding and to mitigate privacy concerns. The home edge system was outlined, and major software components were derived from requirements, following design considerations. To complete this work, system is to be integrated, applying with proper open source software. With the home edge system, user studies will be carried out, verifying our approach. As data pipelines are installed within home, we can understand our family lifestyle without privacy concerns.

ACKNOWLEDGMENT

This research was supported by the MSIT(Ministry of Science and ICT), Korea, under the Grand Information Technology Research Center support program(IITP-2022-2020-0-01612) supervised by the IITP(Institute for Information & communications Technology Planning & Evaluation)

REFERENCES

- [1] S. Feng, P. Setoodeh, and S. Haykin, "Smart home: Cognitive interactive people-centric internet of things," *IEEE Communications Magazine*, vol. 55, no. 2, pp. 34–39, 2017.
- [2] H. Lin and N. W. Bergmann, "Iot privacy and security challenges for smart home environments," *Information*, vol. 7, no. 3, p. 44, 2016.
- [3] *SmartThings API (1.0-PREVIEW)*, <https://developer-preview.smartthings.com/docs/api/public>, Jul. 2022.
- [4] *Google HomeGraph API*, <https://developers.google.com/assistant/smarthome/reference/rest>, Jan. 2021.
- [5] *American Time Use Survey*, <https://www.bls.gov/tus>, Jul. 2021.

¹8*360 + 2*30 + 10*24 = 3.2(MB)

²week: 22.3MB, month: 89.0, quarter: 356.2, year: 1068.5

Performance Evaluation of Metaverse Platform to the Type of Game Server Engine

Dongeon Yoon and Hyosang Lee

*Department of Computer Media Engineering
University of Tongmyong
Tongmyong, Busan 48520, Korea
{ehddjs97 & gytkd9575}@naver.com*

Changseop Lim and Amsuk Oh

*Department of Digital Media Engineering
University of Tongmyong
Tongmyong, Busan 48520, Korea
dlckdtjq123@naver.com, asoh@tu.ac.kr*

Abstract—In this paper, when implementing a video conferencing platform and applying a game server engine to it, we experiment with how different latency is depending on the number of concurrent connectors. As a result, the Amazon Game Lift (AWS) engine showed the best performance with a delay time of 22.146 msec. This experiment will help each individual choose a game server when implementing a metaverse platform.

Keywords—, Latency, Metaverse, Game Server Engine, Platform

I. INTRODUCTION

Recently, as digital transformation accelerates throughout society, metaverse is drawing attention. Companies such as Roblox, Microsoft, and Meta are launching and competing on multiple platforms[1], affecting the economy, culture, education, and financial industries as a whole. Due to this influence, there is also a aspect in which individuals create their own metaverse platforms[2]. When creating a metaverse platform, the game production engine that will make avatars or objects is important, but the server of games that help multi-communication is also important. However, since it is very difficult for an individual to implement a server, several engines that support the game server must be utilized. Therefore, in this paper, we implement a demo-level platform and evaluate communication performance by applying various game server engines. The type of platform implemented is video conferencing that requires a quick response[3].

II. IMPLEMENTATION OF A VIDEOCONFERENCE PLATFORM

First, in this paper, a metaverse platform to be applied to a game server is implemented. The proposed platform is divided into hardware and software areas. VR HMD (Virtual Reality Head Mounted Display) is a VR headset and controller that can be used without a PC for interaction implementation, and uses Oculus Quest 2. A Unity game production engine was used to develop the virtual conference platform, and a Magica Voxel design tool was used to create 3D avatars or objects. Table 1 briefly shows the development environment of the video conferencing platform. Fig. 1 shows the use of the implemented platform.

TABLE I.
DEVELOPMENT ENVIRONMENT FOR VIDEO CONFERENCING PLATFORMS

Field	Area	Name	Development Purpose
Hardware	VR HMD	Oculus Quest 2	Core equipment for interaction implementation with a PC-free VR

This research was supported by the MISP(Ministry of Science, ICT & Future Planning), Korea, under the National Program for Excellence in SW supervised by the IITP(Institute for Information & communications Technology Promotion)(2018-0-018740301001).

			headset released by Facebook
Software	Metaverse Development Platform	Oculus Rift	Running Oculus and Configuring Devices
		Oculus Integration	Integrate Unity with Oculus Hardware
		Unity	Video conferencing platform design and implementation
	3D Design Tools	MagicaVoxel	Create 2D/3D voxel objects (avatar, desk, chair, screen, etc.) for content offer

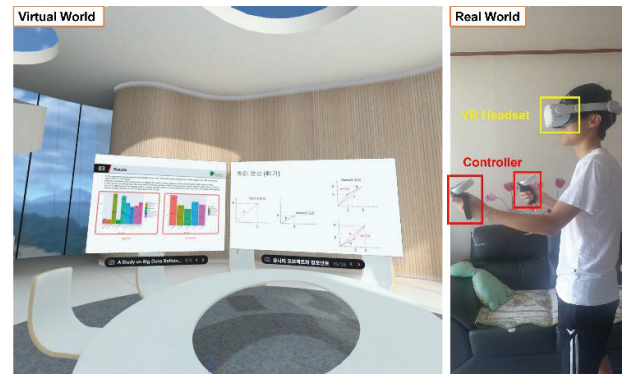


Fig. 1. Running Scenes for Virtual Video Conferencing Platforms

III. PERFORMANCE EVALUATION BY GAME SERVER ENGINE TYPE

In this paper, the difference in access speed according to the number of simultaneous users is measured based on the performance evaluation of the game server engine. In order to give the same conditions, a server connection was attempted from a laptop with a CPU of Ryzen 7-5800H, a GPU of RTX 3060 and a RAM of 32GB. Table 2 shows the specifications of the notebook used for the same experimental conditions.

TABLE II.
NOTEBOOK SPECIFICATIONS FOR SERVER PERFORMANCE ASSESSMENT

Notebook Name	CPU	GPU	RAM	STORAGE
Gigabyte A7 K1 R7	Ryzen 7-5800H(4.4 GHz)	RTX 3060(6GB, GDDR 6)	DDR4 32GB	SSD 1TB

A. Game Server Engine Type

The game server engine for latency measurement was selected based on Supported Languages, Supported Server,

TABLE III.
GAME SERVER ENGINE COMPARISON

Field	Amazon GameLift(AWS)	Monobit Engine	Photon Server(Photon Cloud)
Development Company	Amazon(USA)	Monobit Engine(Japan)	Exitgames(Germany)
Explanation	Management services for deploying, operating, and expanding multiplayer gaming-only gaming servers	Communication middleware and comprehensive server packages	Game Server Engine Helps Multi-Communication
Supported Languages	C++, C#	C++, C#, JavaScript	C++, C#
Supported Server	Windows Server, Amazon Linux	Linux Server(Redhat, CentOS)	Windows Server
Client	-	Windows, iOS, MacOS	Windows, iOS, Android, Steam, XBOX, PS
Supported Game Engine	Unity, Unreal Engine, Cocos2d-x	Unity, Unreal Engine	Unity, Unreal Engine, Corona Labs
Supported DB	MySQL(AuroraDB), DynamoDB(NoSQL)	MySQL	MongoDB, Redis
Features	<ul style="list-style-type: none"> - Support for a diversity of service catalogs - GameLift : Server Infrastructure Management AutoScaling - Player matchmaking - Real-time Monitoring Dashboard - Deploys gaming sessions in the cloud and expands to support a growing player base 	<ul style="list-style-type: none"> - UDP, TCP, and RUDP protocol support - Custom matching lobby and high-speed relay server capabilities - Ideal for implementing small P2P online games and large VR games - Cloud Package Support 	<ul style="list-style-type: none"> - Ready-to-use without server deployment and operations - Provide a cloud environment that is easy to deploy and operate servers - Dedicated servers and custom code plug-ins (Cloud) - Support for UDP, TCP, HTTP, and WebSocket network transport protocols
Weakness	<ul style="list-style-type: none"> - Cost increase as many users grow 	<ul style="list-style-type: none"> - Difficult to use for large projects - Lack of language support 	-

Supported Game Engine, Supported DB, and cloud support. Table 3 is a comparison table of game server engines.

B. Experimental Results

As a result of performance measurements by game engine, there were two simultaneous connectors and the delay time when using Amazon GameLift (AWS) was the shortest at 22.146 msec. On the other hand, there were 10 concurrent connectors and the latency when using the Monobit Engine was the longest at 27.007 msec.

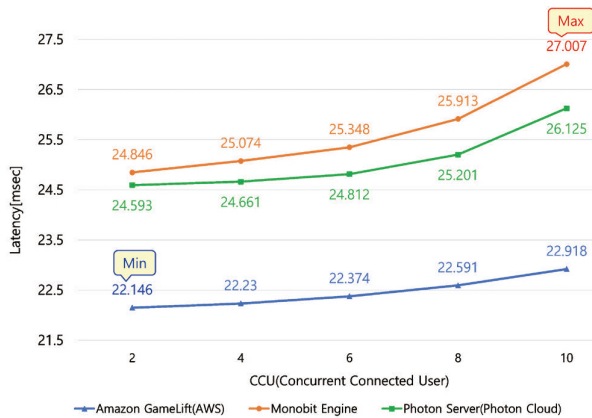


Fig. 2. Latency Measurement Result of Game Server Engine by Number of Concurrent Connected User

IV. CONCLUSION

Due to high entry barriers, the number of individual developers is increasing as metaverse, which was mainly developed by companies, has become a trend due to the development of technology. However, since it is difficult for individuals to implement a game server engine, they wanted to find a game server with optimal latency. First, three servers with many users were selected based on supported languages, supported server, supported game engine, supported DB, and cloud support. The experiment was conducted with the laptop's specification set to be the same, showing the fastest speed when using the Amazon GameLift (AWS) engine with two simultaneous connectors. This study is expected to help platforms that require real-time communication, such as video conferencing platforms.

ACKNOWLEDGMENT

This research was supported by the MISP(Ministry of Science, ICT & Future Planning), Korea, under the National Program for Excellence in SW) supervised by the IITP(Institute for Information & communications Technology Promotion)(2018-0-018740301001).

REFERENCES

- [1] H. Y. Han, "A Study on Typology of Virtual World and its Development in Metaverse" Journal of Digital Contents Society," vol. 9, no. 2, 2008, pp. 317-323.
- [2] S. H. Yoon, "A Case Study On Learning Game Using An Unity Engine" Korean Society of Computer Information, 2016, pp. 327-330.
- [3] Y. K. Bae, "A Study on an Educational Using Plan of Augmented Reality and 3D Technology" Proceedings of the Korea Contents Association Conference, 2011, pp. 365-366.

Lightweight Anomaly Detection based on Embedded A.I. for Early Failure Detection of Industrial Robots

1st Hyuntae Cho
dept. of Digital Media Engineering
Tongmyong University
Busan, South Korea
ORCID 0000-0002-8951-0239

2nd Wooseok Byun
dept. of Electrical Engineering
KAIST
Daejeon, South Korea
ORCID 0000-0002-2720-3102

Abstract—Robots are being used as innovative tools to replace human labor, and the application field of robots is rapidly expanding along with artificial intelligence technology in the era of the Fourth Industrial Revolution. Among them, industrial robots are used in most industrial fields; the automobile, electric and electronic industries are the largest consumers. There have been many attempts to diagnose robot failures, but most of the sensor data is extracted from robots and algorithms or machine learning for diagnosis are being carried out on remote servers or clouds. In this case, accurate diagnosis is difficult when communication costs increase excessively and communication is not smooth. In this paper, we propose an embedded DS-CNN-based lightweight artificial intelligence technology that runs on an embedded system mounted on an industrial robot. In addition, we compare and analyze the performance of high-performance algorithms performed in the server by verifying the proposed method on an actual embedded board.

Keywords—anomaly, fault, DS-CNN, robot, embedded. Deep learning

I. LIGHTWEIGHT ANOMALY DETECTION SYSTEM BASED ON EMBEDDED A.I.

The proposed lightweight anomaly detection aims to operate on ARM Cortex-M4/M7 systems for lightweight embedded systems. In this paper, Depthwise Separable CNN (DS-CNN)^[1] is adopted to operate on the target MCU. The Mel Frequency Cepstral Coefficient (MFCC) function of the measured sound data is applied to input data of the deep neural network. The hidden layer of the proposed DS-CNN consists of six layers, one CNN layer and five DS-CNNs, as shown in Figure 1. Each layer of DS-CNN consists of a series of depthwise convolution, batch normalization/ReLU, pointwise convolution, and batch normalization/ReLU activation function. Finally, the output layer has an average polling layer. A key feature of the proposed method is the use of 8-bit weights and activations instead of floating-point-based weights and activations used on general purpose PCs or servers for high-performance machine learning. We converted the trained model to TensorFlow Lite and encoded the model on the target MCU. Since the proposed method adopts 8-bit weighting and activation, the accuracy of anomaly detection is low. So we added an additional method to measure the data and predicts the anomaly multiple times. If the predicted anomaly result exceeds 75% of the total prediction, the

system is true positive (defect). Otherwise, it is in a normal condition.

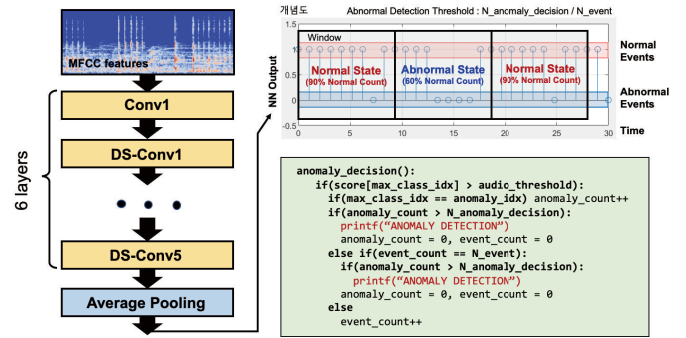


Fig. 1. Conceptual overview of the proposed system.

II. PERFORMANCE EVALUATION AND CONCLUSION

The dataset used for learning is Malfunctioning Industrial Machine Investigation and Inspection (MIMII)^[2], which includes four types of sound data for valves, pumps, fans, and slide rails. This paper only uses slides rail data because it is widely used for industrial robots. The slides rail dataset consists of 26.7 hours of normal data and 7.4 hours of abnormal data. 77% of the total data was used for the training data and 23% was used as the testing data. When floating-point-based weights and activation functions were used in the PC environment, anomaly event classification performance was 95.7% while performance was 80.85% when operation was performed using 8 bits-based weighting and activation functions on the Cortex-M7 MCU. In order to improve performance, we had a set of 60 predictions and votes were conducted. If 60 consecutive predictions are made and 45 are abnormal, it is judged as a true abnormality and a problem occurs in the robot. In this case, performance improved by up to 95%.

REFERENCES

- [1] Y. Zhang, N. Suda, L. Lai, V. Chandra, “Hello edge: Keyword spotting on microcontrollers,” *arXiv preprint arXiv:1711.07128*, 2017.
- [2] H. Purohit, R. Tanabe, K. Ichige, T. Endo, Y. Nikaido, K. Suefusa, Y. Kawaguchi, “MIMII Dataset: Sound dataset for malfunctioning industrial machine investigation and inspection,” *arXiv preprint arXiv:1909.09347*.

Coding Rate Adjustment of Underwater Optical Wireless Communication based on Deep Reinforcement Learning

Huicheol Shin
KIOST
South Korea
shc0305@kiost.ac.kr

Yujae Song
Kumoh National Institute of Technology
South Korea
songyj@kumoh.ac.kr

Yongjae Kim
KIOST
South Korea
yongjaekim@kiost.ac.kr

Abstract—In this work, we analyze the underwater environmental factors that determine the quality of underwater channel when constructing an underwater optical wireless communication (UOWC) link between an underwater sensor node located on the seabed and the unmanned surface vehicle (USV) located on the sea surface. Furthermore, to improve communication performance, we implement a reinforcement learning algorithm that learns optimal coding rate that satisfy the minimum required symbol error rate (SER) using environmental sensor information attached to USV.

Index Terms—Reinforcement learning, underwater optical wireless communication, modulation coding scheme, repetition code

I. INTRODUCTION

Recently, underwater optical radio communication (UOWC) has attracted much attention as a powerful solution for many applications such as underwater data sensing, collecting and processing due to advantages such as high transmission speed, very wide bandwidth, and low latency. However, due to harsh underwater conditions (turbidity, turbulence, temperature, etc.), UOWC faces challenges such as absorption, scattering and attenuation. consequently, these underwater characteristics cause deterioration of UOWC performance, such as reduced transmission distance and increased error rate, thereby degrading the reliability of the network. In order to overcome these challenges, many researchers have recently conducted research such as applying various wavelengths or adjust the modulation coding scheme (MCS) level. [1]–[4]

In this paper, we analyze the performance of optical communication according to irregularly changing attenuation characteristics in an underwater environment and implements a reinforcement learning algorithm to select the optimal coding rate that can satisfy both channel quality and data transmission efficiency required by UOWC network.

II. SYSTEM MODEL

Fig. 1 shows a system model in which underwater wireless optical communication (UOWC) is performed considered in this study. First, the unmanned surface vehicle (USV), which is a receive node for acquiring data, receives the location information of the underwater sensor (transmit node) and then

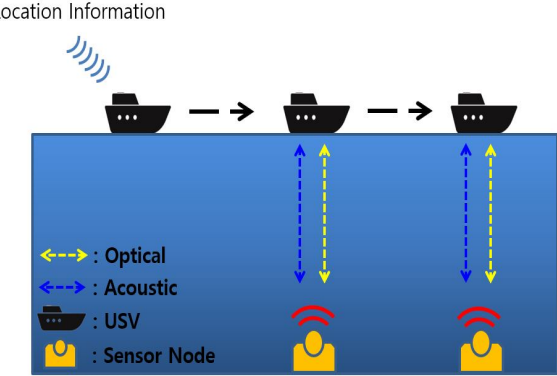


Fig. 1. UOWC system model

moves to the point where underwater sensor is installed using the global positioning system (GPS) information. Thereafter, the USV transmits an acoustic signal to form a laser based UOWC link and performs initial synchronization between the USV and the underwater sensor. The reason why acoustic communication is considered in this process is that unlike optical communication, which is sensitive to misalignment due to its strong straightness, although the transmission rate is slow, the acoustic communication has high reliability due to its wide transmission range and long distance. Subsequently, when the link configuration is completed, USV analyzes the channel quality based on information from the attached environmental sensors. In addition, reinforcement learning is performed based on the sensing data to select the optimal coding rate that can satisfy the required performance and request the underwater sensor to transmit the data to the corresponding MCS level. [5]

To analyze the channel quality of the configured UOWC link, the intensity of the received optical signal is required. The optical signal transmitted through the underwater channel can be calculated by the following equation. [6]

$$P_R = P_T \frac{A_r}{4\pi d^2} e^{-c(\lambda)d}, \quad (1)$$

where P_T is the intensity of the optical signal transmitted

by the sensor node, A_r is aperture size of receive node, d is distance of the UOWC link and $c(\lambda)$ is attenuation coefficient according to wavelength λ .

The received optical signal is converted into an optical current by a photo-diode of an optical modem mounted on the USV. Photo-diodes include PIN photo-diode, avalanche photo-diode (APD), silicon photo-multiplier (SiPM) and in this work, we consider the photo current converted using SiPM, which has a large gain due to its high sensitivity. Accordingly, the photo current converted into SiPM can be represented by the following equation:

$$I_P = \frac{P_R E G q}{h c / \lambda}, \quad (2)$$

where E is the photo detection efficiency (PDE), G is the gain of SiPM, q is the electric charge, h is Planck constant and c is the light speed. Subsequently, when the photo current is obtained, the signal-to-noise ratio (SNR) of the received signal can be calculated as follow:

$$SNR = \frac{I_P}{\sqrt{2qFBG(I_P + (2I_D + I_B))}}, \quad (3)$$

where F is the noise figure, B is the bandwidth, I_D is the dark current noise and I_B is the background noise current. As a result, Bit error rate (BER) of the UOWC link can be calculated based on derived SNR, and the BER is determined differently depending on the modulation technique. In this study, BER using pulse position modulation (PPM) is considered, and the corresponding equation is as follows:

$$BER_{M-PPM} = \frac{1}{2} \operatorname{erfc} \left(\frac{1}{2\sqrt{2}} \sqrt{SNR \frac{M}{2} \log_2 M} \right), \quad (4)$$

When BER is obtained, error probability can be reduced by applying an error correction code (ECC) and the n-bit signal to which ECC is applied is called a symbol. Meanwhile, the symbol error rate (SER) is calculated differently according to the ECC scheme, and the repetition code is considered to measure the performance of UOWC link.

III. SIMULATION

As shown in Fig 2, we analyze the change in BER according to the turbidity, which is one of the environmental factors that determine the channel quality of UOWC link. As a result, it can be confirmed that the higher turbidity causes the rapid increase in the BER of UOWC link. Therefore, we implement reinforcement learning algorithm that selects the optimal coding rate to reduce the error rate.

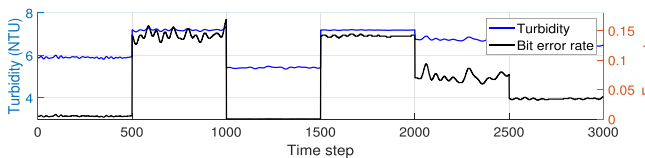


Fig. 2. BER variation according to turbidity

The proposed reinforcement model not only adjusts the coding rate to satisfy the minimum SER required by the UOWC link using the turbidity information and error information in the previous time step, but also minimizes the repetition of bit to ensure efficient use of data capacity.

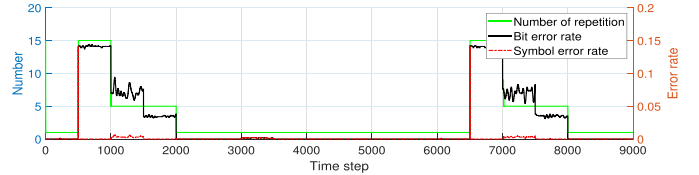


Fig. 3. SER variation according to turbidity

Fig 3 shows the performance result of the proposed reinforcement learning algorithm. It can be confirmed that the repetition code is appropriately adjusted and SER is maintained in order to reduce the BER determined by the turbidity change to the required performance ($SER_{req} = 0.01$).

IV. CONCLUSION

In this work, the channel quality of UOWC link is analyzed based on turbidity data, which is underwater environment information, and reinforcement learning algorithm is implemented to reduce error rate by adopting a repetition code. As a result, it was confirmed that the proposed reinforcement learning model satisfies SER_{req} by finding the optimal coding rate. In the future, based on the corresponding learning result, the channel quality using more environmental information (i.e., temperature, illuminance and water depth) will be analyzed and the simulation will be performed by adopting several ECC schemes.

ACKNOWLEDGMENT

This research was a part of the project titled 'Development of Polar Region Communication Technology and Equipment for Internet of Extreme Things (IoET),' funded by the Ministry of Science and ICT (MSIT)

REFERENCES

- [1] N. Saeed, A. Celik, T.Y. Al-Naffouri and M. Alouini, "Underwater optical wireless communications, networking, and localization: A survey," *Ad Hoc Networks*, vol.94, pp.1-34, 2019.
- [2] H. Kaushal and G. Kaddoum, "Underwater optical wireless communication," *IEEE Access*, vol.4, pp.1518-1547, 2016.
- [3] Y. Song, "Underwater acoustic sensor networks with cost efficiency for Internet of Underwater Things," *IEEE Trans. Ind. Electron.*, vol.68, pp.1707-1716, 2021.
- [4] M. A. Ali, "comparison of modulation techniques for underwater optical wireless communication employing APD receivers," *Research Journal of Applied Sciences, Engineering and Technology*, vol.6, pp.707-715, 2015.
- [5] J. Jeong, S.H. Lim, Y. Song and S.W. Jeon, "Online learning for joint beam tracking and pattern optimization in massive MIMO systems," *IEEE INFOCOM 2020*, pp.764-773, 2020.
- [6] A. Celik et al., "End-to-end performance analysis of underwater optical wireless relaying and routing techniques under location uncertainty," *IEEE Trans. Wirel. Commun.*, vol.19, pp.1167-1181, 2020.

Anti-biofouling for Seawater Battery Systems

Juhyun Kim
Maritime ICT R&D Center
KIOST
Busan, Korea
jhk@kiost.ac.kr

Ahyun Park
R&D Center,
Marine Equipment Technology Solutions
Busan, Korea
ahpark14@gmail.com

Seungjae Baek
Maritime ICT R&D Center
KIOST
Busan, Korea
baeksj@kiost.ac.kr

Yoonchil Kim
Maritime ICT R&D Center
KIOST
Busan, Korea
yckim@kiost.ac.kr

Sungmin Koo
Maritime ICT R&D Center
KIOST
Busan, Korea
smkoo@kiost.ac.kr

Saat Mubarrok
Mulawarman University
Kalimantan Timur, Indonesia
mubarrok@fmipa.unmul.ac.id

Abstract—In this paper, we present two anti-biofouling techniques to efficiently reduce attachment organisms. Specifically, we introduced an electric shock and an UV-C LED devices for seawater battery, and then we analyzed the effectiveness of the techniques by applying them to an actual seawater battery system. A long-term real-sea experimental results showed that both techniques can be a good remedy while UV-C LED showed a better electric power efficiency.

Keywords—sea-water battery, anti-biofouling, electric shock, UV-C

I. INTRODUCTION

In maritime environment, a stable electric power supply is an essential element for the reliable operation of equipments and infrastructures. Especially for a battery-driven system, there are a wide variety of types of batteries: lithium ions (Li-Ion), lithium-polymers (Li-Po), nickel cadmium (Ni-Cd), nickel hydrogen (Ni-Mh), and lead-acid (SLA)[1, 2]. However, all the existing batteries are not designed for the maritime environment, but supposed to be used for the general land condition. Therefore, a corrosion or a breakage of a battery is unavoidable when it is exposed to seawater and in that case, there is a possibility of environmental pollution due to a leakage. Recently, the world's first rechargeable seawater battery, secondary battery that uses seawater as a cathode, are introduced[3, 4, 5, 6]. Simply, seawater battery charges and discharges electrical energy using sodium ions in seawater. Therefore, compared with the conventional batteries, seawater battery can provide same power with twice capacity or can reduce battery system's physical dimension by half. Furthermore, performance degradation caused by repeated charging and discharging is not occur. However, seawater battery is suffered from the biofouling hazards as it exposed to seawater for a long time. Therefore, in this paper, we present two anti-biofouling techniques to efficiently reduce attachment organisms. Specifically, we introduced an electric shock and an UV-C LED devices for seawater battery, and then we analyzed the effectiveness of the techniques by applying them to an actual seawater battery system. A long-term real-sea experimental results showed that both techniques can be a good remedy while UV-C LED showed a better electric power efficiency.

II. ATTACHMENT ORGANISMS REDUCTION TECHNOLOGY

In this paper, an electric shock device and an UV-C LED were installed in the seawater battery system to control attachment organisms. The attachment removal technology using electrical energy has been verified by various environments such as a nuclear power plant intake and so on. In this study, it is designed to minimize power consumption by periodically applying electric shocks. An electric shock is applied by setting a current of up to 400 V and 10 A at an interval of 20 to 255 seconds (Fig. 1). Meanwhile, five UV-C LEDs with sterilization effects were attached to the bottom of the pressure-resistant can of the seawater battery system (Fig. 2). Light having a wavelength of 278 nm is irradiated with a 10 W output, and the irradiation period is configurable.



Fig. 1. Anti-biofouling device(Electric shock device)

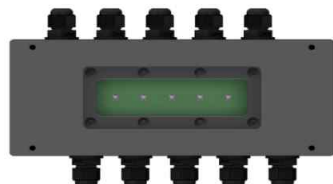


Fig. 2. Anti-biofouling device(UV-C LED)

To verify the performance of the proposed technique, the system and control group to which the proposed technique was applied were installed in the waters of the Namhae Research Institute of the Korea Maritime Science and Technology Institute for two months (Fig. 3, 4).



Fig. 3. Experimental setup(Electric shock experiment)

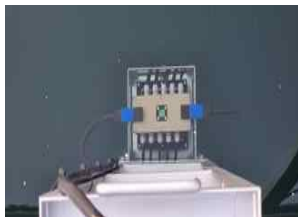


Fig. 4. Experimental setup(Sea-water battery module without UV-C LED)

III. EXPERIMENTAL RESULTS AND CONSIDERATIONS

The results of the electric shock experiment are shown in (Fig. 5, 6). Fifteen days after the start of the experiment, mud was attached to both cell surfaces, and after summer, the cell surface was covered with a large amount of *Serpuia vermicularis*, and over time, seaweeds were occupied by the bryozoa. Comparing Fig. 5 and Fig. 6, it can be confirmed that the electric shock technique showed some effect on reducing the attachment organism, but complete control is impossible.



Fig. 5. Experimental results with electric shock

(Cell condition after 60 days real sea experiment without electric shock)



Fig. 6. Experimental results with electric shock

(Cell condition after 60 days real sea experiment with electric shock)

The results of the UV-C LED experiment are shown in (Fig. 7, 8) As shown in Fig. 7, the seawater battery module without UV-C LED cannot be operated because the attachment covers the entire module and cell surface after 60 days, whereas the module with UV-C LED as shown in Fig. 8 has a small amount of attachment, enabling stable

operation. In addition, an experiment was conducted to adjust the irradiation position and voltage to analyze the suitable illuminance of the UV-C LED. As a result, when irradiating UV-C LEDs with high voltage at a distance of 5cm, it was analyzed that the control effect was the best.



Fig. 7. Experimental results with UV-C

(Module condition after 60 days real sea experiment without UV-C LED)



Fig. 8. Experimental results with UV-C

(Module condition after 60 days real sea experiment with UV-C LED)

ACKNOWLEDGMENT

This work was supported by the Korea Institute of Energy Technology Evaluation and Planning(KETEP) grant funded by the Korea government(MOTIE) (20215610100030, Development and Demonstration of Seawater Secondary Battery Module over 1kWh for Marine Equipment)

REFERENCES

- [1] Helmut Weiss, "Large lithium-ion battery-powered electric vehicles — From idea to reality", 2018 ELEKTRO,2018, pp. 1-5
- [2] Abla Khiareddine, "Techno-economic analysis of the lithium-ion and lead-acid battery in Photovoltaic pumping system", 2019 19th International Conference on Sciences and Techniques of Automatic Control and Computer Engineering (STA), pp. 417-422, 2019
- [3] Kim, Youngjin et al., "High-Capacity Anode Materials for Sodium-Ion Batteries", Chemistry A European Journal 20(38), 11980-11992, (2014).
- [4] Kim, Jae-Kwang et al., "Rechargeable Seawater Battery and Its Electrochemical Mechanism.", ChemElectroChem 2.3 328-332, (2015).
- [5] S. Koo et al., "Sea-water Battery for Maritime Applications", Global Oceans 2020: Singapore – U.S. Gulf Coast, pp. 1-4, Oct. 2020.
- [6] Soedibyo, "Particle swarm optimization based maximum power point tracking for seawater battery application", 2018 IEEE International Conference on Innovative Research and Development (ICIRD), pp. 1-6, 20

Research on the development of Unmanned Boat Applying Sea-water Battery for Observation and Detection

Juhyun Kim

Maritime ICT R&D Center

Korea Institute of Ocean Science &
Technology
Busan, Korea
jhk@kiost.ac.kr

Hyoun Kang

Maritime ICT R&D Center

Korea Institute of Ocean Science &
Technology
Busan, Korea
hkang@kiost.ac.kr

Jaeho Choi

Maritime ICT R&D Center

Korea Institute of Ocean Science &
Technology
Busan, Korea
jaeho@kiost.ac.kr

Sangwoo Kang

Maritime ICT R&D Center

Korea Institute of Ocean Science &
Technology
Busan, Korea
tkddn2845@kiost.ac.kr

Dayu Wiyati Purnaningtyas

Bandung Institute of Technology

Jawa Barat, Indonesia

dayu.purnaningtyas@oceanography.itb.a
c.id

Keywords—Sea-water Battery, USV, Unmanned Surface Vehicle, marine power supply specialized, underwater

Abstract— In this paper developed an unmanned surface vehicle(USV) for observation and detection using sea-water batteries. Existing batteries cause damage and environmental pollution when exposed to seawater, while sea-water batteries are a stable new concept of power supply for seawater flooding for a long time. An USV has mainly used lithium-based batteries as a battery-powered unmanned marine vehicle but the demand for a source of electrical power for stable operation in poor marine environments is increasing. Accordingly, this paper developed an USV with sea-water batteries. Through verification of the real sea, it was confirmed that the USV can be stably operated in the seawater environment, and that it is possible to operate the sonar, the mission module of the USV.

I. INTRODUCTION

The battery used in existing marine devices uses lithium-based or lead-acid batteries, which cause various safety problems such as short use time, damage due to flooding, environmental pollution due to leakage of harmful substances and so on. The Unmanned Surface Vehicle(USV) is an unmanned underwater system developed to conduct underwater exploration and monitoring, and collect marine environmental data. It is generally operated by applying a lithium-based battery. The need for alternative source of electrical power for stable operation in poor marine environments is increasing. This paper develops an USV of a source of electrical power system equipped with a sea-water battery to solve the existing problems. It is possible to dramatically increase the operating time of the USV by applying a stable sea-water battery to seawater immersion.

II. SEA WATER BATTERIES

A. Composition of Sea-water Battery

As shown in Figs. 1 and 2, in the sea-water battery, a lithium-based battery cell and a battery management system (BMS) module for managing the lithium-based battery cell are protected through a water tight housing. The sea-water battery cell used in this paper was 8Wh (2.8 V, 3Ah), size is 160×181×230 (mm), weight is 0.95 kg, and a unit module is 144Wh (12V, 12Ah), 444×167×205 (mm), and weighs is 18 kg.

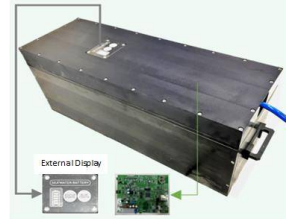
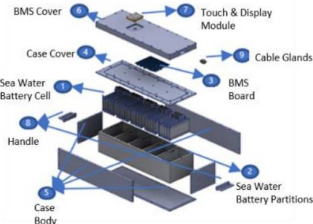


Fig. 1. Sea water battery module



[Fig 2] Sea water battery module details

B. Sea-water Batteries Management System

The sea-water battery has a built-in BMS that specializes in the marine environment for the stable operation of the system. The main functions of BMS are shown in Figure 3.



- A) Battery Monitoring
 - Monitoring charging/discharging conditions and internal temperature and humidity
 - Monitor voltage current between pack and each cell
 - Monitor battery charging and functional status
- B) Battery Protection
 - Overcharge-Overdischarge protection (17.7 V overcharge protection, 10.0 V overdischarge protection)
 - Over-current protection (over 1A)
 - Short circuit protection
- C) Cell Balancing
 - Apply a passive method that discharges the cells with the highest voltage to the lowest current
- D) User Interface
 - Support RS-485, CAN, Bluetooth
 - Check SoC via external display module

Fig. 3. Sea water battery management system

III. USV(UNMANNED SURFACE VEHICLE)

The USV is an unmanned underwater system developed to conduct underwater exploration and monitoring, and collect

marine environmental data. The USV to be developed in this paper provides image storage data and water depth data using a sound speed measuring device, a HD Camera, and a multi-beam, and the specific specifications are as shown in Table 1.

TABLE I.

General specification	
Weight	20kg
Speed	Under 10kn
Size	170 X 88 X 38
Shipping Time	5 hours for 4 batteries/ 25,000mah
Survey Accuracy	RTK ±2cm
Carry	Portable
The lay of the land	Complex terrain navigable
Mountable Sensor	Single beam, ADP multi beam, water quality measurement sensor, etc



Fig. 4. USV (Unmanned Surface Vehicle)

IV. LOCATION AND TEST SCENARIOS

The real sea verification experiment was conducted on a beach located in Dongsam-dong, Yeongdo-gu, Busan.

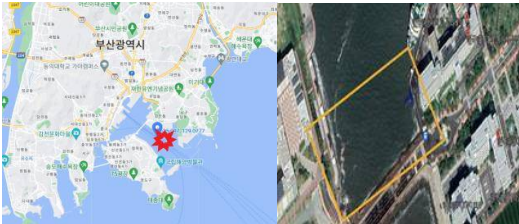


Fig. 5. Experimental location (Yeongdo-gu, Busan)

The sea-water battery were connected to conduct a driving test of multi-beam and communication equipment. As a result of the test, the driving time of the multi-beam and communication equipment without movement of the hull was about 2 hours/test up to the operation from about 10m away from the test bed was possible. The system stability test was performed together by comparing the hull transmission, the motor, the current flow method, the battery operating time measurement, and the posture values (Role, Pitch, Yaw).



Fig. 6. Hull Drive Test

After the stability test of the equipment, an empirical test was conducted to confirm operating time, wave resistance, low temperature resistance, maximum mission distance,

maximum speed measurement, and other operational specifications in the marine environment.

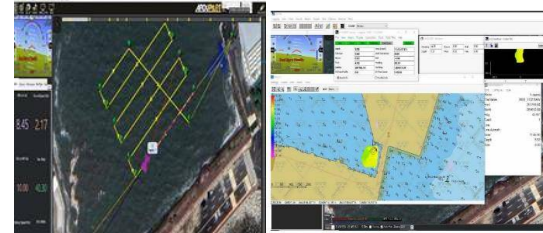


Fig. 7. The Moving Path of Unmanned Surface Vehicle Using

Fig. 8. Acquisition of water depth data using multi-beam

A schematic diagram was created that visualizes a method of exploring the seabed topography through a multi-beam acoustic surveyor mounted on an unmanned surface vehicle along the set route. It is possible to check the water depth by location for each route that the USV moved, and water depth data was calculated using calibration to calculate various data results such as 3D data and grid depth through tidal correction, sound velocity measurement, and false data correction.



Fig. 9. 3D depth data from USV

ACKNOWLEDGMENT

This work was supported by the Korea Institute of Energy Technology Evaluation and Planning(KETEP) grant funded by the Korea government(MOTIE) (20215610100030, Development and Demonstration of Seawater Secondary Battery Module over 1kWh for Marine Equipment)

REFERENCES

- [1] Frölicher, T.L., Fischer, E.M., and Gruber, N., "Marine heatwaves under global warming," *Nature* 560, 360–364, Aug. 2018, DOI: <https://doi.org/10.1038/s41586-018-0383-9>
- [2] Block, B. A., Dewar, H., Farwell, C., and Prince, E. D., "A new satellite technology for tracking the movements of Atlantic bluefin tuna", *Proceedings of the National Academy of Sciences*, 95(16), 9384–9389, Sep. 1998. DOI: <https://doi.org/10.1073/pnas.95.16.9384>
- [3] Kim, Hyojin et al., "Metal-free hybrid seawater fuel cell with an ether-based electrolyte", *Journal of Materials Chemistry A*, 2(46) 10584–10588. Dec. 2014. DOI: <https://doi.org/10.1039/C4TA04937C>
- [4] Bae, H. S., Kim, W.-J., Kim, W.-S., Choi, S.-M., & Ahn, J.-H. (2015, August 5). Development of the SONAR System for an Unmanned Surface Vehicle. *Journal of the Korea Institute of Military Science and Technology*. The Korea Institute of Military Science and Technology. <https://doi.org/10.9766/kimst.2015.18.4.358>
- [5] Ko, S.-H., Kim, D.-H., & Kim, J.-Y. (2013, September 30). Implementation and field test for autonomous navigation of manta UUV. *Journal of the Korean Society of Marine Engineering. Journal of Advanced Marine Engineering and Technology*. <https://doi.org/10.5916/jkosme.2013.37.6.644>

KIO-Gaon: a modular designed Remotely Operated Vehicle for versatile operations

Sungmin Koo
Maritime ICT R&D Center
Korea Institute of Ocean Science & Technology
Busan, Korea
smkoo@kiost.ac.kr

Juhyun Kim
Maritime ICT R&D Center
Korea Institute of Ocean Science & Technology
Busan, Korea
jhk@kiost.ac.kr

Yazid Ridla
Oceanovision
Jawa Barat, Indonesia
yazid.ridla@gmail.com

Seungjae Baek
Maritime ICT R&D Center
Korea Institute of Ocean Science & Technology
Busan, Korea
baeksj@kiost.ac.kr

Abstract—A remotely operated underwater vehicle, commonly called ROV, is an unmanned underwater vehicle operated by an aboard crew via a tethered cable [1]. An ROV is widely used in surveys, science expeditions/inspections, constructions, and military use due to its advantages such as long working time, endurance in deep sea, and elimination of life risking hazards [2]. Generally, an ROV system is divided into three parts: ROV's main body, a ground control system (GCS) for conveying the user's input and for displaying the data gathered by the ROV, and a cable that links the two parts for power supply and communication. A prevalent portion of the ROVs main body is made up of a buoyant material to adjust buoyancy of the body, multiple thrusters for a maneuverability, a variety of sensors and tools that each suit a particular task, a couple of pressure-resistant watertight canisters in which all the non-waterproof devices, such as a controller, are enclosed. All the mentioned components are put together in the main frame. To increase the odds of a successful mission in harsh offshore environments, it would be reasonable to design a ROV specifically tailored to a task. However, this type of design philosophy makes it difficult to expand or modify the ROV to other tasks. For example, it would be difficult (or in some cases impossible) to add more sensors, manipulators, or more canisters. The problem can be moderated by careful design considerations, but the limited number of pre-designed extra auxiliary ports and space could eventually fall short. In this paper, we present a ROV designed with a modular architecture that enables versatile modifications. In particular, we build on a common interface concept for designing the ROV. Any canister with the common interface can be connected or disconnected in a daisy chain manner. Specifically, a canister in the proposed modular architecture follows the rules specified below. First, each canister has ethernet IN/OUT and power IN/OUT ports. Second, each canister has additional I/O ports as required. Third, any canister designed by the above two principles can be connected or disconnected to/from the chain. Thus, whatever devices that are required, the ROV can be easily expanded by connecting additional canisters with the appropriate ports for the devices. As shown in Fig. 1, we adapt a picatinny rail system into the main frame for dynamically changing the ROV structure. For example, canisters can be placed anywhere in the system to meet the requirements as shown in Fig. 2. When the canister structure is changed, it is required to adjust the buoyancy of the ROVs main body. To make adjustment procedure simple, we employ modularized buoyancy materials. In short, an ordinary single piece buoyancy material is

finely chopped into a uniform size and is attached or detached as required as shown in Fig. 3. As shown in Fig. 4, we build the proposed ROV, called KIO-Gaon which means 'KIOST mid-class ROV'. The detailed specifications is summarized in Table 1. We demonstrate the successful operations of the proposed design by conducting field tests in open seas in Korea as shown in Fig. 5.

Keywords—ROV, modular, design, versatility, expandability

REFERENCES

- [1] B. H. Robison, "Midwater research methods with MBARI's ROV," Marine Technology Society Journal, 26(4), Jan., 1993.
- [2] H. G. Greene, D. S. Stakes, D. L. Orange, J. P. Barry, and B. H. Robison, "Application of a remotely operated vehicle in geologic mapping of Monterey Bay, California, USA," in proceedings of the America Academy of Underwater Sciences, 1993.

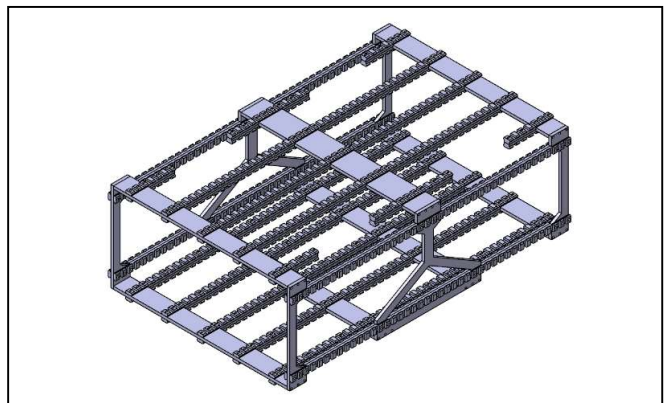


Fig. 1. A rail system based main frame

This work was supported by research grants from Korea Institute of Ocean Science and Technology (PF631910), and "Base research for building a wide integrated surveillance system of marine territory" funded by the Ministry of Oceans and Fisheries (MOF).

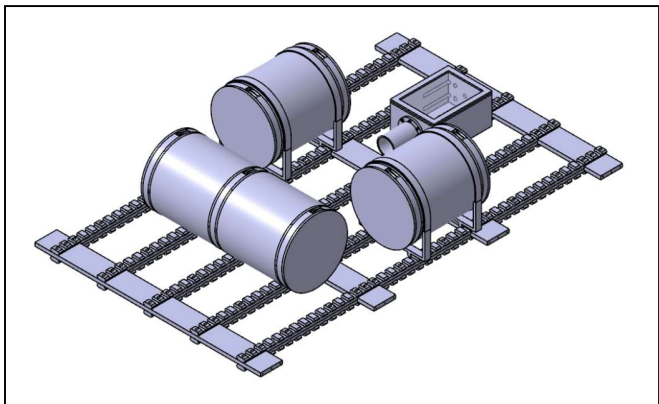


Fig. 2. Canisters placement

TABLE. 1. SPECIFICATIONS

Max' depth	300m
Max' speed	2knots(protected)
L x H x W	1.2m x 0.8m x 0.6m
Launch weight	121kg
Input power	300VDC, 20A
Sensors	Depth, temperature, altimeter, AHRS, DVL, USBL, 1 HD and 5 SD cameras, Sonar

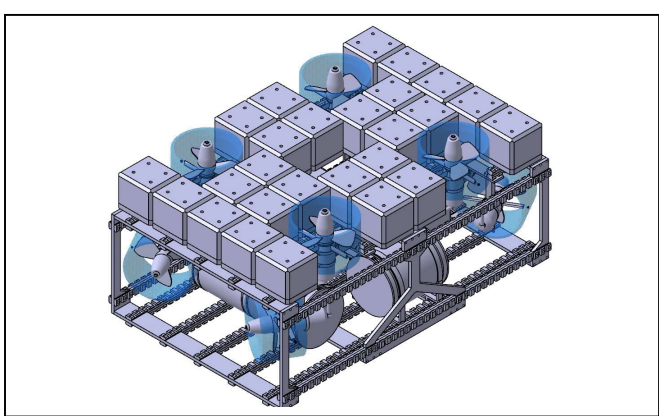


Fig. 3. Design of the ROVs main body

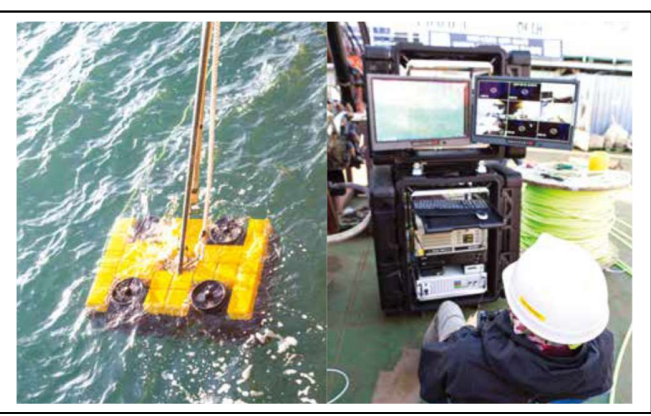


Fig. 5. Field test in Korea

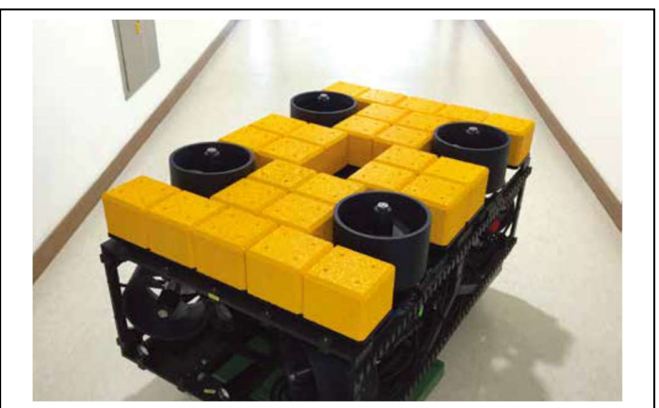


Fig. 4. Implemented ROV (KIO-Gaon)

Improved Efficiency of Small Wind Turbine using Vertical Dual Axis

*Note: Sub-titles are not captured in Xplore and should not be used

Ah Hyun Park
R&D Center
Marine Equipment Technology Solutions
Busan, Republic of Korea
ahpark14@gmail.com

Hyoun Kang
Maritime ICT R&D Center
Korea Institute of Ocean Science and Technology
Busan, Republic of Korea
hkang@kiost.ac.kr

Yong Soo Kang
R&D Center
Dual Wind
Ulsan, Republic of Korea
suto3525@naver.com

Seungjae Baek
Maritime ICT R&D Center
Korea Institute of Ocean Science and Technology
Busan, Republic of Korea
baeksj@kiost.ac.kr

Faizal Ade R. Abdullah
Bandung Institute of Technology
far.abdullah@itb.ac.id

Abstract—In this work, we develop a high-power vertical dual small wind turbine that can be used for power supply of various devices. Existing wind turbines require a strong wind speed to obtain an effective electric power. However, by adopting a coreless-vertical axis structure, a high-power generation efficiency can be achieved at a relatively weak wind speed. In addition, it is possible to improve wind power generation efficiency by up to 150% compared to the existing turbine at general urban wind speeds by developing a vertical dual axis technology to be less affected by wind direction, and upper and lower separated fan structure.

Keywords—small wind turbine, wind power generation efficiency, vertical dual axis

I. INTRODUCTION

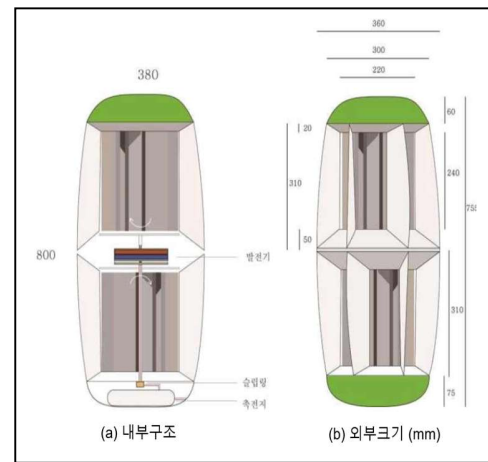
Recently, the new renewable energy has been highlighted due to the exhaustion of fossil fuels and the increase in demand for eco-friendly energy. In particular, wind power generation is the most competitive energy among the renewable energy sources because the power generation efficiency is close to the power generation unit cost of fossil fuels or natural gas. Therefore, researches and developments of wind power generation are actively in progress due to its excellent economic feasibility. Since a large-scale wind power turbine was commercialized in the early 2000s, the improved performance of wind power turbine has been achieved by continuous research developments [1-3]. However, the large wind power turbine is limited due to various problems such as installation conditions, high investment cost, noise/vibration, environmental damage, and maintenance. In addition, it is difficult to secure high-quality usable wind speeds, limiting the installation of a large wind power turbine. Therefore, the small wind power turbines have been actively studied in recent years [4-6]. The small wind power turbine has the various advantages such as relatively low installation costs, maintenance ease, and low noise.

In this work, we develop a 10W-30W class small wind power turbine that can efficiently generate electric power even with low wind speeds. For efficient power generation at low wind speeds, we use axial-flux permanent magnet (AFPM) structure [7-9] that are advantageous for cooling and

miniaturization. The AFPM-type wind power turbine has a simple structure due to direct drive system, and has high energy conversion efficiency caused by a low change in power. In addition, the structure development of vertically arranged fans based on the coreless-type AFPM turbine, which is easy to generate electric energy at low wind speeds, improve wind power generation efficiency. The proposed dual small wind power turbine in this work was actually developed using 3D printing and computer numerical control (CNC) process, and it was confirmed that wind power generation efficiency dramatically improved compared to the existing turbine through performance evaluation experiments.

II. DESIGN AND FABRICATION PROCESS

In order to improve the efficiency of small wind power turbine, in this work, a vertical dual small wind power turbine based on a coreless-type AFPM was designed and fabricated. To overcome the limitation of existing small wind power turbine with weak output power, the vertical dual axis [10,11] technology was applied. As shown in Fig. 1, upper and lower separated fans are designed to rotate in the reverse direction, and each wing is specifically devised for improving generation efficiency.



Identify applicable funding agency here. If none, delete this text box.

Fig. 1. Design of (a) internal structure and (b) external size for vertical dual small wind power turbine.

The vertical dual small wind power turbine designed in this work was fabricated through the following process. First, the outer blade, inner blade, upper and lower plate parts are manufactured using 3D printing and CNC process. Thereafter, the main body and upper and lower plate parts of the turbine are painted, and the turbine part and the main body are assembled. Finally, after connecting the turbine circuit and manufacturing the printed circuit board, the turbine drive and the main body are assembled to complete the fabrication of the vertical dual small wind power turbine.

III. RESULTS AND DISCUSSION

The vertical dual small wind power turbine was completed as shown in Fig. 2(a). The principle of power generation is that the two turbines receive wind from any directions, causing the upper and lower magnet blades to rotate in different directions. Therefore, it can secure twice RPM as fast as existing wind turbines, resulting in three times the voltage (V), twice the current (A) are generated to produce more than four times the power (W).

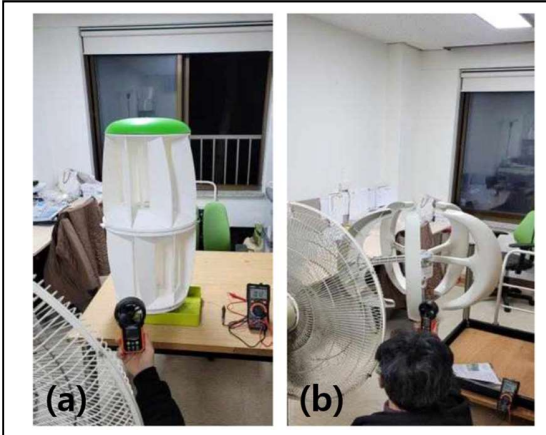


Fig. 2. Wind volume test of (a) small wind power turbine using vertical dual axis and (b) existing small wind power turbine.

To evaluate the performance of wind power generation, the vertical dual small wind power turbine and the existing wind power turbine carried out the wind volume test, respectively. Fig. 3 shows a graph of voltage (V) according to wind speed (m/s) at a current of 200 mA for comparison of wind power generation. As a result, it is confirmed that the wind power generation efficiency of the vertical dual small wind power turbine in general urban wind speeds range of 1 m/s to 5 m/s is improved by 30% to 150% compared to the existing wind power turbine.

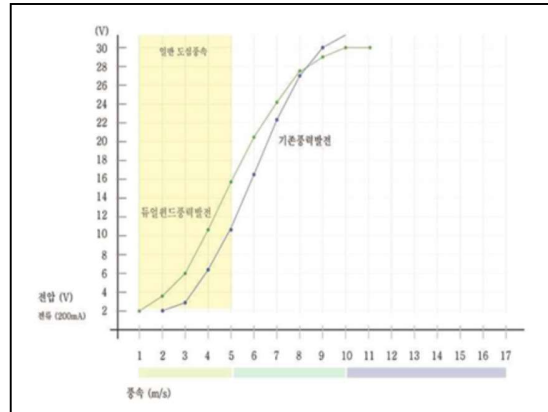


Fig. 3. Generation quantity graph of dual small wind power turbine compared to existing wind power turbine.

IV. CONCLUSION

In summary, we have developed a high-power coreless-type vertical dual small wind power turbine. To overcome the limitation of the existing small wind power turbine with weak output power, a vertical structured fans structure were designed by applying the vertical dual axis technology. The power generation efficiency of vertical dual small wind power turbine is significantly improved in comparison with the existing wind power turbine. In the future, the vertical dual small wind power turbine will be applied to various applications such as streetlight, marine equipment, and power supply of island area, and also expanded to household generator to secure new market.

ACKNOWLEDGMENT

This work was supported by the Korea Institute of Energy Technology Evaluation and Planning (KETEP) grant funded by the Korea government (MOTIE) (20215610100030, Development and Demonstration of Seawater Secondary Battery Module over 1kWh for Marine Equipment)

REFERENCES

- [1] Y. Kumar, j. Ringenberg, S. S. Depuru, V. K. Devabhaktuni, J. W. Lee, E. Nikolaidis, B. Andersen, A. Afjeh, "Wind energy: Trends and enabling technologies", Renewable and Sustainable Energy Reviews, vol. 53, pp. 209-224, September 2015.
- [2] G. M. J. Herbert, S. Iniyam, E. Sreevalsan, S. Rajapandian, "A review of wind energy technologies", Renewable and Sustainable Energy Reviews, vol. 11, pp. 1117-1145, November 2005.
- [3] X. Yin, W. Zhang, X. Zhao, "Current status and future prospects of continuously variable speed wind turbines: A systematic review", Mechanical Systems and Signal Processing, vol. 120, pp. 326-340, October 2018.
- [4] A. Rosenberg, S. Selvaraj, A. Sharma, "A novel dual-rotor turbine for increased wind energy capture", Journal of Physics: Conference Series, vol. 524, pp. 012078-012088, June 2014.
- [5] P. D. Clausen, D. H. Wood, "Recent advances in small wind turbine technology", Wind Engineering, vol. 24, pp. 189-201, May 2000.
- [6] O. Ozgener, "A small wind turbine system (SWTS) application and its performance analysis", Energy Conversion and Management, vol. 47, pp. 1326-1337, October 2005.
- [7] D.-W. Chung, Y.-M. You, "Design and performance analysis of coreless axial-flux permanent-magnet generator for small wind turbines", Journal of Magnetics, vol. 19(3), pp. 273-281, September 2014.

- [8] B. J. Chalmers, W. Wu, "An axial flux permanent magnet generator for a gearless wind energy system", IEEE Transactions on Energy Conversion, vol. 14, pp. 251-257, June 1999.
- [9] T.-U. Jung, J.-S. Cho, "Electromagnetic structural design analysis and performance improvement of AFPM generator for small wind turbine", Journal of Magnetics, vol. 16, pp. 374-378, December 2011.
- [10] T. S. No, J.-3. Kim, J. H. Moon, S. J. Kim, "Modeling, control, and simulation of dual rotor wind turbine generator system", Renewable Energy, vol. 32, pp. 2124-2132, October 2009.
- [11] R. Howell, N. Qin, J. Edwards, N. Durrani, "Wind tunnel and numerical study of a small vertical axis wind turbine", Renewable Energy, vol. 35, pp. 412-422, February 2010.

A Brief Survey of Massive MIMO SWIPT-Enabled IoT Network

Hyunwoo Jung

Department of information and communication technology
Korea Institute Ocean Science and Technology
Busan, Korea
hyunwoo@kiost.ac.kr

Yongjae Kim

Department of information and communication technology
Korea Institute Ocean Science and Technology
Busan, Korea
yongjaekim@kiost.ac.kr

Abstract—A massive multiple-input-multiple-output (MIMO) simultaneous wireless information and power transfer (SWIPT)-enabled system is newly proposed for the internet-of-things (IoT) network. This paper presents a brief introduction to massive MIMO SWIPT-enabled IoT networks and describes related works.

Index Terms—massive MIMO, SWIPT, IoT network

I. INTRODUCTION

IoT refers to a communications network made up of vast amounts of sensors, software, and user devices that share information and coordinate decision-making through connections over the Internet. With the realization of IoT networks, the Internet will become truly ubiquitous. The main problem of IoT network is the limited battery life of devices which significantly restrict the performance of the communication system.

SWIPT is a strong candidate to overcome the aforementioned problem with the capability to prolong the lifetimes of wireless devices. One of the challenges of the SWIPT technique is the large propagation path loss. This will even intensify in the network using millimeter waves for information carriers. One feasible solution to that is the massive MIMO SWIPT-enabled system, a newly proposed idea for future wireless communication. Massive MIMO is a technique that adopts numerous amount of antennas in a base station to provide extremely sharp beams and deliver communication service to a numerous number of users at the same frequency and time resource. Massive MIMO SWIPT-enabled systems can further enhance the spectral and energy efficiency of IoT networks. Since studies summarizing the research work on massive MIMO SWIPT-enabled IoT networks have not been published to date, this paper presents a brief introduction to massive MIMO SWIPT-enabled IoT networks and describes related works.

II. MASSIVE MIMO SWIPT-ENABLED IOT NETWORK

A massive MIMO SWIPT-enabled system is expected to be a viable candidate to be applied in IoT networks which will solve the limited battery resource problem so that the overall network efficiency and reliability will be even more ameliorated.

In [1], a massive MIMO two-way relaying system with SWIPT in IoT networks taking into account power splitting SWIPT scheme and large-scale fading channels is proposed. Two classical and linear relay precoding, i.e., zero-forcing reception/zero-forcing transmission and maximum ratio combining/maximum-ratio transmission are adopted to satisfy the requirements of high rate in the relay system. [2] proposes a SWIPT-enhanced framework for a cell-free massive MIMO scheme capable of servicing both energy harvesting mobile stations and conventional mobile stations. Spatially correlated Rician fading channels and the use of different precoding schemes that are based on different channel estimators differing on the assumed knowledge of the line-of-sight components are considered. [3] proposes a mixed timescale online stochastic successive convex approximation algorithm to solve joint beamforming and power splitting optimization problem in a downlink massive MIMO SWIPT IoT network.

III. CONCLUSION

In this paper, a newly suggested massive MIMO SWIPT-enabled IoT network research concept and its related research work is introduced. We will continue to strive to expand the scope of research on massive MIMO and SWIPT-enabled IoT networks.

ACKNOWLEDGMENT

This research was a part of the project titled ‘Development of Polar Region Communication Technology and Equipment for Internet of Extreme Things (IoET),’ funded by the Ministry of Science and ICT (MSIT)

REFERENCES

- [1] J. Wang, G. Wang, B. Li, H. Yang, Y. Hu and A. Schmeink, “Massive MIMO Two-Way Relaying Systems With SWIPT in IoT Networks,” *IEEE Internet Things J.*, vol. 8, no. 20, pp. 15126-15139, Oct. 2021, doi: 10.1109/JIOT.2020.3032446.
- [2] G. Femenias, J. Garcia-Morales and F. Riera-Palou, “SWIPT-Enhanced Cell-Free Massive MIMO Networks,” *IEEE Trans. Commun.*, vol. 69, no. 8, pp. 5593-5607, Aug. 2021, doi: 10.1109/TCOMM.2021.3083644.
- [3] X. Chen, H. V. Cheng, A. Liu, K. Shen and M. -J. Zhao, “Mixed-Timescale Beamforming and Power Splitting for Massive MIMO Aided SWIPT IoT Network,” *IEEE Wireless Commun. Lett.*, vol. 9, no. 1, pp. 78-82, Jan. 2020, doi: 10.1109/LWC.2019.2942314.

Non-negative Matrix Factorization based Optimization Algorithm for Face Age Prediction

Man Zhang

Dept. Computer & Media Engineering
The Graduate School, Tongmyong University
Busan, Republic of Korea
mandyz0216@gmail.com

Dong Myung Lee

Dept. of Computer Engineering
Tongmyong University
Busan, Republic of Korea
dmlee@tu.ac.kr

Abstract—In this paper, the non-negative matrix factorization (NMF) based optimization algorithm is suggested. The optimization algorithm is used to reduce the dimension of the face feature matrix to obtain the characteristic face, and support vector machines (SVM) is used to train and classify the reduced dimension matrix. This paper aims to estimate the age of face images using the proposed algorithm. Currently, this paper has only progressed to algorithm design, and performance experiments are scheduled to be carried out according to dataset construction and performance metrics soon.

Keywords—face age prediction, negative matrix factorization, K-L divergence, SVM classifier

I. INTRODUCTION

With the progress and development of the times, artificial intelligence technology has developed by leaps and bounds. In this paper, a non-negative matrix factorization (NMF) optimization algorithm is proposed for improving the accuracy of age prediction based on face images.

The traditional NMF uses Euclidean distance and KL divergence to calculate the minimum target distance for minimizing the error of decomposition. Current face recognition-based research methods largely include the following two research ideas. One is a method of recognizing faces by taking a picture of a face based on full face recognition and the other is a feature-based face recognition method.

II. PROPOSED OPTIMIZATION ALGORITHM

NMF dimensionality reduction method can fix the number of features after dimensionality reduction according to needs, greatly reducing image redundant information, and will bring better results in downstream tasks. Firstly, the target image is divided into four parts, and then the features are extracted by using the improved non-negative matrix decomposition. In order to speed up the convergence of non-negative matrix factorization, we only keep non-negative constraints, use the steepest descent method to solve, and add regular term constraints to improve the computational efficiency of the algorithm.

The steps of proposed optimization are as follows:

- A. Initialize random matrix W and matrix H .
- B. Set the upper limit of iteration times and error threshold.
- C. According to H_{kj}^{t+1} and W_{ik}^{t+1} iterate matrices h and W , and end the iteration when the number of iterations reaches the upper limit or the error is less than the threshold.

D. After the iteration, the required matrices W and h can be obtained.

III. FUTURE PROGRESS OF THIS STUDIES

A. Dataset

According to the quantity distribution of each age group, the age span of the data set used in this paper is from 21 to 50 years old, because there is a small amount of data from 1-20 years old and 51-100 years old. The images in the dataset are 128×128 pixels in size.

B. Experimental Environment

The experiment is based on Windows, using PyCharm editor and Python programming to complete the compilation of all codes.

C. Experimental Processes

- 1) Read image data
- 2) Image output quartering
- 3) Use the improved NMF to reduce the dimension of each piece of data
- 4) Each image exhibit and combine four images
- 5) Construct training data and labels
- 6) Split training set and test set
- 7) Support vector machines (SVM) classification
- 8) Call model test results

D. Metrics for Experimentation

The mean absolute error (MAE) and R^2 (R-Square) determination coefficient were used for the evaluation index.

1) MAE is the average value of absolute error, which can better reflect the actual situation of the predicted value Error.

2) R^2 : A measure of the fit of a model.

$$R^2 = 1 - \frac{\sum_i (\hat{y}_i - y_i)^2}{\sum_i (\bar{y}_i - y_i)^2} \quad (1)$$

Where: y_i is the true value, \hat{y}_i is the predicted value. \bar{y}_i is the mean of the true value. The higher the R^2 value, the higher the accuracy of the prediction model.

ACKNOWLEDGMENTS

This research was supported by the BB21plus funded by Busan Metropolitan City and Busan Institute for Talent & Lifelong Education (BIT).

This research was supported by the MISP (Ministry of Science, ICT & Future Planning), Korea, under the National Program for Excellence in SW) supervised by the IITP (Institute for Information & Communications Technology Promotion) (2018-0-018740301001).

UAV-Assisted Real-Time Monitoring and Detection of Maritime Infrastructure Defects

Min Hyuk Kim, Kwonsoon Yong, Abdallah Khreishah*, Sung-Hoon Lim, Wonjong Noh

Division of Software, College of Information and Science, Hallym University

Chuncheon 24252, Republic of Korea

{mhkim1401, ksyong1401}@gmail.com, {shlim, wonjong.noh}@hallym.ac.kr

**Department of Electrical and Computer Engineering, New Jersey Institute of Technology*

Newark, New Jersey 07102 USA

abdallah@njit.edu

Abstract—In this study, we design a UAV-assisted computing platform model that enables real-time monitoring and detection of marine infrastructure defects. As a core algorithm, we propose low-complexity convolutional neural network (CNN) and U-Net structures that identify whether given images have problems and accurately segment the location of the problem. By conducting experiments, we prove the concept of the proposed systems. This study helps to safely check defects in maritime infrastructure at any time and prevent accidents, without human intervention.

Index Terms—Light-weight CNN and U-Net, low communication and computation overhead, marine infrastructure, UAV-assisted classification and segmentation

I. INTRODUCTION

Owing to natural or environmental factors, marine infrastructures are aging rapidly. To maintain the function of aging marine structures and extend their lifespan, continuously and efficiently inspecting and diagnosing these structures is necessary. However, the existing infrastructure inspection methods which mostly rely on human operations, require considerable amount of time, are expensive, and have long inspection cycles. In addition, there are high risk of accidents and most systems require the use of additional facilities. To overcome these limitations and enforce preventive maintenance by performing more efficient facility inspection and diagnosis, recently, facility inspection and diagnosis equipment that use the fourth industrial revolution technologies such as drones, artificial intelligence (AI), and Internet of Things (IoT) have been developed. In particular, the detection of cracks in infrastructures using unmanned aerial vehicles (UAVs) or mobile robots are currently in the conceptualization and commercialization process [1], [2]. Motivated by this trend, our study aims to develop an infrastructure defect detection solution using deep learning-based real-time image processing and mobile technology.

II. SYSTEM MODEL

Figure 1 shows the proposed system structure for monitoring and detecting marine infrastructure defects through real-

This work was supported by the National Research Foundation of Korea (NRF) grant funded by the Korean Government (Ministry of Science and ICT) under Grant 2020R1F1A1069119.

time image processing and mobile technology based on deep learning. The main functions of the proposed system are as follows.

- 1) Aerial vehicles collect image information on maritime structures, run cooperative deep learning algorithms, and then provide an objective diagnosis of the condition of the structure.
- 2) Image analysis and diagnosis in aerial vehicles can be performed in real time.
- 3) The aerial vehicles provide objective diagnostic information to ground mobile robots cooperating with various base stations on the ground.
- 4) The information exchange between aerial vehicles, ground mobile robots, and networks have low communication overhead through efficient data transmission methods.

In particular, in this study, basic concepts were designed and verified for 1) and 2) of the system.

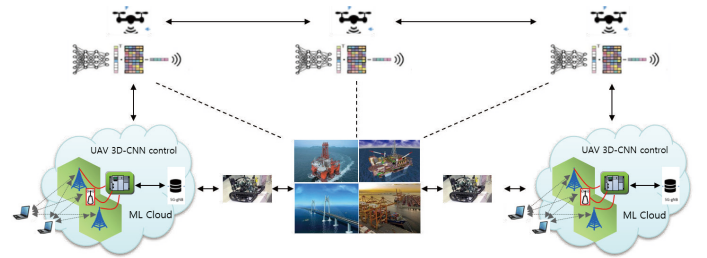


Figure 1. System model: UAV-assisted monitoring and crack detection.

III. PROPOSED CRACK DETECTION ALGORITHM

A. Classification

When an image taken by a UAV is received, for efficient crack detection, 1) gray scaling is applied to each image to reduce computation overhead, and 2) the gray scaled input image is divided into sub-images of size 128×128 pixels. These pre-processing steps help real-time performance by reducing the computation complexity of the machine learning model. The proposed low-complexity CNN model that classifies whether input sub-images have cracks is shown in Fig. 2. This model

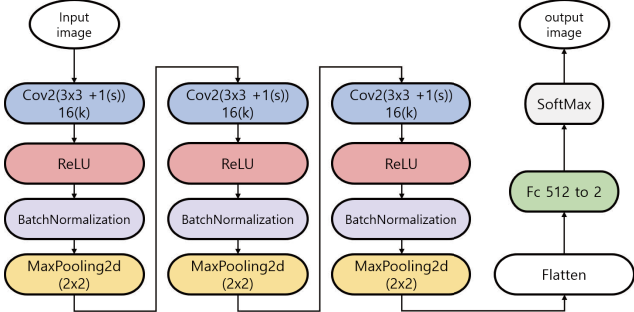


Figure 2. 2D/3D-CNN based crack detection model.

shows sufficient performance using the Kaggle dataset as training data. To generalize the performance for crack variations that may exist in aged structures, we augmented the data using deep convolutional generative adversarial networks (DCGAN). Cracks were detected with a probability of 98.17%.

B. Segmentation

For each sub-image that have been determined to have cracks, pixel-level crack segmentation is performed to further pin-point the cracks. Figure 3 shows a simplified U-Net model for real-time crack segmentation.

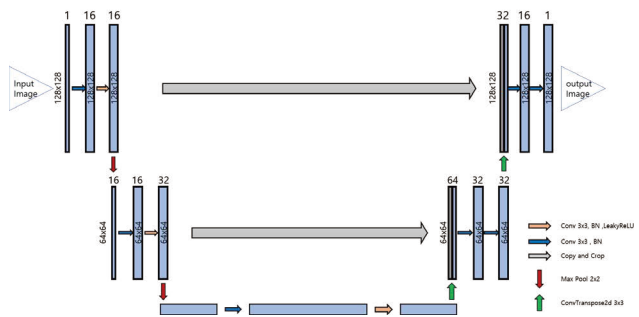


Figure 3. Low-dimensional U-Net architecture.

IV. EVALUATION

In Fig. 4, (a) shows the image acquisition process using a UAV, and (b) shows an acquired target image for crack detection. In (c), the image of (b) is divided into small pieces, and, in (d), all sub-images with cracks are identified by the proposed CNN module. Finally, (e) shows the crack segmentation result from the crack images using the proposed U-Net module.

V. CONCLUSION AND FUTURE WORKS

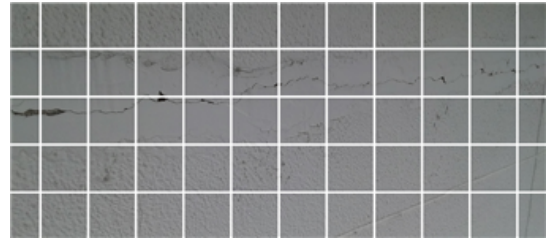
In this study, we designed a system for the real-time monitoring and detection of defects in maritime infrastructure using UAVs. To detect defects in real time and accurately segment the location of the defects, we presented low-complexity CNN and U-Net structures as core parts of the proposed system. Through real implementations and experiments, we presented its proof-of-concept, and confirmed its operations and performance. As future work, we plan to develop cooperative



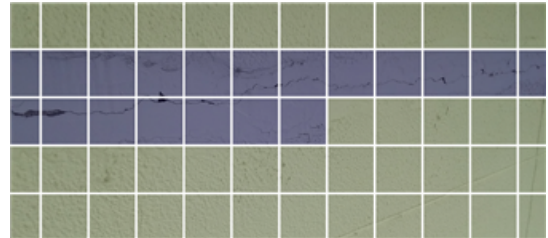
(a) Image acquisition by UAV.



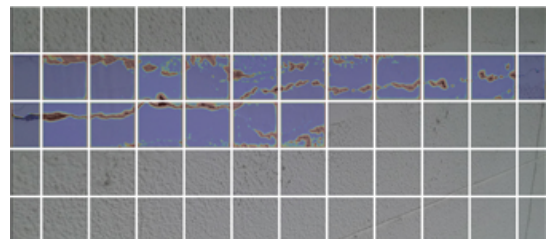
(b) Target crack image.



(c) Fragmented crack image.



(d) Classification of sub-images with cracks.



(e) Crack segmentation.

Figure 4. Crack detection and segmentation example.

machine-learning algorithms between multiple UAVs, as well as communication-efficient information exchange methods.

REFERENCES

- [1] Xiong Peng, Xinguo Zhong, Chao Zhao, Anhua Chen, Tianyu Zhang, 'A UAV-based machine vision method for bridge crack recognition and width quantification through hybrid feature learning,' *Construction and Building Materials*, Vol. 299, 2021,
- [2] Ayele, Yonas Zewdu and Aliyari, Mostafa and Griffiths, David and Drogue, Enrique Lopez, 'Automatic Crack Segmentation for UAV-Assisted Bridge Inspection,' *Energies*, Vol. 13, No. 23, 2020

Self-Supervised MIMO System for Autonomous Underwater Navigation Operations

Simeon Okechukwu Ajakwe, Vivian U. Ihekonye, Dong-Seong Kim, Jae Min Lee

Department of IT Convergence Engineering, Kumoh National Institute of Technology, Gumi, South Korea

(simeonajlove, ihekonyevivian)@gmail.com,(dskim, ljmpaul)@kumoh.ac.kr

Abstract—The need for a cyber-edge and cognitive artificial intelligence (AI)-based security strategy to boost autonomous underwater navigation and prevent heterogeneous attacks from pirates is imperative in maritime operations. This paper proposes a split of super-resolution (SR) to reconstruct the channel state information (CSI) through self-supervised learning for a multiple-input-multiple-output (MIMO) system. Compared with the existing system, a split of SR into two disjoint sub-blocks through transfer learning is used to improve the CSI detailed structures in the reconstruction process. The simulation results show that the proposed system significantly improved the quality of the CSI after reconstruction against the existing system in terms of cosine similarity ρ and normalized mean square error, which are essentials for a MIMO system in improving performance, coverage, reliability, and user experience in 5G underwater networks.

Index Terms—artificial intelligence, autonomous, MIMO, Navigation, Self-supervised learning, split reconstruction.

I. INTRODUCTION

Communications in autonomous underwater navigation requires connected intelligence and security technologies to track and curtail reprisal attacks from non-state actors threatening maritime military and freight operations [1]. Maritime security and surveillance systems span vessel traffic management systems (VTMS), automatic identification systems (AIS), long-range identification and tracking (LRIT) and space-based AIS. Multiple-input-multiple-output (MIMO) system is one of the effective approaches to boost network performance, coverage, and reliability for real-time data streaming and transmission in maritime surveillance.

Over time, the standard compressive sensing (CS) approach and the channel state information (CSI) compression technique have been used to improve the performance of MIMO systems. In contrast to single input single output (SISO), MIMO systems obtain better data rates by combining multiple antennas and single routes in order to acquire communication channel information [2]. Massive MIMO, an improved form of MIMO, increases wireless communication throughput and spectrum efficiency by employing a collection of antennas on both the transmitter and reception sides [3]. However, this method often assumes that CSI is a sparse matrix. Instead, it has a very intricate structure and is not exactly minimalist. As a result, the exact structure of the CSI matrix is altered throughout the compression process, making the CS-based approach ineffective.

In recent times (due to an increase in hardware computational capacity), deep learning models' application has

witnessed a geometric explosion. Several deep learning (DL) models are proposed to solve problems in the communication system and autonomous navigation and surveillance [4]. Authors [5] proposed channel classification and CSI reconstruction based on residual learning technique [6], called as CsiNet, in which a refinement approach was deployed to reconstruct the CSI. However, no consideration was given to the detailed structure of CSI, which resulted in the low quality of reconstructed CSI in the MIMO system. Also, authors [7] combined CNN and Long Short-Term Memory (LSTM) algorithm in reconstructing CSI in an indoor and outdoor environment to improve the performance of the MIMO system. The simulation results show that their model, CsiNet-LSTM outperformed the CsiNet proposed by the authors [6]. However, the computational complexity of the model is relatively high.

This work adopts a similar approach to improve the channel structures' resolution albeit with self-supervised learning (SSL). SSL is a deep learning framework that is just a step closer to embedding human cognition into machines leveraging the least computational complexity and cost of quality labeled data in task performance [8]. Specifically, a masked autoencoder (CSI-MAE), a variant of denoising autoencoder is adopted in this study. Then, transfer learning is applied for domain adaptation to tackle the system with a different domain but has similarities among source and target tasks from a related distribution of the system. The rest of this paper is organized as section II presents the Problem formulation; section III highlights the Simulation results; and section IV concludes the paper.

II. PROBLEM FORMULATION

To reconstruct CSI in a MIMO system, the number of the channel matrix, C is a linear function of the number of antennas, n_a over the subcarriers, n_s . In a spatial frequency domain, the stack structure of a CSI matrix can be represented as $C_m = [C_1, C_2, \dots, C_{n_s}]^C$. Through Discrete Fourier Transformation, C_m is transferred from spatial frequency domain to angular-delay domain given by equation (1).

$$\hat{C} = S_{f_s} \cdot C \cdot A_{f_t}^C, \quad (1)$$

with S_{f_s} containing the sub-carriers matrices; and A_{f_t} having transmitted antennas matrices. However, the value of \hat{C} is large and the compressed version transmitted back to the base station via a feedback channel is of low quality.

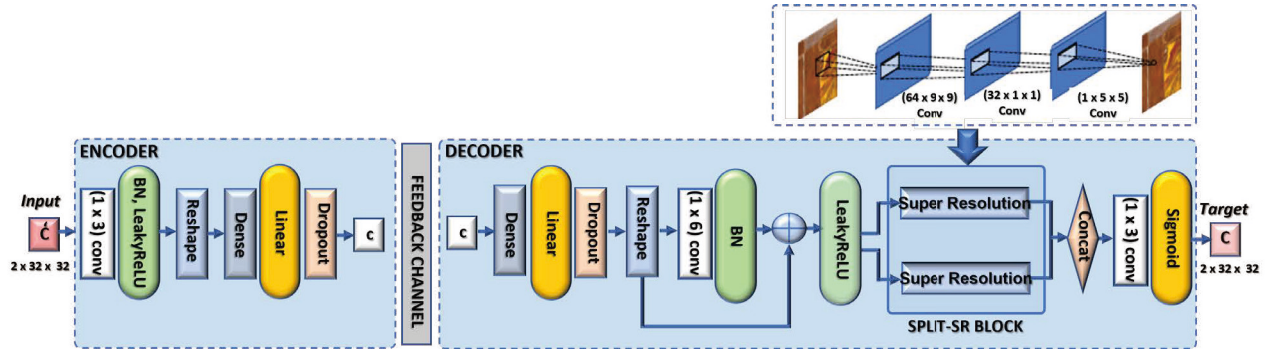


Fig. 1: CSI-MAE Block Diagram for MIMO System CSI Reconstruction

The proposed model, CSI-MAE addresses the large \hat{C} matrix size and quality of reconstructed CSI through an improved denoising autoencoder that compresses (encoder) and reconstructs (decoder) with a split super-resolution (SR) block and transfers learning as seen in Fig. 1.

CSI-MAE model takes two-channel matrices of \hat{C} as input with each having a size of 32×32 for encoding. By using 2 filters (of 1×3 size), the convolutional layer generates two feature maps, which are reshaped and extracted to a fully connected layer (FCL) using batch normalization (BN), leakyReLU as activation function with a dropout of 0.1. This forms a compressed compact version, c of the input. Then, the decoder reconstructs the c . To avoid overfitting and coadaptation of the training data, the FCL scales up a feature of c with a dropout. Thereafter, the input is reshaped and sent to FCL with 2 filters of 1×6 size to improve the network stability. To improve the resolution and quality of the reconstructed image, transfer learning is applied by extracting the weights and biases obtained from the Split-SR convolution block (SRCNN). The proposed architecture is based on Keras API. Hence, the SRCNN (based on TensorFlow backend) is turned into Keras backend. Then, the new equivalent model of super-resolution is built in the network architecture by injecting the extracted pretrained weights and biases into the proposed model. Table I summarizes the configuration of the CSI-MAE model.

III. RESULTS AND PERFORMANCE EVALUATION

The data set used for the generation and simulation of channel modeling is in the work of the authors [9]. The data set was divided into 70%, 20%, and 10% for model training, testing, and validation. To evaluate the channel matrix's ability to recover to its original levels by the models, normal mean square error (NMSE) and cosine similarity (ρ) are used with the adaptive moment estimation (ADAM) optimizer as loss function, using data compression rates; 1/4, 1/16, 1/32, and 1/64. 32 antennas at the BS are used and positioned 20m at the center of a square area in the indoor pico cellular scenario at the 5.3 GHz band. The simulation is carried out on Windows 10 with Intel(R) Core(TM) i5-8500 CPU @ 3.00GHz, 6Core(s), NVIDIA GeForce GT 1030, GPU CUDA:

TABLE I: The CSI-MAE Model Configuration

Layer	Output Shape	Descriptions	Process
Input	(2, 32, 32)		Encoder
Conv2D	(2, 32, 32)	2 x (1x3), BN, Leaky-relu	
Reshape	(2048)	From $2 \times 32 \times 32$ to 2048×1	
Dense	(128)	FCL compress an into C	
Dropout	(128)	Dropout value 0.1	
Dense	(2048)	FCL decompress input on C	
Dropout	(2048)	Dropout value 0.1	Decoder
Reshape	(2, 32, 32)	Reshape back to $2 \times 32 \times 32$	
Conv2D	(2, 32, 32)	2 x (1x6) with BN	
add	(2, 32, 32)	Add LeakyRelu function	
Split	(1, 32, 32)	Split input feeds into Slit-SR block	Split of SR through TL
SR Block	(1, 32, 32)	use ReLu 1 x (5x5)	
SR Block	(1, 32, 32)	use ReLu 1 x (5x5)	
Concat	(2, 32, 32)	Concat each input	Decoder
Conv2D	(2, 32, 32)	2 x (1x3) with sigmoid	

0 (Tesla K80, 11441.1875MB), 36GB RAM. The summary of the simulation result is captured in Table II.

NMSE measures the difference between output (as reconstructed CSI C) and input (as original CSI \hat{C}), defined as:

$$\Rightarrow NMSE = \xi \left[\| \hat{C} - C \|_2^2 * \frac{1}{\| \hat{C} \|_2^2} \right]; \quad (2)$$

TABLE II: NMSE (dB) comparison of CSI reconstruction algorithms

Compression Rates	Models	NMSE (dB) Indoor	NMSE (dB) Outdoor
1/4	CSI-MAE	-16.33	-9.47
	CsiNet [6]	-14.53	-9.58
	Csi-LSTM [7]	5.09	5.27
1/16	CSI-MAE	-10.91	-4.73
	CsiNet [6]	-8.05	-4.51
	Csi-LSTM [7]	6.49	6.17
1/32	CSI-MAE	-7.96	-2.87
	CsiNet [6]	-7.27	-2.60
	Csi-LSTM [7]	-5.70	9.48
1/64	CSI-MAE	-5.92	-2.00
	CsiNet [6]	-4.39	-1.84
	Csi-LSTM [7]	-2.29	-0.13

The results from Table II show that the proposed model, CSI-MAE has the best performance across the different compression rates with the least error value and validation loss when compared with CSiNet and Csi-LSTM both for the indoor and outdoor environments. For instance, at a compression rate of 1/4 of, CSI-MAE achieved -16.33dB and -9.47dB NMSE values, which are much better than 14.53 and 9.58 achieved by CSiNet and 5.09 and 5.27 by the Csi-LSTM model.

Fig 2 and Fig 3 show the performance of CSI-MAE in terms of loss on the training and validation dataset.

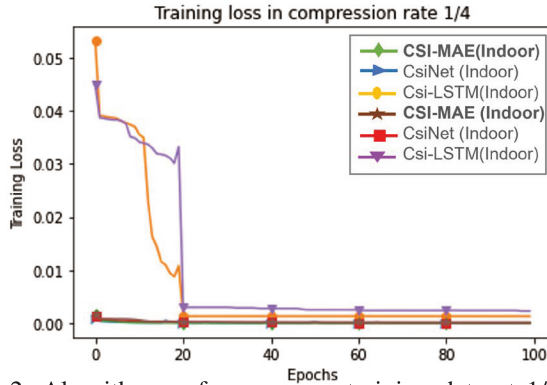


Fig. 2: Algorithm performance on training data at 1/4 compression rate

The result in Fig 2 and Fig 3 confirms that CSI-MAE achieved the lowest loss error both on the training and validation data at 1/4 compression rate than CsiNet and Csi-LSTM for both indoor and outdoor scenarios. The same result is achieved by the proposed model in other compression rates; 1/16, 1/32, and 1/64.

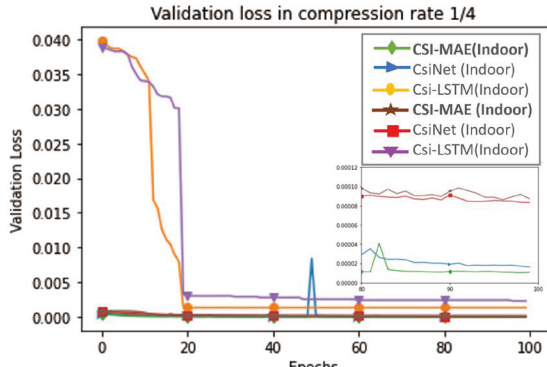


Fig. 3: Algorithm performance on validation data at 1/4 compression rate

The CSI feedback serves as a beamforming vector. The cosine similarity denoted as ρ measures the quality of the beamforming vector.

From Fig. 4, CSI-MAE achieved the highest accuracy in terms of ρ versus CsiNet and Csi-LSTM for different compression rates both in the indoor and outdoor environment. Thus, the proposed split of SR through transfer learning techniques retains effective beamforming gain and reconstructs the CSI closest to the original CSI. Moreover, at the compression

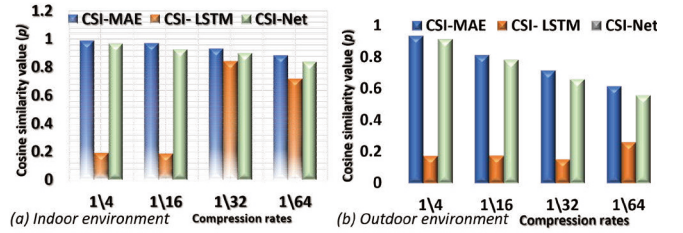


Fig. 4: Comparison of Cosine Similarity (ρ) in different compression rates

rate of 1/64, CSI-MAE continues to perform better than the existing system.

IV. CONCLUSION

This work proposed a novel self-supervised learning model for MIMO systems for CSI reconstruction based on a split of superresolution. The simulation results showed that the proposed model achieved the lowest error values in all data compression rates and higher accuracy than the existing system, justifying its suitability for underwater navigation networks. As in future work, advanced deep learning in terms of layer combination and filter size of each layer will be considered.

ACKNOWLEDGMENT

This research work was supported by Priority Research Centers Program through NRF funded by MEST (2018R1A6A1A03024003) and the Grand Information Technology Research Center support program (IITP-2022-2020-0-01612) supervised by the IITP by MSIT, Korea.

REFERENCES

- [1] S. O. Ajakwe, A. Rubina, D.-S. Kim, and J. M. Lee, "Lightweight CNN Model for Detection of Unauthorized UAV in Military Reconnaissance Operations," in *2021 Korean Institute of Communication and Sciences Fall Conference*, 11 2021. [Online]. Available: <http://www.dbpia.co.kr/journal/articleDetail?nodeId=NODE11022567>
- [2] B. Wang, F. Gao, S. Jin, H. Lin, and G. Y. Li, "Spatial- and frequency-wideband effects in millimeter-wave massive mimo systems," *IEEE Transactions on Signal Processing*, vol. 66, no. 13, pp. 3393–3406, 2018.
- [3] S. O. Ajakwe, C. I. Nwakanma, D.-S. Kim, and J.-M. Lee, "Key Wearable Device Technologies Parameters for Innovative Healthcare Delivery in B5G Network: A Review," *IEEE Access*, vol. 10, pp. 49 956–49 974, 2022.
- [4] S. O. Ajakwe, V. U. Ihekoronye, D.-S. Kim, and J. M. Lee, "DRONET: Multi-Tasking Framework for Real-Time Industrial Facility Aerial Surveillance and Safety," *Drones*, vol. 6, no. 2, 2022.
- [5] T. Huynh-The, C. Hua, Q. Pham, and D. Kim, "MCNet: An Efficient CNN Architecture for Robust Automatic Modulation Classification," *IEEE Communications Letters*, pp. 1–1, 2020.
- [6] C. Wen, W. Shih, and S. Jin, "Deep Learning for Massive MIMO CSI Feedback," *IEEE Wireless Communications Letters*, vol. 7, no. 5, pp. 748–751, Oct 2018.
- [7] T. Wang, C. Wen, S. Jin, and G. Y. Li, "Deep Learning-Based CSI Feedback Approach for Time-Varying Massive MIMO Channels," *IEEE Wireless Communications Letters*, vol. 8, no. 2, pp. 416–419, 2019.
- [8] S. O. Ajakwe, V. U. Ihekoronye, D.-S. Kim, and J. M. Lee, "Adaptive Drone Identification and Neutralization Scheme for Real-Time Military Tactical Operations," in *2022 International Conference on Information Networking (ICOIN)*, 2022, pp. 380–384.
- [9] L. Liu, C. Oestges, J. Poutanen, K. Haneda, P. Vainikainen, F. Qutin, F. Tufvesson, and P. D. Doncker, "The cost 2100 mimo channel model," *IEEE Wireless Communications*, vol. 19, no. 6, pp. 92–99, December 2012.

Aerial Cell Planning Depending on Altitude

Yuna Jeong, Jihyung Kim*, Intae Hwang**, Moon-Sik Lee*

School of Electronics Computer Engineering, Chonnam National University, Gwangju, Korea

*Electronics and Telecommunications Research Institute (ETRI), Daejeon, Korea

**Dept. of Electronic Engineering & ICT Convergence System Engineering, Chonnam National University, Gwangju, Korea

195815@jnu.ac.kr

Abstract—Aerial UEs can have several problems due to frequent handovers when using side beams of a ground cell. QoS degradation, network overload, and delay can lead to a negative effect on the communication system. The higher and faster UAV flies, the more unnecessary handovers occur because it can detect many cells at once during the flight. To reduce unwanted handover events, we emphasize a necessity of a new base station system generating aerial cells. We also explain each different issue at various altitudes and propose novel strategies designed differently depending on the locations of UEs.

Keywords—*Aerial cell, Altitude, Cell planning, Handover, Interference*

I. INTRODUCTION

UAV has been developed over the past decades for several purposes. The technologies related to UAV are getting important with the arrival of 6G wireless communication in three-dimensional space. There are numerous ongoing researches for providing a stable service to many types of aerial vehicles at different altitudes, for example, Air-to-Ground (ATG) communication system or an aerial cell is developing.

Fig. 1 shows some aerial cells formed by two base stations to support aerial vehicles at various altitudes [1]. In the existing system, the terminals in the sky predominantly use side beams to connect to the base stations while devices at ground level use main beam. A group of side beams are spread in various directions, making a problem. The null spaces between several side beams cause frequent handovers. These unwanted handovers by the null spaces and antenna side lobes degrade the resource performance [2]. A solution to reduce the number of handovers is an aerial cell system as shown in Fig. 1. In a cellular system, reusing frequency resources is possible thus it improves an overall efficiency and keep a good connectivity by using handover function. It is difficult to ensure a high reliability and stability if too many handovers occur in this process.

Only with the ground cell, providing a service to various low or high-level aerial vehicles have some difficulties. An aerial cell is therefore a key of the answer but there are still problems. When cell planning is performed at a specific altitude, optimizing and operating for the terminals at another altitude are technically challenging. Assume we formed the cells at a reference altitude of 2,000 m then, interference between main beams get severe at 10 km. At 300 m, side beams fill in the blank area and handover occurs frequently by themselves and null spaces. Therefore, it is necessary to apply different operation methods for each altitude. We deal with this in section III. This methods are essential for seamless communication service, especially in the ATG environment.

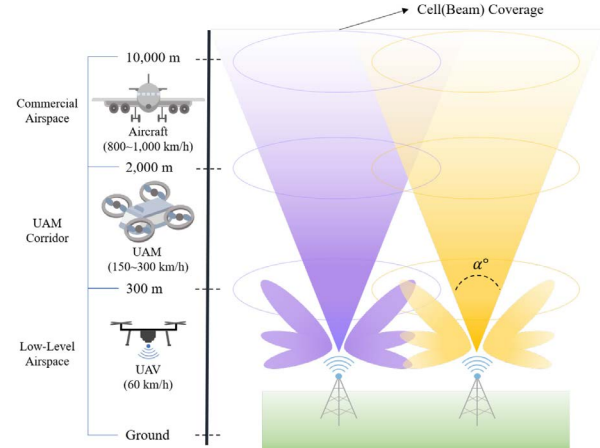


Fig. 1. Aerial vehicles with cell coverage.

II. HANDOVER MECHANISM

To compare reference signals received power (RSRP) at the serving cell and target cell, use equation (1), and then determine whether handover event should be triggered or not by inequality (2).

$$RSRP = Power - Pathloss, \quad (1)$$

$$M_n + O_{fn} + O_{cn} - H_{ys} > M_p + O_{fp} + O_{cp} + O_{ff}, \quad (2)$$

where M_n and M_p represent RSRP measurement values of the neighboring cell and serving cell for each. O_{fn} and O_{cn} are reference signals and offset regarding to neighboring cell. Subscript p means it is related to SpCell [3]. UE decides to perform handover if the requirement of (2) is satisfied during T in Fig. 2.

$$PL = FSPL(d, f_c) + SF + CL(\alpha, f_c), \quad (3)$$

$$FSPL(d, f_c) = 32.45 + 20 \log_{10}(f_c) + 20 \log_{10}(d), \quad (4)$$

where d is a distance between the terminal and the base station. SF and CL stand for shadowing factor and clutter loss for each [4].

III. PROPOSED METHOD FOR CELL PLANNING WITH ALTITUDE

This section describes and explains an aerial cell coverage system for reducing the handover frequency and executing seamless communication in the ATG environment. We also propose to set different events and threshold parameters by altitudes.

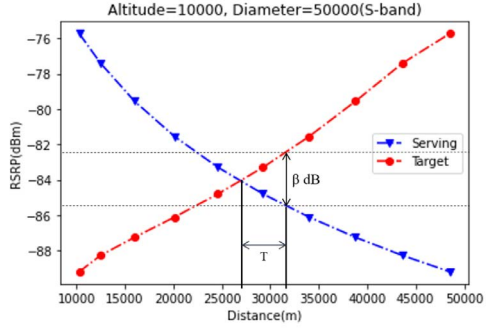


Fig. 2. Handover procedure.

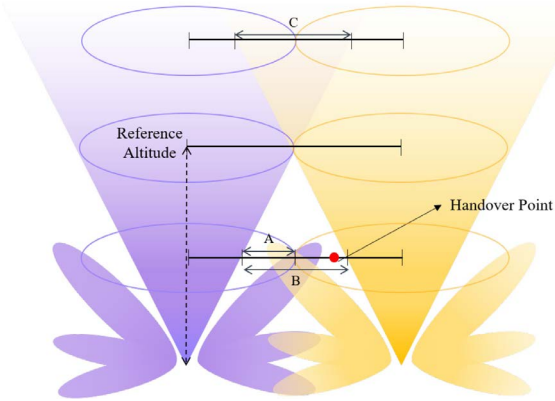


Fig. 3. Various zones depending on altitude in aerial cells.

A. Below the Reference Altitude

At the area lower than the reference altitude, the overlapping area of main beams is reduced as shown in Fig. 3. A group of side beams fill this reduced space rather than remain empty. They cause handover quite often within

TABLE I. HANDOVER MECHANISM IN AERIAL CELL

1:	BS should:
2:	Set reference altitude.
3:	Set thresholds at each altitude.
4:	UE should:
5:	Report its position continuously.
6:	If) UE has lower altitude than reference altitude
7:	If) UE is in A
8:	Use optimized reference values such as H_{ys} .
9:	Evaluate measurement with own threshold at an altitude of the UE.
10:	If) $M_n + O_{fn} + O_{cn} - H_{ys} > M_p + O_{fp} + O_{cp} + O_{ff}$
11:	Start handover.
12:	Else)
13:	Evaluate measurement with own threshold at an altitude of the UE.
14:	If) $M_n + O_{fn} + O_{cn} - H_{ys} > M_p + O_{fp} + O_{cp} + O_{ff}$
15:	Start handover.
16:	Else if) UE has higher altitude than reference altitude
17:	If) UE is in C with handover
18:	BS should apply some technologies to mitigate beam interference.
19:	Else)
20:	Evaluate measurement with own threshold at an altitude of the UE.
21:	If) $M_n + O_{fn} + O_{cn} - H_{ys} > M_p + O_{fp} + O_{cp} + O_{ff}$
22:	Start handover.

the zone B in Fig. 3. Note that the actual handover point is close to the neighboring cell. The threshold added to the RSRP in (2) should be higher than β dB to further increase the handover entry condition in the zone A. After leaving the zone A, handover begins with existing RSRP condition, that is, set two threshold values when determining whether UE needs to handover. In this case, serving BS requires the terminal to report the altitude of it. In short, the main ideas at relatively lower altitude are setting an appropriate threshold for each altitude and getting location information of the terminal so that flexibly apply thresholds.

B. Above the Reference Altitude

At the area higher than the reference altitude, the main beams overlap as shown in Fig. 3. The zone C area requires a method for mitigating interference because the effects of it increase, as the cell edge of the ground. However, applying a power control technology to reduce interference, unlike ground cells, is difficult for an operation up to 10 km. Resource allocation, scheduling, and NOMA technologies can be applied to the zone C accordingly.

Table I presents the proposed method for cell planning with altitude as mentioned in above section A and B.

IV. CONCLUSIONS

To provide an optimal performance for a variety of aerial vehicles, we consider the aerial cell coverage system that can replace the ground cell. This system needs different operating methods for each altitude. At the lower altitude than the reference, it needs to introduce a method that reduces the negative effects of frequent handovers by side beams. Unlike this, some technologies to alleviate interference are needed at relatively higher than the reference altitude. In conclusion, as suggested in this paper, our aerial cell coverage system requires new operation methods, which are different from the ground cell. We expect that they enable to keep the aerial terminals stable in wireless communication.

ACKNOWLEDGMENT

This work was supported by Institute of Information & communications Technology Planning & Evaluation (IITP) grant funded by the Korea government(MSIT) (No. 2021-0-00794, Development of 3D Spatial Mobile Communication Technology).

REFERENCES

- [1] Rakesh Shrestha, Inseon Oh, and Shiho Kim, "A Survey on Operation Concept, Advancements, and Challenging Issues of Urban Air Traffic Management," *Frontiers in Future Transportation*, Volume 2, <https://doi.org/10.3389/ffutr.2021.626935>, pp. 1-20, April 2021.
- [2] Wenbin Dong, Xinhong Mao, Ronghui Hou, Xixiang Lv, and Hui Li, "An Enhanced Handover Scheme for Cellular-Connected UAVs," 2020 IEEE/CIC International Conference on Communications in China (ICCC), pp. 418–423, November 2020.
- [3] 3GPP TR 38.331, "Radio Resource Control(RRC) protocol specification," V17.0.0, pp. 186–187, March 2022.
- [4] 3GPP TR 38.811, "Study on New Radio(NR) to support non-terrestrial networks," V15.4.0, pp. 48–50, September 2020.

Maritime UAV Patrol Tasks Based on YOLOv4 Object Detection

Yi-Yu Chang, John A, Pao-Ann Hsiung, *Senior Member, IEEE*

Dept of Computer Science and Information Engineering

National Chung Cheng University

Minxiong Township, Chiayi, Taiwan

tako19941209@cs.ccu.edu.tw, johnmtech@gmail.com, pahsiung@cs.ccu.edu.tw

Abstract—The maritime patrol personnel usually perform patrol tasks via ships and helicopters in the search and rescue work at sea, which often consumes many resources with human and large patrol tools. The victims call for help, and the rescue unit obtains the ship information but lacks maritime images of the sea and thus cannot control the accident site in time. In this work, we propose an automatic patrol task base on small UAVs and different maritime search patterns corresponding to different sea areas. Maritime images are collected via a deep neural network-based UAV and returned to the search and rescue system in time. The object detection model is trained using images of maritime accidents collected from the network. Maritime accidents can thus be detected by the trained object detection model base on YOLOv4 framework. After maritime detection, we set up an alarm system to classify the danger level of the targets and perform rescue according to the corresponding levels. Finally, an alarm message is sent to the rescuers by Short Message Service (SMS).

Index Terms—Unmanned Aerial Vehicles, Maritime Search and Rescue, Object Detection

I. INTRODUCTION

Numerous maritime accidents, such as ship wrecks, pirate robberies, and fatalities, have occurred endlessly [1]. According to statistics on marine accidents, it was discovered that from 2011 to 2017, there were more than 2,000 maritime accidents in Europe on average annually, and in 2017, there were 1,079 fatalities. The Civil Aviation Administration, which was created in Taiwan reports that there have been 49 marine accidents this year 2019 [2], of which 30 have resulted in fatalities or missing persons. The likelihood of marine accidents is unknown, and such rescue techniques face the issue of a delay in requesting help [3]. The application of UAVs saves humans and also patrols the ship resources in various Ocean Affairs Council, effectively managing the different marine affairs for Taiwan. The serval UAV patrol works in Taiwan effectively monitor the maritime area [4]. The cases of using UAVs for searching for personnel in maritime accidents, such as Zheng et al. [5], proposed a system where rescue units dispatch UAVs with cameras to find victims after a ship sends a distress signal. They compare ship identification with commonly used target identification methods, which include Region-CNN (R-CNN), Single-Shot Multi-Box Detector (SSD), and version 3 of You Only Look Once (YOLOv3). The experimental results show that the recognition accuracy and speed of YOLOv3 can meet

the needs of search and rescue subjects in distress at sea. However, the disadvantage is that the UAV's work is limited by weather factors and the poor sea surface light at night, as target identification would fail under such circumstances. The instability of the maritime environment and the weather conditions will introduce the following challenges: (1) Flight instability of drones at sea. (2) poor image quality captured by the drone's lens under various environmental factors. (3) Target recognition rate is low identification in images under various environmental influences.

Motivation: Currently, the application of drones is extensive, and performance is adequate, such as low power consumption, high flight stability, the image transmission distance of drone, etc. For example, Amaral et al. [6] used target detection methods and team UAVs to monitor and track sea borders. Wang et al. [7] did search and rescue work through UAVs to obtain sea images. They proposed to use a pre-trained convolutional neural network (CNN) to detect the accuracy of the victim's location. Bharati et al. [8] used obstacle detection to avoid collisions when UAVs with cameras are tracking targets. Leira et al. used UAVs to detect icebergs [9] and ice floes in the Arctic to track their movement paths. Maritime object recognition using Convolutional of Neural Network (CNN) models is used to identify the type [10] and direction of ships. However, target identification in the sea does include not only the identification of human figures but also unique environmental characteristics of the ocean, such as the glare projected onto the sea. Therefore, this work proposes a framework for accurately monitoring human figures at sea such that the impact of the sea environment on image recognition is improved, the recognition of partially submerged people is improved, and it achieves an immediate notification.

This work aims to use unmanned aerial vehicles (UAVs) to conduct patrol searches along coastal areas. The first target scenario is a search of the coastal regions and Taiwan location as an example. The second target scenario is maritime area search. In the second scenario, a UAV search is performed from a ship, and the ship is considered as the center point. In both scenarios, we need to consider the limitations of the UAV so that maximal search can be performed within limited resources (power, time, etc.). The most critical problem is the limited power supply on UAVs, thus a handover process

between UAVs during patrol work must be considered. For instance, when the power is insufficient for patrol work, it would be substituted by another UAV with sufficient power.

This work is organized as follows. Section 2 introduces the related work on UAV patrol and object detection. Section 3 presents the assumptions and overall framework for our object detection and alarm system. Section 4 provides the experiment results of our work, and in Section 5, we will give the conclusions and future work.

II. RELATED WORK

In this section, we will review various methods for object identification in such marine scenarios. The related work based on Search and Rescue Based on UAV of Maritime, Search and Rescue Regulations on Maritime, Importance of Image Recognition on UAV and Object-based Detect Methods on Maritime. The international norms on maritime search and rescue follow the international conventions [11] and manuals, which are described in details below. International Convention on Maritime Search and Rescue (SAR) [12], which includes accidents in various fields in Search and Rescue (SAR), aims to develop search and rescue plans. Search and rescue units can cooperate with neighboring SAR organizations, and coordinate the rescue work of personnel at risk on Maritime.

Global maritime and safety Ma et al. [13] used an improved Alexnet model to achieve target classification of maritime on Gaofen-3 spaceborne SAR images. The maritime targets dataset (MTD) consists of boat, cargo ships, container ships, iron towers, oil tankers, and windmills. After training and testing, the model achieved an accuracy of 92.10 of objects. systems (GMDSS) have been added to the SOLAS regulations, which was officially launched in 1992. Initially, the gross tonnage (GT) of life-saving equipment and radio rescue device on the ship are regulated by SOLAS. However, based on the actual situation, the ships of more than 300 GT need to comply with the requirements of the GMDSS.

Ma et al. [13] used an improved Alexnet model to achieve target classification of maritime on Gaofen-3 spaceborne SAR images. The maritime targets dataset (MTD) consists of boat, cargo ships, container ships, iron towers, oil tankers, and windmills. After training and testing, the model achieved an accuracy of 92.10. UAV is becoming increasingly popular, and their applications are more widespread. It is no longer restricted to military purposes. In various applications, UAV has not only strengthened the carrying weight, endurance and the communication technology, but has also improved aerial photography and image transmission technology. The analysis of images is a very important core task, where the identification of objects and events is combined with intelligent learning [14]. The purpose is to reduce the difficulty of people performing a mission in dangerous environments, by getting timely images to assess the situation at an accident site. The following will introduce examples in which image recognition is used by UAV to execute patrol work. Ghahremani et al. [15] proposed a CNN-based cascaded method for long-range object

detection, which can reliably detect smaller objects. In this work, the distant ships can be detected by surveillance cameras. This cascading method can be applied to conventional networks without modifying the trained model or architecture, such as Faster Region-Convolutional Neural Network(Faster R-CNN) or You Only Look One (YOLO) [16]. There are many categories in Computer vision that include picture reconstruction, event monitoring, target tracking, target recognition, machine learning, indexing, image recovery, etc. [66]. Among these categories, target recognition constitute the core of maritime surveillance. There are also many algorithms for target recognition, the common methods include R-CNN and YOLO. The following will introduce the different methods for maritime object detection. Zou et al. [17] and Chen et al. [18] both use the Faster R-CNN model for target recognition, and using the Resnet model to replace the architecture of VGG16 as the detection framework. The former trains the model with the self-made Pascal VOC2007 dataset. The experimental results show that this method has high detection accuracy for identifying different ship targets. The latter uses the HRSC2016 (High-Resolution Ship Collection) dataset for training model, its experimental results show this method can improve the performance of traditional Faster R-CNN detector (72.7 mAP) by about 5 in mAP (mean average precision).

Guo et al. [19] described that accurately locating smaller imaging of vessels is difficult, due to the complicated monitoring environment at sea. They proposed a new PL loss function, this model replaces the original cross-entropy function and constitute a single-stage detector YOLO-H model. This model effectively solves the problem of low precision of model caused by sample imbalance. The authors used the ms-coco dataset for experimental evaluation, the test results obtained a higher AP (average precision) than YOLOv3. Samer et al. [20] proposed a method that can effectively detect small objects at sea. This method uses only 14 training images, while other common object recognition methods require more training images. Because the current technology specifically used for object recognition is mainly a supervised method, a large amount of data needs to be labeled in advance to perform training. Therefore, the author uses a weakly supervised deep learning method for efficient target detection, and only needs some training data labeled with the position of the detection object (bounding box) to get an accurate position.

III. ASSUMPTIONS AND UAV PATROL SYSTEM ARCHITECTURE

In this section, we will illustrate the scenarios for target problem, assumptions that may be encountered during the UAV patrol process and proposed Search And Rescue System UAV Patrol Architecture.

A. Target problem

To search for object of humans at sea, not only the environment at sea is complex, but the UAV used for searching has flying restrictions. Some problems encountered in using UAV for searching at sea are as follows.

UAV Search Area and Route Planning: We have considered two types of Area Searching, including searching along the coastal and beyond the sea surface. Since the environment and range of these two kinds of area are different, it is necessary to develop a suitable searching scheme for different areas. The Route Planning for Maritime Search and Rescue is based on the Search Pattern in the IAMSAR regulations. We will perform the automatic patrol of the drone through the planned search path to detect the accidents on maritime.

Identification of Human and shipwreck at Sea: Human recognition at sea is very difficult, because most of the body is covered by water, and a spherical buoy and circular garbage are all very similar to the head of human, which could cause objects to be mis-recognized. We determine danger events by identifying accidents of spherical objects and ship collision.

B. Assumptions

The following assumptions are made for UAV patrol tasks in this work.

Location Assumptions: The UAV patrol mission is often divided into two scenarios, the sea area is Divided in Taiwan as shown in Figure 1. The first scenario is the UAV patrol near the coast and within 3 nautical mile that we call offshore patrol area. The marine area in Taiwan's regulation is the area of the average high line to 3 nautical miles. The second scenario is that the UAV patrol around a ship outside 3 nautical miles that we call pelagic patrol zone. It is for target ship which is conducting marine activities, and the UAV is carried by the ship to solve the problem of long-range patrol.

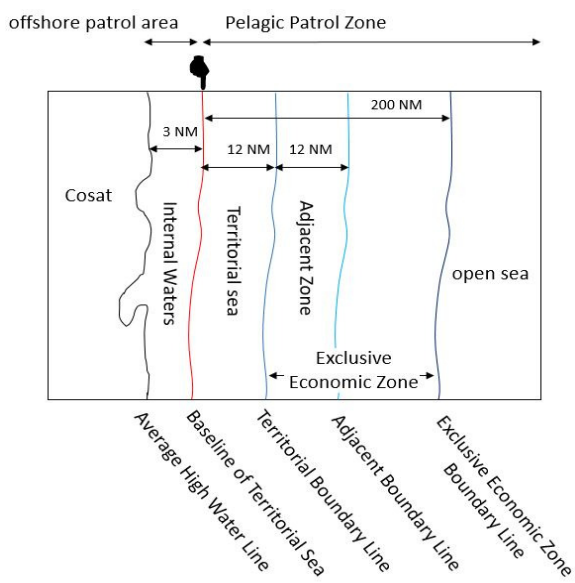


Fig. 1. The marine area in Taiwan [21]

Weather Assumptions: It is suggested by the vendor of UAV device that bad weathers such as raining, fogging, snowing, lightning thunder, and strong wind above level 6

(wind speed 10 mph Feet above) are to be avoided. However, maritime accidents can occur under bad weather, thus whenever rescue or monitoring is required as assessed by the maritime authorities patrol tasks within 3 nautical miles will still be performed. For example, the UAV might fall down during an unstable flight or the UAV take off might be very difficult. Therefore, when ships carrying UAVs cannot navigate due to bad weather, they will not perform marine patrol tasks.

Search Pattern Assumptions: IAMSAR regulations propose different Search Patterns , including (1) Trackline Pattern, (2) Parallel Track Pattern, (3) Creeping Line Pattern, (4) Expanding Square Pattern, and (5) Sector Pattern. The following will explain each search pattern and the corresponding suitable scenes [22].

Notification Assumptions: In maritime work, we divide the images monitored by UAVs into two Danger Levels(DL).

(1) Rescue Alarm: This message will be displayed in two cases. First, when a shipwreck accident is discovered (the ship was tilted, overturned, and the hull did not enter the sea beyond the waterline). Second, when receiving a radio distress signal provided by the ship (IAMSAR requires ships to carry radio mobile equipment). This means that when the rescue unit receives this message, it must immediately dispatch the rescue. The UAV images can assist the rescue unit to confirm the situation at the scene of the accident.

(2) Accident Monitoring: People may be doing water sports in the sea, so it does not necessarily mean an accident. When the system recognizes someone in the sea, it will be deemed necessary to maintain vigilance and continuously monitor the situation.

C. Search And Rescue System UAV Patrol Architecture

This section introduce the design of UAV Patrol System; then we will explain the patrol process on the coast and the sea, and how to apply a pre-trained model for object recognition to the patrol tasks. The proposed architecture consists of patrol UAV, a remote control device, and detection system. The description of the architecture components given in Figure 2 is as follows.

Unmanned Aerial Vehicle (UAV): In our work, a UAV is used to perform maritime accident patrol on the coast and the sea. Maritime rescue includes rescuing targets and positioning information, which will be obtained through the UAV camera, GPS/GLONASS device and UAV Tx/Rx Module. When the UAV performs patrol work, it means that the UAV camera starts to take pictures and obtain all the images within the working range of the drone. Mavic 2 pro UAV has two positioning devices, Global Positioning System (GPS) and Global Navigation Satellite System (GLONSS). In our work, we will use this information to lock the precise location of the target to be rescued. In the patrol work, each photo will be associated with its corresponding positioning information. When the UAV takes a photo, it will take the current location of the photo and transfer the image and the location from the UAV to the mobile device via remote control device. The UAV Tx/Rx Module used to transmission (Tx)and the reception

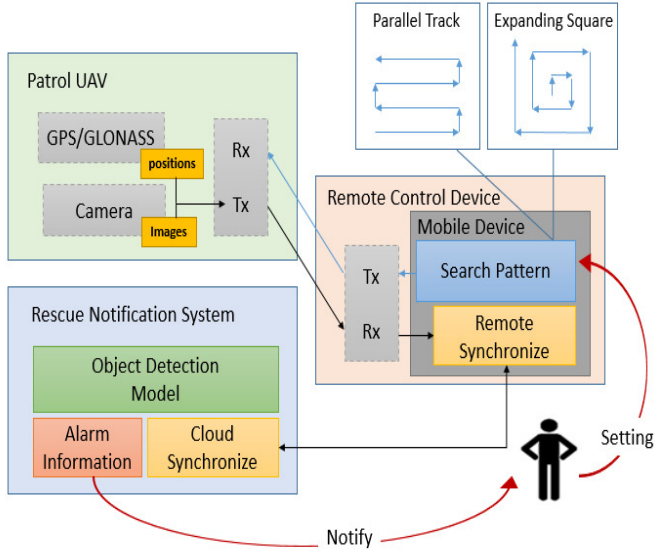


Fig. 2. UAV Patrol System Architecture

module as Rx in UAV. The transmission module is used to transmit the photos and positioning information back to the mobile device through the remote control. It also contains various dynamic information that occurs during UAV patrol missions, such as flight attitude, warning messages of low battery or strong wind. The reception module is used to receive the instructions given by the remote control, which means that the UAV will receive commands for patrol actions, such as the setting of flight height and route planning.

Remote Control Device: Remote control device is the control end of UAV, users will control the flight movement of UAV through the remote control device. In our work, it mainly acts as a bridge between UAV and mobile devices. That the mobile device is used to set UAV parameters. The working modules of remote control device contain Tx/Rx module and mobile device. The Tx/Rx Module of Remote Control Device used to control device, define the transmission module as Tx and the reception module as Rx similar to the UAV Tx/Rx module. It uses the transmission module to give the motion commands of the UAV patrol tasks. The Mobile Devices used to connects via the remote control device to monitor the dynamic information of the UAV patrol tasks. It consists of two modules including (1) Searching Pattern Module which is responsible for setting flight parameters, and (2) Remote synchronize module which collects photos and synchronizes it to the cloud.

Object detection model: Object detection model for object recognition in the rescue notification system to detect objects on a sea surface by processing the images, when there is an object detected and it needs rescue, the rescue unit is alerted.

The Darknet53 of neural network framework to trained an object detection model that recognizes humans. As shown in Figure 3, Darknet53 is composed of Convolutional and Residual and it has 52 convolutional layers and a connected

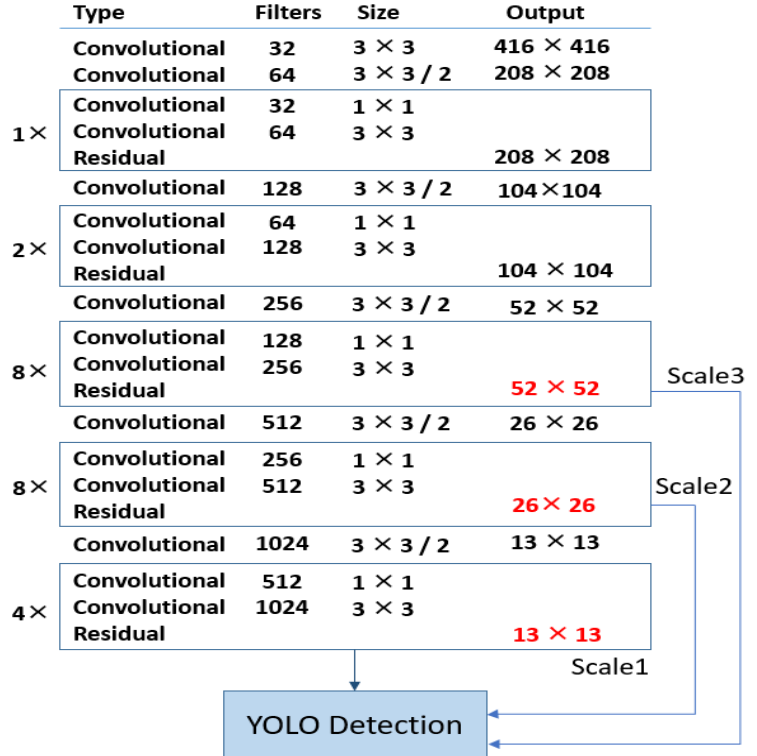


Fig. 3. The Darknet53 structure [23]

layer. The Residual module deepens the network structure and uses a short cut to solve the problem of vanishing gradient. A residual structure contains two convolutional layers, the convolution kernel of the first layer is 1×1 , and the convolution kernel of the second layer is 3×3 . YOLOv3 uses three feature layers to predict the anchor box which used in YOLOv4 as the head. The input size of the preset is 416×416 in the YOLOv3 framework, so the sizes of three feature layers are 52, 26, and 13. A feature layer has three anchor boxes, so there are a total of nine predicted anchor boxes. The training method for the YOLOv4 model is shown in Algorithm 1. The input data is the maritime images, and the objects in the image include humans, ships, and collisions.

D. Maritime UAV Patrol Tasks Design

The proactive rescue consists of the following three steps as proposed in this thesis. First, UAV patrol is used assist to the rescue unit to carry out maritime patrol tasks. Second, target objects at sea are detected through image recognition. Finally, we determine the danger level of the target for notifying the rescue unit.

Figure 4 shows the execution flow of UAV patrol tasks. As soon as the flight parameters and object detection model are set, UAV will be able to start patrol tasks. It will patrol and take pictures on flight parameters and the location of where the image was taken. Then, the transmit current image and location are transmitted via the UAV Tx to the receiver Rx of the remote control. Images and positions in the mobile device

Algorithm 1: YOLOv4 Training Algorithm

Input:

Input(Img, Img_{bbx}, Img_{path}): Maritime dataset;
 // The dependent files of the input image is as following
 1 *Img*: The maritime images;
 2 *Img_{bbx}*: The TXT file of the bounding box coordinates;
 3 *Img_{path}*: The TXT file of the maritime images path;

Output:

Prediction: Image detecting result is *Img(Img_h, Img_s, Img_c)*;
 // The label of output images are as following
 4 *Img_h*: The label of human in the image;
 5 *Img_s*: The label of ship in the image;
 6 *Img_c*: The label of collision in the image;

Variable:

Img: the images for training;

```
// Training
7 while Img do
8   [ Training(Input(Img, Imgbbx, Imgpath));
9 return Prediction();
```

will be synchronized with that in the rescue notification system of cloud. After receiving images, the object detecting model in the cloud will analyze them and then output the detection results. Finally, if a target object of rescue is detected the alarm information module determines the danger level, including (1) Danger level 1, which means it is detected that a human has fallen into the sea. At this time, the alarm information module will notify the rescue unit to monitor this situation. When the monitored humans are determined to be in danger, then the rescue is carried out. (2) Danger level 2, ship has collide. The alarm information module will warn the rescue unit to dispatch personnel to rescue, and the target rescue area is according to the position information of the image associated with the shipwreck.

IV. EXPERIMENTAL SETUP AND RESULTS

In this section, introduce the experimental environment, UAV flight parameter settings, and the difference in parameters used by the object detection model base on YOLOv4. Finally, we will show the warning methods of the rescue objects we care about. The experimental training environments shown in Table I, and experimental environments of patrol tasks are shown in Table II.

The experimental evaluation metrics for the results are average precision (AP), true positive (TP), and false positive (FP) for detecting different classes of objects are presented in Table III. Humans in the sea have an AP of 87.71

Based on the object detection results, which the alarm system classify the maritime accidents of people and shipwrecks.

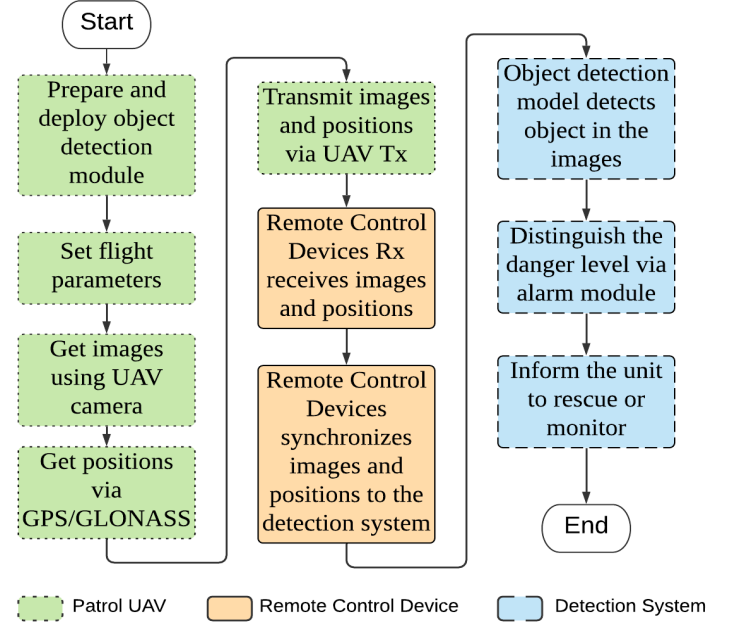


Fig. 4. UAV Patrol Task Flow Chart

TABLE I
TRAINING ENVIRONMENT FOR TRAINING

CPU	Intel (R) Xeon (R) 4110
GPU	NVIDIA GTX 2080Ti 11G
Memory	128 GB RAM
Operating System	Ubuntu 16.04 LTS (Xenial Xerus) (64-bit)
Programming Language	Python v.3.5

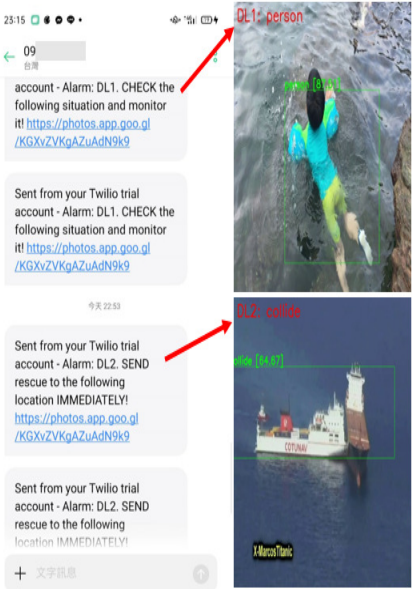
TABLE II
EXPERIMENTAL ENVIRONMENT FOR PATROL TASKS

UAV Device	Mavic 2 Pro
Battery Capacity	3850 mAh
Battery Energy	59.29 Wh
Camera	Hasselblad L1D-20c
Image Transmission	OCUSYNC 2.0
Image Format	JPEG/DNG (RAW)
Video Format	MP4 / MOV (MPEG-4 AVC/H.264, HEVC/H.265)
memory	8G
GNSS	GPS/GLONASS
APP	DJI GO 4

TABLE III
EVALUATION OF MARITIME OBJECTS RECOGNITION

Objects	AP	TP	FP	mAP
Human	87.71	2756	404	3*94.20%
Ship	96.25	772	117	
Collision	98.65	764	25	

When the rescue unit receives the Short Message Service (SMS) of alarm in Figure 5 (a), it will be informed of the danger level and the link of Maritime database to obtain historical detection images in Figure 5 (b).



(a)



(b)

Fig. 5. (a) The alarm SMS of danger level information (b) The images of accident in database

V. CONCLUSIONS AND FUTURE WORK

In this work, we proposed maritime patrol system with object detection model based on YOLOv4 using UAV to assist search work on sea, which not only reduce human resources of victims search work but also avoid the risk of unexpected accidents when personnel is on duty. Also, UAV patrol system reduces the time of seeking help by victims via radio. UAV is combined with the maritime search patterns that can be arranged to patrol specific sea area. We trained the object detection model to make the model learn how to identify the objects on the sea, and achieved mAP of 94.20% for the maritime objects detections including human, ships and collisions in the video images, which is 11% more accurate than the SSD512 method. The detection system is based on deep learning construction to catalog the detected images with danger level, which assist the rescue unit to automatically determine whether the target encounters danger and send rescue message.

For the future works, the identification of danger levels implemented in this work is manual. Danger level identification needs to consider the behaviors of people and define the differences between these behaviors in the marine environment, there is an opportunity to achieve fully automatic identification.

REFERENCES

- [1] California submarine catches fire at sea, kills 4 and missing 30. <https://www.ntdtv.com/b5/2019/09/02/a102656737.html>, Septemper 2019.
- [2] Shipwreck Statistics Tables of Maritime Port Bureau. MOTC for September 2019. <https://www.motcmpb.gov.tw/Information/Detail/80a75abe-4ebe-8c24-467fe4eaecd?SiteId=1&NodeID=406>, August 2019..
- [3] The ship of airport was not dispatched to rescue, that questioned for delayed rescue. <https://hk.appledaily.com/breaking/20200122/4E77HFA64RNPWQGDZIR6IMA744/>, January 2020.
- [4] Yang, Jianhua, Zhaowei Ding, and Lei Wang. "The Programming Model of Air-Ground Cooperative Patrol Between Multi-UAV and Police Car." IEEE Access 9 : 134503-134517, 2021.
- [5] R. Zheng, R. Yang, K. Lu, and S. Zhang. A Search and Rescue System for Maritime Personnel in Disaster Carried on Unmanned Aerial Vehicle. In Proceedings of the IEEE International Symposium on Distributed Computing and Applications for Business Engineering and Science (DCABES), pages 43–47, November 2019.
- [6] G. Amaral, H. Silva, F. Lopes, J. P. Ribeiro, S. Freitas, C. Almeida, A. Martins, J. Almeida, and E. Silva. UAV cooperative perception for target detection and tracking in maritime environment. In Proceedings of the International Conference on OCEANS 2017 - Aberdeen, pages 1–6, June 2017.
- [7] S. Wang, Y. Han, J. Chen, Z. Zhang, G. Wang, and N. Du. A Deep-Learning-Based Sea Search and Rescue Algorithm by UAV Remote Sensing. In Proceedings of the IEEE CSAA Guidance, Navigation and Control Conference (CGNCC), pages 1–5, August 2018.
- [8] S. P. Bharati, Y. Wu, Y. Sui, C. Padgett, and G. Wang. Real-Time Obstacle Detection and Tracking for Sense-and-Avoid Mechanism in UAVs. IEEE Transactions on Intelligent Vehicles, 3(2):185–197, June 2018.
- [9] F. S. Leira, T. A. Johansen, and T. I. Fossen. A UAV ice tracking framework for autonomous sea ice management. In Proceedings of the International Conference on Unmanned Aircraft Systems (ICUAS), pages 581–590, June 2017.
- [10] H. Fu, Y. Li, Y. Wang, and L. Han. Maritime Target Detection Method Based on Deep Learning. In Proceedings of the IEEE International Conference on Mechatronics and Automation (ICMA), pages 878–883, August 2018.
- [11] L. Y. Lin. Taiwan's Maritime Search and Rescue SchemeA Study on the Integrated Planning of the SAR Resources in the Private Sector. January 2005.
- [12] [http://www.imo.org/en/About/Conventions/ListOfConventions/Pages/International-Convention-on-Maritime-Search-and-Rescue-\(SAR\).aspx](http://www.imo.org/en/About/Conventions/ListOfConventions/Pages/International-Convention-on-Maritime-Search-and-Rescue-(SAR).aspx), April 1979.
- [13] M. Ma, H. Zhang, X. Sun, and J. Chen. Maritime targets classification based on CNN using Gaofen-3 SAR images. The Journal of Engineering, 2019(21):7843–7846, August 2019.
- [14] C. D. Rodin, L. N. de Lima, F. A. de Alcantara Andrade, D. B. Haddad, T. A. Johansen, and R. Storvold. Object Classification in Thermal Images using Convolutional Neural Networks for Search and Rescue Missions with Unmanned Aerial Systems. In Proceedings of the International Joint Conference on Neural Networks (IJCNN), pages 1–8, July 2018.
- [15] A. Ghahremani, E. Bondarev, and P. H. N. De With. Cascaded CNN Method for Far Object Detection in Outdoor Surveillance. In Proceedings of the 14th International Conference on Signal-Image Technology Internet-Based Systems (SITIS), pages 40–47, November 2018.
- [16] R. Joseph, D. Santosh, G. Ross, and F. Ali. You only look once: Unified, real-time object detection. In Proceedings of the IEEE conference on computer vision and pattern recognition, May 2016.
- [17] J. Zou, W. Yuan, and M. Yu. Maritime Target Detection Of Intelligent Ship Based On Faster R-CNN. In Proceedings of the Chinese Automation Congress (CAC), pages 4113–4117, November 2019.
- [18] Z. Chen and X. Gao. An Improved Algorithm for Ship Target Detection in SAR Images Based on Faster R-CNN. In Proceedings of the Ninth International Conference on Intelligent Control and Information Processing (ICICIP), pages 39–43, November 2018.
- [19] Y. Guo, S. Wang, H. He, L. Sun, and S. Ma. Research on Boat Identification Based on Improved Loss Function of Deep Convolutional Neural Networks. In Proceedings of the WRC Symposium on Advanced Robotics and Automation (WRC SARA), pages 278–283, August 2019.
- [20] S. Alashhab, A. Gallego, A. Pertusa, and P. Gil. Precise Ship Location With CNN Filter Selection From Optical Aerial Images. IEEE Access, 7:96567–96582, July 2019.
- [21] Enforcement scope. https://www.cga.gov.tw/GipOpen/wSite/ct?xItem=5138_ctNode=891&mp=999, June 2020.
- [22] <https://report.nat.gov.tw/ReportFront/PageSystem/reportFileDownload/C10802957/001>.
- [23] Bosio, Alberto, et al. "A reliability analysis of a deep neural network." 2019 IEEE Latin American Test Symposium (LATS). IEEE, 2019.

DL-Based AUV Position Prediction Using Odometry Data for Internet of Underwater Things

Made Adi Paramartha Putra^{*†}, Nengah Widya Utami[†],

I Gede Juliana Eka Putra[†], Dong-Seong Kim^{*}, and Jae-Min Lee^{*}

^{*}Department of IT Convergence Engineering, Kumoh National Institute of Technology, Gumi, South Korea.

[†]Accounting Information System, STMIK Primakara, Denpasar, Indonesia

[‡]Informatic Engineering, STMIK Primakara, Denpasar, Indonesia

mdparamartha95@kumoh.ac.kr^{*‡}, {widya,[†] gedejep[‡]}@primakara.ac.id, {dskim*, ljmpaul*}@kumoh.ac.kr

Abstract—In this study, a deep learning (DL)-based model to predict an autonomous underwater vehicle (AUV) position is proposed. The proposed DL model uses a deep concatenated multi-layer perceptron (DC-MLP) model with a one-to-one approach, where each position data is predicted separately to minimize prediction error. A real-world dataset from AUV is used to evaluate the performance of our proposed model and baseline model. Based on the comprehensive simulation, the performance of the DC-MLP model outperforms the others in terms of root mean squared error (RMSE), coefficient of determination, and final results of the AUV position prediction.

Index Terms—autonomous underwater vehicle, deep learning, position prediction.

I. INTRODUCTION

Unmanned underwater research is becoming increasingly possible because of developments in marine technology. An autonomous underwater vehicle (AUV) is a device that can travel a predefined path while exploring an underwater area. The AUV will return to the designated location for data processing when the exploration operation is over [1]. Due to the difficulty of underwater circumstances, sensor malfunctions might occur, causing a lot of issues, e.g., failing to classify the target [2] or route diverging from the designed one and consuming more power. Energy consumption is an important aspect in underwater operation, hence an energy efficient route is needed [3].

Additionally, to mitigate the location issue, the author in [4] proposes an AUV location prediction using a data collection scheme. The key idea is that during data collection, the AUV follows the predetermined path and simultaneously updates its location to the nearest sensor nodes while the others send it to their neighbors. A trajectory adjustment mechanism is used to overcome the energy issue from nearest node trajectories. The author also proposes a reliable time mechanism that only allows specific nodes to send data directly to the AUV. Another technique for location prediction in [5] was performed by estimating Doppler shift in the physical layer and reducing AUV communication with a belief propagation-neural network-based location prediction model. The author states that they successfully demonstrated the accuracy of location prediction based on extensive experimental work.

Based on the mentioned studies, there are no comprehensive studies that consider AUV position to be predicted using

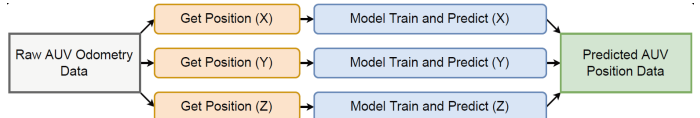


Fig. 1. The proposed one-to-one prediction for the AUV position

odometry data. Therefore, the major contributions of this paper are summarized as follows:

- Proposes a deep learning (DL)-based model to predict AUV position with a low error rate by using the x , y , and z axis from odometry data.
- Apply the one-to-one concept of data prediction to reduce the loss produced by the DL model.
- Comprehensive evaluation of the proposed DL model and the baseline models, e.g., gated recurrent unit (GRU) and long-short term memory (LSTM), using a real-world odometry dataset of AUV.

II. PROPOSED SYSTEM

The proposed one-to-one prediction for the AUV position is depicted in Fig. 1. Initially, the raw AUV odometry data is preprocessed to obtain three different axis positions, namely *position.x*, *position.y*, and *position.z*. Based on a one-to-one approach, each data input forwarded to the DL model will produce a single result. Therefore, each of those data points is forwarded to the proposed DL model to train and predict the next position of the AUV.

The deep concatenated multi-layer perceptron (DC-MLP) is employed from our previous work [6] in environmental data prediction. The model consists of two depths of MLP networks with a concatenation layer to merge the results of both networks. After that, a fully connected (FC) layer is added before the prediction layer. To avoid overfitting, the number of neurons of each MLP network is set to 32, where the FC layer is 8. After the model successfully produce predicted data of each AUV position, the system will combine it together to form an actual AUV position prediction.

III. RESULTS AND DISCUSSION

To evaluate model performance in predicting AUV position using odometry dataset [7], root mean squared error (RMSE)

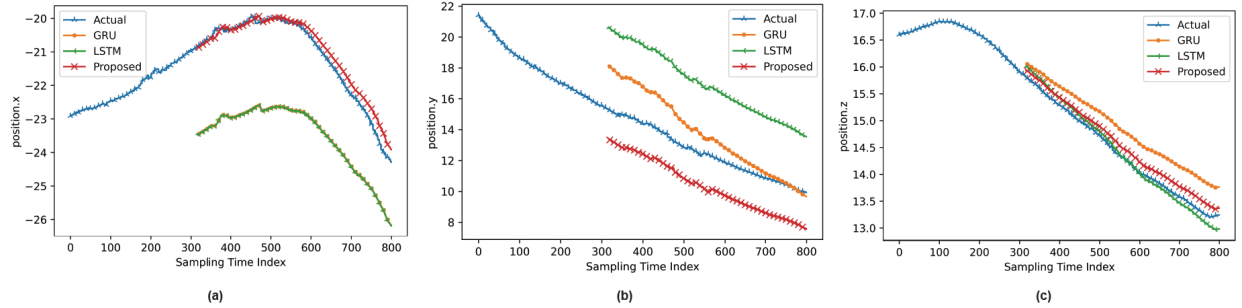


Fig. 2. The AUV actual and predicted position from all models compared. (a) x axis (b) y axis (c) z axis.

TABLE I
PERFORMANCE COMPARISON TO PREDICT AUV POSITION (X, Y, Z)

Model	Position.x		Position.y		Position.z	
	RMSE	R^2	RMSE	R^2	RMSE	R^2
GRU	1.9048	0.9921	4.2256	0.1816	0.5108	0.9788
LSTM	1.8924	0.9922	2.4632	0.7219	0.6260	0.9682
Proposed	1.3633	0.9960	2.7200	0.6609	0.3201	0.9917

and coefficient of determination (R^2) are used. Each position prediction result is evaluated using those two metrics. Comparison between actual data and predicted data from three different models investigated in this paper is illustrated in Fig. 2. As we can see, based on the first 450 predicted data points, the performance of the proposed DC-MLP is better than other models, especially in predicting the x axis. It is because the DC-MLP is able to learn from historical data better than others by using a concatenation layer in the proposed model. To further provide a better understanding of the models' performance, Table I shows RMSE and R^2 for each axis prediction. It can be observed that GRU performs poorly compared to the others for all axis. On the other hand, the LSTM model is able to perform better in predicting the y axis compared to the proposed model. Despite that result, the performance of LSTM is inferior compared to the proposed DC-MLP after combining all axes into one position prediction, as illustrated in Fig. 3.

IV. CONCLUSION

In this research, we employed a one-to-one method with odometry data to develop a DL-based AUV location prediction algorithm. The concatenation layer, a merging layer, and an MLP-based network were used to construct the proposed DL model. Numerous simulation results demonstrated that the suggested DL model outperformed other models in terms of RMSE and R^2 for the three examined axes when it comes to properly predicting AUV placement.

ACKNOWLEDGMENT

This research work was supported by Priority Research Centers Program through NRF funded by MEST(2018R1A6A1A03024003) and the Grand Information

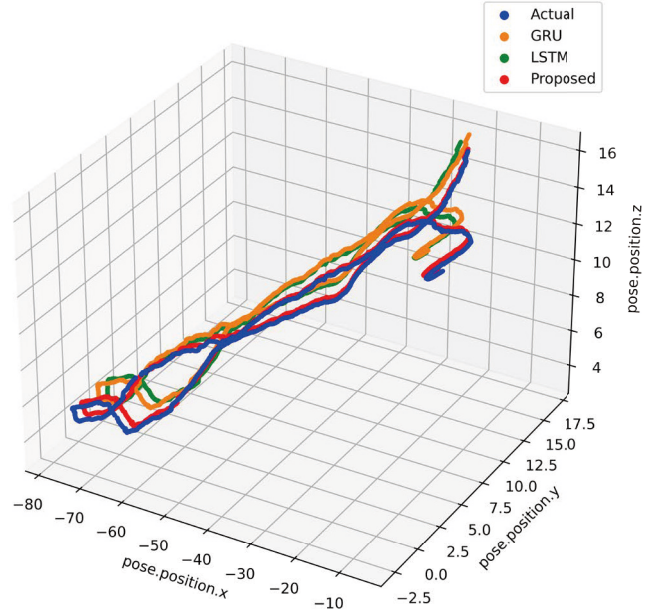


Fig. 3. The predicted AUV position over time based on all models compared.

Technology Research Center support program (IITP-2022-2020-0-01612) supervised by the IITP by MSIT, Korea.

REFERENCES

- [1] Y. Yang, Y. Xiao, and T. Li, "A survey of autonomous underwater vehicle formation: Performance, formation control, and communication capability," *IEEE Communications Surveys Tutorials*, 2021.
- [2] H. Tran-Dang and D.-S. Kim, "Energy-efficient cooperative routing in underwater acoustic sensor networks," *Journal of Advances in Information Technology*, 2019.
- [3] V.-S. Doan, T. Huynh-The, and D.-S. Kim, "Underwater acoustic target classification based on dense convolutional neural network," *IEEE Geoscience and Remote Sensing Letters*, 2022.
- [4] G. Han, X. Long, C. Zhu, M. Guizani, Y. Bi, and W. Zhang, "An auv location prediction-based data collection scheme for underwater wireless sensor networks," *IEEE Transactions on Vehicular Technology*, 2019.
- [5] S. Song, J. Liu, J. Guo, C. Zhang, T. Yang, and J. Cui, "Efficient velocity estimation and location prediction in underwater acoustic sensor networks," *IEEE Internet of Things Journal*, 2022.
- [6] M. A. P. Putra, A. P. Hermawan, D.-S. Kim, and J.-M. Lee, "Energy efficient-based sensor data prediction using deep concatenate mlp," in *IEEE Int. Conf. on Emerging Tech. and Factory Auto. (ETFA)*, 2021.
- [7] A. Mallios, E. Vidal, R. Campos, and M. Carreras, "Underwater caves sonar data set," *The International Journal of Robotics Research*, 2017.

Beam Divergence Angle and Transmission Power Adjustment of Underwater Optical Wireless Communication based on Reinforcement Learning

Huicheol Shin
KIOST
South Korea
shc0305@kiost.ac.kr

Yujae Song
Kumoh National Institute of Technology
South Korea
songyj@kumoh.ac.kr

Yongjae Kim
KIOST
South Korea
yongjaekim@kiost.ac.kr

Abstract—In this paper, we analyze SNR (signal-to-noise ratio) performance between transmission node (i.e., underwater sensors) fixed to the seabed in an underwater wireless optical communication environment and receive node (i.e., ships, unmanned surface vehicles) where shaking occurs due to wind and wave at sea surface. Furthermore, based on the analysis results, we present a deep reinforcement learning based beam divergence angle and transmission power adjustment algorithm for efficient battery operation of the transmit node while minimizing disconnection of underwater optical wireless communication (UOWC) links.

Index Terms—Reinforcement learning, underwater optical wireless communication, beam divergence angle

I. INTRODUCTION

Optical communication in an underwater wireless communication environment has the advantage of providing high transmission speed and low delay communication performance compared to generally used acoustic communication. However, there are limitations such as short transmission distances, and many researchers have recently conducted various studies to overcome them. [1], [2]

This paper performs deep reinforcement learning-based beam divergence angle and transmission power adjustment research to overcome the disconnection of underwater optical wireless communication(UOWC) link due to misalignment between transmission node and receive node.

II. SYSTEM MODEL

In this work, we consider a laser based UOWC network that consists of a transmission node (i.e., underwater sensors) and receive node (i.e., ships, unmanned surface vehicles), as shown in Fig 1. Specifically transmission node is fixed to the sea floor and measure a variety of underwater environment data. Meanwhile, using global positioning system (GPS) information, receive node move to the point where underwater sensor is vertically located according to a pre-determined route.

In an UOWC environment, the signal-to-noise-ratio (SNR) of communication link can be calculated as shown in the following equation. [3]

$$SNR = \frac{I_P}{I_N}, \quad (1)$$

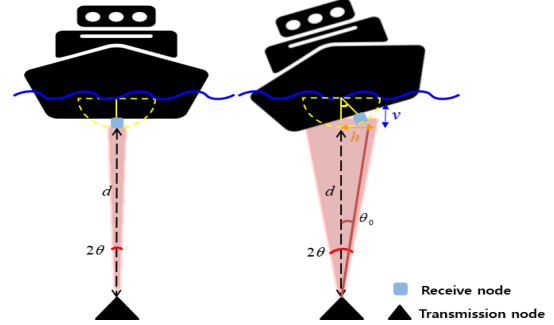


Fig. 1. UOWC system model

where I_P is the received optical current and I_N is noise current. I_P is calculated through the performance of photodiode and received power, of which the received power can be obtained as follows:

$$P_R = P_T \eta_T \eta_R L G, \quad (2)$$

where P_T is the transmission power, η_T and η_R are transmission and receive efficiency, respectively, L is the propagation loss, and G is the geometric gain. The propagation loss of an optical signal in the underwater environment can be calculated as follows:

$$L = \exp \left\{ c(\lambda) \frac{d}{\cos(\theta)} \right\}, \quad (3)$$

where $c(\lambda)$ is the attenuation coefficient, d is distance of communication link and θ is the beam divergence angle of optical signal. The geometric gain of underwater optical channel can be computed as follows:

$$G = \begin{cases} \frac{A_r \cos(\theta_0)}{2\pi d^2 [1 - \cos(\theta)]}, & \theta_0 \leqslant \theta \\ 0, & \text{otherwise,} \end{cases} \quad (4)$$

where A_r is aperture area of optical modem and θ_0 is the inclination angle between transmission and receive node. As shown in Fig. 1, the inclination angle according to the position change of the receive node is determined by the horizontal movement h and the vertical movement v . According to the above equation, G can be obtained only when the beam divergence angle of optical signal at the transmit node is greater

than inclination angle. Accordingly, in order to transmit data in the UOWC, the receive node must be located within the beam range and outside that range, the communication link will be disconnected. Therefore, the transmission node needs to adjust the beam divergence angle larger than the inclination angle. In addition, control of transmission power is also required for efficient battery consumption. To this end, we proposed a two-phase deep Q-network (DQN) based reinforcement learning algorithm for determining the beam divergence angle and transmission power of the transmission node. [4]

III. PROPOSED ALGORITHM

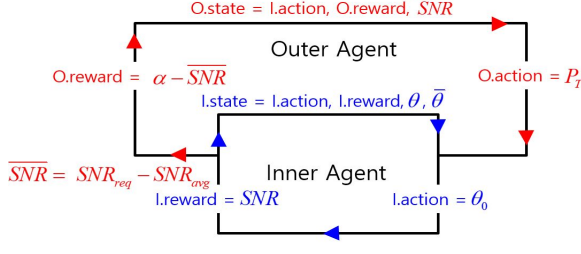


Fig. 2. Two-phase DQN agent

The proposed reinforcement learning model, in which the transmission node is a decision maker, consists of an inner agent and an outer agent, which learn the beam divergence angle and transmission power, respectively. The inner agent and outer agent are learned on state, action and reward information, and each information is shown in Fig. 2.

The inner agent predicts movement and determines the beam divergence angle through repeated learning in an environment where the receive node location is unknown. If $\theta < \theta_0$, the SNR becomes zeros, and when $\theta = \theta_0$, the SNR becomes maximum. The outer agent can obtain a reward using the gap (SNR_{gap}) between the required minimum performance (SNR_{req}) and the average SNR (SNR_{avg}) calculated based on the inner agent learning results during the specific iteration n. thus, the outer agent controls the transmission power so that SNR_{avg} is as close to SNR_{req} as possible.

IV. SIMULATION RESULT

To measure the performance of the proposed algorithm, we performed the simulation in an environment in which the position of receive node changed irregularly.

Fig. 3 shows the learning result of the inner agent that controls the beam divergence angle by learning the movement of the receive node. As a result, it can be confirmed that the beam divergence angle is maintained larger than the inclination angle to prevent the link disconnection. Furthermore, at the same time, the beam divergence angle is close to the inclination angle to increase SNR.

Fig. 4 illustrates the performances when maximizing the transmission power (only inner) and adjusting the transmission power with the outer agent (inner-outer). The performance of the outer agent is better as the difference between SNR_{avg} and SNR_{req} is smaller, that is, the closer the SNR_{gap} is to zero. Therefore, it can be confirmed that the outer agent appropriately controls the transmission power.

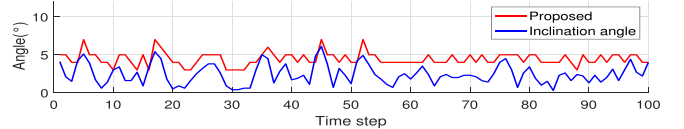


Fig. 3. Inner agent simulation result

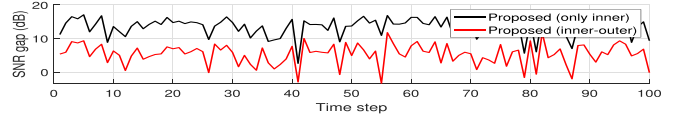


Fig. 4. Outer agent simulation result

Finally, Fig. 5 shows the SNR value according to the change in the beam divergence angle at a specific inclination angle and learning result of proposed algorithm.

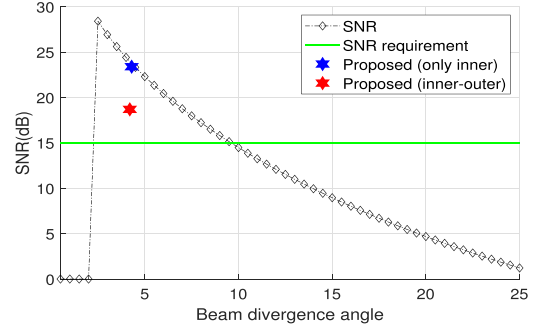


Fig. 5. Reinforcement learning result

V. CONCLUSION

In this work, we implement a beam divergence angle and transmission poser control model base on reinforcement learning for efficient battery operation while predicting irregular movement of receiving node and maintaining communication link. Based on this result, we intend to expand the research to three-dimensions by performing simulation using real-sea motion data.

ACKNOWLEDGMENT

This research was a part of the project titled 'Development of smart maintenance monitoring techniques to prepare for disaster and deterioration of port infra structures', funded by Ministry of oceans and fisheries. Also, this work was supported by the Basic Science Research Program through the National Research Foundation of Korea, Ministry of Education, Science and Technology under Grants NRF2020R1F1A1074175.

REFERENCES

- [1] N. Saeed, A. Celik, T.Y. Al-Naffouri and M. Alouini, "Underwater optical wireless communications, networking, and localization: A survey," *Ad Hoc Networks*, vol.94, pp.1-34, 2019.
- [2] Y. Song, "Underwater acoustic sensor networks with cost efficiency for Internet of Underwater Things," in *IEEE Trans. Ind. Electron.*, vol.68, pp.1707-1716, Feb. 2021.
- [3] A. Celik et al., "End-to-end performance analysis of underwater optical wireless relaying and routing techniques under location uncertainty," *IEEE Trans. Wirel. Commun.*, vol.19, pp.1167-1181, 2020.
- [4] J. Jeong, S.H. Lim, Y. Song and S.W. Jeon, "Online learning for joint beam tracking and pattern optimization in massive MIMO systems," *IEEE INFOCOM 2020*, pp.764-773, 2020..

Single enhancement techniques for underwater stereo vision

Hong-Gi Kim

Maritime ICT R&D Center, KIOST

Busan, Republic of Korea

hgkim@kiost.ac.kr

Jung-Min Seo

Maritime ICT R&D Center, KIOST

Busan, Republic of Korea

jmseo@kiost.ac.kr

Soo Mee Kim

Maritime ICT R&D Center, KIOST

Busan, Republic of Korea

smeekim@kiost.ac.kr

Abstract— In order to ensure safety and efficiency of unmanned underwater works underwater situation visualization is an essential technique among unmanned automatic technologies. Although optical color images are used widely for underwater visualization, physical distortions such as color casting and blurring are occurred in underwater color images and it leads to uncertainty in depth estimation for stereo vision. In this study, we applied image fusion and deep learning techniques to improve the underwater image quality. The performance of single image enhancement techniques was evaluated by underwater image quality measure (UIQM) and underwater color image quality evaluation (UCIQE). Single image enhancement increased quantitatively UIQM and UCIQE by 82.8 % and 35.8 % on the average, respectively and improved the color accuracies of reconstructed red, green and blue – depth (RGB-D) point clouds compared to the original images. Single underwater image enhancement techniques improved the accuracies of depth estimation for underwater stereo vision.

Keywords—Underwater visualization, Unmanned automatic techniques, Underwater stereo vision, Single image enhancement

I. INTRODUCTION

Since safety and efficiency issues always exist in human-based underwater works, unmanned automatic technologies are actively used to overcome the issues. Environmental recognition is essential unmanned automation technology for underwater works, and optical camera is an imaging sensor widely used for underwater visualization. The underwater color image is deteriorated by color casting and blurring due to wavelength-dependent attenuation of the visible light [1]. In this study, we developed a underwater stereo vision system constructed of two optical cameras applying single image enhancement techniques. Also, we evaluated the performances of image enhancement and stereo vision.

II. METHOD

2.1 Underwater stereo vision system

We built an underwater stereo vision system with two commercial underwater cameras (Eagle IPZ/4000, OTAQ, United Kingdom). For geometric calibration of two underwater cameras, we used a self-designed RGB phantom (30 kg, 1.2 x 1.2 m²), which is composed of red, green, and blue colored plates. Two cameras acquired simultaneously 28 image pairs of RGB phantom placed at different depths (2 to 2.3 m) and distances (4 to 5.5 m) from the vision system. A transformation matrix between two camera coordinates was estimated from the corner points extracted on the 28 image pairs.

2.2 Single underwater image enhancement techniques

In order to enhance the optical image pairs for stereo vision, we applied image fusion and deep learning techniques. Image fusion conducts three successive steps of white-balancing,

contrast and edge enhancing by CLAHE and UMP, and fusing of two images enhanced in the second step [2]. Generative adversarial network (GAN) which consists of a generator and discriminator networks was adapted [3]. Training datasets are constructed with two groups of clean and underwater images. And then cycle-consistent adversarial networks (CycleGAN) and underwater GAN (UGAN) were trained to improve the color casting and blurring [4, 5]. We evaluated the enhancement performance by underwater image quality measure (UIQM) and underwater color image quality evaluation (UCIQE) [6, 7].

2.3 Underwater stereo vision

The stereo data was computed after enhancing the image pairs simultaneously taken by two cameras [8]. The conventional processing of image rectification, disparity map estimation RGB-D point cloud reconstruction were performed for underwater stereo vision.

III. RESULT

Fig. 1 compares the original and enhanced underwater images. We confirmed qualitative and quantitative improvement by single image enhancement resulting in UIQM and UCIQE increases by 82.8 % and 35.8 %, respectively. Fig. 2 compares the image pairs of two cameras, the rectified images, the estimated disparity maps, and the reconstructed RGB-D point clouds from the original and enhanced underwater images. We evaluated the color accuracies of the point clouds reconstructed from the original and enhanced underwater images by the difference from the ground data. Single image enhancement was helped to reconstruct more accurate RGB-D point clouds showing the increased color accuracy by 35 % comparing to the point clouds reconstructed from the original underwater images.

IV. CONCLUSION

We developed an underwater stereo vision system of two underwater optical cameras and single image enhancement techniques were applied for obtaining more accurate underwater stereo data. Comparing to original underwater image, the enhancement performance after applying single image enhancement was achieved by increases of 82.8 % and 35.8 % in terms of UIQM and UCIQE, respectively. The color accuracy of the RGB-D point clouds reconstructed from the enhanced underwater images was increased by 35 %



Fig. 1. The original (a) and the enhanced (b) underwater images.

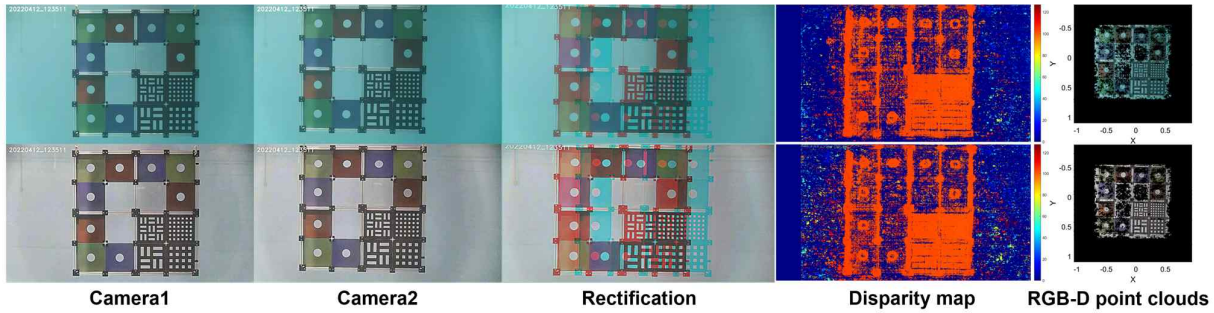


Fig. 2. The simultaneous images taken by two cameras, the rectification images, the estimated disparity maps, and the reconstructed RGB-D point clouds of RGB phantom: underwater data before (top) and after (bottom) enhancement

comparing to ones from the original images. Single underwater image enhancement techniques improved the accuracies of depth estimation for underwater stereo vision.

ACKNOWLEDGMENT

This research was a part of the project titled ‘Development of unmanned remotely construction aided system for harbor infrastructure’, funded by the Ministry of Oceans and Fisheries, Korea and a part of the National Research Foundation of Korea (Development of Underwater Stereo Camera Stereoscopic Visualization Technology, NRF-2021R1A2C2006682) with funding from the Ministry of Science and ICT in 2022.

REFERENCES

- [1] C. D. Mobley and C. D. Mobley, “Light and Water: radiative transfer in natural waters,” Academic Press, 1994
- [2] C. O. Ancuti, C. Ancuti, C. De Vleeschouwer and P. Bekaert, “Color balance and fusion for underwater image enhancement,” IEEE Transactions on image processing, vol. 27, no. 1, pp. 379-393, 2017
- [3] I. Goodfellow, et al., “Generative adversarial nets,” Advances in neural information processing system, vol. 27, 2014
- [4] J. Y. Zhu, T. Park, P. Isola and A.A. Efros, “Unpaired image-to-image translation using cycle-consistent adversarial networks,” In Proceedings of the IEEE international conference on computer vision, pp. 2223-2232, 2017
- [5] C. Fabbri, M. J. Islam and J. Sattar, “Enhancing underwater imagery using generative adversarial networks,” IEEE International Conference on Robotics and Automation, pp 7159-7165, 2018
- [6] K. Panetta, C. Gao, S. Agaian, “Human-visual-system-inspired underwater image quality measures,” IEEE Journal of Oceanic Engineering, vol. 41, no. 3, pp. 541-551, 2015
- [7] M. Yang and A. Sowmya, “An underwater color image quality evaluation metric.” IEEE Transactions on Image Proc, vol. 24, no.12, pp. 6062-6071, 2015.
- [8] R. Hartley and A. Zisserman, “Multiple view geometry in computer vision,” Cambridge university press, 2003

A Brief Survey of Massive MU-MIMO User Scheduling in Various Network

Hyunwoo Jung

*Department of information and communication technology
Korea Institute Ocean Science and Technology
Busan, Korea
hyunwoo@kiost.ac.kr*

Yongjae Kim

*Department of information and communication technology
Korea Institute Ocean Science and Technology
Busan, Korea
yongjaekim@kiost.ac.kr*

Abstract—Massive multiple input multiple output (MIMO) is a technique that adopts a thousand or hundreds of antennas in a base station (BS) to simultaneously deliver communication services to a hundred or dozens of users at the same frequency and time resource. Massive MIMO has several advantages such as low power consumption, high data rate, etc. Together with a massive MIMO regime, user scheduling can further improve the sum rate of wireless networks. Thereby, massive multi-user MIMO (MU-MIMO) scheduling is often considered a promising solution for various wireless communication networks.

In this paper, the research works on massive MU-MIMO user scheduling in different duplex operations, i.e. time division duplex (TDD) and frequency division duplex (FDD), and in different network schemes, i.e. internet-of-things (IoT) network and millimeter wave (mmWave) network, is briefly studied.

Index Terms—massive MIMO, scheduling, massive MU-MIMO scheduling

I. INTRODUCTION

Along with the advent and permeation of advanced communication technologies, e.g., IoT and mmWave networks, a demand for a higher capacity, and lower latency wireless communication has been growing exponentially. To cope with ever-increasing network traffic, massive MU-MIMO that employ spatial and multi-user diversity to further improve the network capacity with a huge number of BS antennas for serving a large number of users have been firstly proposed by Thomas Marzetta [1]. Massive MU-MIMO is a technique that adopts a thousand or hundreds of antennas in a BS to simultaneously deliver communication service to a hundred or dozens of users at the same frequency and time resource. Massive MIMO has several advantages which are low power consumption, system robustness, high spectral efficiency, and most importantly high system capacity.

Meanwhile, billions of user equipments (UEs) are expected to be connected by forming machine-to-machine, machine-to-human, and human-to-human networks in future wireless communication schemes. In such a scenario where there exists a very large number of users, by scheduling UEs that have low channel correlation matrices and low interference with each other, the network sum rate can be further improved. Thereby, massive MIMO and multi-user scheduling are often jointly considered in various wireless communication networks.

However, the investigations summarizing recent research works on massive MU-MIMO scheduling have not been per-

formed yet to the best of the authors' knowledge. Therefore, in this paper, the research works on massive MU-MIMO user scheduling in different duplex operations, i.e. TDD and FDD, and in different network schemes, i.e. IoT and mmWave network, is briefly studied.

II. MASSIVE MU-MIMO USER SCHEDULING

In a massive MU-MIMO regime, simultaneous user scheduling is possible by applying beamforming for the downlink and matched filter for the uplink when the number of BS antennas is larger compared to the number of users [2]. Taking into account an uplink and downlink, choosing duplex schemes in massive MU-MIMO is a crucial issue to make the system trade-off between the complexity and maximum sum rate of the system. In this section, the analysis and related studies of the massive MU-MIMO scheduling algorithms on both TDD and FDD operations are observed.

A. Time division duplex

In general, massive MU-MIMO operates on TDD to reduce the system complexity as TDD operation relies on the channel reciprocity theorem. However, in TDD massive MU-MIMO system, a channel state information (CSI) obtained would be contaminated by pilot transmission from the user of another cell due to the limitations of coherence time [3]. In [4], sum-rate improvement in TDD massive MIMO system with user grouping/cluster technique, intra-group and inter-group user selection algorithm, and antenna scheduling algorithm is studied taking into account zero-forcing and minimum mean squared error precoding schemes. [5] proposes a low-complexity joint antenna selection and user scheduling algorithm using adaptive Markov Chain Monte Carlo algorithm in multi-cell multi-user TDD downlink massive MIMO systems considering a trade-off between network performance and computational complexity. In [6], an optimization framework that jointly solves the user scheduling, power control, and precoding design problem is proposed for massive MIMO downlink systems with imperfect CSI caused by pilot contamination.

B. Frequency division duplex

Although massive MU-MIMO generally operates on TDD, the research on FDD massive MU-MIMO is still important for

compatibility with recent cellular systems as typical cellular systems make use of spectrum dedicated for FDD operation. The disadvantage of FDD operation is that due to the higher dimensionality of massive MU-MIMO, the system consumes a huge spectrum as well as the power to obtain CSI. To mitigate high overhead for the CSI feedback from UEs to BS, the first two-stage precoding called joint spatial division and multiplexing (JSDM) which employs spatial correlation of massive MIMO channel is proposed [7]. In [8], the establishment of the NP-hardness of finding the optimal users scheduling solution in JSDM for the downlink of FDD massive MIMO is proposed. In [9], a new agglomerative clustering method and signal-to-leakage-plus-noise ratio-based cluster scheduling is proposed in order to simplify the user clustering process and suppress the residual inter-cluster interference in two-stage precoding transmission.

III. MASSIVE MU-MIMO WITH UE SCHEDULING IN VARIOUS NETWORK

Because of the high data rate and energy-efficient nature of massive MU-MIMO, the system is often considered a promising solution in various wireless communication networks, such as IoT networks and mmWave networks, where massive connectivity services are expected to be required. In this section, the implementation of massive MU-MIMO with UE scheduling in various network schemes is described.

A. Internet of things network

IoT network is the next generation network scheme where billions of physical layer devices will be connected to the internet, and a huge amount of information will be shared from device to user or from device to device. In a massive MIMO-enabled IoT scenario, the number of UEs would be larger than the number of BS antennas. Thereby, scheduling is a necessary issue to be addressed. [10] proposes a general framework for the analysis of large-scale MIMO-enabled IoT systems involving multiple types of devices with varying configurations and requirements, taking into account the randomness of spatial location and time traffic attributes. Through the analysis results, the optimal number of scheduling by device type, which maximizes spatial average packet throughput while satisfying the device's delay constraints, is investigated.

B. Millimeter wave network

MmWave bands ranging from 30GHz to 100GHz have poor path loss characteristics compared to conventional radio frequency bands ranging below 30GHz. Large antenna arrays in Massive MIMO give the system an extra gain and diversity which provides higher throughput to the system. Therefore, massive MIMO has become a prerequisite for operating in the mmWave networks, i.e. fifth-generation (5G), fifth-generation and beyond (5GB), and sixth-generation (6G) wireless networks. In order to maximize the quality of services of all UEs in the massive MU-MIMO mmWave system, UE scheduling is necessary. [11] proposes a novel proportional fairness-discrete

Fourier transform scheme for mmWave massive MIMO downlink system to jointly optimize user scheduling and hybrid beamforming which considers both system throughput and user fairness.

IV. CONCLUSION

In this paper, various scheduling algorithms in different massive MU-MIMO systems have been studied. A brief analysis and research work with TDD and FDD duplex operation and massive MU-MIMO with UE scheduling in IoT network and mmWave network have been introduced. Based on this research, we will work on the reinforcement learning-based UE scheduling algorithm in a massive MU-MIMO enabled-IoT network.

ACKNOWLEDGMENT

This research was a part of the project titled ‘Development of Polar Region Communication Technology and Equipment for Internet of Extreme Things (IoET),’ funded by the Ministry of Science and ICT (MSIT)

REFERENCES

- [1] T. L. Marzetta, “Noncooperative Cellular Wireless with Unlimited Numbers of Base Station Antennas,” *IEEE Trans. Wirel. Commun.*, vol. 9, no. 11, pp. 3590-3600, Nov. 2010, doi: 10.1109/TWC.2010.092810.091092.
- [2] T. A. Sheikh, J. Bora and A. Hussain, “A Survey of Antenna and User Scheduling Techniques for Massive MIMO-5G Wireless System,” *Conf. Curr. Trends Comput. Electr. Electron. Commun. (CTCEEC)*, Mysore, India, Sep. 2017, pp. 578-583, doi: 10.1109/CTCEEC.2017.8455177.
- [3] O. Elijah, C. Y. Leow, T. A. Rahman, S. Nunoo and S. Z. Iliya, “A Comprehensive Survey of Pilot Contamination in Massive MIMO—5G System,” *IEEE Commun. Surv. Tutor.*, vol. 18, no. 2, pp. 905-923, Nov. 2015, doi: 10.1109/COMST.2015.2504379.
- [4] T. A. Sheikh, J. Bora and M. A. Hussain, “Sum-Rate Improvement in Massive MIMO System with User Grouping and Selection, and Antenna Scheduling Scheme,” *Wirel. Pers. Commun.*, vol. 120, pp. 1043-1056, Apr. 2021. <https://doi.org/10.1007/s11277-021-08503-2>.
- [5] S. Maimaiti, G. Chuai, W. Gao, et al., “A low-complexity algorithm for the joint antenna selection and user scheduling in multi-cell multi-user downlink massive MIMO systems,” *EURASIP J. Wirel. Commun. Netw.*, vol. 208, Aug. 2019, doi: 10.1186/s13638-019-1529-7.
- [6] J. Choi, N. Lee, S. Hong and G. Caire, “Joint User Scheduling, Power Allocation, and Precoding Design for Massive MIMO Systems: A Principal Component Analysis Approach,” *IEEE Int. Symp. Inf. Theory (ISIT)*, Vail, CO, USA, Aug. 2018, pp. 396-400, doi: 10.1109/ISIT.2018.8437617.
- [7] A. Adhikary et al., “Joint Spatial Division and Multiplexing for mm-Wave Channels,” *IEEE J. Sel. Areas Commun.*, vol. 32, no. 6, pp. 1239-1255, June 2014, doi: 10.1109/JSAC.2014.2328173.
- [8] A. Maatouk, S. E. Hajri, M. Assaad and H. Sari, “On Optimal Scheduling for Joint Spatial Division and Multiplexing Approach in FDD Massive MIMO,” *IEEE Trans. Signal Process.*, vol. 67, no. 4, pp. 1006-1021, Feb. 2019, doi: 10.1109/TSP.2018.2886163.
- [9] X. Sun, X. Gao, G. Y. Li and W. Han, “Agglomerative User Clustering and Cluster Scheduling for FDD Massive MIMO Systems,” *IEEE Access*, vol. 7, pp. 86522-86533, June 2019, doi: 10.1109/ACCESS.2019.2923246.
- [10] Q. Zhang, H. H. Yang, T. Q. S. Quek and S. Jin, “Spatiotemporal Modeling of Massive MIMO Systems With Mixed-Type IoT Devices: Scheduling Optimization With Delay Constraints,” *IEEE Internet Things J.*, vol. 8, no. 12, pp. 10146-10159, June 2021, doi: 10.1109/IJOT.2021.3051055.
- [11] X. Gao, X. Wu, Z. Zhang and D. Liu, “Low Complexity Joint User Scheduling and Hybrid Beamforming for mmWave Massive MIMO Systems,” *Pers. Indoor Mobile Radio Commun. (PIMRC)*, London, UK, Oct. 2020, pp. 1-6, doi: 10.1109/PIMRC48278.2020.9217049.

Development of In-Situ Underwater Gamma-ray Spectroscopy System

Jungmin Seo
Maritime ICT R&D Center
Korea Institute of
Ocean Science & Technology
Busan, South Korea
jmseo@kiost.ac.kr

Soo Mee Kim
Maritime ICT R&D Center
Korea Institute of
Ocean Science & Technology
Busan, South Korea
smeekim@kiost.ac.kr

Abstract—Because Korea and neighboring countries, Japan and China are highly dependent on nuclear power generation, it is necessary to monitor periodically the radiation leaks around nuclear power plants. In this study, a underwater gamma-ray spectroscopy system was built with a NaI and PMT-based gamma sensor, a waterproof case and a communication system. We confirmed the normal operation of in-situ acquisition of underwater radiation spectra guaranteeing the waterproofness up to a depth of 3m. The underwater gamma-ray spectrometer can be applied for periodic in-situ monitoring of the accident radiation leakages or the suspicious changes of radiation dose level around nuclear power plants or aquafarms.

Keywords—underwater radiation spectrometer, NaI and PMT based gamma-ray detector, waterproof casing system

I. INTRODUCTION

For environmental radiation measurement, GM tube sensor is generally used, but its life span is relatively short for continuous measurement. On the contrary, the scintillation radiation detector shows the reliable detection efficiency for environmental radiation spectrometry [1-2]. In this study, we built a underwater gamma-ray spectrometer, which can be applied for in-situ monitoring of sudden radiation leakages into ocean, and confirmed its normal operation of measuring gamma-ray spectra and the waterproofness through water tank experiments.

II. UNDERWATER GAMMA-RAY SPECTROSCOPY SYSTEM

The Figure 1 shows the configuration diagram of the in-situ underwater spectroscopy system. We chose a 905-4 scintillation detector (ORTEC, USA), which is constructed with a 3 (dia.) x 3 (len.)-inch NaI(Tl) crystal and a PMT, as gamma-ray sensor[3]. In Crystal, a Cs-137 source with an intensity of 0.1 uCi was used to check whether the detection works normally.[4] Since the selected radiation detector supports the USB communication, the underwater spectroscopy system was configured by changing to POE communication method that can connect power and communication from the outside in order to overcome the limit of USB-based communication distance of 5 m. A USB over IP device converts from USB to Ethernet communication methods for an intermediate data communication.

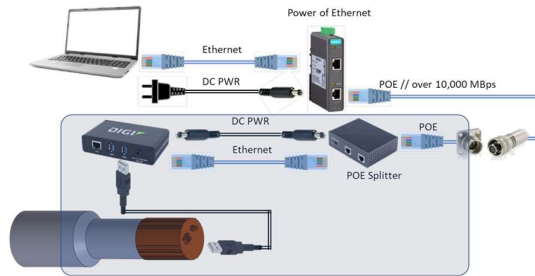


Fig. 1. Construction diagram of underwater spectroscopy system

The water-protective case was designed for minimizing the decrease in the detection performance of the detector and preventing foreign substances such as moisture from penetrating the inside. Figure 2 shows the structure of the designed waterproof casing. The Al-sealed crystal part of the gamma-ray detector was exposed directly to water. An O-ring was applied around it, and the other part of the detector was sealed by applying an O-ring to the other cover. The inside of the protective case is composed of a device that can fix the gamma-ray detector, and a USB over IP device and waterproof connector to communicate the measured spectra.

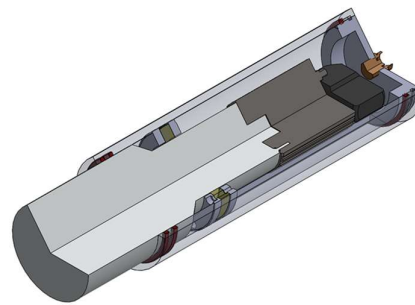


Fig. 2. waterproof case for underwater gamma-ray spectroscopy

Figure 3 shows the completed fabrication and assembly. The waterproof and detection performances were confirmed through water tank experiments.



Fig. 3. Assembled whole system geometry

III. EXPERIMENTS AND RESULTS

The waterproof performance was checked first before assembling the sensor by shutting with a dummy cover. And then the assembled underwater gamma-ray spectroscopy system with the NaI detector was fixed at a depth of 2 m in a water tank. We confirmed that there is no trace of moisture permeation inside the case for 24 hours.

In addition, we checked whether the underwater gamma-ray spectroscopy system can measure normally in the water tank as shown in Figure 4. A Cs-137 point source (0.1 uCi) was placed at various distances (0 and 50 cm) from the waterproofing spectroscopy system and then the gamma-ray spectra was measured for 10 minutes. Also, a background spectrum was measured by removing the Cs-137 point source. Figure 5 shows the measured spectra of background and Cs-137 being apart from the underwater spectroscopy system by 0 cm and 50 cm, respectively. The radiation dose from the source or the atmosphere was measured according to each distance in the water, and it was confirmed that the radiation dose can be sufficiently measured in the water through the above series of experiments.

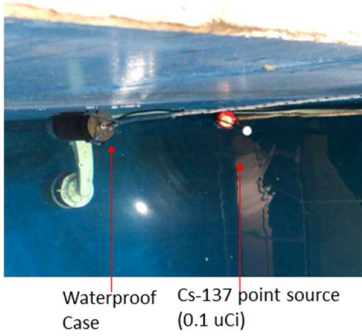


Fig. 4. Experimental set-up for evaluation of detection performance

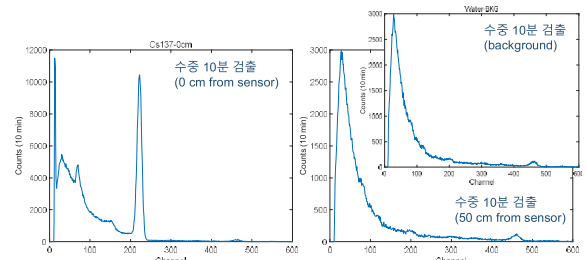


Fig. 5. Measured underwater radiation spectra of background and Cs-137 point source (0.1 uCi) being apart by 0 and 10 cm

IV. CONCLUSION

We constructed an in-situ underwater gamma-ray spectroscopy with a commercial NaI scintillation detector and self-designed waterproof casing. The waterproof casing was designed to guarantee minimizing the reduction of the detection performance. We confirmed the 24-hr waterproofness and the normal operation of measuring gamma-ray spectra by the underwater gamma-ray spectrometer can be applied for periodic in-situ monitoring of the accident radiation leakages or the suspicious changes of radiation dose level around nuclear power plants or aquafarms.

ACKNOWLEDGMENT

This research was a part of the project titled ‘Development of Smart Processing Technology for Sea Foods’, funded by the Ministry of Oceans and Fisheries, Korea.

REFERENCES

- [1] Joohyun Lee, A Study on Development of Radiation Sensor Module for Life Radiation Measurement, KERIS Theses & Dissertations
- [2] Hyunduk Kim, Byunghun Han, Chea-Seok Lee, Gyuseong Cho, Hojong Chang, “Research on Key Technology for realization of living environment radiation(Cs-137) measurement system”, Conference on Information and Control Systems, 2020, pp 472-473
- [3] “905 Series NaI(Tl) Scintillation Radiation Detectors”, ORTEC Homepage, accessed Aug 12, 2020, <https://www.ortec-online.com/products/radiation-detectors/scintillation-detectors/scintillation-detector-types/905-series>
- [4] Seung-Tak Ra, Joo-Hyun Lee, Seung-Ho Lee, “Design of Wide-Range radiation measurement system using GM Tube and NaI(Tl) Detector”, Journal of IKEEE.Vol.21, No.2, 2017, pp. 146-149

Analysis of Signal Processing Using Water Surface Elevation Data

1st UkJae Lee
Coastal Development and Ocean Energy Research Center
Korea Institute of Ocean Science and Technology
Busan, Korea
fukjae@kiost.ac.kr

4th JiYoung Kim
Renewable Energy Group
New & Renewable Energy Laboratory
Kepco Research Institute
Daejeon, Korea
jy_kim@kepco.co.kr

2nd HongYeon Cho
Marine Bigdata Center
Korea Institute of Ocean Science and Technology
Busan, Korea
hycho@kiost.ac.kr

5th Yunzheng Ge
First Institute of Ocean Energy Research Center
Qingdao, China
gyz1248@163.com

3rd DongHui Ko
Coastal Development and Ocean Energy Research Center
Korea Institute of Ocean Science and Technology
Busan, Korea
kodh02@kiost.ac.kr

Abstract— This study proposed additional techniques for wave spectrum analysis using water surface elevation observed by an Oceanographic and Meteorological Observation Tower on the west coast of the Korean Peninsula. The additional techniques used in this study constitute a smoothing method, which can solve the confidence interval range problem of the estimated spectrum in the frequency domain. When the smoothing method was applied, the confidence interval range of the estimated spectrum decreased approximately four times compared to that of the existing estimated spectrum. This increased the accuracy of the estimated peak wave period, and the peak wave period distribution showed variations of 10% and 7.3% at two analysis points. Moreover, for optimal smoothing, the smoothing number according to the range of the significant wave height was calculated using the root mean square error. As the significant wave height increased, the smoothing number increased owing to an irregular spectrum energy density.

Keywords— water surface elevation, smoothing, significant wave height, peak wave period

I. INTRODUCTION

The major parameters for distinguishing irregular oceanographic characteristics are the wave height and period, which are generally analyzed through water surface elevation (WSE, $\eta(t_i)$). With the development of oceanographic observation systems in recent years, wave information that enables various wave analyses can be easily acquired, and the importance of wave observation data has been rising. Methods for analyzing irregular wave characteristics include irregular wave spectrum analysis method, which analysis spectrums in the frequency domain[1]. The spectrum analysis method, which is one of the methods to calculate the major factors of waves, calculates the distribution of wave energy using a frequency function, as well as the period and area corresponding to the frequency of the largest energy density[2]. In addition, it assumes that numerous waves in the ocean are composed of many sine waves with different amplitudes and frequencies. In contrast, Pierson and Marks (1952) and Casas Prat (2008) proposed a wave spectrum analysis method, which was used to study the estimation of spectral distribution in the area of interest, extreme value analysis, and a numerical model of wave deformation through the given parameters (wave height and period) calculated

using observation systems[3],[4]. In the process of calculating the peak wave period among the wave parameters using the wave spectrum analysis method, the spectrum shows two or more peaks owing to the combination of swell waves and winds[5]. Rodriguez and Soares (1999) conducted a study on the bimodal spectrum shape through numerical analysis[6]. In this study, standardized the spectrum analysis method, one of the wave analysis methods, stepwise using WSE data observed through wave observation systems and used a data filter method to apply appropriate wind-wave standards for the Korean Peninsula. In addition, a performance upgrade and application values for the program were proposed through a data smoothing method to improve the accuracy of the calculated spectrums.

II. DATA AND METHOD

A. Observed Data

Korea Electric Power Corporation installed two Oceanographic and Meteorological Observation Towers in the western sea to build an offshore wind farm, which investigates wind and sea conditions. The WaveGuide system, which was developed by Delft in 1996, used in the observation can observe wave heights and directions. It is installed in the meteorological observation tower platform and is controlled by a WaveGuide server, and the data are transmitted by a remote system. The time interval of the observation data (WSE) is 200 ms (0.2 s). The period of the observation data used in this study ranged from July 2013 to July 2014 (approximately 7 months, 170 days excluding omissions) for HeMOSU-1 and from November 2013 to April 2014 (approximately 5 months, 133 days excluding omissions) for HeMOSU-2. The data omissions may result from the system error and maintenance period of the equipment.

B. Signal Processing Analysis

The wave spectrum analysis process is performed in the time domain and the frequency domain, and the analysis is performed through the following process.

- Time Domain : Remove the linear trend, Data window, Data filter

- Frequency Domain : Spectrum periodogram, Data smoothing

The data have a trend and the homogeneity of the data is broken owing to external effects such as tides in the observation data; hence, the data trend must be removed. To verify the trend in time-series data, the Mann-Kendall test, one of the nonparametric statistical techniques, was used, and the mean sea level correction was performed by removing the linear trend. Subsequently, a data window technique was applied to minimize energy leakage that occurs in the domain that is not an integer multiple ($n\Delta f$) of the frequency interval (Δf) when analyzing actual time-series data. This allows more accurate estimations of the spectrum by minimizing both ends of the observation data. Furthermore, various techniques are applicable to the data window, such as cosine, Hamming, Hanning, and Blackman windows. In this study, a cosine window was applied. Meanwhile, regarding the appropriate wind-wave period for removing long and short-term components, criteria were prepared according to the classification of the ocean wave spectrum. The general periods of gravitational waves, which are wind waves excluding capillary and ultra-gravity waves, are classified ranging from 1–3 s to 20–30 s [7],[8]. However, these are very old criteria, and, therefore, it is necessary to apply an appropriate period of winds and waves considering the characteristics of the sea area on the Korean Peninsula, the target area of this study. Thus, based on the review results of the wave observation data in real sea areas [9], the upper limits for 50 years or less and 100 years or more are 16.5 s and 17.5 s, respectively. As a result, this study applied the interval 1–20 s as the criterion for the appropriate wind-wave period. This study corrected the data ($\hat{\eta}(t_i)$) additionally using the Butterworth filter[10]. The FFT is generally used to analyze time-series data calculated through the correction of observation data in the frequency domain. However, to flexibly select the number of data to be analyzed without limiting it to $N = 2^n$ in this study, the periodogram method was applied, which can calculate and convert the Fourier coefficient to the frequency domain. To improve the accuracy of the spectrum estimation, as shown in the following equation, the data smoothing method that applies the bias-variance trade-off theory was used as follows. The bias-variance trade-off is one of the theories used to minimize errors such as overfitting or underfitting in the process of generalizing a random distribution and can be expressed as Eq. (1):

$$E[(\hat{X} - X)]^2 = (X - E(\hat{X}))^2 + (E(\hat{X}) - [E(\hat{X})]^2) \quad (1)$$

where X is the actual spectrum value and \hat{X} is the estimated spectrum. Furthermore, the left side in Eq. (7) is the mean square error (MSE), $E(\hat{X}) - [E(\hat{X})]^2$ is the variance, and $X - E(\hat{X})$ is the bias. In this study, the effect on validation, smoothing of the estimated spectrum was reviewed.

III. RESULT AND CONCLUSION

A. Validation of wave parameter result

Verification of the obtained wave data through this analysis is essential. Thus, the correlation between the wave parameters calculated using the wave spectrum method applied in this study, the wave parameters calculated by the WaveGuide, and the wave observation system was analyzed.

Moreover, additional verifications were performed by applying Parseval's theory. As a result of the correlation analysis for H_s among the wave parameters calculated by applying the two methods, the correlation coefficients (CC) were very high at 0.994 and 0.998, respectively. Meanwhile, as a result of the correlation analysis for T_p , the CCs were calculated as 0.731 and 0.786, respectively. The differences between the two methods may result from the filter and smoothing methods applied in this study.

As a method of verifying the result of the wave spectrum analysis performed in this study, a theory stating that the variance (m_0) of the waveform is equal to the total energy (η_{rms}^2) of the observation data was used. The correlation analysis result of the two parameters for HeMOSU-1 and HeMOSU-2 showed that the CCs between the two parameters were 0.9994 and 0.9991, respectively. These values suggest that the two parameters are statistically equal.

B. Smoothing effect

As a result of calculating the CI of the estimated spectrum, the CI range for the peak part of the estimated spectral density was [46.65, 216.49], and the CI range of the spectral density calculated by smoothing was [12.24, 56.81]. Thus, the CI range became approximately four times smaller than before smoothing. The smoothing number showed an increasing trend at both locations as the significant wave height decreased. This suggests that the application of smoothing had difficulty because of unstable distribution of the wave spectrum. Furthermore, the distribution change patterns of the peak wave period calculated from the estimated spectrum ($S(f_k)$) and smoothed spectrum ($\hat{S}(f_k)$) according to the application of smoothing were analyzed. As a result of a linear correlation test performed to examine the effect of the peak wave period by smoothing, the CCs were 0.829 and 0.856, respectively, showing statistically high correlations. Furthermore, most periods were distributed between approximately 4 and 6 s. Regarding the density distribution change pattern of the peak wave period, depending on whether smoothing was performed or not, generated a significant difference as the null hypothesis was rejected because of the effect of smoothing for both HeMOSU-1 and -2 (p-value < 0.05).

ACKNOWLEDGMENT

This research was part of the project titled 'The development of 1kW-class tidal power generator system capable of supplying power to port facilities (grant number : 20210224)', funded by the Ministry of Oceans and Fisheries, Korea.

REFERENCES

- [1] Mizuguchi, M., 1982. Individual wave analysis of irregular wave deformation in the nearshore zone. *Coast. Eng.* 485–504.
- [2] Thompson, E. F., 1980. Energy spectra in shallow US coastal waters.
- [3] Pierson, W. J., Marks, W., 1952. The power spectrum analysis of ocean-wave records. *AGU*. 33(6), 834–844.
- [4] Casas Prat, M., 2008. Overview of ocean wave statistics.
- [5] Soares, C. G., Carvalho, A. N., 2012. Probability distributions of wave heights and periods in combined sea-states measured off the Spanish coast. *Ocean Eng.* 52, 13–21.
- [6] Rodriguez, G.R., Soares, C. G., 1999. The bivariate distribution of wave height and periods in mixed sea states. *J. Offshore Mech. Arctic Eng.* 121 (2), 102–108.
- [7] Munk, W. H., 1951. Origin and generation of waves. *Scripps Institution of Oceanography La Jolla Calif.*

- [8] Sorensen, R. M., 1967. Investigation of ship-generated waves. *J. Water. Harb. Coast. Eng. Div.* 93(1), 85–102.
- [9] Ministry of Oceans and Fisheries., 2019. Report on the deep water design wave estimation in the Korea (in Korean).
- [10] Butterworth, S., 1930. Experimental wireless and the wireless engineer. *Wireless Eng.* 7, 536.

Movable Visualization System for Exterior Monitoring of Outdoor Infrastructures

Jeong, Hong Guk

Maritime ICT R&D Center, KIOST

Korea Institute of Ocean Science & Technology

Busan, South Korea

wjdfhdrrn@kiost.ac.kr

Lee, Jih Yeong

Maritime ICT R&D Center, KIOST

Korea Institute of Ocean Science & Technology

Busan, South Korea

wlgud0818@kiost.ac.kr

Seo, Jung Min

Maritime ICT R&D Center, KIOST

Korea Institute of Ocean Science & Technology

Busan, South Korea

jmseo@kiost.ac.kr

Kim, Soo Mee

Maritime ICT R&D Center, KIOST

Korea Institute of Ocean Science & Technology

Busan, South Korea

smeekim@kiost.ac.kr

Abstract—In order increase the work safety and efficiency of current human-based status evaluation of port infrastructures, the demand of adopting unmanned automatic evaluation system is growing. In this study, we developed a movable visualization system equipped with a multiple sensor module for exterior monitoring of outdoor infrastructures. The multiple sensor module consisted of two lidars, a stereo camera, and motion sensor. Movement of the multiple sensor module was implemented by remotely controllable toy car. We tested the functional performances of a dual lidar, a stereo, a motion sensor. The measurement error of GPS and IMU of the motion sensor 50 cm and were ± 0.2 degrees. The merged lidar data and stereo helped to visualize the exterior status of the objects to be monitored.

Keywords—Movable visualization system, dual lidar, stereo camera, motion sensor, Exterior monitoring of outdoor infrastructures

I. INTRODUCTION

It is reported that the proportion of port infrastructures older than 30 years in South Korea is about 23% in 2019 and it will be surged up to 47 % in 10 years. Port infrastructures get older, the breakages by aging and natural disaster are increasing. Current exterior status evaluation of port infrastructures relies on human surveys. In order to improve the survey safety and efficiency, the demand of unmanned automatic monitoring systems is growing. In this study, we developed a movable visualization system equipped with multiple sensors such as lidar, stereo camera, and motion sensor. Also, we evaluated the functional performances of the multiple sensors.

II. METHOD

Fig. 1 shows the movable visualization system ($100 \times 44 \times 70 \text{ cm}^3$) equipped with a multiple sensor module. The multiple sensor module consisted of two lidars, a stereo camera, and motion sensor. The lidars and stereo camera are used to visualize the exterior of outdoor infrastructures. The motion sensor provides information on the absolute location and the posture of the movable visualization system. The movement was implemented by a remotely controllable toy car, which can be operated in a speed range of 1 to 4 knots and the vertical motion of the sensor module was implemented to simulate the real monitoring situations at sea.

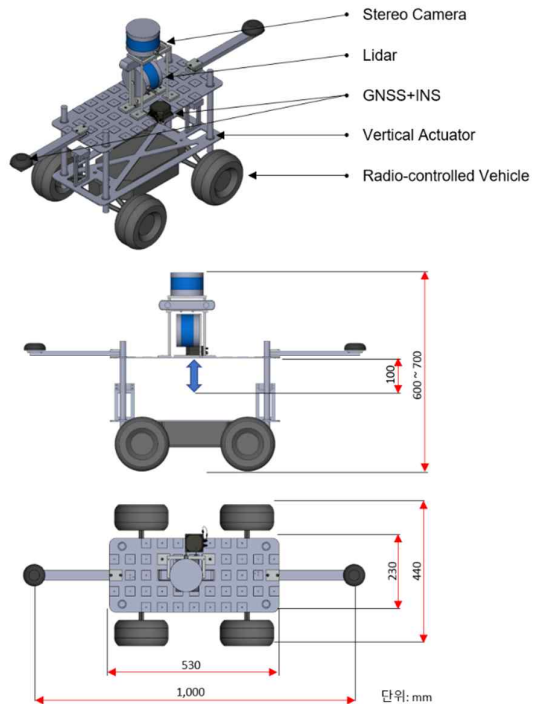


Fig. 1. Movable visualization system implemented by remotely controllable toy car

The multiple sensor module consisted of a dual lidar, a stereo camera, and an integrated motion sensor of global navigation satellite system (GNSS) and inertial measurement unit (IMU) as shown in Fig. 2. The dual lidar (Puck High-Res, Velodyne, USA) of 16 channels were aligned to scan same region and the scanned data were merged to obtain the denser point clouds [1]. A stereo camera (ZED2, Stereo Labs, France) gives RGB-D point clouds of the scanned region [2]. The motion sensor (VN-310, VECTRONAV, USA) measures the synchronized GNSS and IMU data to utilize for motion correction of multiple sensor module and representation of the measured point clouds in absolute coordinate system [3]. In order to measure the reliable global positioning system (GPS) data, two antennas are apart from each other by 1 m.

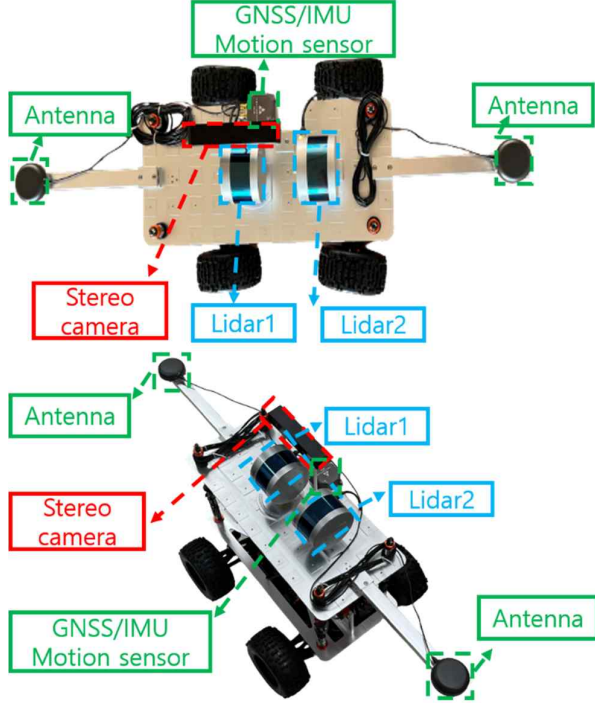


Fig. 2. Multi-visualization sensor module configuration

III. RESULT

The movable visualization system was fixed at a location with a latitude of 35.07 and a longitude of 129.08 and then the GNSS and IMU data were measured for 30 minutes. Fig. 3 shows the accuracy plot of the measured GNSS data resulting in an error range of 40 to 50 cm. Other three plots show the roll, pitch, and yaw in the measured IMU data and the errors are within ± 0.2 degrees.

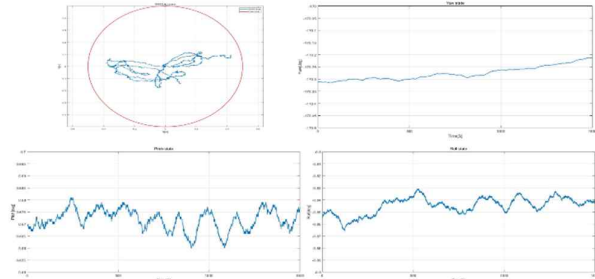


Fig. 3. Accuracy plots of GNSS and IMU data

Fig. 4 shows the visualization data with dual lidar and stereo data. Fig. 4(a) shows the point clouds measured from Lidar1 and Lidar2, as well as the merged dual lidar data. Fig. 4(b) shows an RGB image, mesh representation of point clouds, and colored point clouds obtained by ZED stereo camera. The movable visualization system provided multi-sensor data taken simultaneously by dual lidar and stereo. The merged lidar data was denser than single lidar data and the stereo data give color and three-dimensional posture of the interested object.

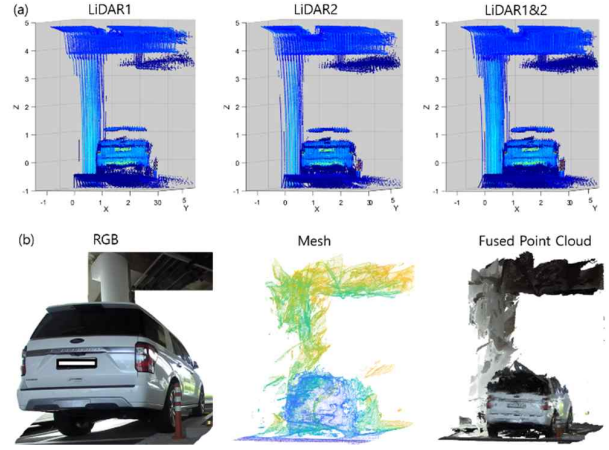


Fig. 4. Visualization data measured by (a) dual lidar and (b) stereo camera

IV. CONCLUSION

We developed a movable visualization system for exterior monitoring of outdoor infrastructure and measured synchronized dual lidar, stereo and GNSS/IMU data. The error ranges of GNSS and IMU sensors were evaluated by 40 to 50 cm and ± 0.2 degrees, respectively. The merged lidar data and stereo helped to visualize the exterior status of the objects to be monitored.

ACKNOWLEDGMENT

This research was a part of the project titled 'Development of smart maintenance monitoring techniques to prepare for disaster and deterioration of port infra structures', funded by the Ministry of Oceans and Fisheries, Korea.

REFERENCE

- [1] Velodyne Lidar, <https://velodynelidar.com/products/puck-hi-res>
- [2] Stereolabs, <https://www.stereolabs.com/zed-2/>
- [3] Vectornav, <https://www.vornav.com/products/detail/vn-310>

Deep Reinforcement Learning-Based Power Allocation in Multi-Cell Massive MIMO

Youngwoo Oh

*Dept. of Computer Engineering
Chosun University
Gwangju, South Korea
ywo@chosun.kr*

Wooyeol Choi

*Dept. of Computer Engineering
Chosun University
Gwangju, South Korea
wyc@chosun.ac.kr*

Abstract—In this paper, we consider a massive multiple-input multiple-output (MIMO) system that has a large number of transmit antennas at the base station serving multiple users in a downlink multi-cell system. In the massive MIMO system, the number of radio frequency chains and the total transmit power is increasing due to a large number of deployed antennas. The conventional energy-efficient optimization techniques are based on iterative numerical algorithms requiring high computational complexity. To solve this problem, we present a deep reinforcement learning-based power allocation scheme to improve the sum-rate and reduce the complexity. The simulation results demonstrate that the reinforcement learning-based power allocation methods achieve higher energy efficiency with lower complexity than existing optimization algorithms.

Index Terms—Massive MIMO, deep reinforcement learning, power allocation

I. INTRODUCTION

The massive multiple-input multiple-output (MIMO) has been utilized to enhance spectral efficiency by serving multiple users simultaneously with a large number of transmitting antennas at a base station (BS). Since the total consumption is proportional to the antennas in the BS, the energy consumption in a massive MIMO system has significantly increased. To this end, various optimization techniques for maximizing the sum-rate and minimizing power consumption have been performed to improve energy efficiency in the massive MIMO system. However, most of the optimization problems are non-convex [1], [2] and require a high computational complexity.

In this paper, we consider a deep reinforcement learning (DRL)-based approach to solve these problems. DRL-based techniques have been rapidly developed in wireless communications. These approaches have demonstrated finding the optimal value faster than the conventional methods and are robust against dynamic changes [3], [4]. Therefore, we propose a DRL-based power allocation scheme to improve the sum-rate performance and reduce the complexity in the massive MIMO systems.

This research was supported in part by Basic Science Research Program through the National Research Foundation of Korea (NRF) funded by the Ministry of Education under grant (No. NRF-2021R1I1A3050535), and in part by 'Technology Commercialization Collaboration Platform' program of the Korea Innovation Cluster (No. 2022-DD-RD-0065).

II. DRL-BASED POWER ALLOCATION

We consider the downlink power allocation for a multi-cell massive MIMO system. All user equipment (UE) is randomly located in N cells, and a BS is deployed in the center of each cell. The BS is equipped with M transmitting antennas and serves K UEs with a single antenna. The received signal at the k -th UE associated with n -th BS is the sum of the desired signal transmitted from n -th BS, the interference from adjacent BSs, and the noise, and can be expressed as

$$y_{n,k} = p_{n,k}g_{n,k}w_{n,k}x_{n,k} + \sum_{j \neq n}^N \sum_{k=1}^K p_{j,i}g_{j,i}w_{j,i}x_{j,i} + n_{n,k}, \quad (1)$$

where $p_{n,k}$, $w_{n,k}$, and $x_{n,k}$ is the transmitted power, the zero-forcing precoding vector, and the downlink signal of n -th BS to k -th UE, respectively, and $n_{n,k}$ is additive white Gaussian noise with variance σ^2 . Therefore, the signal-to-interference and noise ratio (SINR) of the k -th UE connected to n -th BS can be defined as

$$\gamma_{n,k} = \frac{p_{n,k}\|g_{n,k}w_{n,k}\|^2}{\sum_{j \neq n}^N \sum_{k=1}^K p_{j,i}\|g_{j,i}w_{j,i}\|^2 + \sigma^2}. \quad (2)$$

The downlink rate for k -th UE is given by $C_{n,k} = \log_2(1 + \gamma_{n,k})$. The problem of maximizing the sum-rate can be defined as

$$\begin{aligned} & \max_{p_{n,k}} f(p_{n,k}) \\ & \text{s.t. } 0 < p_{n,k} \leq P_{\max}, \quad \forall n, k, \end{aligned} \quad (3)$$

where the $f(p_{n,k}) = \sum_n^N \sum_k^K C_{n,k}$ and P_{\max} is maximum transmission power. The conventional power allocation methods consume high computational time to solve the above problem. Therefore, we apply the DRL algorithms considering the complexity and sum-rate performance. To solve the maximization problem by the reinforcement learning algorithms, we transform it into a Markov decision process (MDP).

The state space consists of the SINR, and the objective function, and can be expressed as

$$S(t) = \{\gamma_{n,k}(t), f(p_{n,k}(t))\}, \quad \forall n, k, \quad (4)$$

The action space $A(t)$ is the set of the downlink transmission power for all BSs to UEs, which is selected by dividing it into

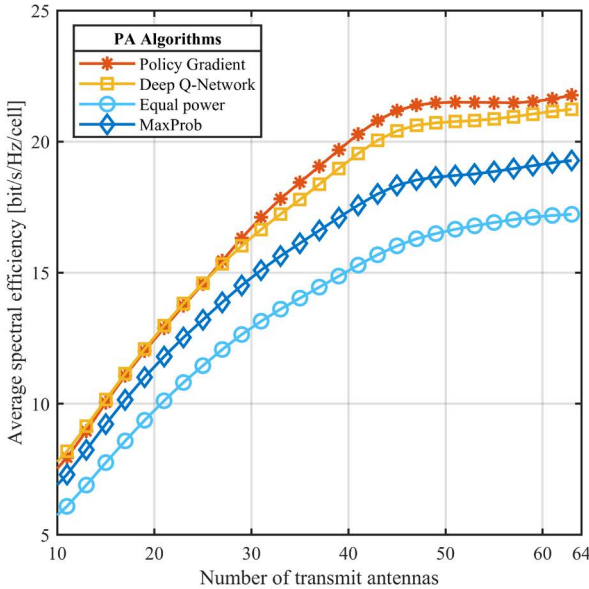


Fig. 1. A performance evaluation of different methods at various BS antennas.

specific steps between P_{\min} and P_{\max} to reduce the complexity. The reward by the state and action spaces is the same as the objective function to maximize the sum-rate, and can be defined as

$$R(t) = f(p_{n,k}(t)) \quad (5)$$

Therefore, the DRL agent trains to obtain as much reward as possible, considering the maximize the sum-rate.

III. SIMULATION RESULTS

This section evaluates the numerical simulation performance for the applied DRL-based power allocation in the multi-cell massive MIMO system. For the massive MIMO system, we consider the number of BS antennas installed to be 64, and the total number of users is 10. In addition, the cell is a radius of 500 m, and the maximum transmitted power of BS is 32 dBm.

We conducted the simulations using both value-based and policy-based DRL algorithms. The deep Q-network (DQN) consists of three fully connected layers of 128, 64, and 64 neurons with a Relu activation function. In addition, we rely on the Adam optimizer and the mean squared error (MSE) loss function. We evaluate the performance of the applied DRL algorithms based on the average spectral efficiency and computational time. The maximum product SINR and equal power algorithms are suggested as benchmarks to compare the DRL algorithms, where we denote the maximum product SINR algorithm as MaxProb.

Fig. 1 presents the performance of the average spectral efficiency of each algorithm at a different number of BS antennas. The results show that DQN and policy gradient achieve higher average spectral efficiency than the suggested benchmark algorithms. The reason is that the DRL agents acquire environmental information, such as states and transmission power, and update it after each episode to determine

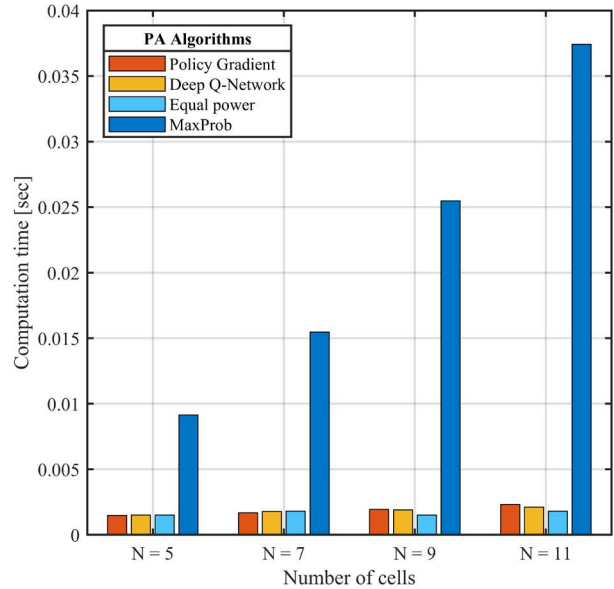


Fig. 2. A comparison of the computational time for each method at different number of cells.

the optimal action. On the other hand, the MaxProb method has a lower performance due to the number of repetitions, the interference of adjacent cells, and the effect of large-scale fading.

Fig. 2 shows the computational time of each algorithm as the number of cells increases. The result demonstrates that the computational time of MaxProb increases exponentially, whereas DRL-based and equal power methods are stable, even though the number of cells increases.

IV. CONCLUSION

This paper presented the DRL algorithms to maximize the sum-rate in a multi-cell massive MIMO system. Through the extensive simulations, we confirmed that the DRL methods can achieve a higher performance of the sum-rate with lower complexity than the existing optimization techniques. Our future work is to perform a joint antenna selection and power allocation method to maximize the spectral efficiency of the massive MIMO systems.

REFERENCES

- [1] L. You, Y. Huang, D. Zhang, Z. Chang, W. Wang, and X. Gao, "Energy efficiency optimization for multi-cell massive mimo: Centralized and distributed power allocation algorithms," *IEEE Transactions on Communications*, vol. 69, no. 8, pp. 5228–5242, 2021.
- [2] J. Choi, N. Lee, S.-N. Hong, and G. Caire, "Joint user selection, power allocation, and precoding design with imperfect csit for multi-cell mmimo downlink systems," *IEEE Transactions on Wireless Communications*, vol. 19, no. 1, pp. 162–176, 2020.
- [3] Y. S. Nasir and D. Guo, "Multi-agent deep reinforcement learning for dynamic power allocation in wireless networks," *IEEE Journal on Selected Areas in Communications*, vol. 37, no. 10, pp. 2239–2250, 2019.
- [4] L. Luo, J. Zhang, S. Chen, X. Zhang, B. Ai, and D. W. K. Ng, "Downlink power control for cell-free massive mimo with deep reinforcement learning," *IEEE Transactions on Vehicular Technology*, vol. 71, no. 6, pp. 6772–6777, 2022.

Collaborative Learning for Cyber-Attacks Classification in Maritime Transportation Systems

Ahmad Zainudin^{*†}, Jung-Hyeon Kim[§], Dong-Seong Kim[§], and Jae-Min Lee[§]

^{*}Department of Electronic Engineering, Kumoh National Institute of Technology, Gumi 39177, Korea

[§]Department of IT Convergence Engineering, Kumoh National Institute of Technology, Gumi 39177, Korea

[†]Department of Electrical Engineering, Politeknik Elektronika Negeri Surabaya, Surabaya, Indonesia

(zai*, trizkim, dskim, ljmpaul)@kumoh.ac.kr

Abstract—Cyber-physical systems (CPS)-based maritime transportation systems (MTS) provide improved navigation, traffic monitoring, real-time tracking, and safety systems. These new features enable intelligent and autonomous capabilities to assert the MTS for increasing connectivity with heterogeneous network devices that impose MTS vulnerability to cyber-attack. This study proposes federated learning (FL)-based multilayer perceptron (MLP) intrusion detection model to maintain data in a decentralized manner, raising privacy concerns. The proposed model was evaluated using publicly available cyber-security benchmarks, CICIDS2017 dataset. Performance evaluation shows that the proposed model outperforms state-of-the-art with an accuracy of 98.79% with computational time of 1.210 ms.

Index Terms—federated learning, intrusion detection, maritime transportation systems

I. INTRODUCTION

Maritime transportation systems (MTS), which is an integrated network of sensor and maritime industry infrastructure entities associated with ports, vessels, navigation systems, shore-based facilities, containers, and autonomous underwater vehicles [1]. The new features that enable intelligent and autonomous capabilities assert the MTS for increasing connectivity with heterogeneous network devices. Moreover, using an integration of cloud and edge devices in large quantities for data gathering can impose MTS vulnerability to cyber-attack [2]. Centralized-based network intrusion detection systems (IDS) requires uploading network traffic features as training data to the cloud server [3]. A Cyber-physical systems (CPS)-based MTS that is concerned with data privacy makes it challenging. Federated learning (FL) moves the training to the edge, where it is closer to data-generating devices. CPS on the vessels locally trains the network traffic data to create a detection model.

Some approaches have been implemented based on centralized-based [4] and federated learning-based intrusion detection and classification of malicious network activities. The authors [5] applied an ML-based malicious detection system for resource-constrained IoT-enabled MTS. This system uses a multi-access edge computing (MEC) platform to perform an online learning model. This approach provides a modified hybrid forgetting mechanism and improved approximate linear dependence to filter the unnecessary data and maintain the detection model up-to-date. This approach [5] perform in a centralized-learning scenario that leads to privacy data issues.

The authors [6] implemented FL-based intrusion detection in the MTS ecosystem. This approach proposes a CNN-MLP model and a FedBatch aggregation algorithm to address the straggler problem in an unstable communication environment. This proposed model evaluated uses the NSL-KDD dataset and got an improved result of 88.1% accuracy. The existing [6] FL-based intrusion detection in MTS means the intrusion detection accuracy is still not enough for recent cyber-attacks. In this study, we propose FL-based collaborative learning using an MLP intrusion detection model for cyber-attack classification and use an up-to-date cyber-security dataset.

Considering the requirements for enhanced privacy scenarios to train an intrusion detection model in CPS-based MTS, this study proposes some contributions:

- We implemented a multilayer perceptron (MLP) intrusion detection model to classify malicious traffic and evaluated it using the cyber-security benchmark CICIDS2017 dataset.
- We proposed an IDS model that uses collaboration FL-based to maintain the privacy requirements in CPS-based MTS. The CPS-based MTS on the vessel locally trains its network traffic data and sends training parameters to the aggregation server. A federated average (FedAvg) was exploited as an aggregation algorithm.

II. FL-BASED CYBER-ATTACK CLASSIFICATION IN MTS

This study proposes a privacy-preserving FL-based intrusion detection system in the MTS ecosystem. Fig. 1 shows the overview of the proposed system. The system consists of an aggregation server on the cloud, and CPS-based ESs on the vessels are denoted as $E = \{e_1, e_2, e_3 \dots e_n\}$. In the first stage, an aggregation server initiates the global model and sends the training parameters such as weight w , bias b , learning rate η values and communication round number R to the agents. The agents received this model as a local model and locally trained their raw data using a local model m_i . After the local training process, the agents send the updated training parameters (Δw and Δb) to the aggregation server. The aggregation server aggregates the updated training parameters from all agents using a federated averaging (FedAvg) algorithm and sends them back to the agents. The system exploits an MLP-based model for network intrusion detection in a CPS-based MTS environment and was evaluated using the CICIDS2017 dataset.

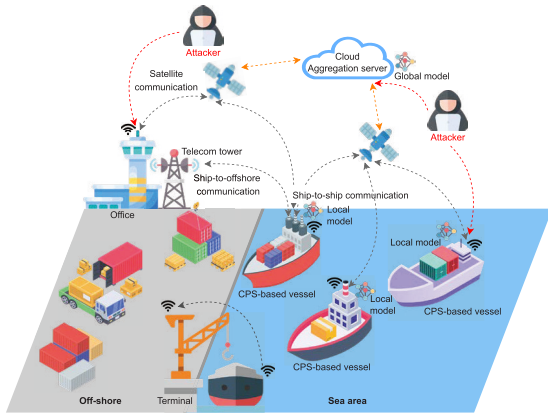


Fig. 1. FL-based cyber-attacks classification in MTS

TABLE I
TRAINING PARAMETERS OF THE PROPOSED MODEL

Parameters	Value	Parameters	Value
Number of classes	5	Learning rate	0.01
Total features	78	Optimizer	SGD
Dense layers	6 (78, 64, 32, 16, 8, 5)	Loss function	Categorical cross-entropy
Communication round	1, 2, 3, 4...10	Activation function	ReLU
Mini-batch size	32	Number of agents	5

This dataset contains benign and four malicious activities (DoS Hulk, PortScan, DDoS, and DoS GoldenEye).

III. EXPERIMENTAL RESULTS AND DISCUSSION

The MLP model was composed of input, output, and four hidden layers (78, 64, 32, 16, 8, 5). The local training uses a mini-batch size of 32 and a learning rate of 0.01 with an stochastic gradient descent (SGD) optimizer and categorical cross-entropy loss function. The training parameters are shown in Table I. Performing the proposed model's accuracy with various communication rounds is shown in Fig. 2. Table. II describes the cyber attack classification accuracy for each class. Comparison performance with the existing model is shown in Table III. The proposed model achieves the best accuracy of 98.78% and a loss of 0.0319 when performing eight communication rounds.

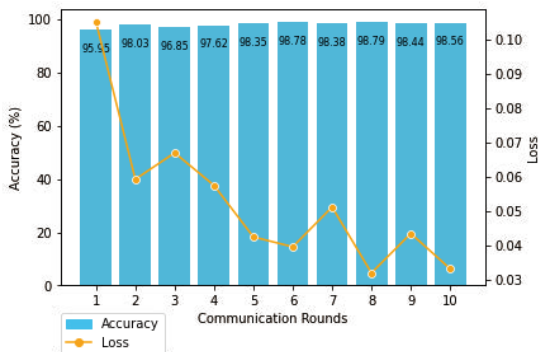


Fig. 2. Proposed Model Performance with Varying Communication Rounds

TABLE II
CYBER ATTACKS CLASSIFICATION ACCURACY FOR EACH CLASS

R	Benign	DoS Hulk	PortScan	DDoS	DoS GE
1	99.74%	90.07%	98.95%	82.08%	0
2	99.11%	92.49%	99.80%	99.27%	99.49%
3	99.89%	93.97%	99.75%	82.15%	95.89%
4	96.61%	99.67%	99.78%	98.64%	97.45%
5	99.29%	93.68%	99.69%	99.58%	95.65%
6	99.38%	96.16%	99.76%	98.37%	99.68%
7	98.03%	98.44%	99.67%	99.10%	96.88%
8	99.41%	95.50%	99.79%	99.67%	98.10%
9	99.50%	94.69%	99.03%	99.47%	81.70%
10	99.48%	98.46%	99.77%	99.54%	97.87%

TABLE III
COMPARISON OF FL-BASED CYBER ATTACKS CLASSIFICATION WITH DIFFERENT MODELS

Model	Accuracy	Loss	Time-cost	Trainable Parameters
CNN	95.37%	0.0885	1.188 ms	12,845
Multi-MLP	96.63%	0.0632	2.196 ms	28,009
CNN-MLP [6]	98.24%	0.0426	1.332 ms	168,729
Proposed Model	98.79%	0.0319	1.210 ms	14,007

IV. CONCLUSION

This study performs FL-based network intrusion detection in the MTS environment. The proposed model was evaluated using the publicly available cyber-security CICIDS2017 dataset. The evaluation results show the proposed model outperforms the other FL-based intrusion classification model with an accuracy of 98.78% and a time cost of 1.210 ms.

ACKNOWLEDGMENT

This work was supported by Priority Research Centers Program through the National Research Foundation of Korea (NRF) funded by the MSIT (Ministry of Science and ICT) (2018R1A6A1A03024003), Korea and the Grand Information Technology Research Center support program (IITP-2022-2020-0-01612) supervised by the IITP (Institute for Information & Communications Technology Planning & Evaluation.

REFERENCES

- [1] P. Kumar, G. P. Gupta, R. Tripathi, S. Garg, and M. M. Hassan, "DLTIF: Deep Learning-Driven Cyber Threat Intelligence Modeling and Identification Framework in IoT-Enabled Maritime Transportation Systems," *IEEE Transactions on Intelligent Transportation Systems*, 2021.
- [2] L. A. C. Ahakonye, C. I. Nwakanma, J.-M. Lee, and D.-S. Kim, "Efficient Classification of Enciphered SCADA Network Traffic in Smart Factory Using Decision Tree Algorithm," *IEEE Access*, vol. 9, pp. 154 892–154 901, 2021.
- [3] G. O. Anyanwu, C. I. Nwakanma, J. M. Lee, and D.-S. Kim, "Novel Hyper-tuned Ensemble Random Forest Algorithm for the Detection of False Basic Safety Messages in Internet of Vehicles," *ICT Express*, 2022.
- [4] G. C. Amaizu, C. I. Nwakanma, S. Bhardwaj, J. Lee, and D.-S. Kim, "Composite and Efficient DDoS Attack Detection Framework for 5G Networks," *Computer Networks*, vol. 188, p. 107871, 2021.
- [5] E. Gyamfi, J. A. Ansere, M. Kamal, M. Tariq, and A. Jurcut, "An Adaptive Network Security System for IoT-Enabled Maritime Transportation," *IEEE Transactions on Intelligent Transportation Systems*, 2022.
- [6] W. Liu, X. Xu, L. Wu, L. Qi, A. Jolfaei, W. Ding, and M. R. Khosravi, "Intrusion Detection for Maritime Transportation Systems With Batch Federated Aggregation," *IEEE Transactions on Intelligent Transportation Systems*, 2022.

FED-MARINE: Federated Learning Framework for DDoS Detection and Mitigation in Maritime-SCADA Network

Love Allen Chijioke Ahakonye, Cosmas Ifeanyi Nwakanma [†], Jae Min Lee, Dong-Seong Kim

*IT Convergence Engineering, [†]ICT Convergence Research Center, Kumoh National Institute of Technology Gumi, South Korea
(loveahakonye, cosmas.ifeanyi, ljmpaul, dskim)@kumoh.ac.kr,*

Abstract—Information and communication technology (ICT) is continually expanding and converging in various industries, particularly in the maritime industry, and this trend will strengthen Maritime supervisory and data acquisition (SCADA) security. However, these application areas have the challenge of mitigating attacks. The Maritime SCADA systems are critical infrastructure requiring protection. This paper proposes a federated learning orchestration to secure the Maritime SCADA from the distributed denial of service (DDoS) strikes.

Index Terms—Internet of Maritime things (IoMT), Intrusion Detection, Maritime SCADA, Maritime security,

I. INTRODUCTION

ICT convergence in the maritime sector has enabled the growth of the Maritime SCADA systems to become large, complicated, and distributed, making them vulnerable to both traditional and emerging threats. Cyber-attacks on maritime SCADA are no longer a speculative issue. The devastating NotPetya virus, for example, crippled the Maersk shipping firm in June 2017 [1], [2]. There have been initiatives to defend such network systems. These efforts include risk management policies on maritime SCADA with their disparate methodologies [3] including firewalls to reduce cases of unauthorized access. The effect of cyber attacks on the Maritime SCADA includes the disruption of services and the enormous catastrophe to the Maritime operations. Thus, it is pertinent to proffer efficient artificial intelligence (AI) based intrusion detection systems (IDS) to alleviate attacks. The onslaught of distributed denial of service (DDoS) poses issues in IIoT SCADA networks and application layers [4], the maritime SCADA is not an exception. This attack can distort the victim server by forwarding many demand traffic to congest the network and overwhelming the malicious network traffic with fake source addresses [4].

Many authors have used AI approaches to predict and detect vulnerability and attacks. Authors [4]–[6], for example, proposed various IDS frameworks. At the moment, industrial breakthroughs such as the machine learning (ML) and IIoT have transformed and impacted daily living as well as a wide range of industries. IIoT has grown ubiquitous due to its application in various fields, including communication and industry in general. However, the Maritime SCADA lacks significant attention to ML approaches to intrusion detection. Most of the

studies on maritime SCADA and security focus on awareness creation, risk assessment analysis, strategies, and training [2], [3], [7]. Thus, this study is the first attempt to propose an ML-based framework based on our knowledge. The proposed approach is a secure federated learning (FL) structure for detecting and mitigating DDoS attacks in maritime SCADA networks.

The traditional ML relies on a server-side dataset split into train and test sets for model training. It is the reverse in the FL approach. Learning from various clients is aggregated and combined on the server-side to derive a new model downloaded on the clients/devices. It is an iterative process and data privacy-sensitive solution [8]. Hence suitable for privacy-constrained devices and operations and low communication delay in the maritime sector. Fig. 1 depicts the model architecture of the proposed framework design.

This study leverages the public federated Edge-IIoT dataset [8] to evaluate the applicability of the proposed framework for a Maritime SCADA IDS system. The contributions of this paper are:

- 1) A novel federated learning (FL) framework structure for DDoS attack mitigation in maritime SCADA network.
- 2) Applicability of the proposed model in detection of other attack types including zero day.
- 3) To validate the reliability of the proposed model in a real-time scenario using Edge-IIoTset and centralized datasets.

II. SYSTEM METHODOLOGY

The goal of the proposed FED-MARINE is to build models across client/devices based on their available stored data while preserving data privacy. This new technique involves downloading the initial model on the server to an available client or device for training. The client starts training with the received model based on the available data in its data store. The new device models are sent to the server for aggregation to derive a global model by learning from all the clients. The server, in turn, pushes the model back unto the clients. This process applies to all eligible clients at the same time. A merged and improved single global model is made available to the clients.

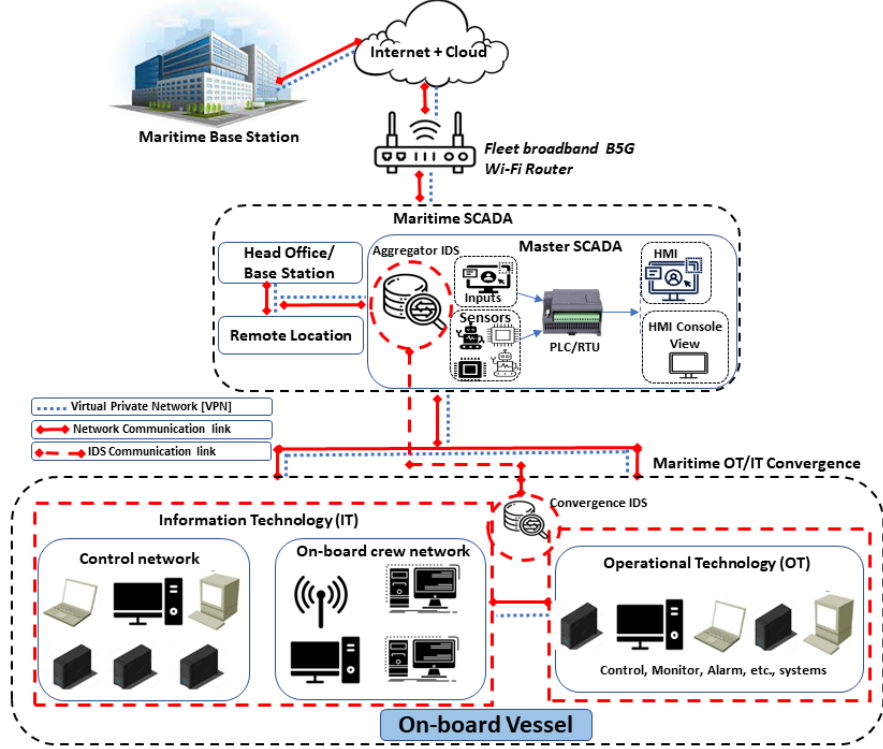


Fig. 1. The Framework of the Proposed Model: FED-MARINE

Algorithms 1 and 2 shows the client and server-side procedures of the proposed FED-MARINE while Fig. 2 illustrates the process of the proposed system model.

Algorithm 1 Client-side Process Algorithm

```

ClientUpdate( $i, \omega$ ): // Run on client  $i$ 
 $B \leftarrow$  (split  $N_i$  into subsets of  $B$ )
for each local epoch  $j$  from 1 to  $Q$  do
    for subset  $a \in B$  do
         $\omega \leftarrow \omega - \eta \nabla \ell(\omega; a)$ 
    end for
    return  $\omega$  to server
end for

```

Algorithm 2 Server-side Process Algorithm

```

ServerExecution:
initialize  $\omega_0$ 
for each circle  $s = 1, 2, \dots$  do
     $m \leftarrow \max(C * I, 1)$ 
     $Y_s \leftarrow$  (random set of  $x$  clients)
    for each client  $i \in Y_s$  in parallel do
         $\omega_{s+1} \leftarrow \text{ClientUpdate}(i, \omega_s)$ 
    end for
     $\omega_{s+1} \leftarrow \sum_{i=1}^I \frac{n_i}{n} \omega_{s+1}$ 
end for

```

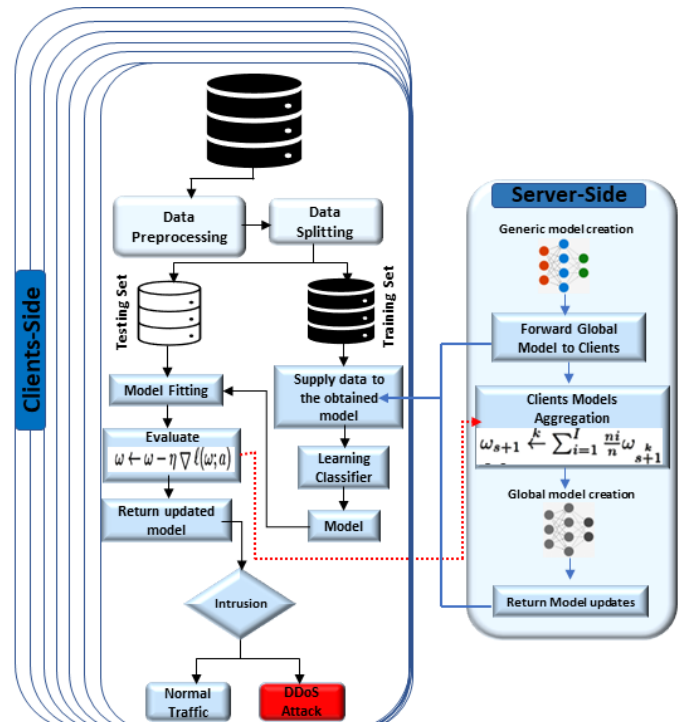


Fig. 2. Process Flow of the Proposed System FED-MARINE

III. PERFORMANCE EVALUATION

Table I illustrates the performance of a deep learning algorithm on the proposed approach to evaluating the federated Edge-IIoT dataset. The experimental result demonstrates the applicability of the proposed framework to the Maritime SCADA network. The proposed approach is relevant to other privacy-constrained networks with intrusion challenges, which can be with any suitable choice of ML algorithms.

TABLE I
MODEL PERFORMANCE ON EVALUATED FEDERATED EDGE-IIOT DATASET

Accuracy(%)	Precision(%)	Recall(%)	AUC
90.83	93.74	88.89	0.9968

IV. CONCLUSION

This study proposed an FL-based approach for Maritime SCADA IDS. The results show that the proposed approach exhibits applicability and significance in attack detection. Therefore, considering the complexity and privacy constraints of the Maritime operations, the proposed approach is suitable for attack mitigation in the target domain. In the future, we intend to evaluate the proposed framework using Maritime SCADA datasets.

ACKNOWLEDGMENT

This research work was supported by Priority Research Centers Program through NRF funded by MEST

(2018R1A6A1A03024003) and the Grand Information Technology Research Center support program (IITP-2022-2020-0-01612) supervised by the IITP by MSIT, Korea.

REFERENCES

- [1] H. Boyes, R. Isbell, and A. Luck, “Good Practice Guide Cyber Security for Ports and Port Systems,” *Institution of Engineering and Technology*, https://assets.publishing.service.gov.uk/government/uploads/system/uploads/attachment_data/file/859925/cyber-security-for-ports-and-port-systems-code-of-practice.pdf, 2020.
- [2] D. Dalaklis, N. Nikitakos, and R. Yaacob, “Cyber Security Training Strategy: Dealing with Maritime SCADA Risks,” in *Proceedings of the International Maritime Lecturers’ Association, Seas of Transition: Setting a Course for the Future*. World Maritime University, 2021, pp. 53–61.
- [3] E.-M. Kalogeraki, S. Papastergiou, H. Mouratidis, and N. Polemi, “A Novel Risk Assessment Methodology for SCADA Maritime Logistics Environments,” *Applied Sciences*, vol. 8, no. 9, p. 1477, 2018.
- [4] G. C. Amaizu, C. I. Nwakanma, S. Bhardwaj, J. Lee, and D.-S. Kim, “Composite and Efficient DDoS Attack Detection Framework for B5G Networks,” *Computer Networks*, vol. 188, p. 107871, 2021.
- [5] M. Andrey Teixeira, T. Salman, M. Zolanvari, R. Jain, N. Meskin, and M. Samaka, “SCADA System Testbed for Cybersecurity Research Using Machine Learning Approach,” *arXiv e-prints*, pp. arXiv–1904, 2019.
- [6] L. A. C. Ahakonye, C. I. Nwakanma, J.-M. Lee, and D.-S. Kim, “Efficient Classification of Enciphered SCADA Network Traffic in Smart Factory Using Decision Tree Algorithm,” *IEEE Access*, vol. 9, pp. 154 892–154 901, 2021.
- [7] I. de la Peña Zarzuelo, “Cybersecurity in Ports and Maritime Industry: Reasons for Raising Awareness on this Issue,” *Transport Policy*, vol. 100, pp. 1–4, 2021.
- [8] M. A. Ferrag, O. Friha, D. Hamouda, L. Maglaras, and H. Janicke, “Edge-IIoTset: A New Comprehensive Realistic Cyber Security Dataset of IoT and IIoT Applications for Centralized and Federated Learning,” *IEEE Access*, vol. 10, pp. 40 281–40 306, 2022.

Indoor Visible Light LOS Channel Estimation using Support Vector Regression

Yeonghae Kim^a, Young Jae Moon^b, Sudhanshu Arya^c, Yeon Ho Chung^{b,*}

^aDepartment of Artificial Intelligence Convergence, Pukyong National University, Busan, Republic of Korea

^bDepartment of Information and Communications Engineering, Pukyong National University, Busan, Republic of Korea

^cResearch Center of Artificial Intelligence, Pukyong National University, Busan, Republic of Korea

Abstract

In this work, we present a supervised machine learning solution to indoor visible light channel estimation in optical wireless communications (OWCs). Specifically, we focus on the estimation of the line of sight (LOS) channel based on the support vector regression (SVR). The objective of this paper is to analyze the performance of supervised learning for channel estimation. In particular, we assume that the training data for the SVR are receiver positions and received power with Gaussian noise; therefore, the input of SVR is receiver positions different from the training data, and the output of SVR is the received power.

Keywords: Channel estimation, machine learning, optical wireless communications, support vector regression, visible light communication

1. Introduction

Recently, optical wireless communications (OWCs) have been regarded as a promising technology for outdoor, indoor, and underwater wireless applications [1, 2, 3]. OWCs transmit data through the optical carriers, i.e., infrared, visible, and ultraviolet, and compared to RF, OWCs have a very high optical bandwidth available, allowing much higher data rates [1].

The future OWC should be capable of good channel modeling and fast channel estimation. To satisfy such requirements, channel estimation using machine learning is being considered [4]. Channel modeling uses several parameters, and if machine learning is used considering all of these parameters, it becomes very complicated and takes a long time to calculate. In this paper, we attempt to estimate the channel using support vector regression (SVR), which is one of the supervised learning techniques. In order to minimize the complexity of machine learning, only the coordinates of receiver are used as input.

2. System Model

2.1. Visible Light based Indoor LOS Communication System Model

A visible-light indoor LOS communication system utilizing one LED is shown in Figure 1. The system model parameters are shown in Table 1.

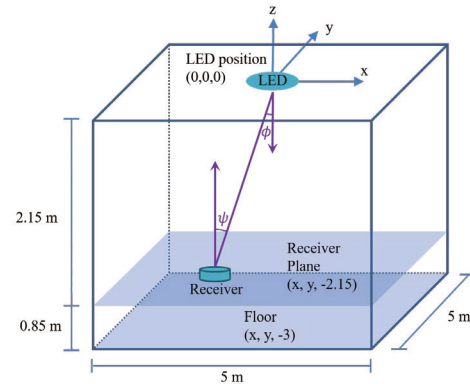


Figure 1. A visible-light indoor LOS communication system utilizing one LED.

Next, we present the LOS communication system model as follows [5, 6]. The transmitter LED is assumed to have a Lambertian radiant intensity,

$$R_0(\phi) = \begin{cases} \frac{m+1}{2\pi} \cos^m(\phi) & \text{for } \phi \in [-\pi/2, \pi/2] \\ 0 & \text{for } \phi \in [\pi/2, \pi] \end{cases} \quad (1)$$

*Corresponding author

Email addresses: rladudgo4567@gmail.com (Yeonghae Kim), 8068joshua@gmail.com (Young Jae Moon), Sudhanshu.arya27@gmail.com (Sudhanshu Arya), yhchung@pknu.ac.kr (Yeon Ho Chung)

Table 1

The parameters of the system model.

Room size	$5 \text{ m} \times 5 \text{ m} \times 3 \text{ m}$
Desk height from the ceiling	2.15 m
LED power (P_{LED})	20 mW
Semi-angle at half power ($\Phi_{1/2}$)	70°
FOV at the receiver	60°
Detector physical area of PD (A_r)	1 cm
Transmission coefficient of optical filter ($T_s(\psi)$)	1.0
refractive index of lens at PD (n)	1.5

where ϕ is the irradiance angle. m is the order of Lambertian emission and is related to LED semiangle at half-power $\Phi_{1/2}$. The DC gain for a receiver located at a distance of d and angle ϕ with respect to the transmitter can be approximated as

$$H_{\text{los}}(0) = \begin{cases} \frac{A_r}{d^2} R_0(\phi) T_s(\psi) g(\psi) \cos \psi & 0 \leq \psi \leq \Psi_c \\ 0 & \psi > \Psi_c \end{cases} \quad (2)$$

where A_r is the detector area, ψ is the incidence angle, $\Psi_c \leq \pi/2$ is the field of view (FOV), T_s is the transmission coefficient of optical filter, and the non-imaging concentrator of gain g is represented by $g = n^2 / \sin^2 \Psi_c$ where n is the refractive index of lens. The received power is $P_r = P_{\text{LED}} \times H_{\text{los}}(0)$. Additive white Gaussian noise (AWGN) σ_n^2 is applied to the received power to create the training data for machine learning. The received power can be represented by

$$P_r = P_{\text{LED}} \times H_{\text{los}}(0) + \sigma_n^2. \quad (3)$$

2.2. Supervised Learning - Support Vector Regression

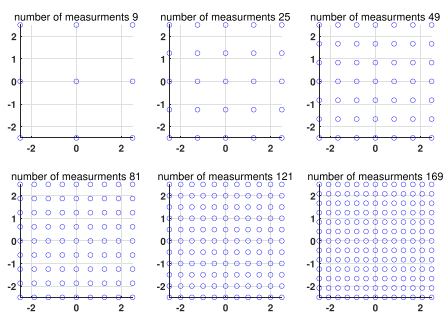


Figure 2. The number and location of measurements.

To estimate the channel, SVR is used among supervised learning techniques. SVR is based on Vapnik's support vector machine [7]. SVR, first introduced by Drucker, aims to create a hyperplane that is most similar to the observed values [8].

The input of the SVR uses the x,y coordinates of the receiver plane and the received power at the corresponding coordinates, and the output is the expected receiving power. Each coordinate collected for learning is shown in Figure 2. The radial basis function (RBF) is used for kernel. In order to find out the prediction performance for each number of measurements and each noise intensity, the training process was carried out separately.

3. Conclusions

In this paper, we have studied the visible light based LOS channel estimation through SVR using position input. Prediction performance will be analyzed according to the several locations of measurement. In addition, we will analyze the prediction performance at the coordinates beyond the learned area, which is the square area, with the transmitter centered and 5 meters wide.

Acknowledgments

This research was supported by Basic Science Research Program through the National Research Foundation of Korea (NRF) funded by the Ministry of Education (2018R1D1A3B07049858).

References

- [1] V. W. S. Chan, Free-space optical communications, *Journal of Lightwave Technology* 24 (12) (2006) 4750–4762. [doi:10.1109/JLT.2006.885252](https://doi.org/10.1109/JLT.2006.885252).
- [2] T. Komine, M. Nakagawa, Fundamental analysis for visible-light communication system using led lights, *IEEE transactions on Consumer Electronics* 50 (1) (2004) 100–107.
- [3] Y. Kim, S. Arya, Y. H. Chung, An optimal energy harvesting scheme for simultaneous lightwave information and power transfer over multi-layer turbulence-induced underwater channel, *Optics Communications* 501 (2021) 127382.
- [4] S. M. Aldossari, K.-C. Chen, Machine learning for wireless communication channel modeling: An overview, *Wireless Personal Communications* 106 (1) (2019) 41–70.
- [5] S. Rodríguez Pérez, R. Pérez Jiménez, F. J. López Hernández, O. B. González Hernández, A. J. Ayala Alfonso, Reflection model for calculation of the impulse response on ir-wireless indoor channels using ray-tracing algorithm, *Microwave and optical technology letters* 32 (4) (2002) 296–300.
- [6] N. Hayasaka, T. Ito, Channel modeling of nondirected wireless infrared indoor diffuse link, *Electronics and Communications in Japan (Part I: Communications)* 90 (6) (2007) 9–19.
- [7] C. Cortes, V. Vapnik, Support-vector networks, *Machine learning* 20 (3) (1995) 273–297.
- [8] H. Drucker, C. J. Burges, L. Kaufman, A. Smola, V. Vapnik, Support vector regression machines, *Advances in neural information processing systems* 9.

Clustering Algorithm for Cooperative Spectrum Sensing in Cognitive Radio Networks

Chunghyun Lee
School of Computer Science and
Engineering
Chung-Ang University
Seoul, Republic of Korea
chlee@uclab.re.kr

Donghyun Lee
School of Computer Science and
Engineering
Chung-Ang University
Seoul, Republic of Korea
dhlee@uclab.re.kr

Junsuk Oh
School of Computer Science and
Engineering
Chung-Ang University
Seoul, Republic of Korea
jsoh@uclab.re.kr

Geeranuch Woraphonbenjakul
School of Computer Science and
Engineering
Chung-Ang University
Seoul, Republic of Korea
geeranuch@uclab.re.kr

Taeyun Ha
School of Computer Science and
Engineering
Chung-Ang University
Seoul, Republic of Korea
tyha@uclab.re.kr

Sungrae Cho
School of Computer Science and
Engineering
Chung-Ang University
Seoul, Republic of Korea
srcho@cau.ac.kr

Abstract—Recently, spectrum sensing schemes are being studied in cognitive radio networks by classifying them into centralized model and decentralized model. A trend is moving from centralized to decentralized as cognitive radio networks focus on increasingly distributed environments in line with the Internet-of-Things. However, these two models each have their pros and cons that complement each other, so there is no guarantee which one is always better. In this paper, we propose an efficient clustering algorithm for secondary users in a clustered cooperative spectrum sensing model that absorbs the advantages of the above two models. The proposed algorithm forms a cluster through two-dimensional spatial correlation and shares sensing information through single-hop transmission between neighbors.

Keywords—Spectrum sensing, Clustered cognitive radio networks, Clustering algorithm

I. INTRODUCTION

As the demand for maritime Internet of Things (IoT) traffic increases significantly, the issue of availability of communication resources has emerged. This is important not only for now but also for the upcoming 6G. To solve this problem, the Spectrum sensing technology was proposed in CRN (Cognitive Radio Network), a communication system composed of PU (Primary Users) and SU (Secondary Users).

In CRN, SUs use Spectrum sensing technology [1]–[4] to detect unused spectrum licensed to PUs and use opportunistically vacant licensed channels. However, the spectral detection results of SU are not always accurate. This is because spectral sensing is greatly affected by various factors such as noise, multipath fading, shadowing, and receiver uncertainty problems [2]. To overcome the inaccuracy of spectrum sensing, many studies have proposed new approaches. As one of these studies, cooperative spectrum sensing techniques have received renewed interest. Cooperative spectrum sensing techniques share detection information between SUs to increase the accuracy of detection results.

Cooperative spectrum sensing models can generally be divided into two types: centralized and decentralized, depending on how SUs share sensing information in the network.

The centralized CRN (C-CRN) model utilizes a coordinator called a fusion center (FC) that gathers sensing

information from the SUs, computes a sensing schedule for the SU, and propagates it to the SU.

Unlike C-CRN, SU shares detection information without FC in decentralized CRN (D-CRN). The sensing schedule is also determined by the each SU. Distributed method appropriates to CRNs spectrum sensing performance since it adapts quickly to network changes. It also has a low power consumption level, which is important in CRNs.

Both models have their pros and cons. The centralized cooperative spectrum sensing model has excellent performance because it aggregates and processes the sensed information uniformly. However, recently CRNs are being applied in a distributed environment, and problems that occur when FC is disabled and excessive load are pointed out as disadvantages.

The distributed cooperative spectrum sensing model distributes these loads to each SU and is quite stable in terms of security. However, compared to the centralized cooperative spectrum sensing model, the complexity is high, and in terms of performance, it cannot surpass FC.

In order to solve this ironic situation, a model that combines the merits of the two models has been proposed. This corresponds to a heterogeneous model [5] that selects an appropriate algorithm according to the search coverage performance of the SU, or a cluster model in which it is processed by dividing it into several clusters. In particular, the clustered model is very suitable for the MEC-IoT environment, and the system model is similar.

In this paper, how a SU efficiently composes a cluster with other SUs in a clustered model and how this affects clustered cooperative spectrum sensing.

II. SYSTEM MODEL

A. Clustered Cooperative Cognitive Radio Networks (CC-CRNs)

The system model of clustered cooperative CRNs is configured as Fig. 1. PU may not exist, and one or more may exist. The probability of existence of PU is determined according to the hypotheses theoretic approach [6]. PU operates based on an omni-directional antenna. PU can use the allocated licensed spectrum with the highest priority. In other words, the PU has the right not to be subjected to any

other interference when in use. SU operates based on a directional antenna. SU senses whether PU is operating through a beam in a specific direction to find an idle spectrum. At this time, when the SU senses the use of the PU for the corresponding spectrum, the interference with the PU in use should be minimized.

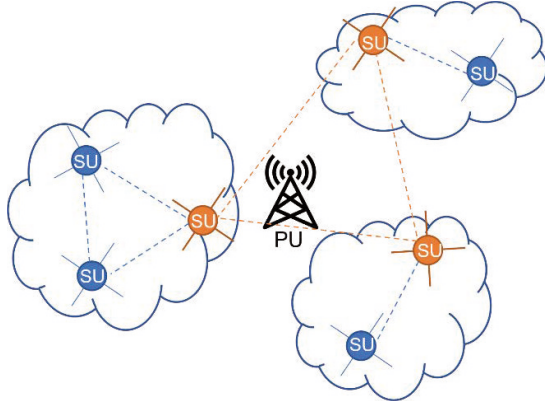


Fig. 1. System model of CC-CRNs

Each SU forms a cluster with adjacent SUs, and one of them is selected as the leader of the cluster. SUs in the cluster are in single-hop communication with adjacent SUs, and can share their sensing information through an underlay control channel.

$P(H_0)$: Probability that PUs are absent.

$P(H_1)$: Probability that PUs are present.

Also, sensing information can be shared between adjacent SUs belonging to different clusters. Therefore, it can be an opportunity to acquire the sensing information of the PU even if it belongs to different clusters.

B. Spectrum Sensing based on Energy Detection

The SU can check whether the PU is being used by detecting the PU signal power γ . That is, if the detected signal power is greater than a certain threshold λ , it is determined that the PU uses the licensed spectrum. In general, this judgment may not always be accurate. In the energy detection method, the accuracy of sensing probability can be improved by finding the optimal threshold.

$$P(H_0) = P(\text{SU fail to detect the PU signal}) = P(\gamma \leq \lambda)$$

$$P(H_1) = P(\text{SU success to detect the PU signal}) = P(\gamma \geq \lambda)$$

III. CLUSTERING ALGORITHM FOR CC-CRNs

In this study, we assume local clustering instead of global FC as Fig. 1. Each local cluster is called LBZ [8] and is defined as follows:

$$LBZ_k = \{SU_i \mid D(i,j) < R, i \in N, \forall SU_j \in LBZ_k\}$$

Where N is number of SUs, k denotes the index of LBZ and $D(i, j)$ denotes the transmission range between SU_i and SU_j . Within each LBZ_k , the LBZ leader basically collects all information from the SU. BZ formed by calculation through two-dimensional spatial correlation elects a leader. The leader calculates the center of the cluster through the two-dimensional coordinates of the SUs and selects the SU

closest to the center as the leader. Basically, SU collects all information of SUs within the same LBZ_k , and send sensing information to the LBZ leader using single-hop communication for the connectivity table as follow algorithm:

Algorithm 1 Local Broadcast Zone Clustering Algorithm

Step 1. Update local sensing information

1. All SU broadcast their local sensing information by single-hop communication.
2. Make connection table.

Step 2. Format LBZ according to definition

3. **for** $i := 0$ to N **do**
- if** SU_i is not contained any LBZ **then**

$$LBZ_k = LBZ_k \cup SU_i$$

- for** $j := i+1$ to N **do**

- if** SU_j is not contained any LBZ **then**

$$if D(i,j) < R then$$

$$LBZ_k = LBZ_k \cup SU_j$$

End if

End if

End for

End if

End for

Step 3. Select the LBZ leader according to cluster centroid

4. Compare between each SU's centroid and cluster centroid.
 5. Update the LBZ leader
-

Cluster spectrum sensing can be performed by applying the cluster LBZ configured as described above to the CRN. The overhead which is generated to FC in the centralized model is distributed across each cluster. The weakness which is caused by attack to FC can be addressed by flexibly changing the cluster leader. Also, unlike distributed models, the complexity is relatively low, and the performance of clusters can be as efficient as centralized models. Also, even if PU sensing fails in the cluster, sensing information is shared through adjacent clusters so that the cluster can know the unknown area.

IV. CONCLUSION

In this paper, spectrum sensing techniques in CRN are introduced to solve the problem of rapidly increasing traffic and insufficient frequency resources due to the advent of the large-scale maritime IoT era. Among them, the clustered spectrum sensing model, which is an efficient model that can compromise this, was introduced by analyzing the pros and cons of the centralized model and the decentralized model. The clustering technique, which is the core of the clustering model, configures a cluster through two-dimensional spatial correlation and selects a leader that can replace FC in the cluster. The centralization problem is solved through flexible leader selection and load balancing. Sensing performance is also guaranteed because this cluster is similar to a split centralized model. There is also an advantage of a distributed model that splits SUs into clusters, which is low in complexity and is suitable for CRNs in partitioned environments. Through these analyzes and algorithms, it is expected that the optimal spectrum sensing technique can be

studied by combining detailed sensing and optimization technique.

ACKNOWLEDGMENT

This studied was supported by the National Research Foundation of Korea (NRF) under Grant NRF-2019R1A2C1090447 funded by the Korea Government (Ministry of Science and ICT).

REFERENCES

- [1] A. Azarfar, J. F. Frigon, and B. Sanso, "Improving the reliability of wireless networks using cognitive radios," *IEEE Communications Surveys and Tutorials*, vol. 14, no. 2, pp. 338-254, April-June 2012.
- [2] I. F. Akyldiz, B. F. Lo, and R. Balakrishnan, "Cooperative spectrum sensing in cognitive radio networks:A survey," *Physical Communication*, vol. 4, pp. 40-62, 2011.
- [3] F. A. Awin, Y. M. Alginahai, E. Abdel-Raheem, and K. Tepe, "Technical issues on cognitive radio-based internet of things sysytems: A survey," *IEEE Access*, vol. 7, pp. 97887-97908, 2019.
- [4] B. Shang, V. Marojevic, Y. Yi, A. S. Abdalla, and L. Liu, "Spectrum sharing for UAV communications: Spatial spectrum sensing and open issues," *IEEE Vehicular Technology Magazine*, vol. 15, no. 2, pp. 104-112, June 2020.
- [5] Z. Gu, Y. Wang, T. Shen, and F. C. M. Lau, "On heterogeneous sensing capability for distributed rendezvous in cognitive radio networks," *IEEE Transactions on Mobile Computing*, vol. 20, no. 11, pp. 3211-3226, November 2021.
- [6] W. Na, J. Yoon, S. Cho, D. Griffith, and N. Golmie, "Centralized cooperative directional spectrum sensing for cognitive radio networks," *IEEE Transactions on Mobile Computing*, vol. 17, no. 6, pp. 1260-1274, 2018..
- [7] L. Li, Y. Qin, and X. Zhong, "A novel routing scheme for resource constraint opportunistic networks: A cooperative multiplayer bargaining game approach," *IEEE Transactions on Vehicular Technology*, vol. 65, no. 8, pp. 6547-6561, 2016.

Deep Reinforcement Learning Based Power Allocation Scheme in Uplink NOMA Systems

Won Jae Ryu

*ICT Convergence Research Center
Kumoh national Institute of Technology
Gumi, Republic of Korea
wj0828@kumoh.ac.kr*

Dong-Seong Kim*

*Dept. of IT Convergence Engineering
Kumoh national Institute of Technology
Gumi, Republic of Korea
dskim@kumoh.ac.kr*

Abstract—Non-orthogonal multiple access (NOMA) has higher spectrum efficiency and throughput than orthogonal multiple access (OMA). In this study, a deep reinforcement learning (DRL) based power allocation scheme for a near and far user is proposed. As the proposed scheme is based on DRL, the near and the far user find appropriate power ratios when they have to transmit signals to the base station (BS) in uplink channels. As the near and the far user send signals in the uplink channels, there is no shared information between them. Therefore, the power allocation in each user will be decided by only the channel state between BS and each user, and the reception of NACK or ACK. When the decision of success of transmissions is decided based on finite blocklength (FBL) regime. The proposed scheme showed that the users can find appropriate power allocation.

Index Terms—Uplink, non-orthogonal multiple access (NOMA), reinforcement learning, power allocation

I. INTRODUCTION

Non-orthogonal multiple access (NOMA) provides high spectral efficiency by superposing signals within the same time, same frequency, and same space as a candidate of technologies for next-generation wireless communications. For decoding the superposed signals, successive interference cancellation (SIC) is adopted to improve spectral efficiency [1], [2]. In this paper, deep reinforcement learning (DRL) [3] based power allocation scheme is adopted for cases where two users share the same frequency, same time, and same space in uplink NOMA systems. In this study, finite blocklength (FBL) is used [4], [5], under the Rayleigh fading channel [6], to confirm whether throughput and error rate requirements are satisfied or not, and DRL is adapted to make transmission power efficient. Using the proposed DRL scheme, simulation results showed that the uplink users were finding out suitable power ratios.

II. SYSTEM MODEL AND PROPOSED SCHEME

In this section, two users who share the same time and the same frequency are assumed in an uplink NOMA system, where there is no grant. Fig 1 describes the uplink NOMA system. As the near-user (NU) is located near the basestation (BS), the received power from the NU to the BS is larger than the received power from the far-user (FU). Using SIC, the signal from NU is decoded first and canceled. Then, the

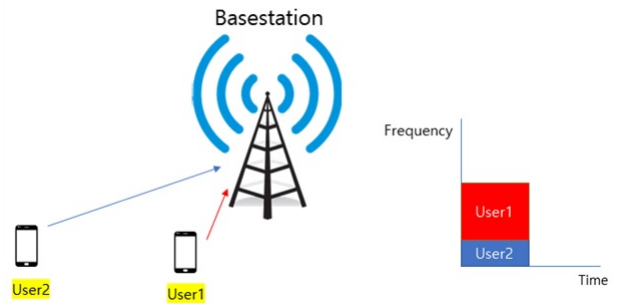


Fig. 1. System Model

signal of FU is decoded after SIC. Equations for each user's signal-to-interference-plus-noise ratio (SINR) are as follows:

$$x_n = \frac{h_n^2 p_n}{h_f^2 p_f + n_o + h_e^2}, \quad (1)$$

$$x_f = \frac{h_f^2 p_f}{n_o + h_e^2}. \quad (2)$$

x_n and x_f are SINRs, h_n and h_f are the channel gains, p_n and p_f are the power ratios for the NU and the FU respectively, h_e is the channel estimation error, and n_o is a Gaussian noise. Based on SINRs acquired by (1) and (2), the decoding error rate can be calculated as follows:

$$\epsilon = Q\left(\frac{C(x) - R}{\sqrt{nV(x)}}\right), \quad (3)$$

$$C(x) = \log_2(1 + x), \quad (4)$$

$$V(x) = 1 - \frac{1}{(1 + x)^2}, \quad (5)$$

$$Q(x) = \int_x^\infty \frac{1}{\sqrt{2\pi}} e^{-\frac{t^2}{2}} dt. \quad (6)$$

Using (3), the decoding error rate can be calculated. $C(x)$ means the Shannon capacity, $V(x)$ means a channel dispersion, and $Q(x)$ means Q-function. If the decoding error rate did not reach a target error rate, the transmission would be assumed failed.

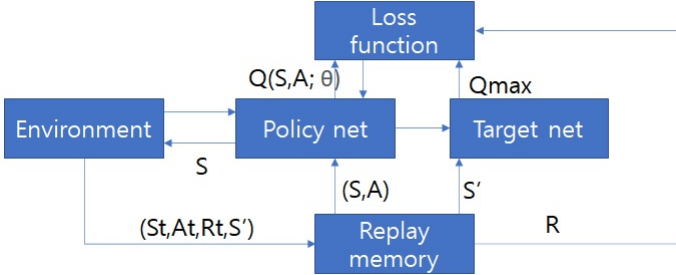


Fig. 2. Structure of DDQN

TABLE I
SIMULATION PARAMETERS AND ENVIRONMENT

Model	Double DQN
Structure	4(input) × 12 × 12 × 10(output)
Activation function	Relu
Optimizer	ADAM
Loss function	Mean square error
Input Parameters	Channel state, blocklength, target data rate, power allocation
Output(Power allocation)	0.1, 0.2, 0.3, 0.4, 0.5, 0.6, 0.7, 0.8, 0.9 1.0
Simulation Environment	Python 3.8.8 (Pytorch)

The proposed DRL model is based on double deep q-learning(DDQN). As shown in Figure 2, two different networks, the policy network, and the target network, are used to reduce overestimation [7]. Therefore, action selection and action evaluation are dealt with separately.

III. SIMULATION

In this study, Rayleigh fading channel model is adopted for the simulation. Using the proposed DRL scheme, a suitable power ratio is selected. If only one user failed transmission, it would be regarded as failed transmission and nack would be sent from BS to the users. Through this procedure, the proposed DRL scheme searches for an appropriate power ratio to successful transmissions. The simulation parameters are shown in Table I. Figure 3 shows the total reward of both FU and NU. X-axis means simulation times, and Y-axis means the reward. The equations of reward for the users are as follows:

$$R_n = \begin{cases} 100 - 50p_n & \text{if ack is received,} \\ 0 & \text{if nack is received,} \end{cases}$$

$$R_f = \begin{cases} 100 - 50p_n & \text{if ack is received,} \\ 0 & \text{if nack is received,} \end{cases} \quad (7)$$

$$R = R_n + R_f.$$

R_n and R_f are rewards for NU and FU, and R is the total reward. Each user gets each reward, based on the rewards, the users search for the appropriate power ratio to maximize the rewards. According to Figure 3, stable transmissions seem possible around 1,000th transmissions.

IV. CONCLUSION

In this study, the appropriate power ratios for transmissions for NU and FU are studied based on the proposed DDQN

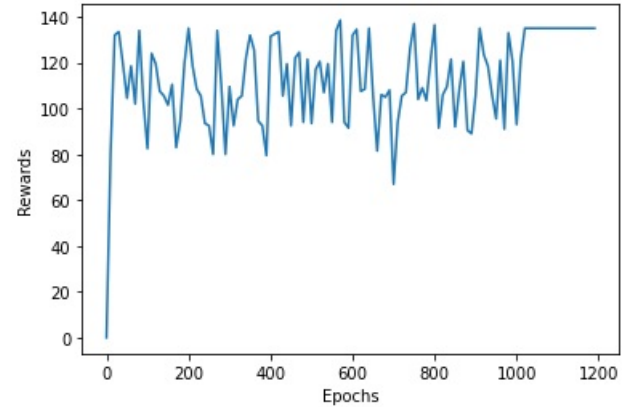


Fig. 3. Simulation results

scheme. As this system is an uplink system, any information between FU and NU is not shared. The only available feedbacks are ack/nack. And, the FBL regime is used to decide transmission fails or successes. Using the proposed DDQN scheme, the simulation results confirm that the users can find appropriate power ratios.

ACKNOWLEDGMENT

This work was supported in part by the Ministry of Science and ICT (MSIT), Korea, under the Grand Information Technology Research Center Support Program, supervised by the Institute for Information and Communications Technology Planning and Evaluation (IITP), under Grant IITP-2022-2020-0-01612, in part by the Priority Research Centers Program under Grant 2018R1A6A1A03024003, and in part by the Basic Science Research Program through the National Research Foundation of Korea (NRF), funded by the Ministry of Education, Science and Technology, under Grant 2022R1I1A1A01069334.

REFERENCES

- [1] Ryu, Won Jae, et al. "On the Performance Evaluations of Cooperative Retransmission Scheme for Cell-Edge Users of URLLC in Multi-Carrier Downlink NOMA Systems." Sensors 21.21 (2021): 7052.
- [2] Higuchi, Kenichi, and Anas Benjebbour. "Non-orthogonal multiple access (NOMA) with successive interference cancellation for future radio access." IEICE Transactions on Communications 98.3 (2015): 403-414.
- [3] Li, Yuxi. "Deep reinforcement learning: An overview." arXiv preprint arXiv:1701.07274 (2017).
- [4] Ryu, Won Jae, and Soo Young Shin. "Performance evaluation of a power allocation algorithm based on dynamic blocklength estimation for URLLC in the multicarrier downlink NOMA systems." Turkish Journal of Electrical Engineering & Computer Sciences 29.1 (2021): 310-320.
- [5] Polyanskiy, Yury, H. Vincent Poor, and Sergio Verdú. "Channel coding rate in the finite blocklength regime." IEEE Transactions on Information Theory 56.5 (2010): 2307-2359.
- [6] Lee, William CY. "Estimate of channel capacity in Rayleigh fading environment." IEEE transactions on Vehicular Technology 39.3 (1990): 187-189.
- [7] Van Hasselt, Hado, Arthur Guez, and David Silver. "Deep reinforcement learning with double q-learning." Proceedings of the AAAI conference on artificial intelligence. Vol. 30. No. 1. 2016.

A Study on Space Diversity Gain of Reflective LoS Channel in Maritime Long Range Communication

Woo Yong Lee

Mobile Communication Research Division,
Telecommunication & Media Research Laboratory
Electronics and Telecommunications Research
Institute (ETRI)
Daejeon, Republic of Korea
wylee@etri.re.kr

Keunyoung Kim

Mobile Communication Research Division,
Telecommunication & Media Research Laboratory
Electronics and Telecommunications Research
Institute (ETRI)
Daejeon, Republic of Korea
kykim12@etri.re.kr

Abstract—A long-distance line of sight (LOS) wireless communication environment, such as an extreme cold area made of seawater and glaciers, is a channel with little electromagnetic wave scattering. A wireless communication system for operating unmanned robot exploration in extreme cold regions such as Antarctica requires a high-speed transmission rate of 10Mbps or more over a long range of 50km or more. It is a very challenging study to apply a beamforming technique using omnidirectional multiple antennas to increase the radio signal strength of a moving vehicle on the terrestrial. In this paper, spatial diversity was analyzed to find out the limit of the maximum beamforming gain in a long-distance line-of-sight reflection channel environment where there is little scattering of electromagnetic waves. In this paper, the maximum spatial diversity gain is analyzed by approximating the line-of-sight reflection communication channel environment as a line-of-sight multiple input/output communication system, and a simulation is performed to find out the maximum spatial diversity gain according to the distance in long-range maritime communication.

Keywords—line of sight, long range communication, spatial diversity gain, spherical surfaces

I. INTRODUCTION

Spatial multiplexing was effective for high-speed communication in an indoor NLOS (Non Line Of Sight) radio channel environment with sufficient electromagnetic wave scattering [1, 2]. But, there is little spatial multiplexing gain in the line-of-sight radio channel with little electromagnetic scatters [2]. On the other hand, spatial diversity can work effectively in line-of-sight radio channels where there is poor electromagnetic scattering [3].

As a method for increasing the spatial diversity gain, a beamforming technique for optimizing the direction of the transmission and reception beams of the array antenna may be used. In previous studies, there was a hierarchical beamforming technique to reduce antenna training time and related overhead [4]. A disadvantage of this hierarchical beam search method lies in the asymmetric region of a wide and narrow beam. Transmitting a wide beam multiple times increases the beam alignment delay. Hierarchical beam search is complicated by needs for a wide dynamic scale of the power amplifier to allocate more power to transmit a wide beam and less power to transmit a narrow beam. To solve this problem, a subarray-based cross-correlation-based beam search technique was proposed under the assumption that the same phase shift is applied to each analog subarray [5]. In addition, a subspace projection-based AoA (Angle of Arrival) estimation technique has been proposed [6]. The phase ambiguity of AoA detection in subarray-based methods is resolved by additional training

symbols, post-processing in the frequency domain, and noise subspace projection and iterative update [7].

The first consideration in developing a high-speed communication system for a wide area is to predict a propagation path in a channel environment in an extreme cold area. The communicable environment is predicted and main specifications of the transceiver are determined. When predicting a propagation path, it is almost impossible to consider all propagation environmental conditions. Therefore, the communication channel environment is modeled and propagation path loss is predicted by considering only the direct and reflected waves, which have the greatest relative influence [8]. In this paper, the theoretical diversity gain according to the distance in the extreme cold environment is analyzed. This simulation result will be introduced and reflected in the design of the communication system for extreme cold areas to be developed in the future.

In this paper, only direct waves and reflected waves that have the greatest relative influence are considered. The spatial diversity gain is analyzed by approximating this communication channel to a 2×2 LoS-MIMO (multiple input/output) communication system. And we simulate the maximum spatial diversity gain in long-distance line-of-sight communication over 50 km.

II. DIVERSITY GAIN ANALYSIS IN SPHERICAL EARTH REFLECTION MODEL

Even when one transmitter tries to transmit to one receiver even in a channel environment where there is little scattering of electromagnetic waves, strong reflections from seawater and glaciers cause interference. We approximate the LOS- 2×2 MIMO channel to analyze the extreme cold region communication causing strong interference. In this case, the relationship causing interference between the transmission x and the reception y is expressed as the region of the reception signal $y \in \mathbb{C}^{2 \times 1}$ as shown in Equation (1).

$$y = Hx + N_0. \quad (1)$$

Here, $H \in \mathbb{C}^{2 \times 2}$: channel vector, $x \in \mathbb{C}^{2 \times 1}$: transmission signal vector, $N_0 \in \mathbb{C}^{2 \times 1}$: AWGN (Additive White Gaussian Noise).

Assuming the spherical reflection channel model [8], the line-of-sight wireless communication system can be viewed as a channel model to transmit data through MIMO antennas, and its shape is shown in Figure 1.

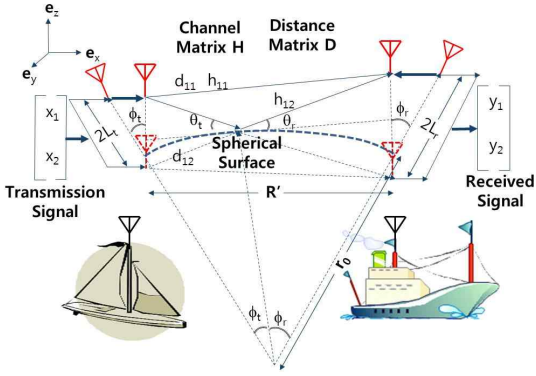


Figure 1. Parametric relationship between transmission and reception in LoS wireless communication system based on spherical reflection channel model.

Where, R' is the effective straight-line range between transmitter and receiver, L_t : the height of the transmitting antenna, L_r : the height of the receiving antenna, the radius of the earth r_0 , R distance from the surface of the earth, the angle of incidence θ_i , the angle of reflection θ_r , and R the spherical movement trajectory. Let $\phi (= \phi_i + \phi_r)$ be the spherical angle of the Earth with respect to. The (m, n) -th complex channel gain h_{mn} in the channel matrix \mathbf{H} can be showed by Equation (2).

$$h_{mn} = \frac{\lambda}{4\pi d_{mn}} e^{-j\frac{2\pi}{\lambda} d_{mn}} \quad (2)$$

The communication distance d_{mn} from the m -th receive antenna to the n -th transmit antenna is expressed as the following (3) when λ is the wavelength of the carrier radio frequency.

$$d_{mn} \cong \tilde{R} \left\{ 1 + 2 \left\{ \frac{(m-1)L_t \cos\phi_t - (n-1)L_r \cos\phi_r}{\tilde{R}} \right\}^2 \right\} \quad (3)$$

When the channel capacity C of the line-of-sight communication system is the transmission power E_x and the received noise N_0 is, it can be expressed as the following equation.

$$C = \log_2 \det \left(I_M + \frac{E_x}{N_0} \mathbf{H} \mathbf{H}^H \right) \quad (3)$$

Here, when approximated by 2×2 line-of-sight multiple input/output channels, $\mathbf{H} \mathbf{H}^H$ is expressed as Equation (5).

$$\mathbf{H} \mathbf{H}^H \cong 2 \left(\frac{\lambda}{4\pi R} \right)^2 \begin{bmatrix} 1 & \frac{2\pi L_t L_r \cos\phi}{\lambda R} \\ \frac{2\pi L_t L_r \cos\phi}{\lambda R} & 1 \end{bmatrix} \quad (5)$$

The spatial multiplexing gain (SMG) is defined as follows when $\text{SNR} \rightarrow \infty$ [3].

$$\text{SMG} = \lim_{\text{SNR} \rightarrow \infty} \frac{\log_2 \det \left(I_M + \frac{\text{SNR}}{m} \mathbf{H} \mathbf{H}^H \right)}{\log \text{SNR}} \quad (6)$$

For the spherical reflection channel model, SMG can be simplified from Equations (5, 6) to the Equation (7).

$$\text{SMG} \cong \frac{1}{2} \log 4 \left\{ 1 - \left(\frac{2\pi L_t L_r \cos\phi}{\lambda R} \right)^2 \right\} \quad (7)$$

Meanwhile, the spatial diversity gain (SDG) is defined as follows when $\text{SNR} \rightarrow \infty$ [3].

$$\text{SDG} = - \lim_{\text{SNR} \rightarrow \infty} \frac{\log \left(\text{SNR}^{-m} \left(1 - \frac{\text{SMG}}{\min(m, n)} \right) + \left(1 - \frac{\text{SMG}}{\min(m, n)} \right) \right)}{\log \text{SNR}} \quad (8)$$

Considering the spherical reflection channel model, SDG from equations (7) and (8) can be approximated by equation (9).

$$\text{SDG} \cong \frac{1}{2} \left[2 - \log 4 \left\{ 1 - \left(\frac{2\pi L_t L_r \cos\phi}{\lambda R} \right)^2 \right\} \right]^2 \quad (9)$$

III. RIS-BASED 2×2 LOS MIMO CHANNEL CAPACITY SIMULATION

Within the maximum transmission distance of 50 km, the carrier frequency is 3 GHz ($\lambda = 10$ cm), and the antenna separation distance is set to $L = 2,000$. At this time, the simulation result of the spatial diversity gain for LoS wireless communication system based on spherical reflection channel model is shown in Figure 2.

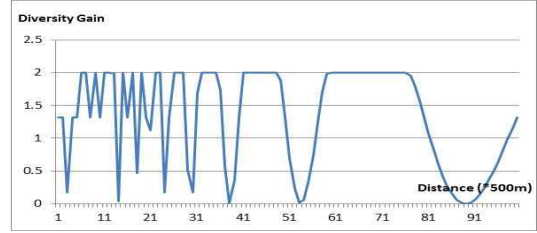


Figure 2. Spatial diversity gain versus distance in a spherical reflection channel model.

ACKNOWLEDGMENT

This paper is a research conducted with the support of the Korea Institute of Marine Science & Technology Promotion (KIMST) funded by the government (Ministry of Science and ICT) in 2022. [No. 2021-0626, Development of Polar Region Communication Technology and Equipment for Internet of Extreme Things (IoET)].

REFERENCES

- [1] E. Telatar, "Capacity of multi-antenna Gaussian channels," *Eur. Trans. Telecommun.*, vol. 10, no. 6, pp. 585–595, Nov. Dec. 1999.
- [2] W. Y. Lee, K. Kim, Y. Kim, and D. Kwon, "A Study on Spatial Multiplexing Gain in LOS- 2×2 MIMO Intelligent Reconfiguration Channel Environment," in Proc. 12th Int. Conf. on ICT Convergence (ICTC), pp. 590–592, Oct. 2021.
- [3] L. Zheng and D. N. C. Tse, "Diversity and Multiplexing: A Fundamental Tradeoff in Multiple-Antenna Channels," *IEEE Trans. Inform. Theory*, vol. 49, no. 5, pp. 1073–1096, May 2003.
- [4] S. Noh, J. Song, and Y. Sung, "Fast Beam Search and Refinement for Millimeter-Wave Massive MIMO Based on Two-Level Phased Arrays," *IEEE Trans. Wireless Commun.*, vol. 19, no. 10, pp. 6737–6751, Oct. 2020.
- [5] J. Zhang, X. Huang, V. Dyadyuk, and Y. Guo, "Massive hybrid antenna array for millimeter-wave cellular communications," *IEEE Wireless Commun.*, vol. 22, no. 1, pp. 79–87, Feb. 2015.
- [6] F. Shu et al., "Low-complexity and high-resolution DOA estimation for hybrid analog and digital massive MIMO receive array," *IEEE Trans. Commun.*, vol. 66, no. 6, pp. 2487–2501, Jun. 2018.
- [7] C. Qin, J. A. Zhang, X. Huang, and Y. J. Guo, "Virtual-subarray-based angle-of-arrival estimation in analog antenna arrays," *IEEE Wireless Commun. Lett.*, vol. 9, no. 2, pp. 194–197, Feb. 2020.
- [8] J. Wang, et al., "Wireless Channel Models for Maritime Communications," *IEEE Access*, vol. 6, pp. 68070–68088, Dec. 2018.

Beamforming and Power Optimization Techniques in Cell-Free Networks

Keunyoung Kim

Mobile Communication Research Division

ETRI

Deajeon, Republic of Korea

kykim12@etri.re.kr

Woo Yong Lee

Mobile Communication Research Division

ETRI

Deajeon, Republic of Korea

wylee@etri.re.kr

Abstract—Cell-free networks are expected to provide uniformly high data rates for all users and considered as a candidate for 6th generation wireless communications. Under various beamforming schemes and optimized power allocation we verifies evenly balanced and high spectral efficiency can be achievable regardless of user's locations and an increasing number of users. Beamforming schemes are chosen to maximize the received power, minimize the received interference, or to maximize the signal to interference and noise ratio. Power allocation schemes are optimized for the same level of these quantities.

Index Terms—Cell-free networks, beamforming, power optimization

I. INTRODUCTION AND SYSTEM MODEL

Cell-free networks are expected as a possible 6th generation mobile technology to provide uniformly high data rates for all users in which multiple access points (APs) are jointly transmit and receive data. Users serving in cell-free networks experience low variations in signal power, low interference, and high signal power [1]. The full potential of cell-free networks will be investigated assuming perfect channel estimation without delay in data transmission. Under various beamforming schemes and appropriate power optimization technique we will evaluate the achievable data rate and verify the performance of cell-free networks.

We consider both the uplink (UL) and the downlink (DL) transmissions of a cell-free network with L single-antenna access points (APs) and K single-antenna users. The schematic diagram for the UL is given in Fig. 1.

II. BEAMFORMING AND POWER ALLOCATION

Beamforming schemes are chosen to maximize the received power, minimize the received interference, or to maximize the signal to interference and noise ratio. The beamforming schemes are summarized in Fig. 2. Power allocation schemes are optimized for the same level of these quantities. We deal with various optimization problems using a unified mathematical framework both for the UL and the DL to provide closed form solutions for different schemes. For optimization

This paper is a research conducted with the support of the Korea Institute of Marine Science & Technology Promotion (KIMST) funded by the government (Ministry of Science and ICT) in 2022. [No. 2021-0626, Development of Polar Region Communication Technology and Equipment for Internet of Extreme Things (IoET)]

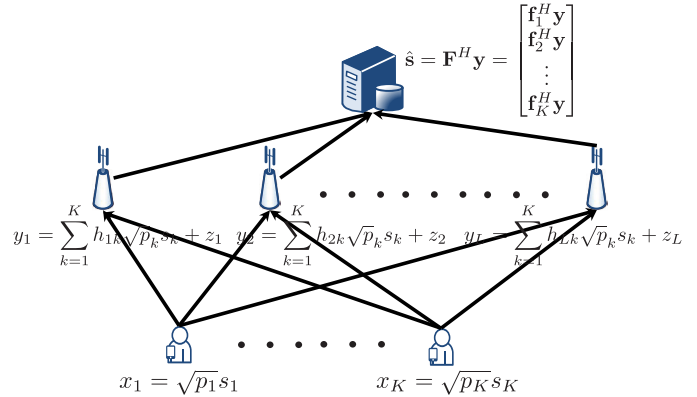


Fig. 1. Uplink system model of cell-free networks.

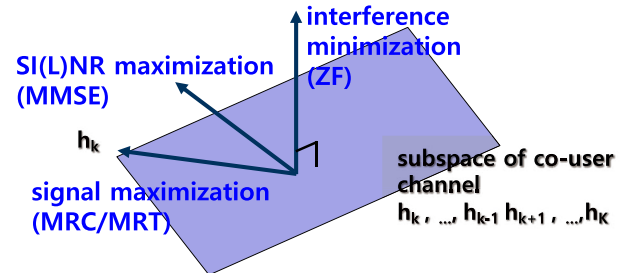


Fig. 2. Summary of beamforming schemes.

problems that do not produce a unique solution, we impose additional objectives such as minimum total transmit power and evenly balanced quantities.

III. EXPECTED RESULTS AND CONCLUSIONS

We will present 2 major results describing almost balanced spectral efficiency of each user. The very steep slope of the cumulative distribution lines will show very little differences in achievable data rate of each user in different locations. A small gap between the lines will indicate small performance degradation with an increasing number of users.

REFERENCES

- [1] Ö. T. Demir, E. Björnson, and L. Sanguinetti, *Foundations of User-Centric Cell-Free Massive MIMO*. Now Foundations and Trends, 2021.

Vessel MMSI Forgery Prevention System

Sung-Hwa Han
Dept. of Information Security
Tongmyong University
Busan, Republic of Korea
shhan@tu.ac.kr

Young-Sik Park
Dept. of Aviation Service
Tongmyong University
Busan, Republic of Korea
okyspark@gmail.com

Abstract—MMSI (Maritime Mobile Service Identify) is a maritime vessel identification number and is used in many countries and various fields. This MMSI is stored in the mobile device in the ship. Malicious users can exploit it by modifying or duplicating the MMSI. This is because the device management subject in which the MMSI is stored is the same as the ship subject. In this study, a certificate-based encrypted MMSI distribution and authentication system was proposed to improve the security environment. Through this, it is possible to identify and deny the abuse of MMSI such as unauthorized modulation.

Keywords—MMSI, Forgery, Certificate, Vessel ID, TPM

I. INTRODUCTION

MMSI is a 9-digit identification number that is widely used in maritime stations and countries to which ships belong. This MMSI is stored in a mobile device and is used for Digital Selective Calling (DSC), Automatic Identification System (AIS), and Emergency Position Indicating Radio Beacon (EPIRB).

A malicious attacker could modify this information. Forged MMSI can cause various marine accidents by making it impossible to track the vessel. In this study, we propose a management system that provides safe MMSI distribution and authentication functions to improve the ship security environment. Through this, the MMSI cannot be arbitrarily modified and cannot be abused.

II. SECURITY THREAT

MMSI is essential for ship operation management. Maritime departments in each country can use the MMSI to determine the direction of a vessel's movement, as well as the location of adjacent vessels.

This MMSI is issued by the ship manager upon application to the Federal Communications Commission (FCC). The ship manager stores the issued MMSI in the mobile device. However, since this mobile device is mounted on the ship, any crew member aboard the ship can access the device. In this environment, a malicious attacker can access the mobile device and tamper with the MMSI.

Such MMSI forgery creates various problems. A malicious attacker can assign the MMSI stored in the mobile device to another vessel or set it to a completely different MMSI. MMSI can be deleted if necessary.

Such MMSI forgery can be used as a tool for various crimes. Vessels that are not at sea can cause vessel collisions. In addition, it will be unable to respond to accidents occurring on adjacent ships.

III. VESSEL MMSI FORGERY PREVENTION SYSTEM

In order to prevent forgery of MMSI, it is necessary to manage MMSI from the initial issuance stage. In this study, we propose a certificate-based MMSI issuance and authentication system.

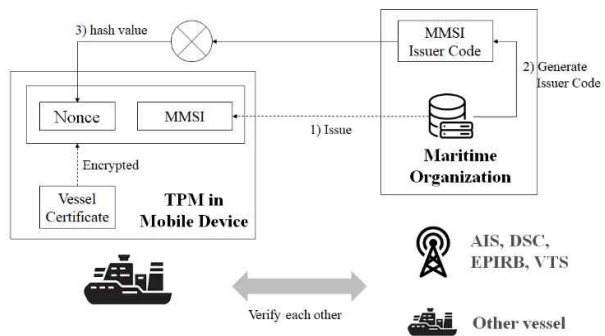


Fig. 1. Vessel MMSI forgery prevention system architecture

Figure 1 shows the MMSI issuance system proposed in this study. When issuing MMSI, it is issued including the nonce distributed by the issuing organization and the ship certificate. Nonce is a hash value including the MMSI and the issuing authority's key. MMSI is used in DSC, AIS, EPIRB, Vessel Traffic Service System(VTS) etc. in vessels. When the vessel is at sea, the MMSI is periodically accredited by maritime authorities.

When a malicious attacker falsifies the MMSI, maritime authorities can immediately recognize it. When a malicious attacker forges the MMSI, it first matches the nonce. Also, in order to forge this nonce, the certificate of the MMSI issuer is required, so this is virtually impossible. In particular, when all issued information including this MMSI is stored in the Trusted Platform Module(TPM), arbitrary modification is virtually impossible.

IV. CONCLUSION

MMSI is an essential element for safe maritime vessel operation. MMSI is an essential element for safe maritime vessel operation. To this end, in this study, an issuance system that cannot forge MMSI was proposed. It is hoped that this study will lead to a healthy marine environment.

REFERENCES

- [1] Lei, J., Chu, X. and He, W., "Trajectory data restoring: A way of visual analysis of vessel identity base on optics," Journal of Web Engineering, pp.413-430, 2021.
- [2] Fu, X., Xiao, Z., Xu, H., Jayaraman, V., Othman, N. B., Chua, C. P. and Lind, M., "AIS data analytics for intelligent maritime surveillance systems," In Maritime Informatics, Springer, Cham, pp. 393-411, 2021.

Density-based contention management for collision avoidance in dense IoT networks

Sejin Choi, Jaewan Lee, Minwoo Kwon, and Yonggang Kim

Division of Computer Science and Engineering, Cheonan-si Chungcheongnam-do,

Kongju National University, Republic of Korea

ygkim@kongju.ac.kr

Abstract—In Internet-of-things (IoT) networks where IoT nodes are densely deployed, collisions among the nodes are highly expected. Although IoT nodes may perform listen-before-talk approach to avoid collisions as in CSMA/CA protocol, the collision probability increases as the density of IoT nodes increases. Instead of using the fixed initial minimum contention window size, we propose to adjust initial contention window size according to the density of the networks. When the collisions are highly expected, the proposed method increases the initial contention window size for collision avoidance. Through the simulation results, we showed that the proposed method is applicable in dense IoT networks.

I. INTRODUCTION

In Internet-of-things (IoT) networks where IoT nodes work as slave nodes and transmit sensed data to the master node, IoT nodes are generally placed in remote and un-reachable places such as maritime environment [1]. Because IoT nodes for sensing the data in remote areas are hard to be connected to power supply, efficient data transmission without significant increase in energy consumption is important to increase lifetime of the nodes. An IoT network following CSMA/CA protocol is assumed to avoid collisions and decrease energy consumption caused by unnecessary transmissions. When a slave IoT node have uplink data, the node transmits ready-to-send (RTS) to the master node. After receiving the clear-to-send (CTS) from the master node, the slave IoT node transmits uplink data to the master node. Note that initial RTS transmission is decided by the back-off process, which is affected by the window size. The back-off time is randomly selected within a contention window size. Although the back-off time is randomly selected, collisions could be easily occurred in networks where a lot of nodes trying to transmit uplink data to the master node. The excessive collisions in dense IoT networks degrade both of the throughput performance and energy efficiency. Kim *et al.* studied contention-based transmission coordination in dense networks [2]. The collisions are occurred by nearby interfering base stations in downlink transmissions. To efficiently coordinate downlink transmissions in dense networks with independently operating base stations, the authors proposed a random number mechanism to decide whether to transmit downlink data.

In this paper, we propose a density-based contention management for uplink transmissions in dense IoT networks. As the density of IoT nodes increases, the collisions among the

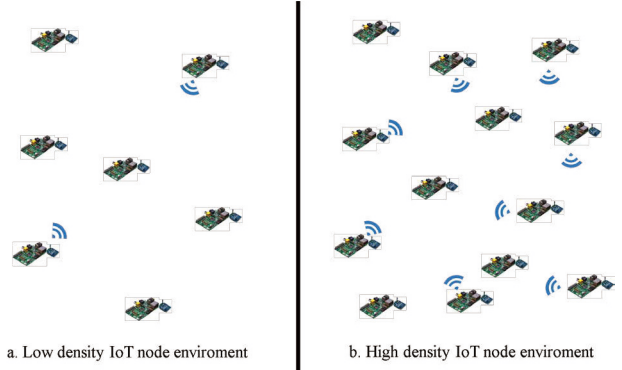


Fig. 1. Collisions according to the density of IoT nodes.

nodes is likely to be occurred more frequently. The proposed method increases the initial contention window size according to the density of the IoT nodes to avoid the collisions. Instead of using the same minimum window size regardless of the density, it is better to increase the initial contention window size when the collisions among the nodes are highly expected.

II. DENSITY-BASED CONTENTION MANAGEMENT

The IoT networks where slave IoT nodes transmit sensed data to the master node is considered. Figure 1 shows IoT network environments according to the density of the slave nodes. As shown in the figure, collisions are highly expected as the density of the nodes increases. Hence, instead of using the same initial minimum contention window size, contention management based on density of IoT nodes is required to decrease collisions and improve uplink transmission performance. Note that the proper collision avoidance increases the energy efficiency and enhance the lifetime of the IoT networks.

Let n_0 be the master node and $\mathcal{N} = \{n_1, n_2, \dots, n_N\}$ be the IoT nodes trying to transmit uplink data to the master node n_0 . The IoT node performs medium sensing to confirm whether the channel is busy before it transmits uplink data to the master node, and postpone its transmission if the channel is busy. When the uplink channel is idle, IoT nodes which have uplink data in their queues try to transmit uplink data after the back-off time to avoid collisions among the nodes. Let ω_{n_i} be the randomly selected back-off time of the station n_i where $\omega \in [0, CW]$ and CW is the contention window size. The station n_i postpones its uplink transmission until

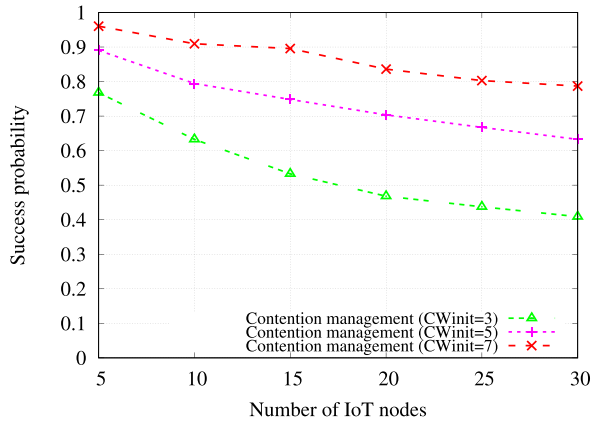


Fig. 2. Transmission success probability according to the density.

the ω_{n_i} counts down to 0. Note that CW becomes double after the unsuccessful transmission until the CW reaches the predefined maximum value CW_{max} .

Although the contention window size increases after the unsuccessful transmission, the contention window size CW does not have to start with the minimum contention value when the collision is highly expected. The proposed method decides the initial contention window size CW_{init} based on the density which can be calculated as

$$CW_{init} = \alpha * D * CW_{min}, \quad CW_{init} \geq CW_{min} \quad (1)$$

where α is the adjustment value and D is the density. Then, the initial back-off value is decided as follows:

$$\omega_{n_i} = [0, CW_{init}], \quad \text{for } \forall n_i \in \mathcal{N}. \quad (2)$$

With the proposed density-based contention management, we decrease the unnecessary contentions and corresponding energy consumption in dense IoT networks.

III. PERFORMANCE EVALUATION

A. Simulation

To evaluate the performance of the density-based contention management method, we constructed IEEE 802.11-based IoT networks by using MATLAB. The IoT nodes transmit uplink data to the AP, and it is assumed that the size of all uplink data is the same. We adjust the initial minimum contention window size to mitigate the collision avoidance in IoT networks. Note that the CW_{init} is deterministically given for simple evaluation.

Figure 2 shows the transmission success probability with regard to the number of IoT nodes. Note that the success probability decreases as the number of IoT nodes increases because of excessive collisions. However, as shown in the results, the success probability of contention management with $CW_{init} = 7$ is better than the one with $CW_{init} = 3$. In addition, the performance gap between them increases as the number of IoT nodes increases. Through simulations, we showed that the proposed density-based contention management increases the uplink performance in dense IoT networks.

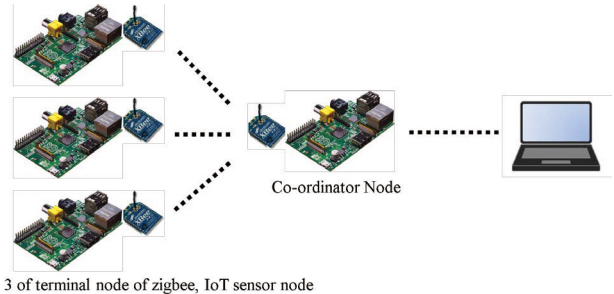


Fig. 3. Test-bed for density-based collision management in IoT networks.

B. Test-bed Implementation

The test-bed for density-based collision management consists of four XBee ZigBee TH module, four Raspberry Pi 4 model B, and four bread board adopter for XBee TH module. Each Raspberry Pi node has ZigBee TH module connected to GPIO port. One Raspberry Pi node works as a master node, and three Raspberry Pi nodes work as slave nodes that transmit uplink data to the master node. The master node is connected to the host computer that manages contention procedure following the density of the nodes. A single uplink channel is assumed for the test-bed. For simple evaluation, the slave nodes transmit same size of uplink data which is fixed as 128 bits. In the slave nodes, 128 bits of data is created every 100 ms and then stored in their queue. After the random back-off depending on the contention window size and RTS/CTS process, the uplink transmission is performed. By adjusting the contention window size, the uplink transmission performance could be evaluated in the test-bed.

IV. CONCLUSION AND FUTURE WORK

In this paper, we studied density-based contention management in dense IoT networks. The proposed method adjusts the initial contention window size according to the density of IoT nodes in the networks. By appropriate adjustment of contention window, the success probability of uplink transmission increases and unnecessary energy consumption caused by collision decreases. Through the simulations, we evaluated the feasibility of the proposed method, and we implemented a test-bed. In the future works, the test-bed would be extended to properly test dense maritime IoT networks. We plan to further develop proposed contention management method by adopting learning approach to dynamically decide contention avoidance procedure in dense maritime IoT networks.

ACKNOWLEDGEMENT

This work was supported by the research grant of Kongju National University in 2022.

REFERENCES

- [1] T. Yang, H. Feng, S. Gao, Z. Jiang, M. Qin, N. Cheng, and L. Bai, "Two-stage offloading optimization for energy-latency tradeoff with mobile edge computing in maritime Internet of Things," *IEEE Internet of Things Journal*, vol. 7, no. 7, pp. 5954–5963, 2019.
- [2] R. Kim, H. Choi, Y. Kim, and H. Lim, "Contention-based transmission coordination for interfering bss in dense mmwave networks," in *International Conference on Information and Communication Technology Convergence (ICTC)*, October 2018.

Transmission Loss Analysis of SATCOM Radomes With Wide Incident Angle

Tae-hyeon Kim

Electronic Engineering

Gyeongsang National University

Jinju-si, Republic of Korea

free4766@gnu.ac.kr

Wang-sang Lee

Electronic Engineering

Gyeongsang National University

Jinju-si, Republic of Korea

wsang@gnu.ac.kr

Abstract— This paper presents analysis of transmission loss for SATCOM(Satellite Communication) radome with wide incident angle. SATCOM radome is mounted on aircraft to protect satellite communication antenna. To protect from external environment and secure electrical performance, SATCOM radome has a sandwich-type structure. Three models of radomes were manufactured for operating frequency of antenna at 10-15 GHz, and transmission loss was compared using calculation and simulation.

Keywords—SATCOM(Satellite Communication), radome, A-sandwich, C-sandwich, Transmission Loss

I. INTRODUCTION

Radome is a dome-shaped structure mounted on a radar or antenna. It prevents degradation of electrical performance and damage to antenna from external environment. In addition, it secures a space for antenna to be installed, and also has effect of maintaining security by preventing external exposure of the antenna. In particular, use of radome is essential because SATCOM(Satellite Communication) radome in this paper is mounted on an aircraft and used for communication with satellite.

Radome surrounds antenna to protect it. For that, radome must be structurally strong enough and at the same time have least effect on performance of antenna[1]. Therefore, dielectrics are mainly used in radomes. For SATCOM radome to be used in aircraft, it must achieve good structural strength performance, light weight, and also have electrical transparency. For this purpose, three models of SATCOM radome using A-sandwich and C-sandwich structures among the styles classified in MIL-7705B[2] were manufactured. Their target frequency is 10-15 GHz. Satellites located at high altitude orbit, so securing communication performance with wide incident angle is required. For analysis of electrical characteristics of these three radomes, theoretical calculation and electromagnetic simulation has proceeded. In this paper, characteristics of radome were compared by transmission losses.

II. TRANSMISSION LOSS ANALYSIS

A. Boundary Value Solution Calculation using MATLAB

In the analysis of SATCOM radome composed of several layers, reflection coefficient and transmission coefficient can be obtained by theoretical calculations through Boundary Value Solution[3]. Magnitude of incident, reflected, and transmitted power is expressed by the following form of matrix.

$$\begin{bmatrix} E_0^+ \\ E_0^- \end{bmatrix} = \left[\prod_{i=1}^N \frac{1}{T_i} \begin{pmatrix} e^{j\gamma_i l_i} & R_i e^{-j\gamma_i l_i} \\ R_i e^{+j\gamma_i l_i} & e^{-j\gamma_i l_i} \end{pmatrix} \right] \frac{1}{T_{N+1}} \begin{pmatrix} 1 & R_{N+1} \\ R_{N+1} & 1 \end{pmatrix} \begin{pmatrix} E_{N+1}^+ \\ 0 \end{pmatrix} \quad (1)$$

Parameters used in the calculation are thickness, permittivity, and loss tangent of each layer. With these parameters, structure of SATCOM radome, and operating frequency, transmission loss can be calculated with MATLAB in short time[4].

B. Full wave Electromagnetic Simulation

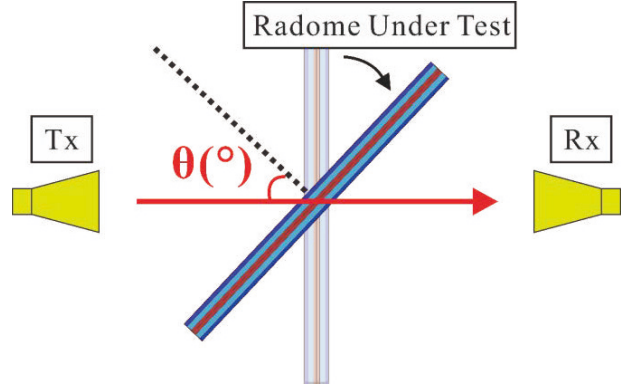


Fig 1. Test condition setup.

Full wave Electromagnetic analysis has been simulated. CST Microwave Studio was used for the simulation. Two 15dBi standard gain horn antennas were used to radiate 10-15 GHz electromagnetic wave. With these horn antennas, S_{21} was measured by setting waveguide port to WR-75 standard waveguide. And each SATCOM radome was modeled and inserted between antennas. Distance between antenna is 40cm. Difference between free space S_{21} without a radome and S_{21} with a radome is a transmission loss[5].

III. RESULTS DISCUSSION

Three SATCOM radome models were used for analysis. One radome model using A-sandwich structure and two radome models using C-sandwich structure were used. Structure of radome is shown in Fig. 3. Parameters in TABLE I were used in test models.

Fig. 2 shows transmission loss by incident angles. A-sandwich radome shows higher transmission loss than C-sandwich radome in generally. At incident angle of 0° and 10° , A-sandwich radome shows maximum transmission loss of 4.8dB and 4.7dB, respectively. On the other hand, both of two C-sandwich models show a lower transmission loss than A-sandwich model. However transmission loss of the C-sandwich model with only E-glass increases up to 4.1dB and 2.4dB, respectively. C-sandwich model with E-glass and Quartz shows stable result than other models under 1.6 and 1.8 dB at the same incident angle. Thereafter, transmission loss is lowered in all models up to incident angle of 70° , and transmission loss increases dramatically up to 3.5dB level near 10 GHz at incident angle of 80° .

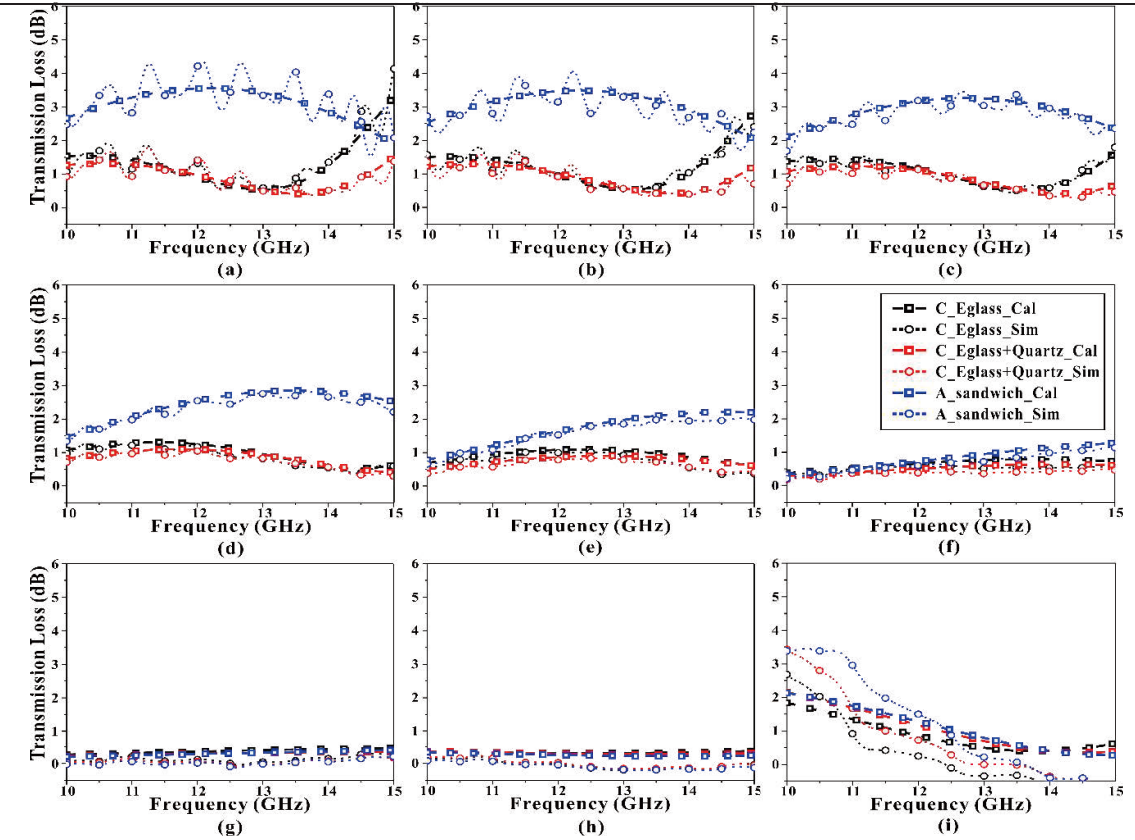


Fig 2. Transmission loss of SATCOM radomes by incident angle, (a) 0°, (b) 10°, (c) 20°, (d) 30°, (e) 40°, (f) 50°, (g) 60°, (h) 70°, (i) 80°.

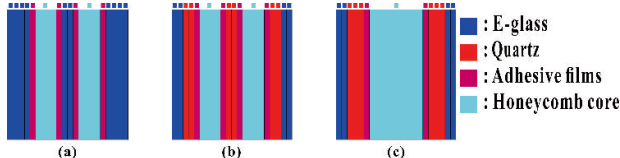


Fig 3. SATCOM radome models under test, (a) C-sandwich with E-glass, (b) C-sandwich with E-glass & Quartz, (c) A-sandwich.

TABLE I. PARAMETERS APPLIED IN RADOMES

Layer	ϵ	$\tan\delta$	Thickness (mm)	
			C-sandwich	A-sandwich
E-glass	4.54	0.017		0.288
Quartz	3.26	0.008		0.298
Adhesive	3.46	0.037		0.25
Honeycomb	1.09	0.003	4.572	9.144

IV. CONCLUSION

As a result of comparing transmission loss of SATCOM radomes through calculation and full wave electromagnetic simulation, two analysis results show very similar tendency. The results for incidence angle of transmission loss are different, showing a low transmission loss at 40° to 70° and a high transmission loss near 10 GHz at 10°. The model using A-sandwich structure has a high transmission loss at the most angles of incidence, and it stands out especially from low angles. So C-sandwich structure is more suitable for

SATCOM radome in the target frequency. Among the C-sandwich models, at results in 0° and 10°, model using only E-glass shows an increase in transmission loss near to 15 GHz. However, model using E-glass and Quartz shows relatively low values, so this model is the best structure.

ACKNOWLEDGMENT

This work was supported by ‘Development of Ku-Band SATCOM Radome for Civil Aircraft using OOA Process’ funded by the Ministry of SMEs and Startups (Korea, MSS). (S3088237), and Institute of Information & communications Technology Planning & Evaluation (IITP) grant funded by the Korea government(MSIT). (No.RS-2022-00156409, ICT innovation human resources 4.0).

REFERENCES

- [1] Qamar, Zeeshan, Jorge L. Salazar-Cerroño, and Nafati Aboserwal. "An ultra-wide band radome for high-performance and dual-polarized radar and communication systems." *IEEE Access* 8 (2020): 199369-199381.
- [2] Military Specification: General Specification for Radomes, MIL-R-7705B, Jan. 1975
- [3] Dennis Kozakoff, Analysis of Radome Enclosed Antennas, Second Edition , Artech, 2009.
- [4] Lien, Fredrik. Modelling and Test Setup for Sandwich Radomes. MS thesis. Institutt for elektronikk og telekommunikasjon, 2014.
- [5] Kurri, Mikko, and Asko Huuskonen. "Measurements of the transmission loss of a radome at different rain intensities." *Journal of Atmospheric and Oceanic Technology* 25.9 (2008): 1590-1599.

Channel Estimation for RIS aided Multi-user SISO system using super-resolution

Jeongbin Seo

Electronics Engineering

Pusan National Univ.

Busan, Republic of Korea

sjb9612@pusan.ac.kr

Donghwan Kim

Electronics Engineering

Pusan National Univ.

Busan, Republic of Korea

dongh@pusan.ac.kr

Suk Chan Kim

Electronics Engineering

Pusan National Univ.

Busan, Republic of Korea

sckim@pusan.ac.kr

Abstract—In this working in process paper, we propose a channel estimation technique for reconfigurable intelligent surfaces aided system using deep back projection networks, which is one of the super-resolution deep learning models. In simulation, the proposed channel estimation technique has better performance than least square method.

Index Terms—Channel Estimation, RIS, Super-Resolution, Deep Learning

I. INTRODUCTION

In this working in process(WIP) paper, we propose channel estimation method using super-resolution deep learning for reconfigurable intelligent surfaces(RIS) aided multi-user single input single output(SISO) system [1]. The proposed channel estimation method has superior channel estimation performance than conventional method.

II. SYSTEM MODEL

We assume that there are a base station(BS) and K users with a single antenna, and one RIS with N passive elements. The users communicate in a time division duplexing method, and the BS estimates the channel in the uplink state by utilizing the reciprocity of the channel. When the $k \in \{1, 2, \dots, K\}$ th user transmits the pilot signal(x_k), the simplified received signal(y_k) by the BS is

$$\begin{aligned} y_k &= \mathbf{h}_{BR}\Phi\mathbf{h}_{RU,k}x_k + w \\ &= \text{diag}(\mathbf{h}_{BR})\mathbf{h}_{RU,k}\phi x_k + w \\ &= \mathbf{h}_k\phi x_k + w, \end{aligned} \quad (1)$$

where the $\mathbf{h}_{BR} \in \mathbb{C}^{1 \times N}$ is the channel between the BS and the RIS, the $\mathbf{h}_{RU,k} \in \mathbb{C}^{N \times 1}$ is the channel between RIS and the k th user, and the $w \in \mathbb{C}^{1 \times 1}$ is additive white Gaussian noise. The Φ and ϕ are the reflection coefficient matrix of RIS and its vectorization form. The \mathbf{h}_k is a cascade channel.

III. PROPOSED CHANNEL ESTIMATION METHOD

We propose a channel estimation technique using DBPN that is super-resolution deep learning models. The proposed channel estimation method estimates the entire channel by inputting fractional channel information into the DBPN. The DBPN used in the proposed method has the following structure: two convolution blocks, a pair of up & down projection blocks, two pairs of dense up & down projection blocks, and

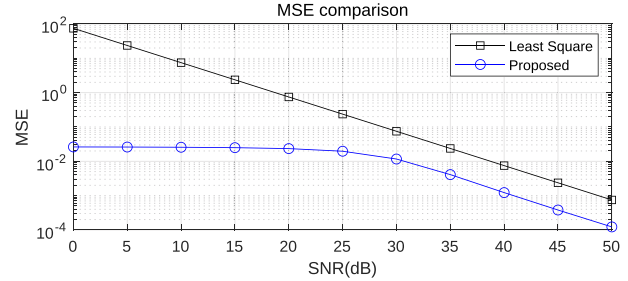


Fig. 1. MSE comparison for channel estimation.

two convolution blocks. The mean square error was used as the loss function.

IV. SIMULATION RESULT

In this chapter, we describes the channel estimation simulation results of the RIS-aided system. The Fig. 1 shows the channel estimation mean square error(MSE) according to the SNR of the proposed channel estimation method and the least square method. The proposed channel estimation method has superior performance than least squares for all SNR.

V. CONCLUSION

In this WIP paper, we proposed a channel estimation method for RIS-aided system using DBPN. The proposed channel estimation method estimates the entire channel with fractional channel information. The proposed channel estimation method has superior performance than least square method.

ACKNOWLEDGMENT

This work was supported by the Technology Innovation Program (or Industrial Strategic Technology Development Program) (00144500, Development of 3D ultrasonic sensor technology for vehicles based on meta structure) funded By the Ministry of Trade, Industry & Energy(MOTIE, Korea)

REFERENCES

- [1] M. A. ElMossallamy, H. Zhang, L. Song, K. G. Seddik, Z. Han, and G. Y. Li, “Reconfigurable intelligent surfaces for wireless communications: Principles, challenges, and opportunities,” *IEEE Transactions on Cognitive Communications and Networking*, vol. 6, no. 3, pp. 990–1002, 2020.

Poster Session

Voice Spoofing Countermeasure Using Residual Convolutional Neural Networks and Self-Attention

Changhwan Go, Wooyeon Choi, and Chanjun Chun*
Dept. of Computer Engineering, Chosun University
309, pilmun-daero, Dong-gu Gwangju 61452, South Korea
20174249@chosun.kr, {wyc, cjchun}@chosun.ac.kr

Abstract—The security of the ASV system was improved through the application of deep learning. However, it is still vulnerable to voice spoofing. Since voice spoofing destroys the security of the ASV system, there is a need for countermeasure. In this paper, we propose a voice spoofing countermeasure using the residual block and the self-attention-based transformer encoder or Bi-LSTM. We employ the LFCC, which is referred to as a cepstral coefficient feature extracted by linear filter banks. In addition, we utilize the dataset of the PA task in ASVspoof2021. ASVspoof2021 is a challenge to develop countermeasures to classify spoof or bonafide and provides datasets recorded in various real environments. We evaluate whether the proposed method classifies voice spoofing better than the conventional voice spoofing detection method.

Keywords—spoofing countermeasure, transformer, LFCC, voice spoofing

I. INTRODUCTION

Spoofing indicates that another person intrudes into the system by forging the user's characteristics. Voice spoofing means a voice forgery attack through a recorded voice. The Automatic Speaker Verification(ASV) system determines whether a user is a registered user using the characteristics of the voice [1]. Since the recorded voice has characteristics similar to the user's live voice, it is difficult for the ASV system to distinguish between the live voice and the recorded voice. Because spoofing through recorded voice destroys the security of the ASV system, it is necessary to develop a countermeasure that can classify it [2].

One of the countermeasures to voice spoofing is the use of deep learning models [3]. Because voice spoofing countermeasures perform effectively with deep learning, there are growing interests in developing deep learning models that classify voice spoofing [4].

In this paper, we propose the voice spoofing countermeasure using the residual block and the self-attention-based transformer encoder [5]. Here, the dataset of the Physical Access(PA) task of the ASVspoof2021 challenge is utilized [6]. The PA task has the purpose of developing voice spoofing countermeasures using datasets labeled with live and recorded speech. We compare the proposed method with the conventional method through the minimum detection cost(t-DCF) [7], and the Equal Error Rate(EER) [8]. A detailed explanation of the proposed method is described in the following Session.

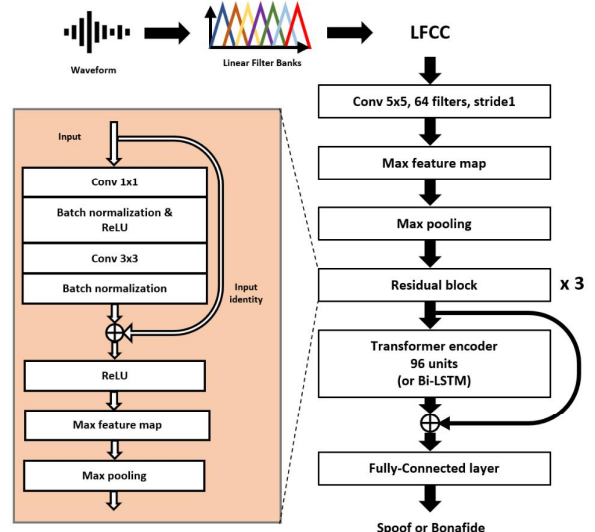


Fig. 1. Architecture of the proposed voice spoofing countermeasure

II. PROPOSED VOICE SPOOFING COUNTERMEASURE

A. Feature

The Linear Frequency Cepstral Coefficient(LFCC) is used as a feature. The LFCC is a cepstral coefficient feature similar to the Mel Frequency Cepstral Coefficient(MFCC). The MFCC reflects the characteristic that a human's auditory perception is more sensitive at low frequencies than at high frequencies. To reflect these characteristics, the mel filter bank applies a narrow filter to the low-frequency band and a wider filter to the high-frequency band. However, the LFCC extracted by the LFBs is extracted from low to high frequency by filters of the same size [9]. We employ the LFCC extracted by applying the 60-dimensional LFBs to hamming windows with 10ms overlap per 20ms from the speech.

B. Architecture

Fig. 1 shows the architecture of our proposed method. It consists of a convolution layer, Max Feature Map (MFM), the three residual blocks, the transformer encoder or the Bi-LSTM, and a Fully-Connected(FC) layer. Our model extracts the feature map through a convolution layer with a 5 by 5 filter and applies it to the MFM that activation function based on the max-out function proposed in Light Convolution Neural Network [10]. The MFM obtains half of the information from feature maps through the element-wise maximum operation. Moreover, it applies max pooling having a kernel size of 2 by 2 and

TABLE I. BI-LSTM & TRANSFORMER HYPERPARAMETER

Hyperparameter	Bi-LSTM	Transformer encoder
Embedding size	(96)	(96)
Hidden state	(96)	(96)
The number of layers	(2)	(2)
Dropout rate	-	(0.4)
FFN	-	(512)
The number of multiheads	-	(4)

TABLE II. MODEL PERFORMANCE ON EVALUATION SET

Model	Evaluation	
	t-DCF	EER(%)
Conventional	CNN-Bi-LSTM	0.9958
	Resnet-Bi-LSTM	0.9919
Proposed	Resnet-Transformer	0.9613
		39.3

passes through 3 residual blocks. After that, the transformer encoder or Bi-LSTM is utilized. Table I shows the hyperparameters of Bi-LSTM and the transformer encoder. The transformer encoder and Bi-LSTM consist of two layers. Moreover, the transformer encoder is employed with 4 multi-head attention. Here, the dropout out of 0.4 is applied to the transformer encoder output. The average of the features extracted from the residual block and the transformer encoder or Bi-LSTM is binary classified through the FC layer. We train 100 epochs and use Adam as the optimizer [11]. The cross entropy is utilized as a loss function.

C. Dataset

We employ the dataset of the PA task in the ASVspoof2021 challenge. The dataset was recorded in various real situations according to the actual distance, sound quality, environment, and room size. The training dataset consists of 8 male and 12 female speakers, and the evaluation dataset contains 21 male and 27 female speakers, respectively. In particular, the training dataset consists of 54,000 utterances, and the evaluation dataset includes 943,310 utterances, respectively.

III. EXPERIMENTAL RESULT

To demonstrate the effectiveness of the proposed voice spoofing detection method, we perform the objective evaluation using the t-DCF and the EER as evaluation indicators. Note that the conventional method uses a model combining CNN and Bi-LSTM [12]. The conventional method is based on the enhanced light CNN architecture and has the characteristic of using the MFM based on the max-out function. The proposed method consists of the residual block with the transformer encoder or the Bi-LSTM. Table II shows the experimental results of each method. The conventional method showed the t-DCF of 0.9958 and the EER of 44.77, respectively. The proposed Resnet-Bi-LSTM provided the DCF of 0.9919 and the EER of 40.34, and the proposed Resnet-Transformer presented the t-DCF of 0.9613 and the EER of 39.3, respectively. The Resnet-Bi-LSTM improved the t-DCF by 0.0039 and the EER by 4.43. Furthermore, the Resnet-transformer improved the t-DCF by 0.345 and the EER by 5.47 over the CNN-Bi-LSTM. Among the three methods, the Resnet-transformer showed the best performance.

IV. CONCLUSION

In this paper, we proposed a voice spoofing countermeasure using the residual block and the transformer encoder. We employed the PA task dataset of ASVspoof2021. In addition, we compared the performance of the proposed method with that of the conventional method using the t-DCF and the EER. As the experimental result, it was confirmed that the proposed method outperformed the conventional method. By improving the model architecture, research on voice spoofing countermeasure is more necessary.

ACKNOWLEDGMENT

This work was supported by the National Research Foundation of Korea(NRF) grant funded by the Korea government(MSIT) (No. NRF-2019R1C1C101159) and 'Technology Commercialization Collaboration Platform' program of the Korea Innovation Cluster(2022-DD-RD-0065).

REFERENCES

- [1] J. H. L. Hansen and T. Hasan, "Speaker recognition by machines and humans: A tutorial review," *IEEE Signal Processing Magazine*, vol. 32, no. 6, pp. 74-99, Oct. 2015.
- [2] Z. Wu, N. Evans, T. Kinnunen, J. Yamagishi, F. Alegre, and H. Li, "Spoofing and countermeasures for speaker verification: A survey," *Speech Communication*, vol. 66, pp. 130-153, Feb. 2015.
- [3] A. Gomez-Alanis, A. M. Peinado, J. A. G. Lopez and A. M. Gomez, "Performance evaluation of front- and back-end techniques for ASV spoofing detection systems based on deep features," in Proc. IberSPEECH, pp. 45-49, Nov. 2018.
- [4] J. A. Nasir, O. S. Khan, and I. Varlamis, "Fake news detection: A hybrid CNN-RNN based deep learning approach," *International Journal of Information Management Data Insights*, vol. 1, no. 1, pp. 1-13, Apr. 2021.
- [5] A. Vaswani, N. Shazeer, N. Parmar, J. Uszkoreit, L. Jones, and A. N. Gomez, "Attention is all you need," in Proc. Advances in Neural Information Processing Systems, vol.30, pp. 6000-6010, Dec. 2017.
- [6] J. Yamagishi, X. Wang, M. Todisco, M. Sahidullah, J. Patino, A. Nautsch, X. Liu, K. A. Lee, T. Kinnunen, N. Evans, and H. Delgado, "ASVspoof 2021: Accelerating progress in spoofed and deepfake speech detection," in Proc. ASVspoof2021 Workshop, pp. 47-54, Sep. 2021.
- [7] T. Kinnunen, H. Delgado, N. Evans, K. A. LEE, V. Vestman, A. Nautsch, M. Todisco, X. Wang, M. Sahidullah, J. Yamagishi, and D. A. Reynolds, "Tandem assessment of spoofing countermeasures and automatic speaker verification: fundamentals," *IEEE/ACM Transactions on Audio, Speech and Language Processing*, vol. 28, pp. 2195-2210, vol. 58, no. 4, Apr. 2020.
- [8] N. Brummer, L. Ferrer, and A. Swart, "Out of a hundred trials, how many errors does your speaker verifier make?," in Proc. Interspeech, pp. 1059-1063, Apr. 2021.
- [9] X. Zhou, D. Garcia-Romero, R. Duraiswami, C. Espy-Wilson and S. Shamma, "Linear versus mel frequency cepstral coefficients for speaker recognition," in Proc. IEEE Workshop on Automatic Speech Recognition & Understanding, pp. 559-564, Dec. 2011.
- [10] X. Wu, R. He, and Z. Sun, "A light CNN for deep face representation with noisy labels," in Proc. IEEE Transactions on Information Forensics and Security, vol. 13, no. 11, pp. 2884-2896, Nov. 2018.
- [11] D. P. Kingma and J. Ba, "Adam: A method for stochastic optimization," in Proc. International Conference for Learning Representations, vol. 8, pp. 1-15, July 2015.
- [12] X. Wang and J.Yamagishi, "A comparative study on recent neural spoofing countermeasures for synthetic speech detection," in Proc. Interspeech, pp. 4259-4263, Mar. 2021.

A study on the control of small Unmanned surface vehicles using disturbance learning

1st Sang Ki Jeong

Maritime ICT R&D Center

Korea Institute of Ocean Science and

Technology

Busan, Republic of Korea

jeongsks313@kiost.ac.kr

2nd Lee Jihyeong

Maritime ICT R&D Center

Korea Institute of Ocean Science and

Technology

Busan, Republic of Korea

wlgud0818@kiost.ac.kr

3rd Park, Haeyong

Maritime ICT R&D Center

Korea Institute of Ocean Science and

Technology

Busan, Republic of Korea

hypark@kiost.ac.kr

4th Hsieh, Wen-Hsiang

Department of Mechanical Design

Engineering

National Formosa University

Yunline, Taiwan

allen@nfu.edu.tw

Ji, Dae Hyeong

Marine Security and Safety Research

Center

Korea Institute of Ocean Science and

Technology

Busan, Republic of Korea

jidae@kiost.ac.kr

Abstract— In this study, the study was carried out on the disturbance learning adaptive control algorithm using a Recurrent Neural Network to apply to the control of the trajectory of the unmanned surface vehicle. There are many difficulties in controlling the movement trajectory of an unmanned surface vehicle in the ocean. [1][2] Current flow in the ocean is a typical disturbance. If the unmanned surface vehicle is not controlled in consideration of disturbance, the performance of the unmanned surface vehicle is deteriorated, and a problem arises that deviates from the correct movement trajectory. Therefore, this disturbance is learned on the move, applied to the control system, and studied the control technology to efficiently control the moving trajectory of the unmanned surface vehicle. [3] To measure the ocean current velocity, GPS is used to measure the ground speed, heading angle, and position (latitude, longitude). And the flow velocity sensor is measured using the velocity at which the hull moves in a fluid having a flow velocity. Based on the calculated velocity and direction of the ocean current the trend is predicted using the learning of the Recurrent Neural Network and applied to the model as a disturbance of the control system. And an Artificial Neural Network PID controller using artificial neural networks was designed to control the trajectory of the unmanned surface vehicle using this. Also, it analyzes whether the moving trajectory of the unmanned surface vehicle is accurately following and validates the control algorithm through simulation and experiment of the applied control system. [4]

its slow movement speed.[5] So it is difficult to obtain high-resolution information by using the medium- and high-speed USV control method using the existing Global Navigation Satellite System (GNSS)-based navigation that ignores Ocean currents.[6][7] Therefore, designed a controller by learning and predicting ocean currents measured in the ocean together with the existing GNSS navigation system and applying them to disturbances in the control system. To learn the ocean currents of the oceans, which are the core of this study, previous data were learned using LSTM to estimate the speed of the next ocean currents, and the output of the controller was determined using this data as a system disturbance. [8] To this end, the speed and direction of the hull's movement are measured using GPS's speed, azimuth, and position (latitude, longitude) data when a small USV moves, and the speed of fluid with a flow velocity is measured using a flow sensor mounted on a small USV. [9] In addition, the control system for controlling the position of the small USV used an ANN-PID(Artificial Neural Networks-PID controller)using an artificial neural network. The ANN-PID controller is designed to control the movement of USV through this as a controller for flexibly coping with disturbances by regulating control gains. Based on these studies, the control results of the small USV were analyzed and the control algorithm was verified through simulation of the applied control system.

II. USV DYNAMICS MODEL AND CONTROL SYSTEM DESIGN

A. USV Dynamics Model

The USV model, which attempts to simulate the control system of this study, is represented by a three-degree of freedom equation that does not consider the components of Roll, Pitch, and Z-direction, which are information related to posture on water.[10] In the motion model, motion characteristics are determined according to inertial force, additional mass, and shape through the definition of the coordinate system and external force component, and it is derived based on coordinate transformation and Newton's six-degree-of-freedom motion equation. Based on this, in the USV's three-degree-of-freedom equation of motion, hydrostatic force, which is a force acting on an external force term, inertial fluid force, viscous damping fluid force, and control fluid force The final model includes the fluid force using each moment is the same as Equations (1) to (3).

I. INTRODUCTION

In this study, to effectively control a small USV(Unmanned surface vehicle) for the investigation of underwater structures in a port, the study has conducted control small USV(Unmanned surface vehicle) by using LSTM (Long Short-Term Memory models) Algorithm to learn the disturbance(Ocean currents) of the ocean and using the predicted disturbance(Ocean currents) information. The small USV used in the port underwater structure survey system travels at a slow speed of 2 to 5 knots to suit the purpose and obtains sonar/image data of the underwater structure, which is greatly affected by the disturbances due to

$$X = X_u|u|u + X_{\dot{u}}\dot{u} + X_{\omega q}\omega q + X_{qq}qq + X_{vr}vr + X_{rr}rr - \sin\theta + F_x + N_x \quad (1)$$

$$Y = Y_v|v|v + Y_{r|r|}\dot{r}|r| + Y_y\dot{v} + Y_f\dot{r} + Y_{ur}ur + Y_{wp}wp + Y_{pq}pq + Y_{uv}uv + \cos\theta\sin\varphi + F_y + N_y \quad (2)$$

$$N = N_v|v|v + N_{r|r|}\dot{r}|r| + N_y\dot{v} + N_f\dot{r} + N_{ur}ur + N_{wp}wp + N_{pq}pq + N_{uv}uv + (x_GW - x_BB)\cos\theta\sin\varphi + \sin\theta + N_z \quad (3)$$

B. USV Control Algorithm

In this study, the speed of ocean currents is learned and used as a control factor of a small USV, so the control algorithm must design a controller that can respond appropriately to external information. Therefore, the controller applied to the small USV designed ANN-PID using an artificial neural network. The ANN-PID controller is an algorithm that can vary the control gain according to the current error.

III. USV OCEAN CURRENTS LEARNING MODEL & USV SIMULATOR

A. Analysis of Ocean currents

In this study, the velocity of ocean currents was measured using a sensor that can measure ocean currents. Fig. 1 shows the method of detecting the velocity of ocean currents using an ocean current measuring sensor.

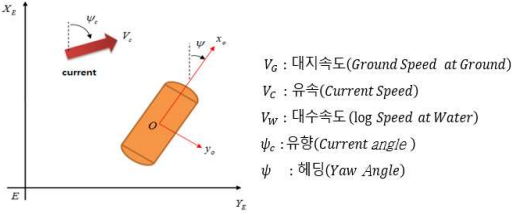


Fig. 1. The coordinate system of the fluid speed measurement dummy

To measure the flow velocity, GPS can be used to measure Ground Speed, Heading Angle, latitude, and longitude, and the flow velocity sensor can measure the speed (water speed) at which the hull moves in the fluid with the flow velocity. Using these two sensors, calculate the speed of the ocean currents. Based on this, to detect the velocity of ocean currents in a sensor mounted on a moving object, the velocity of ocean currents is detected using Equations 4~5.

$$V_G = V_w + V_c \quad (4)$$

The relationship between the SOG(Speed over the ground) and the SOA(Speed through the water) are shown in Equation 4. Since the SOG, SOA, and flow velocity are expressed in the magnitude and direction of the velocity, the vector of the magnitude and direction is divided by x and y.

$$\begin{aligned} V_G &= [|V_G|\cos\psi, |V_G|\sin\psi] \\ V_w &= [|V_w|\cos\psi_w, |V_w|\sin\psi_w] \\ V_c &= [|V_c|\cos\psi_c, |V_c|\sin\psi_c] \end{aligned} \quad (5)$$

And divided in each direction, the force at the three speeds can be expressed as Equation 5 by the relationship between the magnitude of the vector and the Earth's fixed coordinate system.

B. Learning Ocean Currents

Using the measured ocean currents data, we predicted ocean currents using LSTM, a type of RNN. This is to predict the velocity of the next ocean currents and apply them to the output of the control system. If the magnitude of the disturbance can be accurately known, the precision of the ANN-PID control algorithm applied in this study can be improved. The formula for LSTM used for learning ocean currents is Equation 6.[11]

$$\begin{aligned} f_t &= \text{sigmoid}(W_f \cdot [h_{t-1}, x_t] + b_f) \\ I_t &= \text{sigmoid}(W_i \cdot [h_{t-1}, x_t] + b_i) \\ O_t &= \text{sigmoid}(W_o \cdot [h_{t-1}, x_t] + b_o) \\ h_t &= O_t * \text{softsign}(C_t) \\ C_t &= f_t * C_{t-1} + I_t * \tilde{C}_t \\ \tilde{C}_t &= \text{softsign}(W_c \cdot [h_{t-1}, x_t] + b_c) \end{aligned} \quad (6)$$

The measured data was normalized and converted into data having a size between 0 and 1. And three gates (forget gate, input gate, output gate) are denoted by f_t , I_t , and O_t , respectively, and two outputs are denoted by h_t , and C_t . Also, the parameters of LSTM are W_i , W_f , W_o , W_c . Finally, \tilde{C}_t is a new output of the input gate, and the output of I_t is determined according to the degree of its reflection. In general, function tanh is used in BasicLSTMCell, but in this study, function softsign showed better results empirically. And the Adam Optimizer optimization function was used.

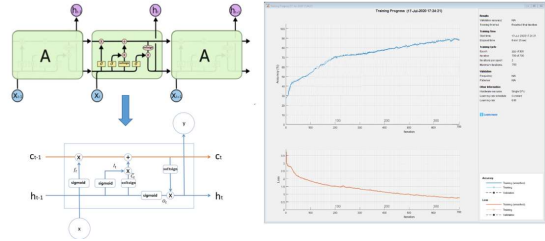


Fig. 2. Structure of LSTM(left) and Training Progress(right)

C. USV Control Algorithm Using LSTM

To combine the external force prediction model using LSTM and the ANN-PID controller, the control system as Fig. 3 was designed. And based on this, a simulator was designed using Matlab / Simulink to check the validity of the small USV's ocean currents learning algorithm and control algorithm.

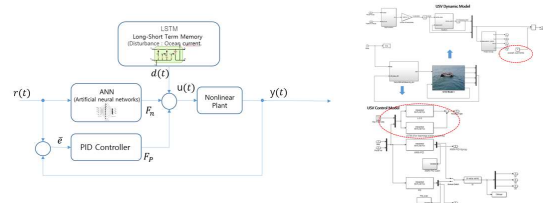


Fig. 3. USV Control Algorithm Using LSTM(left) and USV simulator(right)

USV simulator uses two artificial neural networks to learn external force and design a PID control system using artificial neural networks, and based on this, determines the input of the nonlinear system. It includes the USV's three-degree-of-

freedom equation of motion, a learning model for learning fluid forces and external forces, and an ANN-PID controller.

IV. LEARNING RESULTS OF OCEAN CURRENTS USING LSTM

The prediction of ocean currents was applied to the LSTM model designed in this study using the measured data of ocean currents tested in the real sea. And the validity of the simulation was verified by comparing the data predicted through the model with the actual data. The real sea data used in this study are the same as Fig. 4 (left). Data was measured for 150 minutes, and a graph of Fig. 4 (right) was derived based on this data. In the graph of Fig. 4 (right), green represents 2,000 data out of 4500 measured data, and this data is data used for training and testing. Also, blue is actual data, and red is data predicted by learning the previous 2000 data.

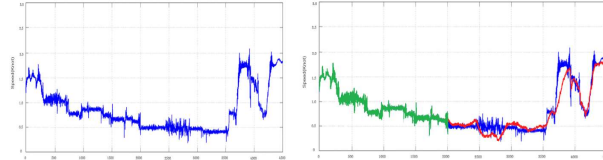


Fig. 4. Ocean current measurement(left) and prediction(right) data

In the predicted graph (red), there is an error in the section where the measured data changes rapidly, but the error between the actual data and the predicted data showed an average of 0.12 knots. Based on the above results, a simulation was performed for controlling the movement of the USV. In this simulation, two-dimensional (X, Y) movement at sea was simulated, and the changing control gain and the movement trajectory of the USV were shown. Ocean currents The actual measured data was inserted into the simulation as a data table. Then, the movement trajectory of the state without applying the predicted ocean currents is compared with the movement trajectory when the external force is learned and applied to the control system. At this time, each varying control gain is shown together.

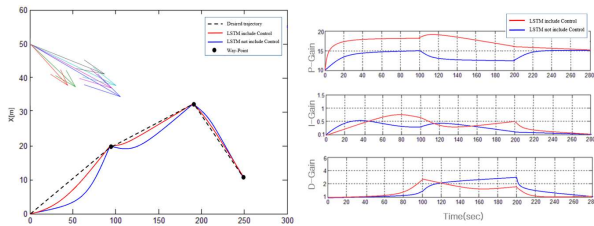


Fig. 5. 2D (X-Y) USV simulation results(left) and Control gain(right)

In Fig. 5 (left), arrows indicate the magnitude and direction of ocean currents, and the trajectory of the USV is shown in red by learning an external force using LSTM and applying this learned data and the ANN-PID controller. And the case where only the ANN-PID control algorithm was applied without learning is shown in blue. As shown in the simulation results, when the USV is controlled using the learning data about the external force, it can be confirmed that it converges to the desired trajectory faster than the existing ANN-PID. At this time, each control gain is shown in Fig. Same as 5 (right).

V. CONCLUSION

In this study, to improve the control performance of low-speed small USV, we propose prediction through the learning of ocean currents and the ANN-PID control algorithm using it. The proposed algorithm learns the measured data using the LSTM algorithm, predicts the subsequent ocean current based on it, and applies the predicted data to the control output as a control factor to improve the performance of the controller. To verify this, we designed a 3-DOF small USV model including fluid force, implemented an LSTM algorithm to predict disturbance, and designed an ANN-PID controller. And the data was processed stably through standardization of input data. Finally, as a result of verifying the control algorithm applied to the USV, it was confirmed that the same system and control algorithm was used, but the control performance was different depending on whether the prediction data of the external force was applied.

REFERENCES

- [1] Mousazadeh H, Jafarbiglu H, Abdolmaleki H, et al. Developing a navigation, guidance and obstacle avoidance algorithm for an Unmanned Surface Vehicle (USV) by algorithms fusion. *Ocean Engineering* 2018; 159: 56-65.J. Clerk Maxwell, A Treatise on Electricity and Magnetism, 3rd ed., vol. 2. Oxford: Clarendon, 1892, pp.68–73.
- [2] Edin Ormedic, Geoff Roberts. Thruster fault diagnosis and accommodation for open-frame underwater vehicle. *Control Engineering Practice* 2004; 12:1575-1598
- [3] Xin G, ZZhongjun H, Jun C. Data-based flooding fault diagnosis of proton exchange membrane fuel cell systems using LSTM networks. *Energy and AI* 2021; 4: 100056
- [4] Saleem Md A, Diwakar G, Dr. Satyanarayana MRS. Detection of Unbalance in Rotating Machines Using Shaft Deflection Measurement during Its Operation. *IOSR-JMCE* 2012; 3: 08-20
- [5] Daxiong J, Xin Y, Shuo L, Yuangui T, Yu T. Model-free fault diagnosis for autonomous underwater vehicles using sequence Convolutional Neural Network. *Ocean Engineering* 2021; 232: 108874
- [6] Alex Graves. Supervised sequence labeling with recurrent neural networks. Ph.D. thesis, Technical University Munich, 2008.
- [7] Jinhao L, Chao L, Dongxiang J. Fault diagnosis of wind turbine based on Long Short-term memory networks. *Renewable Energy* 2019; 133: 422-432
- [8] Shen Y, Ding S, Xiaochen X, Hao L. A Review on Basic Data-Driven Approaches for Industrial Process Monitoring. *IEEE TRANSACTIONS ON INDUSTRIAL ELECTRONICS* 2014; 61: 6418-6428
- [9] Dae-Gi Kim · Gyo-Young Hong · Dong-Man Ahn · Seung-Beom Hong · Min-Seok Jie. Turbojet Engine Control of UAV using Artificial Neural Network PID. *Journal of Advanced Navigation Technology*. 2014; 18;2: 107-113.
- [10] Yuvraj V. Parkale. Comparison of ANN Controller and PID Controller for Industrial Water Bath Temperature Control System using MATLAB Environment. *International Journal of Computer Applications*. 2012; 53;2.
- [11] Koohong Kang. Network Anomaly Detection Technologies Using Unsupervised Learnin. *Journal of The Korea Institute of Information Security & Cryptology*. 2020;30;4: 617-629.

A study on the swarm control algorithm of Unmanned Surface Vehicles

1st Jihyeong Lee

Maritime ICT R&D Center

Korea Institute of Ocean Science and
Technology

Busan, Republic of Korea

wlgud0818@kiost.ac.kr

2nd Sang Ki Jeong

Maritime ICT R&D Center

Korea Institute of Ocean Science and
Technology

Busan, Republic of Korea

jeongsk313@kiost.ac.kr

3rd Park, Haeyong

Maritime ICT R&D Center

Korea Institute of Ocean Science and
Technology

Busan, Republic of Korea

hypark@kiost.ac.kr

Abstract—In this study, to overcome the limitations of a single unmanned surface vehicle(USV), a study was conducted on the swarm control algorithm of the USV. Among the various swarm control methods, a leader-follower swarm control was selected and studied, and the performance of the swarm USV control algorithm proposed in this study was verified through an actual sea area test.

Keywords—swarm control algorithm, Unmanned Surface Vehicle, Leader-Follower swarm control

I. INTRODUCTION

The multi-object system using swarm control has a wider range of missions such as search and environmental investigation than the single-entity system. In addition, by using multiple objects at the same time, there are various advantages such as improved mission performance, increased efficiency, and reduced energy[1][2]. The study of the swarm control algorithm is receiving a lot of attention. In existing studies related to swarm control, the methods of swarm control are classified into behavior-based swarm control, virtual structure swarm control, and leader-follower swarm control[3]. Although each swarm control method has various advantages and disadvantages, in particular, the leader-follower swarm control algorithm is easy to understand mathematically and easy to implement, and in theory, it is possible to increase the number of followers unlimitedly[4][5]. Therefore, in this study, a USV with a leader-follower swarm control algorithm was developed, and the performance of the swarm control algorithm was verified through experiments in the sea area.

II. SYSTEM STRUCTURE

A. System structure of USV

In this study, to apply the leader-follower swarm control algorithm, two USVs, Leader and follower, of the same structure equipped with two thrusters were manufactured. The hull of the USV used in this study was adopted in the form of a catamaran, which is strong in rolling and pitching, and excellent in stability and straight-line driving characteristics, considering that it is operated in a marine environment that is highly affected by disturbances such as waves and currents[6]. In addition, it was manufactured using a rubber material that has excellent waterproof and corrosion resistance and is advantageous for shock absorption. Fig.1 is a picture of the developed USV, and Table.1 is the specification of the USV.

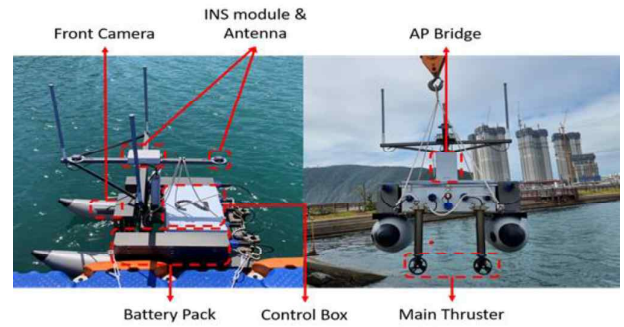


Fig. 1. Structure of Leader & Follower USV

TABLE I. SPECIFICATION OF USV

Size(L*W*H)	1500*920*920(mm)
Weight	60(kgf)
Navigation Sensor	Custom GNSS Marineinnotec K-STAR
Battery	25.9V 75Ah(Li-ion)
Camera	Hanhwa-security QNO-6012R
Main Controller	MSI Cubi 5 10M
AP Bridge	GT-Wave 860s
Thruster	CiLab T80-60

B. Monitoring program

The monitoring program is designed to collect various data such as posture, direction angle, and speed of the leader and follower USV, and to deliver control commands to the leader and follower USV. It was made using “Visual studio C#”, and it was made so that the operator could easily check the data and check the behavior of the platform. Fig.2 is the GUI configuration of the manufactured operation program.



Fig. 2. Configuration of Monitoring Program

III. SWARM CONTROL ALGORITHM

To maintain swarm formation in swarm control using the leader-follower swarm control method, a virtual point must be created at a location where a certain distance and angle are to be maintained from the leader USV, and the follower USV must follow the point. The virtual point followed by the follower USV can maintain a certain distance and angle no matter what form the actual leader USV moves, so it is possible to maintain the desired swarm formation. The error between the virtually generated point and the trajectory followed by follower USV may be expressed as in Equation (1).

$$\begin{bmatrix} e_{x2}(t) \\ e_{y2}(t) \\ e_{z2}(t) \end{bmatrix} = \begin{bmatrix} \cos(\theta_F(t)) & \sin(\theta_F(t)) & 0 \\ -\sin(\theta_F(t)) & \cos(\theta_F(t)) & 0 \\ 0 & 0 & 1 \end{bmatrix} \begin{bmatrix} d_x^d(t) - d_x(t) \\ d_y^d(t) - d_y(t) \\ \theta_F^d(t) - \theta_F(t) \end{bmatrix} \\ = \begin{bmatrix} d_x^d(t) \cos(\phi_{ref} + e_{\theta_2}(t)) - d_x(t) \cos(\phi(t) + e_{\theta_2}(t)) \\ d_y^d(t) \sin(\phi_{ref} + e_{\theta_2}(t)) - d_y(t) \sin(\phi(t) + e_{\theta_2}(t)) \\ \theta_L(t) - \theta_F(t) \end{bmatrix} \quad (1)$$

Here, $[X_F(t), Y_F(t), \theta_F(t)]$ denotes the position of the follower, $[d_x^d(t), d_y^d(t)]$ denotes the position of the virtual point to be followed by the follower, and $\theta_F^d(t)$ denotes the azimuth to the following point. $\theta_F^d(t)$ is the same as the leader's azimuth angle $\theta_L(t)$ so it is possible to express it differently. Therefore, when Equation (1) is developed, the error between the virtual generation point and the follower and the following trajectory is express in the form of Equations (2-a), (2-b), (2-c).

$$e_{x2}(t) = (X_L(t) - X_F(t)) \cos(\theta_F(t)) + (Y_L(t) - Y_F(t)) \sin(\theta_F(t)) + d_{ref} \sin(\phi_{ref} + \theta_L(t) - \theta_F(t)) \quad (2-a)$$

$$e_{y2}(t) = -(X_L(t) - X_F(t)) \sin(\theta_F(t)) + (Y_L(t) - Y_F(t)) \cos(\theta_F(t)) + d_{ref} \sin(\phi_{ref} + \theta_L(t) - \theta_F(t)) \quad (2-b)$$

$$e_{\theta_2}(t) = \theta_L(t) - \theta_F(t) \quad (2-c)$$

Here, using the calculated $[e_{x2}(t), e_{y2}(t)]$, the distance error $d_{\theta_2} = \sqrt{e_{x2}(t)^2 + e_{y2}(t)^2}$ between the virtual point and the follower may be obtained.

IV. RESULT OF ACTUAL SEA AREA TEST

The performance test of the swarm control algorithm was conducted off the coast of Korea Maritime and Ocean University. The test was conducted by placing the leader and followers at different positions and different direction angles and entering four Waypoints to see if followers perform their duties while maintaining the leader and swarm formation well. Fig.3 is a conceptual diagram of the experiment, and Fig.4 is a graph showing the test result

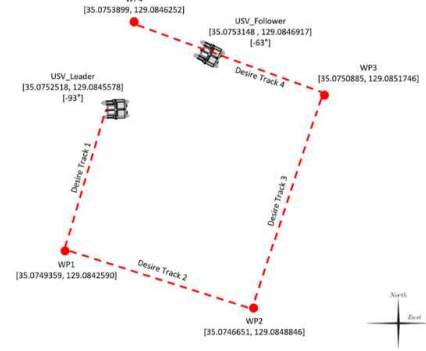


Fig. 3. Diagram of Multi Point Swarm Control Test

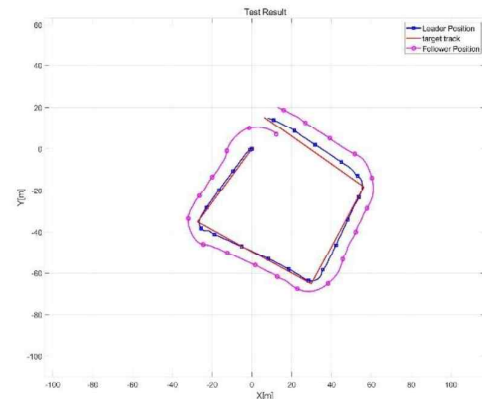


Fig. 4. Result of Multi Point Test

V. CONCLUSION

This research conducted a study on the Leader-Follower swarm control algorithm to overcome the limitations of a single object system. For research, we have developed USV to perform actual missions, and we have developed a swarm control algorithm for transplantation into USV. In addition, the performance of the algorithm proposed in this study was verified through the test in the actual sea area.

REFERENCES

- [1] D.Cruz, J. Mcclintock, B. Perteet, A.A.O.Orqueda, Y.Cao and R.Fierro, "Decentralized cooperative control", Proceeding of IEEE Control System Magazine, 2007, pp. 58-78.
- [2] Y.Gu, B.Seanor, G.Campa, M.R.Napolitano, L.Rowe, S.Gururajan and S.Wan, "Design and flight testing evaluation of formation control laws", Proceeding of IEEE Trans. On Control Systems Technology, 2006, vol.14, pp. 1105-1112
- [3] K.R.Lee, "Design of Decentralized Behavior-Based Network for the Formation Control and the Obstacle Avoidance of Multiple Robot", Proceeding of Ajou University, 2018
- [4] S.B.Park, J.H. Park, "A study on the formation control algorithms of Multi-Obstacles collision avoidance for autonomous Navigation of swarm marine unmanned moving vehicles", Proceeding of Journal of the KNST, 2020, 3(1), pp. 56-61.
- [5] M.H.Tak, J.S.Kim, Y.H.Joo, S.H.Ji, "Formation Control for the Obstacle Avoidance of Swarm Robots based Leader-Follower Robots", Proceeding of the Korean Institute of Electrical Engineers, 2013, 10, pp. 171-172
- [6] Molland A.F., J.F. Wellicome, and P.R.Couser, "Resistance experiments on a systematic series of high speed displacement catamaran form:variation of length-displacement ratio and breadth-draught ratio", Proceeding of ship Science Report, 1994, pp. 71

Fingerprint-aided Coordinated mmWave Beam Selection for mmWave UAV Communications

Yuna Sim

dept. of ICT Convergences System

Engineering

Chonnam National University

Gwangju, Republic of Korea

sya8325@naver.com

Seungseok Sin

school of Electronics and Computer

Engineering

Chonnam National University

Gwangju, Republic of Korea

ssskit7@naver.com

Yuna Jeong

school of Electronics and Computer

Engineering

Chonnam National University

Gwangju, Republic of Korea

yuna1538@naver.com

Jihun Cho

dept. of ICT Convergences System

Engineering

Chonnam National University

Gwangju, Republic of Korea

hoony1992@naver.com

Sangmi Moon

dept. of IT Artificial Intelligence

Korea Nazarene University

Cheonan, Republic of Korea

moonsm@kornu.ac.kr

Intae Hwang

dept. of Electronic Engineering and

dept. of ICT Convergence System

Engineering

Chonnam National University

Gwangju, Republic of Korea

hit@jnu.ac.kr

Abstract—In this paper, we propose a fingerprint-based beam selection and cooperation scheme for millimeter-wave (mmWave) unmanned aerial vehicle (UAV) communication. The proposed scheme constructs an offline fingerprint database for beam selection and performs online beam cooperation. In the offline phase, the best beam index from serving cells and the interference beam indexes from neighboring cells are stored. In the online phase, the best beams and interference beams are determined using the information from the fingerprint database instead of an exhaustive search, and the beam cooperation is performed to improve the signal-to-interference-plus-noise ratio for aerial user equipment. System-level simulations are performed to assess the UAV effect based on the 3GPP new radio mmWave and UAV channel models. Simulation results show that the proposed beam selection scheme can reduce the beam sweeping overhead and inter-cell interference.

Keywords—beam cooperation, beam selection, fingerprint, mmWave, UAV.

I. INTRODUCTION

In the past few years, unmanned aerial vehicles (UAVs) have been increasingly employed in civilian applications, such as for aerial surveillance, traffic control, photography, package delivery, and communication relaying.

Millimeter-wave (mmWave) communication, which utilizes the wide available bandwidth above 28 GHz, is a promising technology to achieve high-rate UAV communication [1]. While mmWave communication has been extensively investigated for 5G-and-beyond cellular systems, its application to cellular-connected UAV systems faces both new opportunities and challenges. On the one hand, as mmWave signals are vulnerable to blockage, the line-of sight (LoS)-dominating UAV–base station (BS) channels offer the most favorable channel conditions for the practical application of mmWave communication. On the other hand, the high UAV altitude and mobility require the development of efficient mmWave beamforming for 3D mmWave UAV–BS channels. The beamforming technology can determine the best beam direction formed by multiple antenna elements for user equipment (UE) to maximize the transmission rate and improve the energy efficiency.

In this paper, we propose a fingerprint-based beam selection and cooperation scheme for mmWave UAV communication. The proposed scheme constructs an offline fingerprint database for beam selection and performs online

beam cooperation. In the offline phase, the best beam index from serving cells and the interference beam indexes from neighboring cells are stored. In the online phase, the best beams and interference beams are determined using the information from the fingerprint database instead of an exhaustive search, and beam cooperation is performed to improve the signal-to-interference-plus-noise ratio (SINR) for aerial UEs.

II. FINGERPRINT-AIDED COORDINATED MMWAVE BEAM SELECTION

A. Construction phase of offline Fingerprint Database

Table I. Example of fingerprint for the cell b

Aerial UE						
P_1		P_2		...	P_A	
b_1^*		b_2^*		...	b_A^*	
I_ID_1	\tilde{b}_1^1	I_ID_1	\tilde{b}_2^1		I_ID_1	\tilde{b}_A^1
I_ID_2	\tilde{b}_1^2	I_ID_2	\tilde{b}_2^2		I_ID_2	\tilde{b}_A^2
Terrestrial UE						
P_{A+1}		P_{A+2}		...	P_{A+T}	
b_{A+1}^*		b_{A+2}^*		...	b_{A+T}^*	

The measurement is performed in each cell by assigning the terrestrial and aerial UEs to each fingerprint spot, and the measurement content includes the fingerprint position, service cell ID and corresponding optimal beam ID. If the UE is an aerial UE, the interference cell IDs and the corresponding strongest interference beam IDs also need to be measured. Then, the measurement result is saved in the corresponding fingerprint database, i.e., a set of all the fingerprint information within a cell coverage area. Each fingerprint database is divided into two parts, namely the terrestrial and aerial fingerprint datasets. Table I shows the fingerprint database of the cell b , in which P_a ($a=1,2,\dots,A$) and P_t ($t=A+1, A+2, \dots, A+T$) are the aerial and terrestrial fingerprint position, respectively. I_ID_i ($i=1,2$) is an interference cell ID for a fingerprint position, b_i^* is the optimal beam ID for P_t , and b_a^* and \tilde{b}_a^i are the optimal beam ID and the strongest interference beam ID, respectively, corresponding to the interference cell i for P_a . Note that the number of interference cells is two ($i=1,2$) because we

consider the intra-site joint transmission (JT) for aerial UEs, as will be discussed in the following subsections.

During the construction phase of the offline fingerprint database, the UE of each fingerprint position performs the beam selection. In the 5G standard, the main procedure for beam selection is beam sweeping, which transmits a set of predefined beams to cover the spatial area. Among them, beam sweeping exhaustively searches for the optimal beam transmitted by the service cell and the strongest interference beams caused by the adjacent cells. Here, we assume that all the beams generated by the same cell are orthogonal and the same beam serves multiple UEs through a time-division multiplexing mechanism to avoid intra-cell interference .

B. Coordinated Beam Selection

In the online phase, the BS can further determine to which fingerprint dataset of the service cell of the UE the matched fingerprint position belongs. If the matched fingerprint position is in the aerial fingerprint position, the UE can be identified as an aerial UE. When a UE is a terrestrial UE, the serving cell only needs to transmit the best beam to the UE according to the beam ID corresponding the matched fingerprint position. As the aerial UEs experience LoS propagation conditions for more cells with higher probability, in comparison with terrestrial UEs, the aerial UEs receive interference from more cells in the downlink. Therefore, JT is applied to improve the performance of an aerial UE. In this study, multiple cells belonging to the same site are coordinated, and data are jointly transmitted to the UEs. As intra-site JT-coordinated multi-point is already supported in 3GPP standardization, enhancements are not required. With beam cooperation for aerial UE, the interference from the neighboring cells is reduced because a neighboring cell is converted from the interference signal to the desired signal.

III. SIMULATION RESULTS

System-level simulations are performed to assess the UAV effect based on the 3GPP NR mmWave and UAV channel models [2,3]. The following schemes are simulated for comparison:

- (1) Random beam selection (R-BS): each UE is served with only its serving cell, and the beams are selected randomly from among all the beams.
- (2) Exhaustive search beam selection (ES-BS): each UE is served with only its serving cell, and the beams are selected via an exhaustive search.
- (3) Beam selection with single-cell transmission (SC-BS): each UE is served with only its serving cell, and fingerprint-based beam selection is used.
- (4) Beam selection with JT (JT-BS): the same as scheme (3), but intra-site JT is used for aerial UEs.

Fig. 1 plots the CDF of the SINR for schemes (1) to (4), where the aerial UE ratio is 50% (5 aerial UEs per cell). The proposed beam selection (JT-BS) can achieve a higher SINR than the other scheme.

Fig. 2 plots the CDF of the SINR for schemes (3) and (4) in cellular-connected UAV communication when the aerial UE ratios are 7.1% (case 3) and 50% (case 5). With the increase in the number of aerial UEs, the inter-cell beam interference increases, and the value of SINR in scheme (4) is significantly improved compared with that in scheme (3).

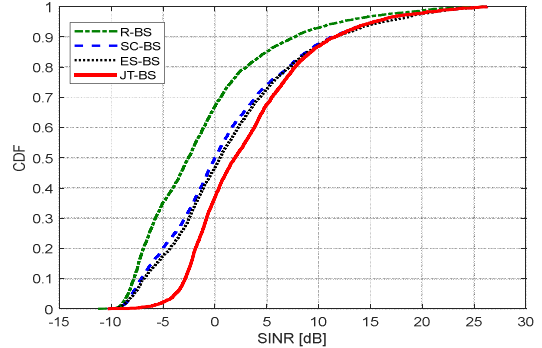


Fig. 1. CDF of the SINR for scheme (1)-(4).

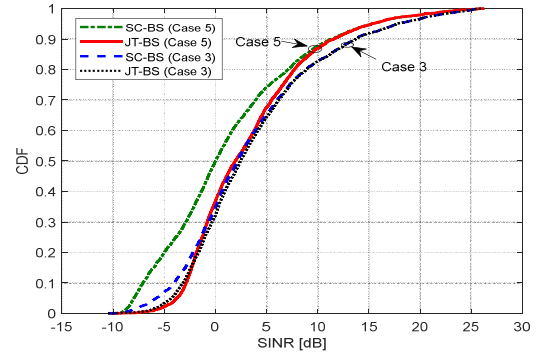


Fig. 2. CDF of the SINR for scheme (3) and (4).

IV. CONCLUSION

In this paper, we proposed a fingerprint-based beam selection and cooperation scheme for mmWave UAV communication. The proposed scheme constructs an offline fingerprint database for beam selection and performs online beam cooperation. The simulation results showed that the proposed beam selection scheme could reduce the beam sweeping overhead and inter-cell interference.

ACKNOWLEDGMENTS

"This work was supported by the National Research Foundation of Korea (NRF) grant funded by the Korea government(MSIT: Ministry of Science and ICT) (2020R1I1A1A01073948 and 2021R1A2C1005058)." "This research was supported by the BK21 Fostering Outstanding Universities for Research (FOUR) Program (5199991714138) funded by the Ministry of Education (MOE, Korea) and National Research Foundation of Korea (NRF)." "This research was supported by the Ministry of Science and ICT (MSIT), Korea, under the Innovative Human Resource Development for Local Intellectualization support program (IITP-2022-RS-2022-00156287) supervised by the Institute for Information & communications Technology Planning & Evaluation (IITP)." "This research was supported by the Ministry of Science and ICT (MSIT), Korea, under the ICT Challenge and Advanced Network of HRD (ICAN) program (IITP-2022-RS-2022-00156385) supervised by the Institute of Information & communications Technology Planning & Evaluation (IITP)." "

REFERENCES

- [1] Z. Xiao, P. Xia, and X.-G. Xia, "Enabling UAV cellular with millimeter-wave communication: potentials and approaches," *IEEE Commun. Mag.*, vol. 54, no. 5, pp. 66–73, May 2016.
- [2] 3GPP Technical Report 36.777, "Technical specification group radio access network; Study on enhanced LTE support for aerial vehicles (Release 15)," V15.0.0, Dec. 2017.
- [3] 3GPP Technical Report 38.901, "Study on channel model for frequencies from 0.5 to 100 GHz (Release 16)," V16.1.0, Dec. 2019

Experiments of Long-Range Underwater Communication in the East Sea

Donghyeon Kim

Department of Convergence Study on the Ocean Science and Technology
Korea Maritime and Ocean University
Busan, Korea
0000-0002-1839-1666

Jeongha An

Department of Radio Communication Engineering
Korea Maritime and Ocean University
Busan, Korea
zung706@gmail.com

Jeasoo Kim

Department of Ocean Engineering
Korea Maritime and Ocean University
Busan, Korea
jskim@kmou.ac.kr

Kiman Kim

Department of Radio Communication Engineering
Korea Maritime and Ocean University
Busan, Korea
kimkim@kmou.ac.kr

In-soo Kim

Agency of Defense Development
Changwon, Korea
kis171@add.re.kr

Abstract—Since 2018, several long-range underwater communication experiments have been conducted in the East Sea along various tracks (at least over 23 km range). These experiments aim to (a) understand and confirm the features of long-range propagation in the East Sea, and (b) research the feasibility of long-range underwater communication over tens of kilometers. This paper introduces three long-range underwater communication experiments and the communication results achieved using time reversal processing.

Index Terms—Long-range underwater communication, Deep water, East Sea, time reversal processing

I. INTRODUCTION

With the development of long-range autonomous underwater vehicles, a necessity for technology development that can communicate stably even over long-range for efficient ocean monitoring has emerged [1], [2]. Long-range underwater communication is challenging because of increased transmission loss, channel temporal and spatial variations, and time-spread of signals created by long-range propagation. SIO and JAMSTEC are conducting various experiment-based research for long-range underwater communication [1], [3]. However, no sea-going experiments aimed at long-range underwater communication were conducted in Korea before 2018 [4]. The purpose of this paper is to research the feasibility of long-range underwater communication in the East Sea using sea-going experimental data.

II. SEA-GOING EXPERIMENTS IN THE EAST SEA

Since 2018, three long-range underwater communication experiments have been conducted in the East Sea (the east of Pohang, Korea). Fig. 1 shows the experimental site where three experiments were carried out, with the experiment names as follows: (1) Biomimetic Long-range Acoustic Communication experiment (BLAC18), (2) Application-adaptive Covert Underwater Acomm. EXperiment 2020 (ACUA-EX20), (3) ACUA-EX22. The water depth of this site is the deep water

with a maximum depth of 1,700 m, and the squares and circles indicate the location of the source and the vertical line array (VLA), respectively. During all experiments, the source was suspended in the research vessel, and the VLA was moored at the bottom. Unlike other experiments, ACUA-EX20 utilized the towed source. In all experiments, the maximum and minimum ranges are 23 and 90 km, respectively.

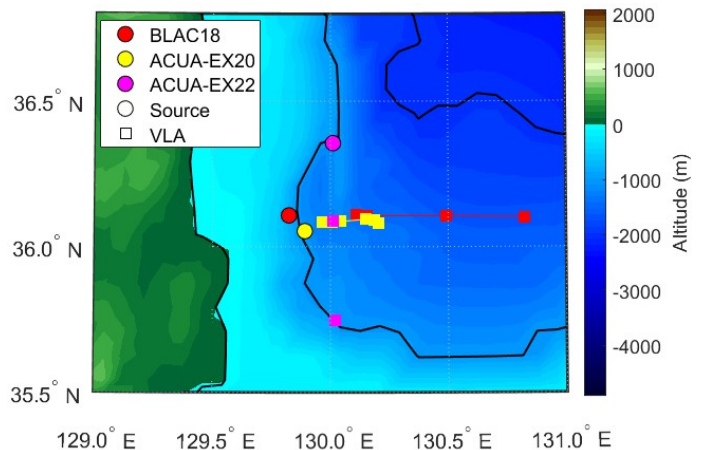


Fig. 1. Experimental site.

The source signal consisted of a chirp signal for estimating the channel impulse response, guard time, and communication data. Channel variation due to time can occur in the signal as the duration of the signal increases. As a result, data for communication was designed to be as short as possible. An M-sequence signal, a training symbol, and a payload comprised the communication data. The M-sequence signal was utilized to estimate Doppler and synchronization, whereas the training symbol was used to apply the equalizer following time reversal processing (TRP).

III. TIME REVERSAL PROCESSING

Because of TRP's ability to mitigate inter-symbol interference and improve signal-to-noise ratio through temporal compression in underwater environments with large multipath spreads, it has been utilized in underwater communication. The TRP approach allows the reconstruction of source signal from matched filtering of received signals and the CIR. [5],

$$\hat{S}(\omega) = \mathbf{R}(\omega)\mathbf{W}^H(\omega), \quad (1)$$

where $\mathbf{H}(\omega)$ and $\mathbf{R}(\omega)$ denote the CIR between the source and the array and the received signal obtained from the array, respectively. And $\hat{S}(\omega)$ denotes the reconstructed source signal.

IV. RESULTS

ACUA-EX20/22 data were selected as representatives of the three experiments. During ACUA-EX20, the communication signals were designed with various modulation types; quadrature phase-shift keying (PSK), 8PSK, 8 quadrature amplitude modulation (QAM), and 16QAM. Scatter plots are illustrated in Fig. 2 to show the communication results based on TRP [6]. The bit error rate of 16QAM was under 2%, and all other signals achieved error-free.

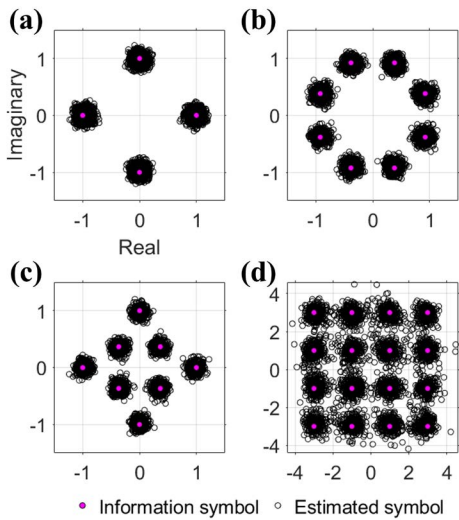


Fig. 2. Scatter plots of various modulation types after TRP: (a) quadrature PSK, (b) 8PSK, (c) 8QAM, and (d) 16QAM.

ACUA-EX22 was conducted in May 2022. We are analyzing this experiment and will present the communication result of one case as an example in this paper. During ACUA-EX22, communication signals were transmitted at two different ranges (30 and 68 km), with the difference from prior experiments being the location of the receiver with respect to the source. The source in BLAC18 and ACUA-EX20 was located on the east side of the receiver, whereas the source in ACUA-EX22 was located on the south side of the receiver. Fig. 3 shows a scatter plot of the binary PSK modulated signal transmitted at 68 km, illustrating error-free.

From the communication results with two experiments, the feasibility of long-range communication was confirmed to be successful even when propagation was north-south rather than east-west.

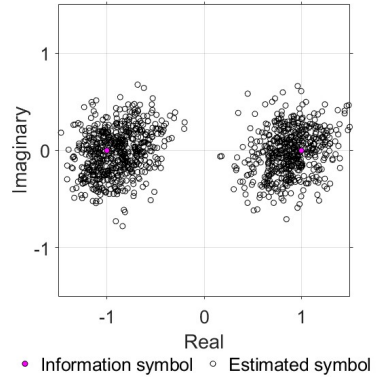


Fig. 3. Scatter plot at a range of 68 km in ACUA-EX22.

V. CONCLUSIONS

After 2018, long-range underwater communication experiments were conducted in the East Sea, and the communication data were decoded with time reversal processing. With BER performance of up to 2%, the feasibility of long-range underwater communication in the East Sea was researched.

ACKNOWLEDGMENT

This work was supported by the Agency for Defense Development, South Korea, under Grant No. UD200010DD.

REFERENCES

- [1] T. Shimura, H. Ochi, Y. Watanabe, and T. Hattori, "Demonstration of time-reversal communication combined with spread spectrum at the range of 900 km in deep ocean," *Acoustical Science and Technology*, vol. 33, no. 2, pp. 113–116, 2012.
- [2] F. Mosca, G. Matte, and T. Shimura, "Low-frequency source for very long-range underwater communication," *The Journal of the Acoustical Society of America*, vol. 133, no. 1, pp. EL61–EL67, 2013.
- [3] H. Song, S. Cho, T. Kang, W. Hodgkiss, and J. Preston, "Long-range acoustic communication in deep water using a towed array," *The Journal of the Acoustical Society of America*, vol. 129, no. 3, pp. EL71–EL75, 2011.
- [4] J.-H. Lee, G.-H. Lee, K.-M. Kim, and W.-J. Kim, "Sea trial results of long range underwater acoustic communication based on frequency modulation in the east sea," *The Journal of the Acoustical Society of Korea*, vol. 38, no. 4, pp. 371–377, 2019.
- [5] H. C. Song, W. S. Hodgkiss, W. A. Kuperman, W. J. Higley, K. Raghukumar, T. Akal, and M. Stevenson, "Spatial diversity in passive time reversal communications," *The Journal of the Acoustical Society of America*, vol. 120, no. 4, pp. 2067–2076, 2006.
- [6] D. Kim, J. Kim, and J. Y. Hahn, "Verification of the feasibility of higher-order modulation for long-range communication in deep water," *The Journal of the Acoustical Society of Korea*, vol. 40, no. 5, pp. 428–438, 2021.

Utility-Centric Partial Offloading in Parked Vehicle-assisted Multi-access Edge Computing

Xuan-Qui Pham and Dong-Seong Kim

ICT Convergence Research Center, Kumoh National Institute of Technology, Korea

Email: {pxuanqui, dskim}@kumoh.ac.kr

Abstract—Recently, parked vehicle-assisted multi-access edge computing (PVMEC) has been promoted to address the computation resource limitation of conventional MEC paradigms by leveraging the opportunistic resources of parked vehicles (PVs). In this paper, we devise a partial offloading scheme that allows mobile devices to partially process their tasks locally and partially offload to a MEC server or a neighboring PV to maximize the system utility in regard to the latency and the cost of computation resources. Evaluation results verify the superiority of the proposed scheme.

Index Terms—parked vehicle-assisted multi-access edge computing, partial offloading, resource allocation.

I. INTRODUCTION

Multi-access edge computing (MEC) allows mobile devices (MDs) to offload their compute-intensive tasks to MEC servers attached to base stations (BSs) [1]. However, deploying massive MEC servers to cover all network areas for computation offloading is infeasible regarding capital expenditure, and can be a waste of resources if the user demand changes.

Hence, parked vehicle-assisted multi-access edge computing (PVMEC) has been proposed to leverage the opportunistic computing resources of parked vehicles (PVs) for helping MEC servers executing the offloaded tasks. In [2]–[4], the authors studied workload allocation between several PVs and a MEC server aiming to optimize the overall computing offloading cost. However, these works handled a single large task without considering the local computing capacity of requesting devices. In [5], the authors performed PV clustering in PVMEC, and then proposed an offloading scheme to minimize the latency of offloaded tasks considering local execution at the requesting devices. Nevertheless, this work neglects the computing offloading cost. In addition, most of related works concentrate on full offloading strategies, where the task is completely executed locally or completely offloaded.

Different from related works, we propose a partial offloading scheme, where a computation task requested by MD can be offloaded for remote execution on either a MEC server or a PV in a partial manner. The offloading utility is expressed from the perspective of MDs based on the gain of latency reduction and

This research was financially supported by the MSIT (Ministry of Science and ICT), Korea, under the Grand Information Technology Research Center support program (IITP-2022-2020-0-01612) supervised by the IITP (Institute for Information & Communications Technology Planning & Evaluation), and Priority Research Centers Program (2018R1A6A1A03024003) through the National Research Foundation of Korea (NRF) funded by the Ministry of Education, Science and Technology.

the cost of using computing resources. Concretely, the main contributions are manifold. First, we formulate the partial offloading problem under an optimization problem with regard to maximize the system utility. Second, we derive a solution with the joint consideration of task assignment, resource allocation, and offloading ratio. Finally, we verify the promising of the proposed scheme via preliminary results.

II. SYSTEM MODEL

The PVMEC paradigm includes a MEC server attached to a BS. The set of MDs and PVs are represented by $\mathcal{N} = \{1, 2, \dots, N\}$ and $\mathcal{M} = \{1, 2, \dots, M\}$, respectively. The PV selection can be performed periodically by the BS using the technique in [2]. By adopting a time-slot model, each MD requests a computation task indicated by (d_i, v_i, c_i) during each slot. Here, d_i denotes the size of input data, v_i denotes the workload density, and $c_i = d_i v_i$ denotes the amount of CPU cycles to finish the task. In the partial offloading mechanism, each MD i locally processes $(1 - \alpha_i)d_i$ bits and offloads the remaining to the MEC server, indexed by 0, or a PV $j \in \mathcal{M}$ by the MEC or D2V offloading mode, respectively. Here, α_i represents the offloading ratio variable.

The partial local computation latency is

$$t_{ij}^l = \frac{(1 - \alpha_i)c_i}{f_i^l}. \quad (1)$$

where f_i^l represents the computing capacity of MD i .

The partial offloading latency from MD i to computing node $j \in \mathcal{M} \cup \{0\}$ is

$$t_{ij}^{off} = \frac{\alpha_i d_i}{R_{ij}} + \frac{\alpha_i c_i}{f_{ij}}, \quad (2)$$

where R_{ij} are the transmission rate following the path-loss model in [6]. f_{ij} denotes the computing resources allocated to MD i by computing node j . Here, the time to return the computation results is omitted [7]. We also consider that at a time slot, a PV can execute at most one MD because of the resource constraint. Therefore, $f_{ij} = F_j$, if $j \in \mathcal{M}$, where F_j represents the computing capacity of the PV j . The total completion time is $t_{ij} = \max\{t_{ij}^l, t_{ij}^{off}\}$.

Let $\mathbf{x} = \{x_{ij} | i \in \mathcal{N}, j \in \mathcal{M} \cup \{0\}\}$ be the computation offloading vector denoting whether task i is offloaded to node j ($x_{ij} = 1$) or not ($x_{ij} = 0$). The utility is defined as follows:

$$U_i = \sum_{j \in \mathcal{M} \cup \{0\}} x_{ij} U_{ij} = \sum_{j \in \mathcal{M} \cup \{0\}} x_{ij} [g_t(t_i^l - t_{ij}) - p_j f_{ij}], \quad (3)$$

where g_t denotes the unit gain of latency reduction, t_i^l is the latency of completely local computation, and p_j denotes the

unit price of computing resources at computing node j . We express the problem formulation as follows:

$$\max_{\mathbf{x}, \boldsymbol{\alpha}, \mathbf{f}} \sum_{i \in \mathcal{N}} U_i \quad (4)$$

$$\text{s.t. } \min t_{ij}, \quad \forall i \in \mathcal{N}, j \in \mathcal{M} \cup \{0\}, \quad (4a)$$

$$\sum_{j \in \mathcal{M} \cup \{0\}} x_{ij} \leq 1, \quad \forall i \in \mathcal{N}, \quad (4b)$$

$$\sum_{i \in \mathcal{N}} x_{ij} \leq 1, \quad \forall j \in \mathcal{M}, \quad (4c)$$

$$\sum_{i \in \mathcal{N}_0} f_{i0} \leq F_0, \quad (4d)$$

$$x_{ij} \in \{0, 1\}, 0 \leq \alpha_i \leq 1, \quad \forall i \in \mathcal{N}, j \in \mathcal{M} \cup \{0\}. \quad (4e)$$

where (4a) ensures the latency minimization. (4b) and (4c) represents the association between the MD and the computing node. (4d) represents the computation capacity constraint of the MEC offloading mode. And (4e) bounds the variables.

III. PROPOSED SOLUTION

In partial computation offloading, the latency minimization for an MD i is reached when $t_{ij}^l = t_{ij}^{off}$. For the MEC offloading mode, the allocated computing resources can be calculated from (1) and (2) as follows:

$$f_{i0} = \frac{\alpha_i c_i}{(1 - \alpha_i)c_i/f_i^l - \alpha_i d_i/R_{i0}}. \quad (5)$$

Then the utility of MD i in the MEC offloading mode is calculated as follows:

$$U_{i0}(\alpha_i) = \frac{g_i c_i}{f_i^l} \alpha_i - \frac{p_0 c_i f_i^l R_{i0} \alpha_i}{c_i R_{i0} - (c_i R_{i0} + d_i f_i^l) \alpha_i} \quad (6)$$

The offloading ratio must satisfy $\alpha_i \leq c_i R_{i0} / (c_i R_{i0} + d_i f_i^l)$ to guarantee that $f_{i0} \geq 0$. It can be calculated as follows:

$$\alpha_i^* = \begin{cases} 0, & A_0 \leq 0 \\ A_0, & \text{otherwise} \end{cases} \quad (7)$$

where $A_0 = \frac{c_i R_{i0} - R_{i0} f_i^l \sqrt{p_0 c_i / g_i}}{c_i R_{i0} + d_i f_i^l}$. Note that the above equation is obtained by letting the derivative $\frac{\partial U_{i0}}{\partial \alpha_i} = 0$. Due to the page limitation, the detail is not presented here.

For the D2V offloading mode, the optimal offloading ratio is calculated as follows:

$$\alpha_i^* = \frac{c_i R_{ij} F_j}{c_i f_i^l R_{ij} + (c_i R_{ij} + d_i f_i^l) F_j}. \quad (8)$$

Then the task assignment can be solved under the 0-1 integer programming problem in regard to variable \mathbf{x} .

IV. PRELIMINARY RESULTS AND DISCUSSIONS

In our simulation, we consider a single cell network setting with one BS furnished with a MEC server. The BS covers a $200 \text{ m} \times 200 \text{ m}$ region where there are 20 MDs, and 10 PVs. Table I summarizes simulation settings.

The performance of our proposal is compared to that of the *MEC only* scheme, which partially offloads the computational tasks to only the MEC server and adopts the proposed resource allocation and offloading ratio solution. Fig. 1a shows the system utility versus the number of MDs. In case of small number of MDs ($N = 5$), both have the same performance since the computation tasks is only partially offloaded via

TABLE I: Simulation parameters.

Parameter	Value
MD's communication radius	50 m
A task: d_i and v_i	[50,150] KB; [1,2] Megacycles/KB
Computation capacity of MDs	[0.5,1] GHz
Computation capacity of PVs	[1,1.5] GHz
Computation capacity of the MEC server	10 GHz
MDs' transmission power	30 dBm
Bandwidth of channel	10 MHz
Path loss coefficient	-3.4
Noise power	-114 dBm
Unit gain of latency reduction	2.5
Unit price of computing resource	0.1

the MEC offloading mode for optimal resource allocation. As N increases, more MDs can gain advantage from offloading, so the system utility increases. Moreover, our proposal can significantly outperform the *MEC only* scheme since the computation tension of the MEC server can be relieved by utilizing D2V offloading optimally. Similar observation can be found in Fig. 1b when we fix $N = 20$ and increase the input data size. The performance advantage gained by our proposal over the *MEC only* scheme in this case is even greater than in the case of increasing the number of MDs.

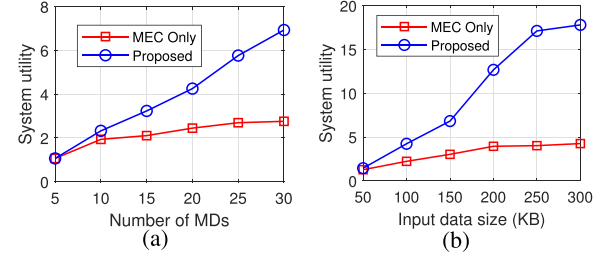


Fig. 1: Performance evaluation under different: (a) Number of MDs, (b) Input data size.

V. CONCLUSION

In this paper, we proposed an efficient utility-centric partial computation offloading scheme, considering the optimization of both the MEC and D2V offloading fashions. The preliminary results showed the potential of the proposed scheme in improving the system utility in PVMEC paradigms. Deeper investigation is left for future work.

REFERENCES

- [1] X.-Q. Pham *et al.*, “Joint service caching and task offloading in multi-access edge computing: A qoe-based utility optimization approach,” *IEEE Communications Letters*, vol. 25, no. 3, pp. 965–969, 2021.
- [2] X. Huang *et al.*, “Parked vehicle edge computing: Exploiting opportunistic resources for distributed mobile applications,” *IEEE Access*, vol. 6, pp. 66 649–66 663, 2018.
- [3] J. Zhang *et al.*, “Optimal task assignment with delay constraint for parked vehicle assisted edge computing: A stackelberg game approach,” *IEEE Commun. Lett.*, vol. 24, no. 3, pp. 598–602, 2020.
- [4] Q. Peng *et al.*, “A task assignment scheme for parked-vehicle assisted edge computing in iov,” in *2021 IEEE 93rd Veh. Technol. Conf. (VTC2021-Spring)*, 2021, pp. 1–5.
- [5] C. Ma *et al.*, “Parking edge computing: Parked-vehicle-assisted task offloading for urban vanets,” *IEEE Internet Things J.*, vol. 8, no. 11, pp. 9344–9358, 2021.
- [6] X.-Q. Pham *et al.*, “Partial computation offloading in parked vehicle-assisted multi-access edge computing: A game-theoretic approach,” *IEEE Trans. Veh. Technol.*, pp. 1–6, 2022.
- [7] ———, “Joint node selection and resource allocation for task offloading in scalable vehicle-assisted multi-access edge computing,” *Symmetry*, vol. 11, no. 1, 2019.

Prospect and Industry Issues of Metaverse and Digital Twin Adoption in Nigerian Maritime

Cosmas Ifeanyi Nwakanma [‡], Judith Nkechinyere Njoku [‡], Cajethan Onyekachi Okafor [†], Dong-Seong Kim ^{*}

[‡]*ICT Convergence Research Center, *IT Convergence Engineering, Kumoh National Institute of Technology Gumi, South Korea*

[†]*Maritime Management Technology, Federal University of Technology, Owerri, Nigeria*

(cosmas.ifeanyi, Judithnjoku24, dskim)@kumoh.ac.kr, [†]cajethan.okafor@futo.edu.ng

Abstract—This work reviewed the potentials and need for Metaverse, Digital twin and enhancement of maritime communication infrastructure in Nigerian maritime sector. The preliminary review results reveal the need for a more robust digital twin platform for maritime communication fault detection detection and evaluation in real time. Similarly, Metaverse promises to be a veritable platform for maritime transportation, communication, and vessel maintenance training. Adopting these technologies can help improve Nigerian's linear shipping connectivity index.

Index Terms—Africa, digital twin, maritime security, metaverse, onboard maritime communications,

I. INTRODUCTION

Digitalization is pushing various industries beyond their historical boundaries and opening up a plethora of new opportunities that will improve the productivity, efficiency and sustainability of shipping and logistics [1]. One of such digital transformations is digital twin (DT) technology and, more recently, the Metaverse. The Nigerian maritime sector is very important, and as a consumer nation that both produces and exports oil, Nigeria depends heavily on imported goods from other countries, most of which are brought in through seaports [2]. Hence, it is pertinent that the prospects of DT and Metaverse in the maritime sector be examined.

To that end, it will focus on answering the following research questions:

- 1) What do Metaverse and Digital Twins mean?
- 2) What are the prospects and the application of Metaverse and Digital Twins in the Maritime industry?
- 3) What are the benefits and challenges of Metaverse and Digital Twins adoption in the Nigerian Maritime industry?

II. BACKGROUND AND RELATED WORKS

The IEEE Standard Association defined the Metaverse as “*an open-ended digital reality and culture that connects various virtual worlds by operating at multiple levels: parallel to, overlaid on, or interactive with the physical domain through increasing developments in interface technologies and real-time data sharing*” [3], [4]. On the other hand, DT involves representing a system or physical object such as a vessel in digital format. The vessel is equipped with a range of sensors relevant to its primary functional areas in order to gather data. The digital copy is later modified using this

information once it has been sent to a processing system [5]. The Metaverse applies DT technology to map the real world into the virtual world in near real-time. The concept of DT adaption for vessels system performance is depicted in Fig. 1 [6]. As illustrated, historical data, industry data, and event and alarm logs are obtained from the physical maritime vessel and used to tune the DT version. The data received is fed into the DT and a base algorithm. The output of the DT is synthetic sensor data, which gets fed into a black box algorithm for the purpose of prediction. To ensure accuracy and reduce the gap between the virtual and physical vessel, the base algorithm is used to finetune the black box algorithm. DT twin vessels enable the use of simulation data to include different events that are nearly never captured by historical data. They also ensure that an exhaustive number of datasets can be generated with diverse variants. As a result of employing DT, the scope can be further increased and controllability improved.

About 60% of all seaborne trade in west and central African regions is accounted for by the marine sector in Nigeria. [7]. However, the country has yet to achieve optimal capacity utilization and the associated revenue benefit as a result of low pace or near non-adoption of state-of-the-art and disruptive technologies such as metaverse, DT, and the challenges of onboard maritime communications.

In [7], examining the industry stakeholder issues preventing the adoption of modern technology in the Nigerian maritime sector, authors posited that the shipyard's infrastructure is outdated and inadequate to leverage its vast water resources for maritime services. However, the work was limited to qualitative evaluation and security issues [8], with no specific technology option in focus.

The authors of [4] reviewed the applicability of Metaverse to data-driven intelligent transportation system using two case studies. Their survey provided the motivation for further research into the role of metaverse and the transportation industry maritime inclusive.

While DT is well researched for maritime industries, Metaverse research focused on the aviation or road transportation industries (see Tables II and III). This is the first study that examines the possible prospects of Metaverse in the maritime industry for a developing country as they combat with lack or substandard transportation infrastructure [9].

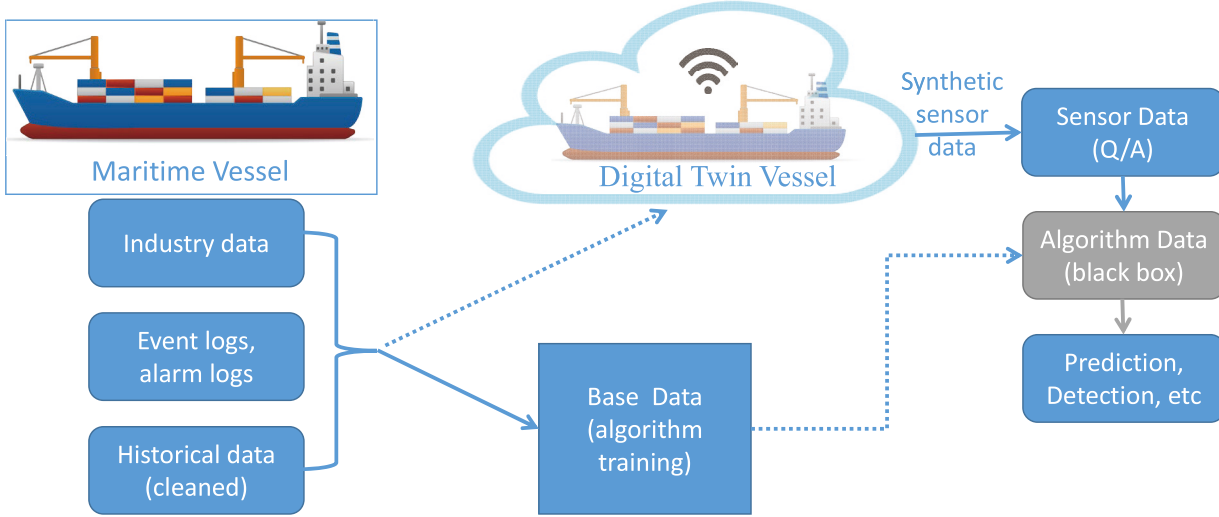


Fig. 1. Digital Twin Adoption for the Vessel System prediction showing the Prediction Algorithms

III. REVIEW METHODOLOGY

This study conformed to the PRISMA (preferred reporting items for systematic reviews and meta-analyses) methodology. In this review the following search terms were used; “Metaverse”, “Digital twin”, and “Maritime transport”, to find previous studies. The following are the database sources for article collection: *IEEE Xplore*, *Wiley*, *MDPI*, and *Taylor and Francis* though core collection were limited to *IEEE Xplore*. Furthermore, only articles written in English language were considered for inclusion. As shown in Fig. 2, 82 documents were obtained after the first search through four databases and other sources. 36 of these documents were excluded as a result of duplication. After screening for relevance, 8 more documents were excluded. Afterwards, 15 articles were excluded based on eligibility. The remaining 23 documents were screened and split into 14 documents for qualitative analysis and 9 documents for quantitative analysis.

The review results are enumerated in Tables II and III, where the prospects and open issues of Metaverse and DT were analyzed respectively. The inference is that, Nigeria needs to adopt Metaverse, DT, and other digital technologies to improve her maritime sector by benchmarking countries that have set in motion the use of these technologies.

TABLE I
PUBLICATIONS USED IN THIS REVIEW

Database source	No. of documents	% Freq
IEEE Xplore	9	39.13
Taylor and Francis	1	4.34
Wiley	1	4.34
MDPI	2	8.69
Other sources	10	43.5
Total	23	100.00

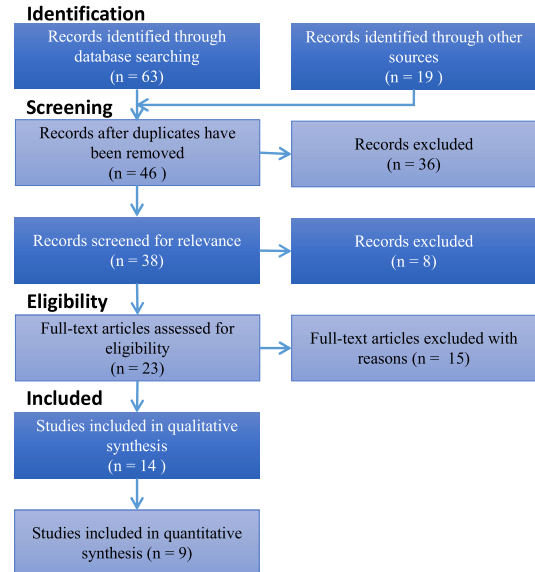


Fig. 2. The PRISMA flowchart

IV. PROSPECTS AND OPEN RESEARCH AREAS IN NIGERIA

The maritime industry’s adoption of metaverse and DT is projected to help achieve the ‘decarbonization’ goal towards attaining zero emissions from ships by 2050 [1], [2]. Hence, the DT offers several benefits. These benefits include but are not limited to: enhancing port and terminal efficiency; better vessel design; and vessel operation. Efficient fleet management; providing situation awareness for all parties involved; optimizing the entire supply chain; and improving safety and security. DT offers workflow prediction and risk mitigation in the real world based on the observed input data. [1].

TABLE II
METAVERSE PROSPECTS AND OPEN ISSUES

Paper	Prospects	Open Issues
[4]	Metaverse potential for intelligent transport	Several enabling technologies are yet to be fully met for full-blown “meta vehicles”
[10]	Promote model training for connected and autonomous vehicles (CAV)	Considering the predicted trajectory for CAV integrated framework
[11]	Aircraft maintenance and can be extended to ship or vessel mainenance	Differentiating millions of parts in aircraft or vessel maintenance knowledge
[12]	Effective for rebranding maritime business and reaching out to the young customers	The use of nonfungible token (NFT) for transparent maritime payment solutions.
[13]	Metavehicle concept for the realization of cyber-physical-social-system (CPSS).	6S: safety, security, sustainability, sensitivity, smartness, systems

TABLE III
DIGITAL TWIN PROSPECTS AND OPEN ISSUES

Paper	Prospects	Open Issues
[14]	Enhancement of scene recognition for search and rescue (SAR) in maritime	Real-time detection and long response time is a challenge in maritime SAR
[15]	Security evaluation of maritime transport using ‘maritime silk road data’	The need to incorporate multi-relay functionality to improve it’s performance.
[16]	ship maintenance using variational autoencoder for fault detection of maritime components onboard	limited to two (2) fault types. Need for robust platforms for fault evaluation.
[17]	Ship maneuvering under wind or no wind influence	Evaluating the role of waterway scenarios in the presence of static and dynamic obstacles.

DT and Metaverse applications to the Nigerian maritime industry are projected to help with performance monitoring, operational cost reduction, and improvement in overall efficiency using tracking technologies in the vessels to collect real-time data from vessels [2]. Also, Metaverse and DT can help in the reduction of greenhouse gas (GHG) emissions. The Nigerian maritime sector is rapidly expanding and need DT, and Metaverse to improve it’s operation, and manage the ports for increased efficiency and output maximization [2].

Although the ship traffic, container port traffic, and gross registered tonnage of Nigeria maritime is increasing, the use of state-of-art marine technologies infrastructure support is limited [18]. The linear shipping connectivity index score used to measure the degree to which countries are connected to international shipping networks has experienced a consistent fall from 23.7 in 2015 to 21.3 in 2020 as shown in Fig. 3 [19].

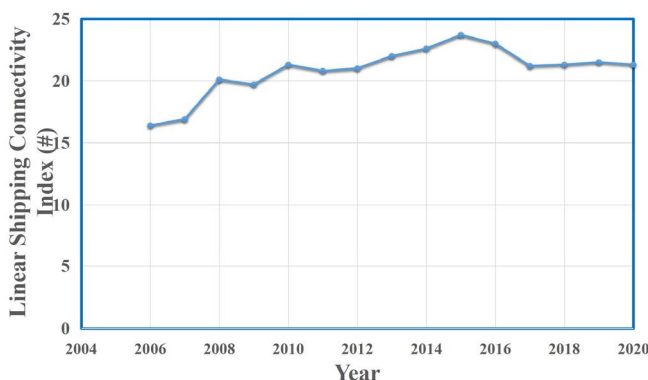


Fig. 3. Linear Shipping Connectivity Index (maximum value in 2004 = 100)-Nigeria

A. Maritime and Shipping Application Case Study

The following areas dominate the focus of experts working on DT and Metaverse for the maritime sector: decision making support, remote control and monitoring, maintenance and condition monitoring [5]. Specifically to ship’s system modelling, the following are major industry case studies: ship hydrodynamics, ship hull structure, marine diesel engine, ship trajectory speed and fuel consumption, propulsion system, ship electric power and ship behaviour [5].

TUAS Metaverse for Maritime Sector: In February 2021, the Turku University of Applied Sciences (TUAS) took the step to develop its own Metaverse for the maritime sector known as the TUAS Metaverse [20]. The TUAS platform is expected to be applicable to smart factory, DT allowing for remote operation and monitoring. TUAS was successfully demonstrated in a porting harbor environment for fire monitoring and fighting under delay-aware simulation condition of 500ms [20].

Port of Rotterdam Container 42: According to Boyles in [21], the Port of Rotterdam adopted the IBM DT to transform its operation into becoming one of the leading ports in the world as confirmed by the World Economic Forum in 2017 [21]. It is projected that with the use of the IBM DT, this port might be the first digital port by 2030. Currently, the port has “Digital Dolphins”, smart quay walls and sensor-equipped buoys in addition to the Container 42 [21].

Saipem 7000 Vessels and ShipManager Hull Software: hhhh ShipMANager Hull is a 3D DT of crane and pipeline vessels developed by DNV. SAIPEM fleet project partnered adopted the ShipManager Hull to support fleet management, periodic inspections and dry-dock repairs optimal planning [22].

Military Sealift Command: A DT is being built for Military Sealift Command’s cargo ammunition carriers with

assistance from General Electric (GE). The data gathered from marine equipment, including variable frequency drives, propulsion motors, diesel engines, and generators, is used to compare the actual output of the vessel to the predicted one. Any anomalies that point to potential engine failure or other vital infrastructure issues are identified and addressed before they occur, enhancing the availability, effectiveness, operations, and readiness of their assets and missions. The DT also enables remote diagnostics and monitoring [23].

V. CONCLUSION

The DT and Metaverse application in the maritime sector is still at the infant stage. This work reviewed the applicability of Metaverse and DT to the maritime sector with a focus on the enabling technologies needed to improve the economic potential of the Nigerian maritime industry. Nigeria's linear shipping connectivity index have been on the decline since 2015. It is a future research direction to present an exploratory research into how the combined use of DT and Metaverse can improve the maritime connectivity in Nigeria.

ACKNOWLEDGMENT

This research work was supported by Priority Research Centers Program through NRF funded by MEST (2018R1A6A1A03024003) and the Grand Information Technology Research Center support program (IITP-2022-2020-0-01612) supervised by the IITP by MSIT, Korea.

REFERENCES

- [1] J. Loh, "Many uses of Digital Twins in Maritime Industry," in *Digital Transformation, Maritime News*, May 30, 2022. [Online]. Available: <https://maritimefairtrade.org/the-many-uses-of-digital-twins-in-maritime-industry/>
- [2] F. Okote, "Digitalisation: Making Nigerian ports globally competitive," in *Businessday*, September 10, 2019. [Online]. Available: <https://businessday.ng/columnist/article/digitalisation-making-nigerian-ports-globally-competitive>
- [3] "The IEEE Global Initiative on Ethics of Extended Reality (XR) Report—Metaverse and Its Governance," *The IEEE Global Initiative on Ethics of Extended Reality (XR) Report—Metaverse and Its Governance*, pp. 1–31, 2022.
- [4] J. N. Njoku, C. I. Nwakanma, G. C. Amaizu, and D. S. Kim, "Prospects and Challenges of Metaverse Application in Data-Driven Intelligent Transportation Systems," *IET Intelligent Transport System*, (Early View), 2022. [Online]. Available: <https://doi.org/10.1049/itr2.12252>
- [5] N. Assani, P. Matić, and M. Katalinić, "Ship's Digital Twin—A Review of Modelling Challenges and Applications," *Applied Sciences*, vol. 12, no. 6039, 2022. [Online]. Available: <https://doi.org/10.3390/app12126039>
- [6] K. B. Ludvigsen and S. Øyvind, "Digital Twin for Blue Denmark: Danish Maritime Authority," in *Digital Twin Report for DMA: DNV GL Maritime*, no. 2018-0006, Rev. A, 2018. [Online]. Available: <https://www.iims.org.uk/wp-content/uploads/2018/04/Digital-Twin-report-for-DMA.pdf>
- [7] N. M. Ikpogu, "Barriers to Technology Adoption Among Maritime Industry Stakeholders in Nigeria," in *Walden Dissertations and Doctoral Studies*, no. 10805, 2021. [Online]. Available: <https://scholarworks.waldenu.edu/dissertations/10805>
- [8] E. Etuk, "Challenges of Curbing Criminality in Nigeria's Maritime Domain and its Attendance Implications on Youth Empowerment," *Advances in Social Sciences Research Journal*, vol. 7, no. 9, pp. 533–537, 2020. [Online]. Available: <https://doi.org/10.14738/assrj.79.8915>
- [9] C. Uzondu, S. Jamson, and G. Marsden, "Road safety in Nigeria: unravelling the challenges, measures, and strategies for improvement," *International Journal of Injury Control and Safety Promotion*, vol. 0, no. 0, pp. 1–11, 2022, pMID: 35895320. [Online]. Available: <https://www.tandfonline.com/doi/abs/10.1080/17457300.2022.2087230>
- [10] Y. Ren, R. Xie, F. R. Yu, T. Huang, and Y. Liu, "Quantum Collective Learning and Many-to-Many Matching Game in the Metaverse for Connected and Autonomous Vehicles," *IEEE Transactions on Vehicular Technology*, pp. 1–12, 2022.
- [11] A. Siyaev and G.-S. Jo, "Neuro-Symbolic Speech Understanding in Aircraft Maintenance Metaverse," *IEEE Access*, vol. 9, pp. 154494–154499, 2021.
- [12] N. Kshetri, "Web 3.0 and the Metaverse Shaping Organizations' Brand and Product Strategies," *IT Professional*, vol. 24, no. 2, pp. 11–15, 2022.
- [13] F.-Y. Wang, "MetaVehicles in the Metaverse: Moving to a New Phase for Intelligent Vehicles and Smart Mobility," *IEEE Transactions on Intelligent Vehicles*, vol. 7, no. 1, pp. 1–5, 2022.
- [14] Z.-Z. Guo, K. Wang, J.-Y. Qin, X.-B. Li, D.-C. Ran, and Y. Shen, "An Intelligent Maritime Scene Frame Prediction Based on Digital Twins Technology," in *2021 IEEE 1st International Conference on Digital Twins and Parallel Intelligence (DTPI)*, 2021, pp. 25–28.
- [15] J. Liu, C. Li, J. Bai, Y. Luo, H. Lv, and Z. Lv, "Security in IoT-Enabled Digital Twins of Maritime Transportation Systems," *IEEE Transactions on Intelligent Transportation Systems*, pp. 1–9, 2021.
- [16] P. Han, A. L. Ellefsen, G. Li, F. T. Holmeset, and H. Zhang, "Fault Detection With LSTM-Based Variational Autoencoder for Maritime Components," *IEEE Sensors Journal*, vol. 21, no. 19, pp. 21903–21912, 2021.
- [17] Y. Shuai, G. Li, J. Xu, and H. Zhang, "An Effective Ship Control Strategy for Collision-Free Maneuver Toward a Dock," *IEEE Access*, vol. 8, pp. 110140–110152, 2020.
- [18] A. E. Faith, "The Maritime Industry of Nigeria. Challenges and Sustainable Prospects," *DANUBIUS WORKING PAPERS*, vol. 1, no. 1, pp. 20–31, 2019. [Online]. Available: <https://dj.univ-danubius.ro/index.php/DWP/article/view/126>
- [19] World-Bank, "Linear Shipping Connectivity Index (maximum value in 2004=100)- Nigeria," in *Data Bank*, 2020. [Online]. Available: <https://data.worldbank.org/indicator/IS.SHP.GCNW.XQ>
- [20] M. Luimula, T. Haavisto, D. Vu, P. Markopoulos, J. Aho, E. Markopoulos, and J. Saarinen, "The Use of Metaverse in Maritime Sector – A Combination of Social Communication, Hands on Experiencing and Digital Twins," *Accelerating Open Access Science in Human Factors Engineering and Human-Centered Computing (AHFE)*, vol. 31, pp. 115–123, 2022. [Online]. Available: <http://doi.org/10.54941/ahfe1001513>
- [21] R. Boyles, "How the Port of Rotterdam is using IBM digital twin technology to transform itself from the biggest to the smartest," *IBM Business Operations Blog*, August 29, 2019. [Online]. Available: <https://www.ibm.com/blogs/internet-of-things/iot-digital-twin-rotterdam/>
- [22] R. G. S. Buøen, "DNV supplies ShipManager Hull software to realize Saipem 7000's digital twin," *DNV Maritime News Blog*, August 13, 2019. [Online]. Available: <https://www.dnv.com/news/dnv-supplies-shipmanager-hull-software-to-realize-saipem-7000-s-digital-twin-154798>
- [23] M. Singh, R. Srivastava, E. Fuenmayor, V. Kuts, Y. Qiao, N. Murray, and D. Devine, "Applications of Digital Twin across Industries: A Review," *Applied Sciences*, vol. 12, no. 5727, 2022. [Online]. Available: <https://doi.org/10.3390/app12115727>

A Study of Open-Source Network Simulator

Jae Woo Kim

ICT Convergence Research Center
Kumoh national institute of Technology
Gumi, Republic of Korea
jaewookim@kumoh.ac.kr

Ki-Hyeob Kwon

ICT Convergence Research Center
Kumoh national institute of Technology
Gumi, Republic of Korea
navkwon@kumoh.ac.kr

Dong-Seong Kim

Dept. of IT Convergence Engineering
Kumoh national institute of Technology
Gumi, Republic of Korea
dskim@kumoh.ac.kr

Abstract—This study analyzed the simulation method for the currently used open source network simulation tool and classified it according to the simulation method. Furthermore, based on the simulation method, we propose a simulation tool selection guide for effective network simulation design.

Index Terms—Network Simulator, Open-Source, Virtualization

I. INTRODUCTION

Network simulation tools allow various developers to pre-test network environments before configuring expensive real-world environments. Therefore, various network simulation tools have been developed according to each requirement, and studies to analyze network simulation tools have also been conducted [1]- [2]. Network simulations virtualize channels for intercommunication from terminal nodes such as PCs to network nodes such as switches, routers, and relays to form a network environment on a computer. Meanwhile, the advantages of open-source network simulation and each simulation tool are being analyzed and studied to select network simulation tools [3]. This short paper summarizes the network simulation methods and the open-source network simulators according to each method. In addition, we derive some items to consider when selecting network simulation tools and propose a guide to simulation methods and tool selection.

II. TWO METHOD OF NETWORK SIMULATOR AND SELECTION GUIDE

The open-source network simulation tool can be divided into two types according to the network simulation method as shown in Figure 1. First, it is a virtualization simulation method. The virtualization simulation method is a method of creating a virtual machine (VM) using the virtualization method on the operating system kernel and configuring one network node for each virtual machine to perform the simulation. It can be said to be an emulation method that virtually imitates actual network equipment on a PC. Second, the discrete event simulation method can be said to be a method of programming and modeling network nodes within general application software and performing simulation by defining events. Discrete event simulation methods can construct flexible network simulation environments such as programming in various scenarios and detailed settings. Table 1 shows the types of open source network simulation tools according to two methods. The purpose of the network simulation is

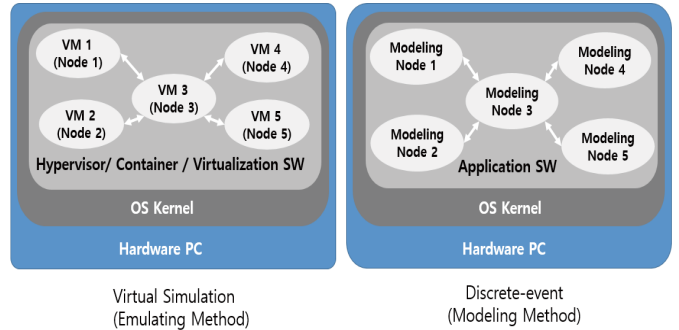


Fig. 1. Two Network Simulation Methods

TABLE I
OPEN SOURCE NETWORK SIMULATION TOOLS BY THE METHODS

Simulation Method	Tool
Virtual Simulation	CORE, Mininet, Cloonix, EVE-NG, GNS3, IMUNES, Containerlab, Kathara, vrnetlab
Discrete-Event	NS2, NS3, OMNET++, JSIM, Shadow

to verify the functionality and performance of the network topology or protocol in detail. Functional verification is to check the network operation function before building an actual network. Virtualization methods are suitable for functional verification. Performance verification is to propose a new protocol algorithm and test its performance. For performance testing, discrete event simulation tools that are easy to implement algorithms are suitable. If the network configuration includes equipment from a particular manufacturer, it has the advantage of selecting tools to support the manufacturer's equipment library. In order to quickly implement a simulation environment, there is an advantage of selecting a simulation tool that supports the GUI. In addition, selecting simulation tools that support the programming language according to the programming capabilities possessed by the developer has an advantage in ease of simulation configuration. The reliability of the simulation results is more reliable because the method of emulating the actual equipment uses a library that reflects the performance of the equipment manufacturer as it is. And it can be seen that simulation tools with more active communities are reliable.

ACKNOWLEDGMENT

This research was supported by Basic Science Research Program through the National Research Foundation of Korea(NRF) funded by the Ministry of Education(2022R1I1A1A01071058,2018R1A6A1A03024003).

REFERENCES

- [1] KHAN, A. R., BILAL, S. M., OTHMAN, M."A performance comparison of open source network simulators for wireless networks", *IEEE international conference on control system, computing and engineering*, pp.34-38, Nov 2016.
- [2] Siraj, Saba, A. Gupta, and Rinku Badgugar,"Network simulation tools survey", *International Journal of Advanced Research in Computer and Communication Engineering*, pp.199-206, 2012.
- [3] Gupta, Suraj G., et al., "Open-source network simulation tools: An overview.", *International Journal of Advanced Research in Computer Engineering Technology*, pp.1692-1635, 2013

Primary User Emulation Attack Detection

Vladimir Shakhov

Department of Electrical, Electronic
and Computer Engineering

University of Ulsan

Ulsan, Korea

shakhov@mail.ulsan.ac.kr

Abstract— Leading IT industry experts are seriously concerned about the low reliability of IoT technologies, especially those based on wireless networks. Cognitive radio solves some of these problems and also provides opportunities for efficient use of the spectrum. However, intrusions that are specific to cognitive radio systems have appeared. We consider one of the most devastating attacks of this type, called the primary user emulation attack. We propose an efficient approach to intrusion detection based on statistical sequential analysis. Performance analysis is also provided.

Keywords—*intrusion detection, cognitive radio, primary user emulation attack, statistical sequential analysis*

WORK IN PROGRESS

Primary User Emulation Attack (PUEA) poses a serious security risks to cognitive radio systems. In its most general form, the attack can be described as follows. The intruder fakes the signal characteristics of primary users. The consequence of this is that secondary users erroneously identify the actions of the intruder as those of the primary user. They refrain from competing for prime user channels. Due to the decrease in the number of channels, the quality of service degrades. Also, an attacker can unfairly take these channels for his sole use.

Investigations are currently underway to detect and counter PUEA. For example, the researchers discussed a taxonomy of PUEA attackers, the success conditions for PUEA, and how the attack affects cognitive radio systems [1]. Also, the signature based method of intrusion detection is offered. This approach is based on the use of an auxiliary two-level database. For these purposes, energy consumption information and location verification are utilized. To mitigate the impact of PUEA on the performance of cognitive radio networks, it is proposed to reserve some of the channels. In some cases, this can improve the situation with the blocking of secondary users, but this measure in itself worsens the network performance. An alternative method of intrusion detection also requires information about the location of the main users and the strength of the received signal. This is the general approach used in many publications. The following three-stage algorithm is used to detect an attack [2]. The signal parameters are sequentially tracked, the transmitter power estimate is calculated, and the transmitter location is calculated based on the distributed information coming from the network nodes. A decision is then made as to whether the transmitter is in good faith or an intruder. With this approach, information about the location of the transmitters must be known in advance. However, in mobile networks, the location of network nodes is usually random. Recently, a variety of ML-based approaches have been proposed to classify whether the received signal is a main user signal or a malicious main user emulation signal. For example, in [3] authors use the signal-to-noise ratio and

Renyi entropy of the energy signal as input to a support vector machine. However, the training set may become outdated due to the mobility of the network nodes.

We develop a low complexity and reliable approach to detect PUEA in cognitive radio systems. We assume that the attacker cannot use the spectrum when the primary user (PU) is transmitting. However, when the PU is not transmitting, the intruder can transmit a spoofed PU signal to avoid the secondary users (SU) being able to use the free spectrum. Thus, SU must determine if the received signal is from the PU or the intruder. The decision rule is based on energy observations. Observations are processed using sequential statistical analysis. Our hypothesis is that the appearance of an intruder leads to changes in the parameters of the random process that displays these observations. Thus, we need to detect the moment of change in the distribution of the random process as soon as possible. The detection algorithm is known as the cumulative sums method (CUSUM). The incoming random values for the algorithm are energies levels observations in sequential time moments. If $\xi(t_j), j > 0$ is the observed energy level and an attack is implemented, then the observed random process, $\{\xi(t_j)\}$ changes own properties. Let T_{alarm} be the moment of time when the decision about PUEA presence is generated. A change-point detection method is as follows

$$S_0 = 0,$$

$$S_i = \max(0, S_{i-1} + \Delta_i).$$

Here Δ_i is a function of observations ξ_i (e.g. the log-likelihood ratio). The alarm is defined as follows:

$$T_{alarm} = \inf \{i \geq 1 : S_i > h\}$$

Generally, the threshold h is defined by simulation to get the tradeoff between efficient detection and false alarm rate.

ACKNOWLEDGMENT

This work was supported by a National Research Foundation of Korea (NRF) grant through the Korean Government (MSIT) under Grant NRF-2020R1IIA1A01065692.

REFERENCES

- [1] R. Yu, Y. Zhang, Y. Liu, S. Gjessing and M. Guizani, "Securing cognitive radio networks against primary user emulation attacks," IEEE Network, vol. 29, no. 4, pp. 68-74, July-August 2015.
- [2] R. Chen, J. -M. Park and J. H. Reed, "Defense against Primary User Emulation Attacks in Cognitive Radio Networks," IEEE Journal on Selected Areas in Communications, vol. 26, no. 1, pp. 25-37, Jan. 2008.
- [3] E. Cadena Muñoz, L. F. Pedraza Martínez, and J. E. Ortiz Triviño, "Detection of Malicious Primary User Emulation Based on a Support Vector Machine for a Mobile Cognitive Radio Network Using Software-Defined Radio," Electronics, vol. 9, no. 8, p. 1282, Aug. 2020.

A Study on the Problems and Solutions in the NFT Ecosystem

Yongbin Choi and Amsuk Oh

Department of Digital Media Engineering
University of Tongmyong
Busan 48520, Korea
asoh@tu.ac.kr

Abstract— Web 3.0 currently used as a decentralized web in conjunction with blockchain technology. In this web 3.0 service, NFT serves as a certificate of digital content, that is, ownership. In order to register and trade this, an underlying platform is essential. In addition, by creating and building this platform, it is possible to preoccupy the leading position in the web 3.0 era. Therefore, this paper aims to study the underlying technology that actively used in metaverse, games, etc. through the development of the NFT platform.

Keywords—, NFT, Klaytn, Platform, Blockchain

I. INTRODUCTION

The NFT platform is a system that connects creators, producers, and customers to transaction entities, creating new business models through efficient transaction record management and real-time transactions, and responding to trends arising from the new WEB3.0 market [1-2]. Since there is still a lack of NFT platforms in Korea, overseas sites are being used, so the transaction market has moved overseas, and accessibility of domestic users and creators is significantly decreasing. Leading development is urgently needed to actively respond to rapidly changing environmental changes in the web ecosystem, such as increasing diversity and volatility in demand along with rapid technological development. Recently, the blockchain industry is actively using NFT to cope with metaverse, games(G2E), etc. [3-4]. The problems and requirements in the domestic NFT ecosystem are as follows.

TABLE I.

PROBLEMS AND REQUIREMENTS IN THE NFT ECOSYSTEM

Field	Problem	Solution
Fee	High transmission costs using ETH	Low fee using Klaytn
Transmission Speed	Low transmission rate using ETH	High transmission speed using Klaytn
Price volatility	High price volatility of ETH	Low price volatility of the Klaytn

Therefore, among these problems derived above, major matters such as commission, transmission speed, and price volatility are to be presented using Klaytn in this paper.

This research was supported by the MISP(Ministry of Science, ICT & Future Planning), Korea, under the National Program for Excellence in SW supervised by the IITP(Institute for Information & communications Technology Promotion)(2018-0-018740301001).

II. NFT TROUBLESHOOTING DETAILS AND METHODS

In this paper, based on Clayton Blockchain Technology(KIP17), we would like to present an ‘NFT platform’ to improve transaction convenience between creators and T buyers, and the research details are as follows.

- ①Wallet : Address issuance and balance confirmation module
- ②Klay Coin Transfer : Both internal address and external address transfer
- ③Klay Coin Transmission History : Klay Coin Transmission History Module
- ④Contract : Contract issuance and management module for NFT transaction records
- ⑤NFT Metadate : NFT Metadata Definition Module
- ⑥NFT : NFT Management Module
- ⑦NFT Transaction : NFT (Token) Trading Module
- ⑧NFT History : NFT Transaction History Module

A. Wallet’s Development

Wallet manages the address for coin transactions with NFT, the Klaytn Coin owned by the user, and the NFT owned by the user, and manages the payment account to register the address and pay the fee by creating the Creator and User, The detailed functions are as follows.

TABLE II.

DETAILS OF WALLET

Function	Content	Grafting technology
Account management	<ul style="list-style-type: none">• Creating an account, deleting• Check account list• Balance check	<ul style="list-style-type: none">① Using the Wallet API② FrontEnd : Codeigniter③ BackEnd : nodejs④ Save DB
Payment account management	<ul style="list-style-type: none">• Create and delete a payment account• Payment account list check• Balance check	<ul style="list-style-type: none">① Using the KSA Wallet API② FrontEnd : Codeigniter③ BackEnd : nodejs④ Save DB

B. Game Server Engine Type

Contract is a digital electronic function that allows individuals(P2P) to enter into desired contracts without inserting a third guarantee agency in the middle. KIP-17 is a non-fungible Token(NFT) contract standard defined by

Klaytn and is built using the KIP-17 API to easily generate and manage KIP-17 tokens.

TABLE III.
DETAILS OF CONTRACT

The game server engine for latency measurement was selected based on Supported Languages, Supported Server.

Function	Content	Grafting technology
Contract management	<ul style="list-style-type: none"> • Contract Distribution (2-3. Related to Klay Transaction) • Contract inquiry 	<ul style="list-style-type: none"> ① Using the KAS-17 API ② FrontEnd : Codeigniter ③ BackEnd : nodejs ④ Save DB

C. Klay Transaction Development

Klay Transaction is a module for Klay coin transmission to pay the amount and gas fee for NFT transactions.

TABLE IV.
DETAILED FEATURES OF KLAY TRANSACTION

Field	Problem	Solution
Basic Transaction	<ul style="list-style-type: none"> • Send Klay 	<ul style="list-style-type: none"> ① Using the Wallet API ② FrontEnd : Codeigniter ③ BackEnd : nodejs ④ Save DB

III. CONCLUSION

This paper presents an underlying technology that can be actively used in metaverse, games, etc. through the development of the NFT platform to study problems and solutions in the NFT ecosystem. Through this base technology, the following expected effects are expected.

- Leading positional occupation through market preoccupation
- The Trend of Metaverse, G2E Game, and NFT according to the Changes of the WEB3.0 Era
- Create value-added value by installing a variety of additional items beyond simple image and video transactions
- Promote transactions by providing a platform that pays low fees to creators
- Blockchain ensures security safety and integrity and reduces data management costs

ACKNOWLEDGMENT

This research was supported by the MISP(Ministry of Science, ICT & Future Planning), Korea, under the National Program for Excellence in SW) supervised by the IITP(Institute for Information & communications Technology Promotion)(2018-0-018740301001).

REFERENCES

- [1] “Klaytn Mainnet: Cypress – The First Blockchain for Everyday Life,” <https://www.klaytn.com/>
- [2] Klaytn team, “Klaytn Design,” https://docs.klaytn.com/klaytn/design_2019
- [3] Andreas Meier and Henrik Storrie, “Blockchain = Distributed Ledger + Consensus”, HDM Praxis der Wirtschaftsinformatik, Volume 55, Issue 6, pp. 1139-1154, December 2018.
- [4] Joseph Abadi and Markus Brunnermeier, “Blockchain Economics”, Princeton University, June 2018.



ICMIC 2022

International Conference on
Maritime IT Convergence

<http://icmic-conf.org/>